International Journal of Geophysics

Implementation of Short- and Medium-Term Earthquake Forecasts

Guest Editors: Rodolfo Console, Koshun Yamaoka, and Jiancang Zhuang

Implementation of Short- and Medium-Term Earthquake Forecasts

International Journal of Geophysics

Implementation of Short- and Medium-Term Earthquake Forecasts

Guest Editors: Rodolfo Console, Koshun Yamaoka, and Jiancang Zhuang

Editorial Board

Contents

Hindawi Publishing Corporation
International Journal of Geophysics
Volume 2012, Article ID 217923, 2 pages
doi:10.1155/2012/217923

Editorial

Implementation of Short- and Medium-Term Earthquake Forecasts

Rodolfo Console,[1] Koshun Yamaoka,[2] and Jiancang Zhuang[3]

[1] *Istituto Nazionale di Geofisica e Vulcanologia, 00143 Roma, Italy*
[2] *Graduate School of Environmental Studies, Nagoya University, Nagoya 464-8601, Japan*
[3] *Institute of Statistical Mathematics, Tokyo 106-8569, Japan*

Correspondence should be addressed to Rodolfo Console, console@ingv.it

Received 11 March 2012; Accepted 11 March 2012

The cases of the recent destructive earthquakes that occurred with impressive frequency in Sichuan (China, 2008), Italy (2009), Haiti (2010), Chile (2010), New Zealand (2010), and Tohoku (Japan, 2011) have shown that, in present state, scientific researchers have achieved little or almost nothing in the implementation of short- and medium-term earthquake prediction, which would be useful for disaster mitigation measures.

This regrettable situation could be ascribed to the present poor level of achievements in earthquake forecast. In fact, although many methods have been claimed to be capable of predicting earthquakes (as numerous presentations on earthquake precursors regularly show at every international meeting), the problem of formulating such predictions in a quantitative, rigorous, and repeatable way is still open.

In the last decade some short- and intermediate-term forecasting models have been proposed in a way that can provide us with the estimate of earthquake occurrence probability in a specific window of their origin times, epicentral coordinates, and magnitudes. They have been rigorously tested in both prospective and retrospective ways against observed seismic activity. However, it seems that these applications are still far away from our practical purposes (see [1], for a comprehensive review of the progress achieved in the last ten years on seismicity-based earthquake forecasts).

On the other hand, another problem of practical implementation of earthquake forecasting could be due to the lack of common understanding and exchange of information between the scientific community and the governmental authorities that are responsible for earthquake damage mitigation in each country: they operate in two different environments, they aim at different tasks, and they generally speak two different languages. In particular, the way how seismologists should formulate their forecasts and how they should transfer them to decision-makers and to the public is still a tricky issue. The case that seven scientists belonging to the Committee on Seismic Risk of the Italian Civil Protection Agency were legally prosecuted after the May 5th, 2009, L'Aquila earthquake is a clamorous example of this kind of problems [2]

It is clear that the formulation of probabilistic earthquake forecasts with large uncertainties in space and time and very low probability levels is still difficult to be used by decision-making people. In real circumstances the authorities deal with critical problems related to the high cost of evacuating the population from an area where the scientific methods estimate an expected rate of destructive earthquake as one in many thousand days, while they require much more deterministic statements. A new name, "operational earthquake forecasting," has been given to the process of providing usable information on future earthquakes or ongoing seismic sequences. An extensive report on the potential of such a process has been written by the International Committee appointed by the Italian Civil Protection Agency [3].

In this special issue, we were aiming to assess the status of the art of earthquake forecasts and their applicability. Therefore, we invited authors to report methods and case

studies that could concretely contribute or, at least seemed promising, to improve the present frustrating situation, regarding the practical use of earthquake forecasts. Seven contributions out of the 22 submissions to this special issue were accepted.

Two contributions present reviews of the present status of earthquake forecasting and its validation. One of them, titled "*Precursor-like anomalies prior to the 2008 Wenchuan Earthquake: a critical-but-constructive review*" by T. Ma and Z. Wu, is a critical review of more than 200 papers reporting the retrospective analysis of precursory anomalies observed prior to the 2008 Wenchuan earthquake in China. The material collected and used for the analysis contains a wide range of precursor-like anomalies observed at different time scales. These anomalies include, among others, seismicity changes, deformation measurements, strain/stress measurements, physical variations, gravity recordings, ionospheric anomalies, and geothermal and atmospheric anomalies. Some of the observations show consistent characteristic times, such as 2–4 days and 1-2 years, which may reveal the preparation and approaching process of this great inland earthquake, and suggest the need for further investigation. A more quantitative approach in statistical sense is considered in "*Evaluating the RELM test results*" by M. K. Sachs et al. They start from the results of the Regional Earthquake Likelihood Models (RELM) test for earthquake forecasting. Five different forecasting methods were considered in the test. In particular, the authors utilize a methodology developed in the atmospheric sciences, specifically for tornadoes, to compare the forecast results. The best forecasts are about one order of information significance better than random forecasts. The paper also includes a discussion on alternative methods of evaluation of the performance of RELM forecasts and on the relative merits of alarm-based versus probability-based forecasts.

Two papers report case studies on different kinds of earthquake precursors. One of them, titled "*Spatiotemporal relationship between geodetic and seismic quantities: a possible clue to preparatory processes of $M \geq 6.0$ inland earthquakes in Japan,*" is by Kawamura et al. They aimed to formulate a model to characterize the physical conditions associated with large earthquake occurrence. In their study, they focused on assessing the relationship between geodetic and seismic quantities and attempted to find the pair of related quantities that most likely indicates preparatory processes of large earthquakes in Japan. Their study revealed that the pair of absolute dilatation rate and seismic energy shows the highest statistical performance. The second paper of this group is titled "*Medium-term earthquake forecast using gravity monitoring data: evidences from the Yutian and Wenchuan earthquakes in China*, by Y. Zhu and F. B. Zhan. They review the gravity monitoring data and methods that had allowed a medium-term forecast of the Yutian and Wenchuan, 2008 earthquakes in China. This paper suggests that gravity changes derived from regional gravity monitoring data could potentially be a useful medium-term precursor of large earthquake, but significant additional research is needed to evaluate and validate this hypothesis.

Other two papers deal with ongoing research projects on earthquake precursors aiming at the development of physical models. One of these is "*The new avalanche-like stochastic model for parameterization of seismicity and its application to the South Sakhalin Island seismicity*," by M. V Rodkin and I. Tikhonov. In this paper, the seismic process is regarded as an assemblage of randomly developing episodes of avalanche-like relaxation. Such a model is considered as an alternative to the model based on the concept of SOC (self-organized criticality). An advantage of this approach consists in a clear physical meaning of the model parameters. An anomalous increase of the parameter called "metastability" was found in connection with two earthquakes occurring in the southern Sakhalin Island in 2006 and 2007, which indicates an increase in probability of the occurrence of a future earthquake. The next paper, with the ambitious title of "*A deterministic approach to earthquake prediction*," by V. Sgrigna and L. Conti, addresses the importance of combining ground and space observations of earthquake precursors. The authors describe a few projects and experiments carried out with the aim of providing support to the theoretical interpretation of seismogenic processes.

The final contribution, "*Probabilistic seismic hazard analysis for Yemen*," by R. Mohindra et al. is a typical example of probabilistic seismic hazard assessment (PSHA) based on the recognition of the principal seismic sources in and around the territory of Yemen. It was recognized that the largest contribution to the PSHA comes from the West Arabian Shield seismic zone.

Acknowledgment

We thank many anonymous reviewers for their careful reviews and constructive suggestions in improving each submission.

Rodolfo Console
Koshun Yamaoka
Jiancang Zhuang

References

[1] K. F. Tiampo and R. Shcherbakov, "Seismicity-based earthquake forecasting techniques: ten years of progress," *Tectonophysics*, vol. 522-523, pp. 89–121, 2012.

[2] N. Nosengo, "Italy puts seismology in the dock," *Nature*, vol. 465, no. 7301, article 992, 2010.

[3] T. H. Jordan, Y.-T. Chen, P. Gasparini et al., "Operational earthquake forecasting. State of knowledge and guidelines for utilization," *Annals of Geophysics*, vol. 54, article 4, 2011.

Hindawi Publishing Corporation
International Journal of Geophysics
Volume 2012, Article ID 406278, 20 pages
doi:10.1155/2012/406278

Research Article

A Deterministic Approach to Earthquake Prediction

Vittorio Sgrigna[1] and Livio Conti[2]

[1] *Dipartimento di Fisica and Sezione INFN, Università Roma Tre, 84 Via della Vasca Navale, 00146 Roma, Italy*
[2] *Facoltà di Ingegneria, Università Telematica Internazionale UNINETTUNO, Corso Vittorio Emanuele II 39, 00186 Roma, Italy*

Correspondence should be addressed to Livio Conti, conti.livio@gmail.com

Received 14 July 2011; Revised 27 January 2012; Accepted 6 February 2012

Academic Editor: Yamaoka Koshun

The paper aims at giving suggestions for a deterministic approach to investigate possible earthquake prediction and warning. A fundamental contribution can come by observations and physical modeling of earthquake precursors aiming at seeing in perspective the phenomenon earthquake within the framework of a unified theory able to explain the causes of its genesis, and the dynamics, rheology, and microphysics of its preparation, occurrence, postseismic relaxation, and interseismic phases. Studies based on combined ground and space observations of earthquake precursors are essential to address the issue. Unfortunately, up to now, what is lacking is the demonstration of a causal relationship (with explained physical processes and looking for a correlation) between data gathered simultaneously and continuously by space observations and ground-based measurements. In doing this, modern and/or new methods and technologies have to be adopted to try to solve the problem. Coordinated space- and ground-based observations imply available test sites on the Earth surface to correlate ground data, collected by appropriate networks of instruments, with space ones detected on board of Low-Earth-Orbit (LEO) satellites. Moreover, a new strong theoretical scientific effort is necessary to try to understand the physics of the earthquake.

1. Introduction

In our opinion, the investigation of possible earthquake prediction must be carried out on a deterministic basis. Unfortunately, at the moment, the study of the physical conditions that give rise to an earthquake and the processes that precede a seismic rupture of an ordinary event are at a very preliminary stage and, consequently, the techniques of prediction of time of origin, epicentre, and magnitude of an impending earthquake now available are below standard.

Therefore, the present level of knowledge is unable to achieve the objective of a deterministic prediction of an ordinary seismic event, but it certainly will in a more or less distant future tackle the problem with seriousness and avoiding scientifically incorrect, wasteful, and inconclusive shortcuts, as sometimes has been done. It will take long time (may be years, tens of years, or centuries) because this approach requires a great cultural, financial, and organizational effort on an international basis. It implies the need for carrying out combined ground and near-Earth space continuous observations of the so-called earthquake precursors, coseismic and postseismic phenomena, as well as the development of appropriate theoretical models able to justify the observations in order to understand the physical mechanisms underlying the earthquake preparation and occurrence. So, ground networks of instruments in the major seismic areas of the Earth and Low-Earth-orbit (LEO) multi-instrument satellites, as well as laboratory and theoretical investigations, will be necessary to address the study carried out by coordinate teams of researchers and specialists in the different scientific and technical fields of the physics of the Earth system. Probably, the pressure of act more quickly sometimes gives bad advise. An example of such behaviour has been given even on the occasion of the recent destructive seismic event occurred in Japan last March 2011 when, also inside groups of the scientific community, reckless statements were raised hinting the hypothesis (and someone has actually said) that earthquake prediction is possible, especially if it is possible there will be financial support and some kind of scientific coordination.

Remember that the 2011 March 11 05:46:23 UTC Tohoku earthquake (near the East coast of Honshu, Japan), also knows as the Great East Japan Earthquake, had magnitude 9.0; location 38.322°N, 142.369°E; depth 32 km. It was the Japan's most powerful earthquake since records began and has struck the north-east coast, triggering a massive tsunami. The Japanese National Police Agency has confirmed 15.550 deaths, 5.688 injured, and 5.344 people missing across twenty-tow prefectures, as well as about 225.000 buildings damaged or destroyed [1].

In the face of such huge disaster, the above-mentioned claims on the earthquake prediction must be considered as regrettable. They were issued through mass media and even within a pseudoscientific context, and appearing as a kind of "scientific looting." Such false statements can only be used to take advantage of the disaster, maybe to obtain more easily research funds or for a greater visibility within the scientific community, civil services, and authorities that need to take adequate measures for assistance and protection of the population and reconstruction of houses and infrastructures. To justify the concept of earthquake prediction, "noises" are often introduced thus confusing different concepts such as earthquake precursor, seismic hazard, earthquake warning, and earthquake forecasting. A similar disgraceful behaviour does not produce any result useful to science or to society.

This "vulnus" inside the scientific community cannot easily be healed and overcame, since mediocre minds are as able to organize themselves as brilliant ones. So, self-referential poor groups of researchers are easily formed and can also permeate international peer-review systems.

But any honest scientist knows that the way to go is almost always one more long and tiring. It requires intelligence, time, perseverance, and scientific humility and honesty.

As mentioned above, a possible contribution to a deterministic earthquake prediction approach may be given by observations and physical modelling of earthquake precursors aimed at seeing, in perspective, the earthquake phenomenon within the framework of a unified theory able to explain the causes of its genesis, and the dynamics, rheology, and microphysics of its preparation, occurrence, postseismic relaxation, and interseismic phases. Unfortunately, up to now what is lacking is the demonstration of a causal relationship (with explained physical processes and looking for a correlation) between data gathered simultaneously and continuously by space observations and ground-based measurements. In doing this, modern and/or new methods and technologies have to be adopted to try to solve the problem.

Within this framework, a few projects and experiments have been carried out on the subject by our team and accompanied by specific theoretical interpretations. They are reported in the paper. As an introduction and justification to these studies and also to avoid confusion, we try to clarify some basic concepts on the matter, critical and methodological aspects concerning deterministic and statistic approaches, and their use in earthquake prediction and warning.

The earthquake prediction and damage prevention methods, as well as the analysis of lithosphere-atmosphere couplings associated with the preparation of seismic events, are the introductory and basic elements of the paper. They will be discussed in this section.

1.1. Earthquake Damage Prevention and Deterministic Prediction Concepts. It is well known that earthquakes are a manifestation of significant ground rock deformation events, that is, episodic deformations of the upper and, more or less, brittle layers of the Earth's lithosphere. These can be classified as fast seismic ruptures, slow earthquakes, and subseismic events. Since the energy released during large earthquakes affects human life, the development and application of appropriate and efficient techniques to defend society from these destructive effects are necessary. At the present time, only two suitable approaches are available: damage prevention and prediction methods.

Earthquake damage prevention implies the development of methods for evaluating seismic risks in order to enable disaster assessment and techniques for use in estimating seismic risk, with the ultimate aim of reducing damage produced by earthquakes through reliable means. The prevention of damage is achievable with existing state of knowledge. In this approach, a great importance lies in the optimization of methods necessary to determine the three main factors—vulnerability, value, and hazard—which define seismic risk.

In contrast, the deterministic prediction of the time of origin, hypocentral (or epicentral) location, and magnitude of an impending earthquake is an open scientific problem. The reason for this is that such predictions are based on the detection of the so-called earthquake precursors or pre-earthquake phenomena, and the physical interpretation of these is a very complicated matter.

At this point, a few main concepts on precursor detectability must be considered. First, it must be clear that reducing "physics of the earthquake" only to the creation of fault rupture and consequent seismic wave propagation is to oversimplify the problem. In fact, it has been repeatedly observed that part of the accumulated (preseismic) elastic energy is also converted to other kind of energies (electromagnetic, acoustic, heat, etc.) and that these conversion mechanisms are probably similar to that of seismic energy. Moreover, observations during interseismic and preseismic periods indicate that large earthquakes are often preceded by signals of different natures (the so-called earthquake precursors), of which the mechanical (tilt and strain), gaseous (helium and radon), and electromagnetic ones have been demonstrated to be the most significant manifestations (see this paper and also [2]). However, the study of the physical conditions that give rise to an earthquake and of the processes that precede a seismic rupture is at a very preliminary stage and, consequently, the techniques of prediction available at the moment are below standard.

In trying to by-pass these difficulties, many investigators have likely been attracted by a statistical prediction approach based on the so-called earthquake forecasting method, that is, the probability of occurrence of an event in a given geographical location, within assigned values of magnitude and time ranges. However, even though the forecasting

methods, such as those of the M8 and CN algorithms (e.g., [3–5]) or of the acceleration deformation approach (e.g., [6]) have reached a very good level of maturity and can display a good level of importance and practical use, they overlap with the seismic hazard concept, one of the three factors used to estimate seismic risk. This could result in a possible ambiguity in the application of earthquake prediction and earthquake damage prevention approaches, which could give rise to a kind of "methodological noise" that would be capable of introducing systematic errors in the use of the two methods. We, therefore, believe that it should be better to pursue the deterministic prediction approach even if a reliable deterministic method of earthquake prediction will presumably be available only in the more distant future.

This conclusion is also confirmed by the underestimated expectation of earthquake prediction in a relatively short period of time based on the basis of seismic precursor studies carried out in the last decades. As mentioned above, the physics of earthquakes has been demonstrated to be a very complicated matter. Nevertheless, research with this aim continues with a critical view, new ideas, and thorough investigations, and the results seem to be promising. Therefore, we propose to carry out studies based on the physics of earthquake precursors, including the necessary field measurements in seismic areas and appropriate laboratory and theoretical investigations to corroborate the observations.

Progress in this area could be due not only to increased amounts and accuracy of ground field measurements, careful attention to errors in data, and improved understanding of earthquake source mechanics, but also—and possibly most importantly—to a new approach based on observations from space.

But how to reach a deterministic seismic prediction by earthquake precursors needs to be better clarified since it is considered by several authors that such an approach seems to be unadvisable because for a deterministic prediction the space localization (epicentre or hypocenter), the time of origin, and the energy or magnitude of an impending earthquake are required at the same time. A possible method on how in principle to practically predict earthquakes with precursory phenomena is proposed at the beginning of Section 3.

1.2. Seismoelectromagnetic Emissions and Couplings between Solid Earth and Near-Earth Space. A great contribution for constructing a deterministic prediction model arises by pre-earthquake (or precursory) phenomena, since they may help in understanding the physical mechanisms underlying the preparation phase of a seismic event. It has been shown that in the Earth's crust, rock microfracturing preceding a seismic rupture may cause local surface deformation fields, rock dislocations, charged particle generation and motion, electrical conductivity changes, gas emission, fluid diffusion, electrokinetic (EKE), piezomagnetic, and piezoelectric effects. It has also been proposed that charge carriers could be activated in dry rocks mainly by the increasing external stress. These mechanisms have been considered as the main sources of the so-called seismoelectromagnetic emissions (SEME) consisting of broad-band (from DC to a few tens of MHz) electromagnetic (EM) fields observed at the Earth's surface and in the near-Earth space (neutral and ionised atmosphere and magnetosphere). Electromagnetic emissions (EMEs) radiated from the Earth's surface and produced as a consequence of earthquake preparation and occurrence, or by human activities, demonstrated to propagate through the near-Earth space and to cause perturbations of electric and magnetic fields and Van Allen radiation belt particle precipitations, ionospheric variations of temperature and density of the ionic, and electronic plasma components in the topside ionosphere. These perturbations are detectable by Low-Earth-Orbit (*LEO*) satellites [2, 7–9].

Within this framework, natural disasters, such as earthquakes, and the impact of anthropogenic EME waves (power line harmonic radiation, VLF transmitters, HF broadcasting stations) in the near-Earth space can also be considered as coupling elements of the lithosphere-atmosphere-ionosphere-magnetosphere interactions. All above mentioned suggests that to better investigate the phenomenon earthquake, simultaneous and coordinated space and ground-based observations in seismic areas have to be carried out. The main problem in this studies is to reconcile near-Earth space perturbations only with the propagation of SEME-waves through the atmosphere and magnetosphere, filtering from the data the impact of atmospheric EME waves during thunderstorm activity, and effects of sun and cosmic rays in the geomagnetic cavity.

Space observations are being performed or are going to be carried out, in the ionosphere-magnetosphere transition region, and a few satellite missions (Demeter, QuakeSat, Sich-1 M, Compass-1/2, Esperia, Egle, Arina, Ausonia, etc.) have already been carried out and/or are proposed from 2001 until the present [2, 10–15].

The basic premise is that observations of different ground and space seismic precursors as well as laboratory experiments on rocks and the development of theoretical models, all of which aimed at placing the phenomenon "earthquake" within the framework of a unified theory, would be able to explain the causes of its genesis, and the dynamics, rheology, and microphysics of its preparation, occurrence, postseismic relaxation and interseismic phases. The physical system to be considered includes solid Earth and nearEarth space with related couplings and perturbations. Also, it is hoped that a better scientific coordination on an international basis between diverse teams of researchers would smooth out and integrate different methodological approaches relatively to each other for a better use of the different competences, instruments, and databases. Up to now what is lacking is the demonstration of a causal relationship with explained physical processes and looking for a correlation between data gathered simultaneously and continuously by space observations and ground-based measurements. That is why we believe that the best approach is to plan and design coordinated and simultaneous ground-based measurements (carried out by appropriate networks of instruments in available test sites on the Earth surface) to be correlated with multiparametric space observations onboard satellites,

together with the development of appropriate methods of data analysis and theoretical modeling. To this end, we have installed the TELLUS tilt network in the seismic area of the Central Apennines of Italy. This network will, in the near future, also include magnetometers and specific devices to detect electric field. Results obtained by the TELLUS network have been reported [16]. Within the framework of a guest investigation programme we have studied data collected in the topside ionosphere by the DEMETER microsatellite, proposed a specific *LEO* satellite project (ESPERIA) and built and tested in space two ESPERIA instruments (the EGLE magnetometer and ARINA particle detector). At the same time, we also have made first attempts to develop a theoretical model of the genesis and propagation of preearthquake electromagnetic emissions in the lithosphere and near-Earth space [7, 15, 17–19].

In 2007, after an IUGG resolution in support of ESPERIA (2007 IUGG resolution number 5) for an ionospheric space mission, we submitted to the Italian Space Agency (ASI) a new space project (AUSONIA), with more large scientific objectives than those of ESPERIA. AUSONIA includes the monitoring and mapping of the ionosphere and of the Earth magnetic field and also the study of tropospheric transient emissions [14]. Then, AUSONIA can investigate both perturbative and steady-state phenomena.

Next two sections will clarify basic concepts concerning hypocentral focal zone and epicentral precursory area (Section 2) and refer to reliable results reported in literature about earthquake precursors (Section 3) and their possible use as seismic predictors. The following Sections 4-5 report the ESPERIA and AUSONIA space mission projects and the description and testing of the first ESPERIA and AUSONIA instruments: the EGLE magnetometer and ARINA particle detector.

2. Hypocentral Preparation Focal Zone and Epicentral Precursory Area

The most familiar brittle lithospheric deformation event is defined as *ordinary* earthquake, that is, a deformation, fracture, structure, and phase transformation phenomenon, which releases suddenly a large amount of the elastic energy stored in the medium and is accompanied by a substantial fraction of energy radiated as elastic (seismic) waves. Seismic wave energy is a certain part (from about 1 to 10%) of total (radiated and not radiated) energy, and it is usually assumed as an estimate of the total energy of the earthquake. Moderate and strong earthquakes, with magnitude from 5.0 to 9.0, have energy and seismic moment [20] approximately in the range 10^{12}–10^{18} J and 10^{17}–10^{22} Nm, respectively, as given by the following well-known relationships (in cgs units) between energy (E), scalar seismic moment (M_0), and surface earthquake magnitude (M_S):

$$\begin{aligned} \log E &= 11.8 + 1.5M_S, \\ \log M_0 &= 1.5M_S + 16.1. \end{aligned} \tag{1}$$

But reducing "physics of the earthquake" only to the creation of fault rupture and consequent seismic wave radiation is to oversimplify the problem. It has been repeatedly observed that part of the accumulated *preseismic* elastic energy is also converted to other kind of energies (electromagnetic and acoustic ones, heat, etc.) and these (yet unknown) conversion mechanisms are probably similar as that to seismic energy. The understanding of such preseismic processes is fundamental to plan and design earthquake prediction techniques on a deterministic basis, that is, based on the so-called *seismo-associated phenomena* or *earthquake precursors*. The latter are phenomena of different types (seismic and nonseismic ones) accompanying the characteristic deformation of rocks during *earthquake preparation time* or *preseismic period*, and associated with changes in physical conditions in the so-called *preparation focal zone (volume)* as defined by standard *dilatancy-diffusion* and *crack-avalanche* "dilatancy" models [21–23].

Until now, no exhaustive physical models have been proposed and accepted by the scientific community to be used for a deterministic earthquake prediction approach. What is known on the topic is that in the time interval preceding a seismic fracture, stress and strain energy are accumulated in a fault asperity. Most of investigators consider reasonable to assume this increasing and concentrating stress at depth as a cause of the anelastic volumetric increase (dilatancy) of a relatively small portion of rock, and consequent rock dislocation and microfracturing. This volume of cracked rock at depth (*preparation focal zone*) is considered as a primary local source of precursor signals. These signals propagating in the surrounding medium allow the earthquake precursors to be observed in a finite region of the Earth's surface (*precursor area*). Then, in principle earthquake precursors can be used to indicate the impending occurrence of a seismic event. Characteristic sizes of the preparation focal zone and of the precursor area have been estimated by Dobrovolsky et al. [24, 25]. They found the volume (V) of soft inclusion (cracked rock) at depth in the lithosphere versus magnitude (M), is described as follows:

$$V_{\max} = 10^{(1.24M-4.47)}\ \text{km}^3, \tag{2}$$

which for a spherical volume of radius (r) gives:

$$r = 10^{0.414M-1.696}\ \text{km}. \tag{3}$$

The dimension of the precursor region at the earth surface is defined [24] by the radius (R) of the Earth's surface area where preseismic strain changes exceed tidal strains ($\approx 10^{-8}$), as follows

$$R = 10^{0.43M}\ \text{km}. \tag{4}$$

Relationships between preseismic strain ε, magnitude M, and distance R are

$$\begin{aligned} \varepsilon &= \frac{10^{1.5M-9.18}}{R^3} \quad \text{for } M < 5.0, \\ \varepsilon &= \frac{10^{1.3M-8.19}}{R^3} \quad \text{for } M \geq 5.0. \end{aligned} \tag{5}$$

For comparison, we report in Table 1 the characteristic dimensions of the preparation focal zone at depth (i.e., the

source of earthquake precursors) with those of the precursor region at the Earth's surface. Data are obtained for $4.0 \leq M \leq 7.0$ events, in the simple case of a preparation focal area modelled by a spherical volume (V) and in presence of a homogeneous medium.

It can be seen that by basing on the model by Dobrovolsky et al. [24] characteristic sizes of preparation focal area at depth are relatively small (from a few hundred meters to a few ten of kilometres) when compared with those of the precursor region at the Earth's surface (from a few tens of kilometres to about one thousand of kilometres).

We stress that this result is only valid for local deformation (tilt and strain) and for a homogeneous Earth's crust containing a soft inclusion simulating the rheological behaviour of a preseismic dilatants volume of cracked rock. When a more realistic and complicated geometry and structure is assumed for the Earth's crust in a seismic region and/or when other kinds of earthquake precursors than mechanical ones are considered (for instance electric and magnetic fields), a new general and more specific physical model must be proposed to determine the above-mentioned r and R sizes of the preparation focal zone and precursor area. In particular, the presence of discrete geodynamic structures (crustal blocks) in seismic regions (see, [16, 26]) implies that a preseismic deformation (tilt and strain) field may propagate at different distances and velocities in the different directions from the preparation focal area. This anisotropic space and time distribution of the preseismic deformation field mainly depends on dimensions, geometry, structure, and rheology of crustal blocks and their transition zones [7, 17].

Finally, empirical semilogarithmic relationships have also been proposed by several authors between magnitude M of an impending earthquake and precursory time ΔT (interval between the onset time of a precursor signal and the time origin of the earthquake). One of such relationships proposed by Rikitake [27] is

$$\log \Delta T = 0.76\, M - 1.83. \tag{6}$$

Concerning nonmechanical earthquake precursors, a model of preseismic electromagnetic emissions is in preparation, which first results have been reported in international meetings [7, 12, 28].

3. More Reliable Ground and Space Earthquake Precursors

In general, earthquake precursors can be divided in the two classes of so-called seismic and nonseismic phenomena. In the class of seismic phenomena are included seismic gap, decreasing (seismic quiescence) and increasing background seismicity, and change in the seismic wave velocity. The list of nonseismic phenomena includes numerous earthquake precursors of very different types as phenomena directly reconciled with local deformations (ground elevations and tilts, strains in rock, water levels in wells, etc.) or of other kind as electric and magnetic fields, EM emissions, electric resistivity in rock, acoustic emissions, gas exhalations (mainly radon and helium), and so forth. The time scale of an earthquake prediction attempt is by convention generally classified as short term (≈hour–days), long-term (≈years–decades), intermediate-term (≈weeks–years), according to the expected time interval to the earthquake (precursor time). Really, only short-term and intermediate term time scales can be considered for a true deterministic earthquake prediction methods, since long-term one, in practice, can be identified with the seismic assessment of the seismic hazard of a given zone and, then, associated with the statistical probability for the occurrence of large earthquakes.

Table 1: Sizes of earthquake preparation zone (r) and precursor region (R) for $4.0 \leq M \leq 7.0$.

M	r (km)	R (km)
4.0	0.1	52
5.0	2.5	141
6.0	6.0	380
7.0	41.3	1023

3.1. A Possible First Empirical Approach to Deterministic Earthquake Prediction Based on Precursory Phenomena. A deterministic earthquake prediction method based on precursory phenomena has not yet been proposed. At this purpose, the combination of simultaneous and continuous observations of mechanical medium-term precursors and electromagnetic short-term ones in selected seismic test areas could be of particular importance in determining, within the time interval of the short-term precursory time (hour-days), the epicentre, the magnitude and time of occurrence of an impending earthquake.

In principle, as a first empirical approach, a possible method could be to combine the most reliable medium-term and short-term earthquake precursors, as follows.

(a) First Warning/Alert. One could imagine using the onset times of the anomalous medium-term (weeks-months) tilt and strain signals recorded by the multi-instrument network working in the seismic test area as a first-time warning.

(b) Second (Final) Warning/Alert. A second (final) time warning could be associated with the onset times of the first anomalous short-term (hour-days) electromagnetic signals pointed out by the same instrumental network. Then, the uncertainty in the estimate of time origin of the event will be ranging from ∼1 hour to days.

(c) Epicenter/Hypocenter. An estimate of the future epicenter could be attempted by the time shifts between the onset times of the different medium-term anomalous mechanical signals observed by the instrumental network and on the basis of the velocity of propagation of the preseismic deformation front through the crust block structures of the observed test area. This velocity is calculated to be of the order of 1 cm/s [16, 29–31]. But this value must be determined for each test area.

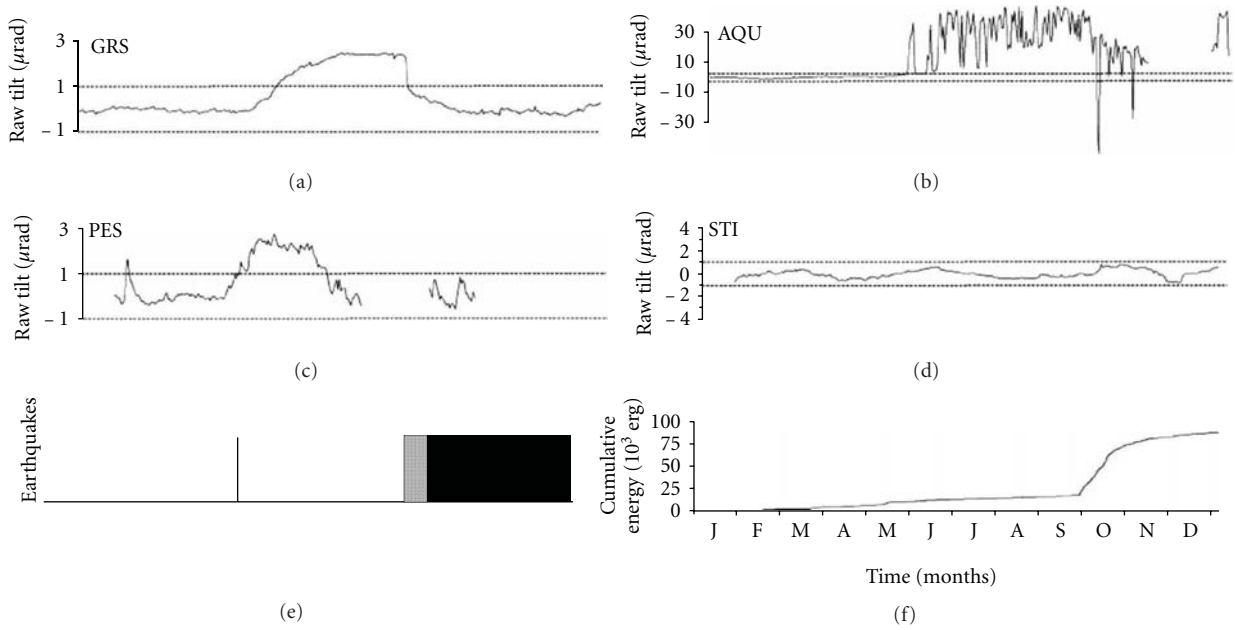

Figure 1: Original figure from the paper by Sgrigna and Malvezzi [16]. Fault creep events recorded during the year 1997 at the GRS (plot (a)), AQU (plot (b)), PES (plot (c)), STI (plot (d)) tilt sites, before the Sept 26, 1997 Umbria-Marches earthquakes ($M = 5.7$; 6.0). Plot (e) shows selected earthquakes (e equal/greater than 10−8). A vertical bar marks a single event M4.4 occurred on May 12; two adjacent shadow and black rectangles of arbitrary amplitude represent two time intervals characterized by the occurrence of a preseismic swarm (lasting a few weeks with a peak event M4.4 on September 3), and of several thousands of aftershocks recorded in the following months, respectively. The two main shocks M5.7; 6.0 of September 26 occurred in the time interval between those marked by shadow and black areas. Plot (f) is the cumulative energy released by earthquakes in 1997.

(d) Magnitude. Finally, the magnitude could be roughly estimated on the basis of the empirical relationships between magnitude and precursory time (e.g., (6) in Section 2) by the time shifts between the onset times of all the couple of medium-term and short-term signals observed at each site of the instrumental network. The use of amplitudes of such signals to calculate the magnitude appear to be more questionable since some spatial differential amplification effects (site effects) are observed in the different sites (then, in the different blocks) where instruments are located. An example of such site effect can be observed in Figure 1.

But before applying, any deterministic method of prediction quantitative specific physical models, unavailable at moment, must be proposed for each test area in order to describe the geodynamics and rheology of crustal blocks and relative transition zones, as well as the physical mechanisms underlying the mechanical and electromagnetic preseismic sources. In particular, to justify the observations is necessary to model the shape, onset times, and durations of precursory signals, thus, reconciling them with the preseismic source behaviour and characteristics (space localization, dimensions, geometry, space orientation, rock yielding conditions, and catastrophic rupture mechanisms).

Only at this stage, an exhaustive and general physical interpretation of such precursors could be of help in reducing the uncertainty (physical error) in the estimation of the epicentral position, magnitude, and time of origin of an impending earthquake, then in contributing to define an acceptable deterministic earthquake prediction. Up to now, there have been systematic observations of mechanical intermediate-term and electromagnetic short-term precursors, which have been shown to be more suitable for the above-mentioned future applications. To give an idea (though not exhaustive) of the state-of-the-art in the topic, the main results are presented here for ground and space observations and divided into intermediate-term and short-term precursors, respectively. A significant ground intermediate-term mechanical precursor is shown in Section 3.2 and a summary, even not exhaustive, of the principal characteristics of ground and space short-term SEME precursors is reported in sub-Section 3.3 (Tables 2 and 3).

3.2. Ground Creep-Related Intermediate-Term Precursors. A number of interesting results concerning anomalous surface tilt variations observed in local seismic regions during earthquake preparation have been reported over the years. They include the observation and modeling of creep-related tilt perturbations [16, 31, 32], precursory tilts detected before local and teleseismic earthquakes [29, 33], coseismic and postseismic tilts [34, 35]. These anomalies are easily detectable by tiltmeters [16, 31, 36–38] and considered by many authors [17, 29, 31, 33, 39–43] to be intermediate-term earthquake precursors. The transmission of substantial stress over large distances has been debated [7, 16, 44].

Continuous hourly ground tilt data collected by the TELLUS tiltmeter network from 1981 to the present in the seismic region of the Central Apennines of Italy

Table 2: A summary of ground-based short-term (hour-days) SEME precursors.

Observations	Modeling
EKE changes. B field changes. Ground potentials [59–61].	Streaming Potentials by saline water moving through porous rocks [62, 63]. Stress applied effects to rocks containing piezoelectric materials [64–67].
ULF-ELF SEME [68–71]. ULF-HF SEME [26, 72–77]. VLF E field changes [78, 79].	EM behaviour of rocks [55, 80–83]. Rocks become a source of highly mobile electric carriers that increase electric conductivity and propagate through the rock as a charge cloud [84].
E field changes and gas emissions by rock microfracturing [31, 85, 86].	Number and dimensions of microcracks and redistribution of pore fluids. Motion of saline pore fluids and formation of intergranular water film [55, 86].
Low-frequency SEME Laboratory investigations about conversion of accumulated preseismic elastic energy to EM energy [87].	Rock as "igneous rock battery" due to the activation of positive hole charge carriers by stress. Dislocation movement leading to bond breaking of Si–OO–Si peroxy links [87].
Mechanical and EM signals from laboratory to geophysical scale [88].	First attempts to justify effects of applied stress on rocks [88].

Table 3: A summary of space-based short-term (hour-days) SEME precursors. Symbol ⇒ means *then.*

Observations	Modeling
Ionospheric E, B fields changes [8, 51, 54, 89–101]	SEME-waves generation ⇒ Lithospheric lowpass filter on ULF-HF-waves ⇒ ULF-ELF SEME-waves may reach the Earth surface and enter into near-Earth space [86, 98, 99, 102–109].
Ionospheric plasma temperature and density changes TEC. Decrease at the ionospheric F2 peak $f0F2$ [110–112].	ULF-ELF SEME-waves-Ionospheric plasma interaction mechanisms [71, 103, 113, 114].
SEME-waves. Van Allen radiation belt particle precipitation. PBs (Particle Bursts) [8, 18, 48–50, 53, 115–118].	Alfven-wave radiation (from DC to some hundred Hz) propagates along the geomagnetic field lines ⇒ Resonant wave-particle interaction at the radiation belt boundary with trapped electrons and protons from a few MeV to several tens of MeV ⇒ Particle precipitation as a result of pitch angle diffusion [7, 8, 50, 51, 92, 119].
Variations in the atmospheric conductivity profiles [98, 99].	Fair weather currents [98]. Modification of spectral content of ELF-VLF radio noise during lightning discharges [99].
ULF SEME-waves and VLF SEME-waves from Satellite Intercosmos-24 [89].	ULF emissions of 0.2 nT penetrate through the ionosphere ⇒ cyclotron interaction with protons of 0.5–5 MeV near the magnetic equatorial plane ⇒ Proton distribution function becomes unstable for the Cherenkov VLF radiation of 0.1–20 kHz [119].
Amplitude and phase variations of radio-signal propagating in the earth-ionosphere wave guide). Disturbances in Omega and Loran VLF radio-waves propagation [120–122].	Abnormal ionisation in the lower ionosphere [121].
Short-term electric field strength attenuation of the Radio Monte Carlo (RMC) LF radio-signal [26].	Tropospheric radio defocusing mechanisms [26].
Atmospheric anomalies caused by VHF SEME-waves [123].	Significant enhancement of VHF EM-waves beyond line-of-sight [123].

has systematically provided evidence of intermediate-term-earthquake tilt precursors [16]. An example of creep-related intermediate-term tilt precursors detected by the TELLUS network has been pointed out by Sgrigna and Malvezzi [16] on the occasion of the Umbria-Marches seismic sequence with two main shocks ($M = 5.7$ and 6.0) with epicentres very close one each other (about 3 km) occurred on September 26, 1997, at 00:33 and 9:40 UTC, respectively. Figure 1 is the original figure taken from the paper by Sgrigna and Malvezzi [16] to which we invite to refer for the description of geodynamics of local crustal block system, characteristics of seismicity, and selection criteria for earthquakes and residual tilt signals.

The main features of the intermediate-term preseismic tilts reported in Figure 1 may be summarized as follows (Figure 1)

(1) Raw tilt data, filtered by meteorological and secular tectonic effects, revealed intermediate-term preseismic tilts with a shape, amplitude, and time duration similar to those already obtained in the same area [16, 31, 42, 43].

(2) Tilts are shifted in time relative to each other, indicating a possible propagation of the preseismic strain field from the preparation focal area to the tilt sites, through the rigid blocks of the region [26, 45] separated by inclined transition zones, filled by fault viscoelastic material [16, 29, 39, 46].

(3) A characteristic so-called site effect is evident in the signal amplification observed at the AQU tilt site when comparing amplitudes of this signal with those recorded at GRS and PES.

(4) Experimental values for the velocity of propagation are in agreement with previous results.

(5) The intermediate-term preseismic tilts have been interpreted as viscoelastic creep strains in the fault material, due to the propagation of stress-strain fields from the dilatant focal area to the observation sites.

(6) One-dimensional and two-dimensional numerical models have been proposed to justify qualitatively the main features (tilt anomaly shape and onset time delay and decay of anomaly amplitude with distance from the earthquake preparation zone) of the preseismic ground tilt behaviour [17, 26, 30]. Horizontal movements of rigid crustal blocks were also considered by Gabrielov et al. [47].

3.3. Ground and Space Short-Term Seismo-Associated EME Signals. Studies of seismoelectromagnetic emissions (SEME) have been developed for a few decades both at the Earth's surface and in the near-Earth space (atmosphere, ionosphere, and magnetosphere).

In recent years, interest has been increasing in the SEME signals consisting of a broad band (from approximately DC to a few tens of MHz) EM fields generated and transmitted by seismic sources into the near Earth's space before, during and after an earthquake. SEME characteristics and detectability as well as the effects they provoke in space (ionospheric and magnetospheric perturbations), have a very interesting and promising nature as a short-term earthquake predictor.

Several significant ground and space observations and modelling of such precursors are summarized in Tables 2 and 3, respectively.

Note that in the case of very shallow and strong earthquakes, when the size of the preparation focal zone is greater than the hypo-central depth (see relations (4) and (5)), also the higher frequency content of DC-HF SEME radiation could be transmitted from the Earth's surface to the near space.

Concerning radiation belt particle precipitation most preseismic PBs have been collected by satellites near the South Atlantic Anomaly (SAA) at altitudes generally between about 400 and 1200 km [48–50]. Moreover, the lower limit of the portion of the ionosphere-magnetosphere transition zone (i.e., the altitude where preseismic EME-waves may be captured in the geomagnetic field lines and, then, propagate up to the inner radiation belt) has been estimated from PBs space observations and resulted to be around 300–500 km [8, 51]. Besides, the lifetime of the longitudinal drift of PBs is determined by the particle loss rate during particle interaction with the residual atmosphere of the Earth. A lifetime of the order of several tens of minutes is obtained for electrons and protons of several tens of MeV [52]. During this time, particles may drift longitudinally around the Earth along the L-shell corresponding to the EME ground source location [50, 53].

This is a crucial factor for a possible use of preseismic PBs as an earthquake predictor since the longitudinal drift makes the PB detection possible by particle detectors installed on board satellites.

Another important factor is the opposite drift direction of positive- and negative-charged particles, which in principle could allow the location of EME wave-particle interaction zone (i.e., the PBs space source location) to be identified.

Nevertheless, there is still an open debate on the mechanism to be invoked in order to justify the phenomenology under study and, in particular, whether the very low amplitude ULF/ELF EM waves may reach the inner Van Allen radiation belt and cause the above-mentioned coupling phenomena. In fact, the electric and magnetic components of these EME-waves are estimated to be of only some fraction of mV/m(Hz)1/2 and of some fraction of nT/(Hz)1/2 or less, respectively [54]. A qualitative representation of the space phenomenology is presented in Figure 2.

4. The AUSONIA "Space Scientific Platform"

After a first satellite project named *ESPERIA* (Earthquake investigations by Satellite and Physics of the Environment Related to the Ionosphere and Atmosphere) was planned and designed for the Italian Space Agency (ASI) with objectives to only detect seismic precursors, a second more complete satellite project named *AUSONIA* was proposed with aim at also studying other phenomena of the near-Earth space accompanying those associated with seismic events and which may interact with precursor signals. For a correct approach to an earthquake precursors study, all these signals must be recognized, isolated, and filtered from the data. A detailed technical description of the ESPERIA space mission concept can be found in the ASI Phase A Report [12] and in Sgrigna et al. 2008.

AUSONIA (Advanced mUlti-Instrument Satellite for a combined Observation of magNetosphere, Ionosphere, Atmosphere, and associated phenomena) is an Italian space project proposal submitted to the Italian Space Agency (ASI) within an ASI AO for earth observation [14]. AUSONIA was planned and designed by an Italian Consortium led by the Roma Tre University of Rome (Vittorio Sgrigna, *Principal Investigator*).

The aim of the AUSONIA project is to design and construct a small space platform planned with an multiinstrument payload and a LEO mini-satellite mainly concerned with the monitoring and mapping of the ionosphere-magnetosphere transition region. The scientific program is based on coordinated, continuous, and simultaneous space and ground-based observations, and on mutual data comparison with other missions of similar quality.

AUSONIA was proposed after the IUGG resolution in support of ESPERIA (2007 IUGG resolution N.5) (http://www.iugg.org/resolutions/), which welcomes the planning of several nations to launch ionospheric monitoring satellite missions. As mentioned above AUSONIA includes both the study of perturbative phenomena in the topside ionosphere (already planned for ESPERIA) and the field mapping of the same region to give a contribution in defining the IGRF and IRI models.

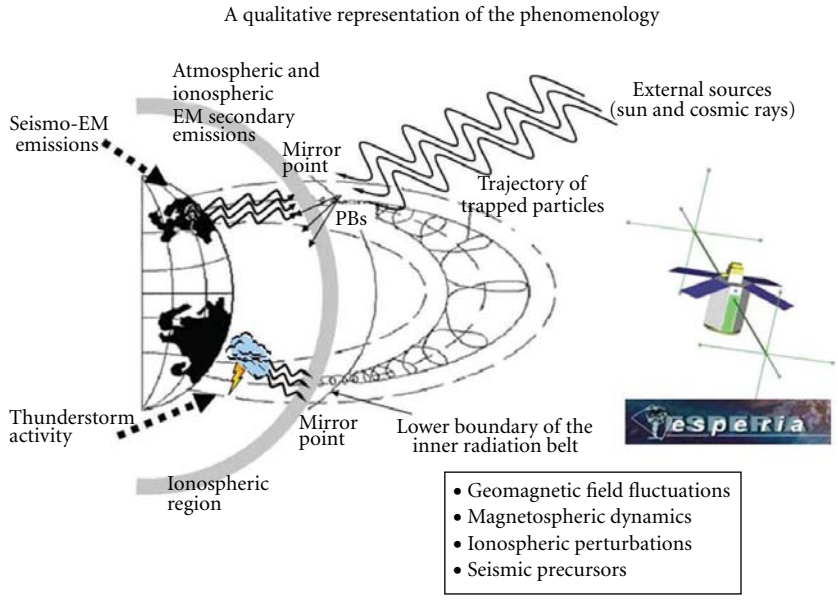

Figure 2: A schematic representation of the solid earth and near-Earth space (atmosphere, ionosphere, magnetosphere) with main associated physical phenomena: seismo-EM emissions, their propagation and interaction with ionospheric plasma and magnetospheric trapped particles, cosmic rays and solar effects into the magnetosphere, and tropospheric TLE and TGF emissions. Trajectories of charged particles trapped by the geomagnetic field lines are represented in a meridian plane.

4.1. AUSONIA Scientific Aims. Scientific and methodological aspects of the AUSONIA space project are reported in Table 4.

4.2. Experiments Planned on Board the AUSONIA Satellite. On the AUSONIA satellite are planned five experiments, MAGIA, ELECTRA, LUCE, CIELO, and TERRA. They are devoted to monitor geomagnetic field, plasma, and particle environment in the ionosphere-magnetosphere transition zone as well as to study optical/UV and X/gamma emissions induced by tropospheric activity. The MAGIA (MAGnetic Instrument Array) experiment is constituted by a scalar, a fluxgate, and a 3-axes search-coil magnetometers to detect stationary, lower-frequency and higher-frequency magnetic field. The magnetometers are installed on the tips of two deployable booms (Boom_M_Right and Left, each one 5 meters long from the satellite spacecraft) to reduce the electromagnetic interference from the satellite equipments. The ELECTRA (ELECTRic field Analyser) experiment consists of 4 electric preamplified probes, each one installed on the tips of 4 meters deployable booms (4 meters long, called ELECTRA_Zenith, TAN, Right, Left) to allow to measure the 3 electric field components in the frequency range from about DC up to about 10 MHz). The MAGIA and ELECTRA sensors can highlight the correlation with lightnings and reconstruct the dynamics of the electromagnetic atmosphere-ionosphere. These measurements are also essential to study the LEP (lightning-induced electron precipitation) and all the phenomena of disturbance of the Van Allen belt-induced storms, in the AUSONIA project are included optical and UV detectors devoted to the observation of TLEs with high spatial and temporal resolution in specific frequency bands. Measurements are taken with video cameras and photometers with the hope of reconciling the need for high capture rate with the high-resolution image. The optical-UV for these observations are concentrated in the experiment LUCE in two separate blocks oriented to nadir and to limb, respectively. Each block consists of 2 cameras with filters optimized for the shooting of red sprites (VID1) and lightning (VID2), respectively, and 4 photometers (PH1, 2,3,4) for UV-visible measurements. The main characteristics of the LUCE experiment are summarized in Table 5. The precipitation of particles of the Van Allen belts was observed by several satellite missions, but many questions need an answer about the temporal and spatial stability of the Van Allen belts and the dynamics of interaction disturbances associated with magnetic storms, the electromagnetic emissions of tropospheric origin, the EM emissions of anthropogenic origin, and so forth. Other themes of topical scientific interest are the X and gamma emissions from the troposphere (TGF). They represent a background for satellite missions such as AGILE designed to explore gamma bursts from the sky. To study of these phenomena, the TERRA detector is designed to be installed on board the AUSONIA satellite. The experiment consists of two identical modules: TERRA_Nadir and TERRA_Tan oriented to Nadir and in the opposite the speed of the satellite, respectively. X- and gamma-ray detectors will be constantly active during the optical and EM measurements to allow to investigate the characteristics and origin of the TGF and their correlation with TLE. TERRA aims at revealing X- and gamma-ray bursts (TGF) from the Earth's troposphere. This to map TGF phenomena, to measure the X-ray spectrum observed range and determine the mechanisms that generate them, to observe the precipitation of

Table 4: Science and methods of the Ausonia project.

	Scientific objective	Expected results	International collaborations
Geomagnetic field mapping	Main field and secular variation will be the principal goals.	Contribution to the IGRF. A better knowledge of the Earth's core dynamics, secular variation, field inversions and crustal anomalies. 3D reconstruction of the mantle conductivity.	Synergy with SWARM mission, INGV ground network and SEGMA-ULF geomagnetic networks.
Monitoring of ionosphere and plasmasphere	Simultaneous measurements of local changes in the topside ionosphere and space and time variability of plasmasphere.	Contributions to the IRI model, ionospheric tomography, study of space weather events by in situ measurements and plasmaspheric TEC investigations.	Collaboration with NASA missions C/NOFS and STPSAT1. Use of CITRIS-like detector to collect signals from CERTO satellite and DORIS radio beacons terrestrial network. Comparisons with INGV and DIAS ionosonde data.
Detection of transient phenomena associated with thunderstorms	Detection of tropospheric transient luminous emissions (TLE), lightnings, terrestrial gamma ray flashes (TGF) and related energy transfer (~0,25–1GW) from troposphere to iono-magnetosphere.	Understanding of TLE e TGF effects in the framework of the ionosphere-magnetosphere couplings.	Complementary observation campaigns of TLE e TGF phenomena to be carried out with the TARANIS satellite.
Study of iono-magnetospheric perturbations due to EM emissions of terrestrial origin	Study of the possible effects produced in the near-Earth space by EM emissions of seismic and volcanic origin.	The AUSONIA team can take profit from the expertise of the previous ESPERIA project (see the 2007 IUGG resolution N.5, http://www.iugg.org/resolutions/).	The AUSONIA team is guest investigator of the DEMETER mission to study whistlers and radiation belt particles.
Investigation of Van Allen particle fluxes and tropospheric X/γ rays	Study of temporal stability of the Van Allen radiation belts, detection of particle precipitation and tropospheric and cosmic X/γ emissions.		A few key persons of the AGILE mission are also members of the AUSONIA team.

particles from the Van Allen belts induced magnetic storms, tropospheric phenomena, seismoelectromagnetic emissions and emissions from anthropogenic EM, to measure range, direction, and temporal variation of the flow of precipitating charged particle, to reveal the runaway electrons, to study the interactions between whistler waves and trapped particles, to generate a trigger signal upon detection of a TGF and enable the acquisition of other experiments such as LUCE, to gather information on the length, height, changes in TGF, and to acquire a statistically significant amount of TGF events as a function of local time, geomagnetic conditions, and so forth.

Figure 3 illustrates the general satellite layout.

Planned experiments and instruments and their positioning on board the AURONIA satellite are reported in Table 5.

4.3. Mission Characteristics. At this overpreliminary step, the final parameters have not yet been completely defined. In Table 6, values are given for a MITA platform solution and a sun-synchronous orbit. The satellite orbit altitude has be chosen to optimise observations at the sunrise-sunset local time for a better identification of seismo-induced ionospheric disturbances. In fact, as reported by Molchanov and Hayakawa [55, 56] and Chuo et al. [57], an increase in the sporadic E-layer critical frequency at the terminator time (sunrise and sunset) is observed within 5 days before the earthquake that determines a corresponding increase in the D-layer electron density and a variation of the VLF propagation at the terminator time. Should AUSONIA be installed on board of another spacecraft, budgets, volume, orbit inclination, and altitude can be changed accordingly.

4.4. Comparisons between AUSONIA and Other Missions. In Table 7, the AUSONIA payload is compared with that of others missions of similar quality. It appears evident the AUSONIA capability in carrying out multiparametric measurements, as well as its character of "small scientific platform" for earth observation.

5. The EGLE and ARINA Space Experiments

A few ESPERIA instruments (such as the particle detectors LAZIO and ARINA, and the search-coil magnetometer EGLE) have been built and tested in space [15, 19, 58]. EGLE was a technological demonstrator installed on board the International Space Station (ISS) on April 15, 2005, within the LAZIO-EGLE experiment of the ENEIDE mission, which has been coordinated by the European Space Agency (ESA)

Table 5: AUSONIA experiments and their positioning on board the satellite.

	Experiment	Module/Code	Probe/Instrument	Positioning/Pointing mode
Geomagnetic measurements	**MAGIA** (MAGnetic Instrument array)	MAGIA_Scalar	Scalar magnetometer	Boom_M_Right
		MAGIA_Flux-Gate	Flux-gate Magnetometer	Boom_M_Right
		MAGIA_Search-Coil	Search-coil Magnetometer	Boom_M_Left
Electromagnetic measurements	**ELECTRA** (ELECTRic field analyser)	ELECTRA_Zenith	Electric probe	Boom_E_Zenit
		ELECTRA_Tan	Electric probe	Boom_E_Tan
		ELECTRA_DX	Electric probe	Boom_E_DX
		ELECTRA_SX	Electric probe	Boom_E_SX
Ultraviolet and Optical measurements	**LUCE** (transient LUminous emissions combined experiment)	LUCE_Nadir_VID1	Video-camera sprite	Nadir
		LUCE_Nadir_VID2	Video-camera lightning	
		LUCE_Nadir_PH1,2,3,4	Photometer 1,2,3,4	
		LUCE_Limb_VID1	Video-camera sprite	Limb
		LUCE_Limb_VID2	Video-camera lightning	
		LUCE_Limb_PH1,2,3,4	Photometer 1,2,3,4	
Plasma measurements	**CIELO** (Combined ionospheric experiment in low earth orbit)	CIELO_GPS	Gps	Zenith
		CIELO_PLASMA	LP, RPA, plasma driftmeter	Along the same direction of the satellite velocity
High-energy particles and X-gamma rays measurements	**TERRA** (circumTerrestrial high-energy paRticle and X-gamma ray analyser)	TERRA_Nadir	High-energy particles and X-gamma rays detector	Nadir
		TERRA_Tan	High-energy particles and X-gamma rays detector	In the opposite direction to the satellite velocity

Table 6: AUSONIA satellite mission characteristics.

Orbit	Sun-synchronous circular orbit 98° inclination Altitude between 600 to 800 km (TBD). See also notes after Table 3 in Section 3.3 Revisit time: ≤24 h
Budgets	Power satellite total: ~270 W (Payload total: 120 W; platform total: 150 W) (TBD) P/L data: ~306 kbps (36,5 Gbit of daily data, margin included) (TBD) Payload mass: ~120 kg (TBD)
Attitude orbit control system	Attitude determination: 0.001° (TBD) Attitude Accuracy (3 axes): 0.1° (TBD) 3 reaction wheels, 3 magnetic coils, 2 star trackers, 3 gyroscopes, GPS receivers, three-axis magnetometer, 10 sun sensors
Spacecraft	Platform MITA or other platform of similar quality (TBD) Nadir pointing Thrusters applied to the platform (constant altitude and/or possible orbit changes) (TBC)
Mission duration	3 years

Table 7: AUSONIA instrument payload compared with that of other missions of similar quality.

			AUSONIA	SWARM	TARANIS	DEMETER	FORMOSAT-2	ASIM (ISS)	VARIANT
Scalar magnetometer			×	×					
Flux-gate magnetometer			×	×					×
Search-coil magnetometer			×		×	×			×
Electric Probes			×		×	×			×
Langmuir probe			×	×		×			
Plasma driftmeter			×	×					
Optical-UV Detector		Nadir	×		×			×	
		Limb	×				×	×	
Particle Detectors	Nadir	Charged particles	×		(Low energy)				
		X/γ	×		×			(Low energy)	
	Limb	Charged particles	×			(Low energy)			
		X/γ	×					(Low energy)	

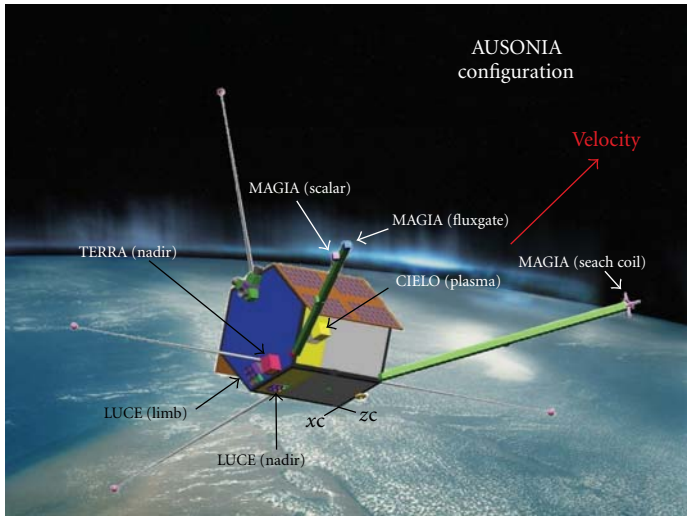

Figure 3: Schematic representation of the AUSONIA satellite project.

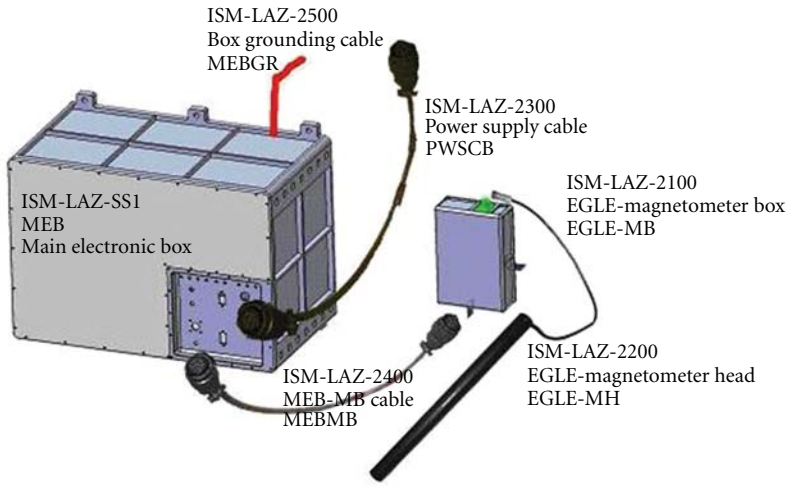

Figure 4: EGLE experimental setup.

Figure 5: EGLE inside the PIRS module of the ISS. Arrows indicate MEB (left), EGLE-MB (front), and EGLE-MH (right).

and received contributions from the Italian National Institute of Nuclear Physics (INFN) and Regione Lazio. The launch of ARINA occurred on June 15, 2006, within the PAMELA mission. ARINA will perform particle measurements on a quasipolar orbit RESURS DK-1 Russian *LEO* satellite. Data from ARINA, EGLE, and TELLUS may be studied together with those collected by DEMETER, through the Demeter Guest Investigator Programme.

5.1. The EGLE Magnetic Experiment on Board the International Space Station. The main goal of the EGLE experiment was to test in space an original very broad band search-coil magnetometer and associated data acquisition system based on the 1-Wire technology. The duration of the mission was of 10 days (15 April–25 April 2005).

The characteristics of the EGLE magnetometer are also important within the ISS applications. In fact, the monitoring of the EM environment on board the ISS needs both an appropriate observation methodology and a corresponding experimental equipment design. The continuous monitoring of the EM environment on board the ISS by an advanced magnetic experiment in the ULF-HF band is important in the following areas:

(a) search of space weather conditions in equatorial, middle-latitude, and subauroral ionosphere;

(b) geophysical research of plasma-wave processes connected to solar-magnetosphere-ionosphere-atmosphere-lithosphere interactions;

(c) investigation of the possible relationships between seismic activity and ULF-VLF phenomena possibly related to earthquakes;

(d) continuous monitoring of ULF-ELF-VLF activity in the near-Earth space including ELF-VLF pollution;

(e) Monitoring of natural and man-made variations of the plasma-sphere caused by whistlers.

(f) investigation of EM background and space weather phenomena;

(g) investigation of the effects of the large ISS structure on the propagating wave-front.

The LAZIO-EGLE experiment aims at performing measurements involving:

(1) the radiation environment;

(2) the magnetic environment inside the ISS.

The experiment includes the high-precision low-frequency magnetometer EGLE (Esperia's Geomagnetometer for a Low-frequency wave Experiment). EGLE is able to measure the intensity and variations in the magnetic field within the ISS and to correlate these measurements with those of particle fluxes. The study of these effects is important to detect electromagnetic field variations and particle pitch angle distribution of the precipitating particles. EGLE experiment is also the first test in space of a data acquisition system based on the 1-Wire technology.

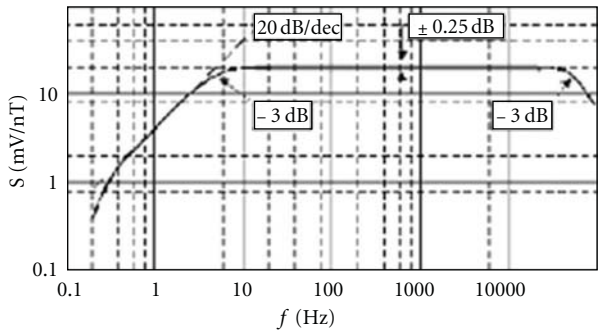

Amplitude-frequency response of the EGLE magnetometer

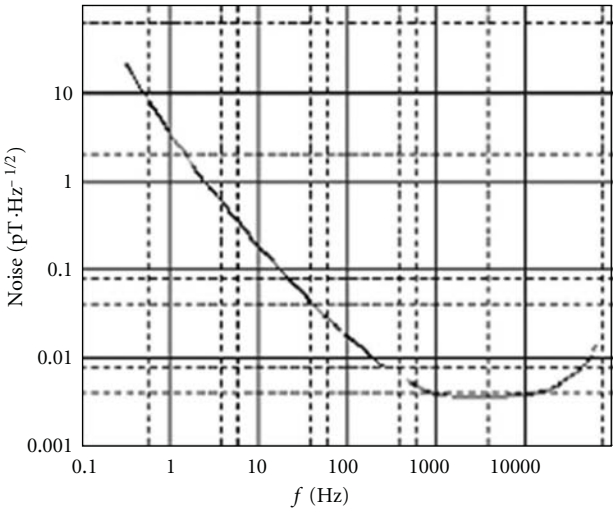

Noise spectral density

Basic technical specifications of the EGLE probe MH.	
Frequency band of receiver signals	0.5 ÷ 50000 Hz
Shape of transfer function	linear—flat
Type of output	Symmetrical
Transformation factor at both output terminals:	
(i) at linear part(0.5–5 Hz)	f 4 mV/(nT Hz)
(ii) at flat part (5–5000 Hz)	20 mV/nT
Transformation factor error:	
(i) at flat part of band pass without edges	± 0.25 dB
(ii) at flat part band pass edges	3 dB
Magnetic noise level, pT Hz$^{-1/2}$:	
(i) at 5 Hz	0.4
(ii) at 100 Hz	0.02
(iii) at 5 kHz	0.004
(iv) at 50 kHz	0.02
Nominal output load	200 pF 50 kΩ
Power supply voltage	± (15 ± 0.2)V
Power consumption	300 mW
Temperature range of operation	– 30 C ÷ + 50 C
Outer dimensions (without prominent parts)	l = 400 mm d = 32 mm
Length of output cable	0.7 m
Weight	320 g

Figure 6: Frequency response and noise spectral density of the EGLE search-coil magnetometer together with technical specifications of the EGLE probe.

The EGLE magnetometer consists of (Figure 4) the following

(i) a single axis search coil probe, the EGLE magnetometer head (MH);

(ii) an electronic interface with amplifiers, filtering, and data acquisition unit (EGLE MB box);

(iii) a 2-m long cable to connect LAZIO MEB and EGLE MB;

(iv) a 1-Wire to RS232 serial adapter on the LAZIO pc tower.

Magnetic field signals detected by the EGLE-MH probe are amplified, filtered, and recorded by the EGLE acquisition and data handling board located in the EGLE-MB box. The EGLE magnetometer magnetic field data are collected in four frequency bands (DC through to 20 Hz raw data; 0.5–40 Hz; 500 Hz–5 kHz; 20–40 kHz integrated r.m.s. data).

Gaps between these frequency ranges have been chosen to filter well-known spurious artificial signals produced inside ISS.

The advantages of using EGLE device are:

(i) high-accuracy measurements;

(ii) small dimensions and mass;

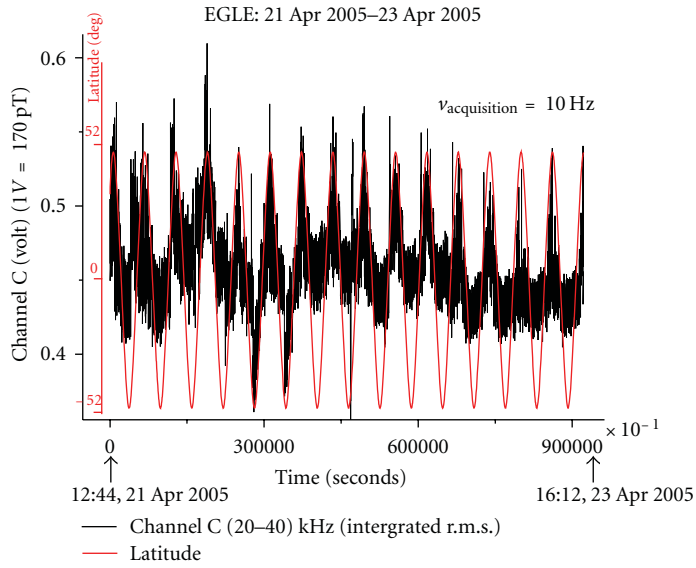

Figure 7: An example of magnetic data in the frequency band (20–40) kHz, recorded by the EGLE instrument on board the ISS during the period of the mission (15 April–25 April 2005). Superimposed to the signal is shown the latitude variation of the ISS.

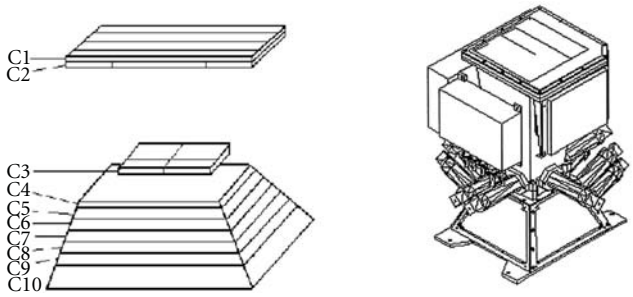

C1–C3: Trigger coincidence scintillation telescope
C4–C10: Scintillation calorimeter
C11-C12: Scintillation anticoincidence detectors

Figure 8: ARINA space instrument layout.

(iii) low power consumption;

(iv) data acquisition via 1-Wire technology;

(v) a standard ISS power supply of the device.

The peculiar characteristic of the 1-Wire technology prompted us to use it in the EGLE experiment to test its possible application in satellite EM measurements where the necessity to hold magnetic sensors far from the satellite body by expanding booms is an important factor for magnetic cleanness (see architecture of electric and magnetic probes in the ESPERIA payload). In fact, the use of 1-Wire technology can strongly reduce the numbers of wires necessary to connect many remote magnetic and electric probes (necessary in these types of investigations) with the central electronic unit located in the satellite body.

Figure 5 depicts the LAZIO-EGLE installation inside the PIRS section of the ISS. As can be seen, MEB (left), EGLE-MB (front), and EGLE-MH (right) are fixed by Velcro tags to the ISS wall. The characteristic frequency response of the EGLE probe is reported in Figure 6. An example of data recorded on board ISS is shown in Figure 7. As it can be seen, part of the ULF frequency band can also be detected by this sensor. This is an unusual characteristic for a search-coil probe and characterizes EGLE as an original broad-band magnetometer, which in a few satellite applications can allow a significant mass reduction by avoiding the use of flux-gate sensors.

5.2. The ARINA Particle Experiment on Board a LEO Satellite. The ARINA experiment consists of a proton-electron telescope to be installed on board the polar LEO Russian satellite RESURS-DK1 within the PAMELA mission. The orbit is elliptic, with an altitude ranging from 300 to 600 km and an inclination of 70.4 degree. The duration of the mission will be ≥3 years. The scientific objective of the experiment is to detect fluxes of high-energy charged particles (3 ÷ 100 MeV), from the inner radiation belt and to correlate them with seismic activity.

The main features of the ARINA instrument are reported in Figure 8. As can be seen from this figure, the instrument consists of a set of scintillation detectors C1–C12 made on the basis of polystyrene, which are viewed by photomultipliers (PMTs), the event recording system, the data acquisition and processing system (DAPS), the power supply system (PSS), and the command unit (CU). Detectors C1–C12 are functionally combined into three systems: the hodoscopic trigger system HTS (detectors C1–C3), the scintillation calorimeter SC (detectors C4–C9), and the anticoincidence system ACS (detectors C10–C12). Each of the detectors C1 and C2 consists of four strips directed perpendicularly and positioned just one under another. Detector C3 is situated below detectors C1 and C2 and has a mosaic structure (six elements). Each mosaic element is viewed by its own PMT. This type of assembly enables the angle of incident

particle to be determined. The geometry and dimensions of detectors C1–C3 define the instrument aperture and the geometric factor. The scintillation calorimeter can comprise the detector C3 in addition to another set of detectors, C4–C9. It provides the separation of the protons and electrons and enables the particle energy to be measured by the number of detectors, passed by the particle up to its stop; that is, it is used the range of the particle in the stack of detectors. The ACS consists of the detector C10 and lateral detectors C11 and C12, and it is needed to exclude the particles moving in the opposite direction (from the bottom to upward) from being recorded as well as all directions beyond the aperture.

6. Conclusion

In this paper, we aimed at giving a contribution to earthquake precursor studies. At this purpose, ground and space observations and modeling have been presented together with specific space projects. In particular, we have clarified different methodological aspects on damage prevention and prediction approaches used to defend society from such destructive events as earthquakes and provided a short summary of the scientific background of ground and space observations on earthquake precursors together with relative first theoretical interpretations. Also a possible first empirical approach to deterministic earthquake prediction based on medium-term and short-term ground and space precursory phenomena has been given. The latter consists of EM emissions radiated from the Earth's surface and produced as a consequence of earthquake preparation and occurrence, or by human activities. They demonstrated to cause ionospheric perturbations that are detectable by *LEO* satellites. Within this framework, we have described the ESPERIA satellite project designed for detecting seismo-associated effects in the topside ionosphere and first ESPERIA instruments (LAZIO-EGLE and ARINA), which have been tested in space. But a field mapping of the topside ionosphere also demonstrated to be an important factor to contribute in defining both the IGRF and IRI magnetic and ionospheric models, as well as the monitoring of TLE and TGF tropospheric phenomena that have recently assumed a relevant importance. An IUGG resolution of 2007 in support of ESPERIA and, more generally, of an ionospheric mission with all the above elements as scientific objectives, triggered us in proposing the AUSONIA space project.

Acknowledgment

The authors declare that they do not have any relation with all commercial devices mentioned in our paper, and that there is no conflict of interest for any of them.

References

[1] Japanese National Police Agency, *Countermeasures for the Great East Japan Earthquake*, http://www.npa.go.jp/archive/keibi/biki/higaijokyo_e.pdf.

[2] V. Sgrigna, A. Buzzi, L. Conti, P. Picozza, C. Stagni, and D. Zilpimiani, "Seismo-induced effects in the near-earth space: combined ground and space investigations as a contribution to earthquake prediction," *Tectonophysics*, vol. 431, no. 1–4, pp. 153–171, 2007.

[3] V. I. Keilis-Borok, "Intermediate-term earthquake prediction," *Proceedings of the National Academy of Sciences of the United States of America*, vol. 93, no. 9, pp. 3748–3755, 1996.

[4] V. I. Keilis Borok and A. Soloviev, *Non Linear Dynamics of the Lithosphere and Earthquake Prediction*, Springer, Berlin, Germany, 2003.

[5] A. Peresan, V. Kossobokov, L. Romashkova, and G. F. Panza, "Intermediate-term middle-range earthquake predictions in Italy: a review," *Earth-Science Reviews*, vol. 69, no. 1-2, pp. 97–132, 2005.

[6] A. Tzanis and F. Vallianatos, "Distributed power-law seismicity changes and crustal deformation in the SW Hellenic ARC," *Natural Hazards and Earth System Science*, vol. 3, no. 3-4, pp. 179–195, 2003.

[7] V. Sgrigna, R. Console, L. Conti et al., "Preseismic natural emissions from the Earth's surface and their effects in the near earth space, A project for monitoring earthquakes from Space," *American Geophysical Union*, vol. 83, no. 19, article S356, 2002, abstract no. T22B-10.

[8] V. Sgrigna, L. Carota, L. Conti et al., "Correlations between earthquakes and anomalous particle bursts from SAMPEX/PET satellite observations," *Journal of Atmospheric and Solar-Terrestrial Physics*, vol. 67, no. 15, pp. 1448–1462, 2005.

[9] S. A. Pulinets, "Space technologies for short-term earthquake warning," *Advances in Space Research*, vol. 37, no. 4, pp. 643–652, 2006.

[10] M. Long, A. Lorenz, G. Rodgers et al., "A cubesat derived design for a unique academic research mission in earthquake signature detection," in *Proceedings of the 16th Annual/USU Conference on Small Satellites*, pp. 1–17, Logan, Utah, USA, August 2002.

[11] M. Parrot, "The micro-satellite DEMETER," *Journal of Geodynamics*, vol. 33, no. 4-5, pp. 535–541, 2002.

[12] V. Sgrigna, "(Principal Investigator), esperia science team, ESPERIA phase a report," Italian Space Agency (ASI), Program for Scientific Missions dedicated to Earth Sciences, Rome, Italy, 2001.

[13] V. Sgrigna, A. Buzzi, L. Conti, P. Picozza, C. Stagni, and D. Zilpimiani, "The ESPERIA satellite project for detecting seismic-associated effects in the topside ionosphere. First instrumental tests in space," *Earth Planets and Space*, vol. 60, pp. 463–475, 2009.

[14] V. Sgrigna, the Ausonia Collaboration, The AUSONIA space project, Proposal submitted to the Italian Space Agency, 2008.

[15] P. Picozza, (PAMELA/ARINA collaboration), The PAMELA Mission, 2003, http://wizard.roma2.infn.it/pamela/index.htm.

[16] V. Sgrigna and V. Malvezzi, "Preseismic creep strains revealed by ground tilt measurements in central Italy on the occasion of the 1997 Umbria-Marche Apennines earthquake sequence," *Pure and Applied Geophysics*, vol. 160, no. 8, pp. 1493–1515, 2003.

[17] V. Sgrigna, C. D'ambrosio, and T. B. Yanovskaya, "Numerical modeling of preseismic slow movements of crustal blocks caused by quasi-horizontal tectonic forces," *Physics of the Earth and Planetary Interiors*, vol. 129, pp. 313–324, 2002.

[18] L. Conti, A. Buzzi, and A. M. Galper, "Influence of the seismic activity on the inner Van Allen radiation belt," in *Proceedings of the 10th Scientific Assembly of the International Association of Geomagnetism and Aeronomy (IAGA '05)*, p. 46, Toulose, France, July 2005, Session Division I, GA101: Monitoring

earthquakes and volcanic activity by magnetic, electric and electromagnetic methods; IAGA2005-A-01518.

[19] V. Sgrigna, "Description and testing of ARINA and LAZIO/EGLE instruments in space within the ESPERIA mission project and the DEMETER guest investigation programme," in *DEMETER Guest Investigator Workshop*, Paris, France, May 2005.

[20] T. Lay and T. C. Wallace, *Modern Global Seismology*, Academic Press, San Diego, Calif, USA, 1995.

[21] A. M. Nur, "Dilatation, pore fluids and premonitory variation of TP/TS travel time," *Bulletin of the Seismological Society of America*, vol. 62, pp. 1217–1222, 1972.

[22] C. H. Scholz, "A physical interpretation of the Haicheng earthquake prediction," *Nature*, vol. 267, no. 5607, pp. 121–124, 1977.

[23] V. I. Mjachkin, W. F. Brace, G. A. Sobolev, and J. H. Dieterich, "Two models for earthquake forerunners," *Pure and Applied Geophysics PAGEOPH*, vol. 113, no. 1, pp. 169–181, 1975.

[24] I. P. Dobrovolsky, S. I. Zubkov, and V. I. Miachkin, "Estimation of the size of earthquake preparation zones," *Pure and Applied Geophysics PAGEOPH*, vol. 117, no. 5, pp. 1025–1044, 1979.

[25] I. P. Dobrovolsky, N. I. Gershenzon, and M. B. Gokhberg, "Theory of electrokinetic effects occurring at the final stage in the preparation of a tectonic earthquake," *Physics of the Earth and Planetary Interiors*, vol. 57, no. 1-2, pp. 144–156, 1989.

[26] F. Bella, M. Caputo, G. Della Monica et al., "Crustal blocks and seismicity in the Central Apennines of Italy," *Nuovo Cimento della Societa Italiana di Fisica C*, vol. 21, no. 6, pp. 597–607, 1998.

[27] T. Rikitake, "Earthquake precursors," *Bulletin of the Seismological Society of America*, vol. 65, pp. 1133–1162, 1975.

[28] L. Conti, A. Cirella, V. Malvezzi, and V. Sgrigna, "A model for the propagation of preseismic electromagnetic fields through lithospheric and atmospheric media," in *Proceedings of the 1st General Assembly, European Geosciences Union*, p. 337, Nice, France, April 2004.

[29] R. G. Bilham, "Delays in the onset times of near-surface strain and tilt precursor to earthquakes," in *Earthquake Prediction: An International Review*, P. J. Simpson and P. G. Richards, Eds., pp. 411–421, Geophysical Union, Washington, DC, USA, 1981.

[30] F. Bella, P. F. Biagi, M. Caputo et al., "Very slow-moving crustal strain disturbances," *Tectonophysics*, vol. 179, no. 1-2, pp. 131–139, 1990.

[31] F. Bella, P. F. Biagi, M. Caputo et al., "Possible creep-related tilt precursors obtained in the Central Apennines (Italy) and in the Southern Caucasus (Georgia)," *Pure and Applied Geophysics PAGEOPH*, vol. 144, no. 2, pp. 277–300, 1995.

[32] S. McHugh and M. J. S. Johnston, "A review of observations and dislocation modeling of some creep-related tilt perturbations from central California," in *Terrestrial and Space Techniques in earthquake Prediction*, A. Vogel, Ed., pp. 181–201, Vieweg and Sohn, Braunschweig, Germany, 1979.

[33] R. G. Bilham, J. Beavan, K. Evans, and K. Hurst, "Crustal deformation metrology at lamont-doherty geological observatory," *Earthquake Prediction Research*, vol. 3, pp. 391–411, 1985.

[34] W. Thatcher and N. Fujita, "Deformation of the mikata rhombus: strain buildup following the 1923 kanto earthquake, Central Honshu, Japan," *Journal of Geophysical Research*, vol. 89, pp. 2102–2106, 1984.

[35] S. Ozawa, T. Nishimura, H. Suito, T. Kobayashi, M. Tobita, and T. Imakiire, "Coseismic and postseismic slip of the 2011 magnitude-9 Tohoku-Oki earthquake," *Nature*, vol. 475, no. 7356, pp. 373–377, 2011.

[36] C. E. Mortensen and M. J. S. Johnston, "The nature of surface tilt along 85 km of the San Andreas fault-preliminary results form a 14-instrument array," *Pure and Applied Geophysics PAGEOPH*, vol. 113, no. 1, pp. 237–249, 1975.

[37] R. G. Bilham and R. J. Beavan, "Strains and tilts on crustal blocks," *Tectonophysics*, vol. 52, no. 1–4, pp. 121–138, 1979.

[38] A. Nur, H. Ron, and O. Scotti, "Fault mechanics and the kinematics of block rotations," *Geology*, vol. 14, no. 9, pp. 746–749, 1986.

[39] Y. Ida, "Slow-moving deformation pulses along tectonic faults," *Physics of the Earth and Planetary Interiors*, vol. 9, no. 4, pp. 328–337, 1974.

[40] A. K. Pevnev, "Earthquake prediction: geodetic aspects of the problem," *Izvestija Akademija Nauk SSSR. Fizika Zemli*, vol. 12, pp. 88–98, 1988.

[41] A. K. Pevnev, "Deterministic geodetic prediction of preparation areas of strong crustal earthquakes," *Earthquake Prediction*, vol. 11, pp. 11–23, 1989.

[42] F. Bella, R. Bella, P. F. Biagi, A. Ermini, and V. Sgrigna, "Possible precursory tilts preceding some earthquakes ($3.0 \leq M \leq 3.8$) occurred in Central Italy between February 1981 and June 1983," *Earthquake Prediction Research*, vol. 4, pp. 147–154, 1986.

[43] F. Bella, P. F. Biagi, M. Caputo, G. Della Monica, A. Ermini, and V. Sgrigna, "Ground Tilt anomalies accompanying the main earthquakes occurred in the central apennines (Italy) during the period 1986–1989," *Il Nuovo Cimento C*, vol. 16, no. 4, pp. 393–406, 1993.

[44] R. J. Geller, "Debate on VAN," *Geophysical Research Letters*, vol. 23, no. 11, 1996.

[45] F. Salvini, "Block tectonics in thin-skin style-deformed regions: examples from structural data in the central apennines," *Annali di Geofisica*, vol. 36, pp. 97–109, 1993.

[46] F. Bella, P. F. Biagi, A. Ermini, V. Sgrigna, and P. Manjgaladze, "Possible propagation of tilt and strain anomalies: velocity and other characteristics," *Earthquake Prediction Research*, vol. 4, pp. 195–209, 1986.

[47] A. M. Gabrielov, T. A. Levshina, and I. M. Rotwain, "Block model of earthquake sequence," *Physics of the Earth and Planetary Interiors*, vol. 61, no. 1-2, pp. 18–28, 1990.

[48] V. P. Pustovetov and A. B. Malyshev, "Space-time correlation of earthquakes and high-energy particle flux variations in the inner radiation belt," *Cosmic Research*, vol. 31, pp. 84–90, 1993.

[49] E. A. Ginzburg, A. B. Malishev, I. P. Proshkina, and V. P. Pustovetov, "Correlation of strong earthquakes with radiation belt particle flux variations," *Geomagn Aeronomy*, vol. 34, pp. 315–320, 1994.

[50] A. M. Galper, S. V. Koldashov, and S. A. Voronov, "High energy particle flux variations as earthquake predictors," *Advances in Space Research*, vol. 15, no. 11, pp. 131–134, 1995.

[51] S. Y. Aleksandrin, A. M. Galper, L. A. Grishantzeva et al., "High-energy charged particle bursts in the near-Earth space as earthquake precursors," *Annales Geophysicae*, vol. 21, no. 2, pp. 597–602, 2003.

[52] M. Walt, *Introduction to Geomagnetically Trapped Radiation*, Cambridge University Press, 1994.

[53] M. E. Aleshina, S. A. Voronov, A. M. Galper et al., "Correlation between earthquake epicenters and regions of

high-energy particle precipitations from the radiation belt," *Cosmic Research*, vol. 30, no. 1, pp. 79–83, 1992.

[54] M. Parrot, J. Achache, J. J. Berthelier et al., "High-frequency seismo-electromagnetic effects," *Physics of the Earth and Planetary Interiors*, vol. 77, no. 1-2, pp. 65–83, 1993.

[55] O. A. Molchanov and M. Hayakawa, "On the generation mechanism of ULF seismogenic electromagnetic emissions," *Physics of the Earth and Planetary Interiors*, vol. 105, no. 3-4, pp. 201–210, 1998.

[56] O. A. Molchanov and M. Hayakawa, "Subionospheric VLF signal perturbations possibly related to earthquakes," *Journal of Geophysical Research*, vol. 103, pp. 17489–17504, 1998.

[57] Y. J. Chuo, J. Y. Liu, S. A. Pulinets, and Y. I. Chen, "The ionospheric perturbations prior to the Chi-Chi and Chia-Yi earthquakes," *Journal of Geodynamics*, vol. 33, no. 4-5, pp. 509–517, 2002.

[58] V. Sgrigna, F. Altamura, S. Ascani et al., "First data from the EGLE experiment onboard the ISS," *Microgravity Science and Technology*, vol. 19, no. 5-6, pp. 70–74, 2007.

[59] M. J. S. Johnston and R. J. Mueller, "Seismomagnetic observation during the 8 July 1986 magnitude 5.9 North Palm Springs earthquake," *Science*, vol. 237, no. 4819, pp. 1201–1203, 1987.

[60] P. Varotsos, K. Alexopoulos, M. Lazaridou-Varotsou, and T. Nagao, "Earthquake predictions issued in Greece by seismic electric signals since February 6, 1990," *Tectonophysics*, vol. 224, no. 1–3, pp. 269–288, 1993.

[61] K. Nomikos, F. Vallianatos, I. Kaliakatsos, E. Sideris, and M. Bakatsakis, "The latest aspects of telluric and electromagnetic variations associated with shallow and intermediate depth earthquakes in the South Aegean," *Annali di Geofisica*, vol. 40, no. 2, pp. 361–374, 1997.

[62] A. B. Draganov, U. S. Inan, and Y. N. Taranenko, "ULF magnetic signatures at the Earth surface due to ground water flow: a possible precursor to earthquakes," *Geophysical Research Letters*, vol. 18, no. 6, pp. 1127–1130, 1991.

[63] Y. Bernabé, "Streaming potential in heterogeneous networks," *Journal of Geophysical Research B*, vol. 103, no. 9, pp. 20827–20841, 1998.

[64] J. R. Bishop, "Piezoelectric effects in quartz-rich rocks," *Tectonophysics*, vol. 77, no. 3-4, pp. 297–321, 1981.

[65] P. Varotsos, N. Sarlis, M. Lazaridou, and P. Kapiris, "Transmission of stress induced electric signals in dielectric media," *Journal of Applied Physics*, vol. 83, no. 1, pp. 60–70, 1998.

[66] F. Freund, "Charge generation and propagation in igneous rocks," *Journal of Geodynamics*, vol. 33, no. 4-5, pp. 543–570, 2002.

[67] I. Stavrakas, C. Anastasiadis, D. Triantis, and F. Vallianatos, "Piezo stimulated currents in marble samples: precursory and concurrent-with-failure signals," *Natural Hazards and Earth System Science*, vol. 3, no. 3-4, pp. 243–247, 2003.

[68] Y. A. Kopytenko, T. G. Matiashvili, P. M. Voronov, E. A. Kopytenko, and O. A. Molchanov, "Detection of ultra-low-frequency emissions connected with the Spitak earthquake and its aftershock activity, based on geomagnetic pulsations data at Dusheti and Vardzia observatories," *Physics of the Earth and Planetary Interiors*, vol. 77, no. 1-2, pp. 85–95, 1993.

[69] A. C. Fraser-Smith, P. R. McGill, R. A. Helliwell, and O. G. Villard, "Ultra low frequency magnetic field measurements in southern California during the Northridge Earthquake of 17 January 1994," *Geophysical Research Letters*, vol. 21, no. 20, pp. 2195–2198, 1994.

[70] V. S. Ismaguilov, Y. A. Kopytenko, K. Hattori, P. M. Voronov, O. A. Molchanov, and M. Hayakawa, "ULF magnetic emissions connected with under sea bottom earthquakes," *Natural Hazards and Earth System Sciences*, vol. 1, pp. 23–31, 2001.

[71] K. Ohta, K. Umeda, N. Watanabe, and M. Hayakawa, "ULF/ELF emissions observed in Japan, possibly associated with the Chi-Chi earthquake in Taiwan," *Natural Hazards and Earth System Sciences*, vol. 1, pp. 37–42, 2001.

[72] J. W. Warwick, C. Stoker, and T. R. Meyer, "Radio emission associated with rock fracture: possible application to the great Chilean Earthquake of May 22, 1960," *Journal of Geophysical Research*, vol. 87, no. 4, pp. 2851–2859, 1982.

[73] K. Oike and T. Ogawa, "Electromagnetic radiations from shallow earthquakes observed in the LF range," *Journal of Geomagnetism & Geoelectricity*, vol. 38, no. 10, pp. 1031–1040, 1986.

[74] M. J. S. Johnston, "Review of electric and magnetic fields accompanying seismic and volcanic activity," *Surveys in Geophysics*, vol. 18, no. 5, pp. 441–475, 1997.

[75] S. Uyeda, K. S. Al-Damegh, E. Dologlou, and T. Nagao, "Some relationship between VAN seismic electric signals (SES) and earthquake parameters," *Tectonophysics*, vol. 304, no. 1-2, pp. 41–55, 1999.

[76] K. Eftaxias, P. Kapiris, J. Polygiannakis et al., "Experience of short term earthquake precursors with VLF-VHF electromagnetic emissions," *Natural Hazards and Earth System Science*, vol. 3, no. 3-4, pp. 217–228, 2003.

[77] F. Vallianatos, D. Triantis, A. Tzanis, C. Anastasiadis, and I. Stavrakas, "Electric earthquake precursors: from laboratory results to field observations," *Physics and Chemistry of the Earth*, vol. 29, no. 4–9, pp. 339–351, 2004.

[78] A. Nardi and M. Caputo, "Perspective electric earthquake precursors observed in the Apennines," in *Proceedings of the 8th Workshop on Non Linear Dynamics and Earthquake Prediction*, ICTP, October 2005.

[79] A. Nardi and M. Caputo, "Perspective electric earthquake precursors observed in the Apennines," *Bollettino di Geofisica Teorica ed Applicata*, vol. 47, pp. 3–12, 2006.

[80] S. K. Park, M. J. S. Johnston, T. R. Madden, F. D. Morgan, and H. F. Morrison, "Electromagnetic precursors to earthquakes in the ulf band: a review of observations and mechanisms," *Reviews of Geophysics*, vol. 31, no. 2, pp. 117–132, 1993.

[81] M. Merzer and S. L. Klemperer, "Modeling low-frequency magnetic-field precursors to the Loma Prieta earthquake with a precursory increase in fault-zone conductivity," *Pure and Applied Geophysics*, vol. 150, no. 2, pp. 217–248, 1997.

[82] V. Surkov, "ULF electromagnetic perturbations resulting from the fracture and dilatancy in the earthquake preparation zone," in *Atmospheric and Ionospheric Electromagnetic Phenomena Associated with Earthquakes*, M. Hayakawa, Ed., pp. 371–382, TERRAPUB, Tokyo, Japan, 1999.

[83] M. Hayakawa, Y. Kopytenko, N. Smirnova, V. Troyan, and T. Peterson, "Monitoring ULF magnetic disturbances and schemes for recognizing earthquake precursors," *Physics and Chemistry of the Earth, Part A*, vol. 25, no. 3, pp. 263–269, 2000.

[84] F. Freund, "On the electrical conductivity structure of the stable continental crust," *Journal of Geodynamics*, vol. 35, no. 3, pp. 353–388, 2003.

[85] G. Areshidze, F. Bella, P. F. Biagi et al., "Anomalies in geophysical and geochemical parameters revealed on the occasion of the Paravani ($M = 5.6$) and Spitak ($M = 6.9$)

earthquakes (Caucasus)," *Tectonophysics*, vol. 202, no. 1, pp. 23–41, 1992.

[86] Z. Guo, B. Liu, and Y. Wang, "Mechanism of electromagnetic emissions associated with microscopic and macroscopic cracking in rocks," in *Electromagnetic Phenomena Related to Earthquake Prediction*, M. Hayakawa, Ed., pp. 523–529, TERRAPUB, Tokyo, Japan, 1994.

[87] F. T. Freund, A. Takeuchi, and B. W. S. Lau, "Electric currents streaming out of stressed igneous rocks—a step towards understanding pre-earthquake low frequency EM emissions," *Physics and Chemistry of the Earth*, vol. 31, no. 4–9, pp. 389–396, 2006.

[88] K. Eftaxias, V. Sgrigna, and T. Chelidze, "Mechanical and electromagnetic phenomena accompanying pre-seismic deformation: from laboratory to geophysical scale," *Tectonophysics*, vol. 431, no. 1–4, pp. 1–5, 2007.

[89] O. A. Molchanov, O. A. Mazhaeva, A. N. Golyavin, and M. Hayakawa, "Observation by the Intercosmos-24 satellite of ELF-VLF electromagnetic emissions associated with earthquakes," *Annales Geophysicae*, vol. 11, pp. 431–440, 1993.

[90] C. J. Rodger, R. L. Dowden, and N. R. Thomson, "Observations of electromagnetic activity associated with earthquakes by low-altitude satellites," in *Atmospheric and Ionospheric Electromagnetic Phenomena Associated with Earthquakes*, M. Hayakawa, Ed., pp. 697–710, TERRAPUB, Tokyo, Japan, 1999.

[91] M. B. Gokhberg, V. A. Morgounov, and E. L. Aronov, "On the high frequency electromagnetic radiation during seismic activity," *Dokladi Akademii Nauk USSR*, vol. 248, pp. 1077–1081, 1979.

[92] V. I. Larkina, V. V. Migulin, O. A. Molchanov, I. P. Kharkov, A. S. Inchin, and V. V. Schvetsova, "Some statistical results on very low frequency radiowave emissions in the upper ionosphere over earthquake zones," *Physics of the Earth and Planetary Interiors*, vol. 57, pp. 100–109, 1989.

[93] M. Parrot and M. M. Mogilevsky, "VLF emissions associated with earthquakes and observed in the ionosphere and the magnetosphere," *Physics of the Earth and Planetary Interiors*, vol. 57, no. 1-2, pp. 86–99, 1989.

[94] S. V. Bilichenko, F. S. Iljin, E. F. Kim et al., "ULF response of the ionosphere for earthquake preparation processes," *Doklady Akademii Nauk USSR*, vol. 311, pp. 1077–1080, 1990.

[95] O. N. Serebryakova, S. V. Bilichenko, V. M. Chmyrev et al., "Electromagnetic ELF radiation from earthquake regions as observed by low-altitude satellite," *Geophysical Research Letters*, vol. 19, pp. 91–94, 1992.

[96] V. M. Chmyrev, N. V. Isaev, O. N. Serebryakova, V. M. Sorokin, and Y. P. Sobolev, "Small-scale plasma inhomogeneities and correlated ELF emissions in the ionosphere over an earthquake region," *Journal of Atmospheric and Solar-Terrestrial Physics*, vol. 59, no. 9, pp. 967–974, 1997.

[97] C. C. Lee, J. Y. Liu, C. J. Pan, and K. Igarashi, "The heights of sporadic-E layer simultaneously observed by the VHF radar and ionosondes in Chung-Li," *Geophysical Research Letters*, vol. 27, no. 5, pp. 641–644, 2000.

[98] S. A. Pulinets, K. A. Boyarchuk, V. V. Hegai, V. P. Kim, and A. M. Lomonosov, "Quasielectrostatic model of atmosphere-thermosphere-ionosphere coupling," *Advances in Space Research*, vol. 26, no. 8, pp. 1209–1218, 2000.

[99] M. Hayakawa, O. A. Molchanov, and A. P. Nikolaenko, "Model variations in atmospheric radio noise caused by preseismic modifications of tropospheric conductivity profile," in *Seismo Electromagnetics: Lithosphere-Atmosphere-Ionosphere Coupling*, M. Hayakawa and O. A. Molchanov, Eds., pp. 349–352, TERRAPUB, Tokyo, Japan, 2002.

[100] A. Buzzi, L. Conti, A. M. Galper et al., "Sismo-electromagnetic emissions," in *Proceedings of the NATO Advances Study. Institute on 'Sprites, Elves and Intense Lightning Discharges'*, M. Fullekrug, E. A. Mareev, and M. J. Rycroft, Eds., vol. 225 of *NATO Science Series II: Mathematics, Physics and Chemistry*, pp. 388–389, Springer, 2006.

[101] M. Parrot, "Statistical study of ELF/VLF emissions recorded by a low-altitude satellite during seismic events," *Journal of Geophysical Research*, vol. 99, pp. 23339–23347, 1994.

[102] M. A. Fenoglio, M. J. S. Johnston, and J. D. Byerlee, "Magnetic and electric fields associated with changes in high pore pressure in fault zones: application to the Loma Prieta ULF emissions," *Journal of Geophysical Research*, vol. 100, no. 7, pp. 12–958, 1995.

[103] O. A. Molchanov, M. Hayakawa, and V. A. Rafalsky, "Penetration characteristics of electromagnetic emissions from an underground seismic source into the atmosphere, ionosphere and magnetosphere," *Journal of Geophysical Research*, vol. 100, pp. 1691–1712, 1995.

[104] R. Teisseyre, "Generation of electric field in an earthquake preparation zone," *Annali di Geofisica*, vol. 40, no. 2, pp. 297–304, 1997.

[105] V. V. Grimalsky, I. A. Kremenetsky, and Y. G. Rapoport, "Excitation of EMW in the lithosphere and propagation into magnetosphere," in *Atmospheric and Ionospheric Electromagnetic Phenomena Associated with Earthquakes*, M. Hayakawa, Ed., pp. 777–787, TERRAPUB, Tokyo, Japan, 1999.

[106] F. Vallianatos and A. Tzanis, "A model for the generation of precursory electric and magnetic fields associated with the deformation rate of the earthquake focus," in *Atmospheric and Ionospheric Electromagnetic Phenomena Associated with Earthquakes*, M. Hayakawa, Ed., pp. 287–305, TERRAPUB, Tokyo, Japan, 1999.

[107] V. M. Sorokin, V. M. Chmyrev, and A. K. Yaschenko, "Electrodynamic model of the lower atmosphere and the ionosphere coupling," *Journal of Atmospheric and Solar-Terrestrial Physics*, vol. 63, pp. 1681–1691, 2001.

[108] N. Gershenzon and G. Bambakidis, "Modeling of seismo-electromagnetic phenomena," *Russian Journal of Earth Sciences*, vol. 3, pp. 247–275, 2001.

[109] Y. Fujinawa, T. Matsumoto, and K. Takahashi, "Modeling confined pressure changes inducing anomalous electromagnetic fields related with earthquakes," *Journal of Applied Geophysics*, vol. 49, no. 1-2, pp. 101–110, 2002.

[110] J. Y. Liu, Y. I. Chen, Y. J. Chuo, and C. S. Chen, "A statistical investigation of preearthquake ionospheric anomaly," *Journal of Geophysical Research A*, vol. 111, no. 5, Article ID A05304, 2006.

[111] K. Heki, "Ionospheric electron enhancement preceding the 2011 Tohoku-Oki earthquake," *Geophysical Research Letters*, vol. 8, Article ID L17312, 5 pages, 2011.

[112] H. Tsuji, Y. Hatanaka, T. Sagiya, and M. Hashimoto, "Coseismic crustal deformation from the 1994 Hokkaido-Toho-Oki earthquake monitored by a nationwide continuous GPS array in Japan," *Geophysical Research Letters*, vol. 22, no. 13, pp. 1669–1672, 1995.

[113] E. Blanc, "Observations in the upper atmosphere of infrasonic waves from natural or artificial sources: a summary," *Annales Geophysicae*, vol. 3, no. 6, pp. 673–688, 1985.

[114] Y. Zaslavski, M. Parrot, and E. Blanc, "Analysis of TEC measurements above active seismic regions," *Physics of the Earth and Planetary Interiors*, vol. 105, pp. 219–228, 1998.

[115] A. M. Galper, V. B. Dimitrenko, N. V. Nikitina, V. M. Grachev, and S. E. Ulin, "Interrelation between high-energy charged particle fluxes in the radiation belt and seismicity of the earth," *Cosmic Research*, vol. 27, article 789, 1989.

[116] S. A. Voronov, A. M. Galper, S. V. Koldashov et al., "Increases in high energy charged particle fluxes near the South Atlantic magnetic anomaly and the seismicity of the earth," *Cosmic Research*, vol. 28, pp. 789–791, 1990.

[117] Y. I. Galperin, V. A. Gladyshev, N. V. Jordjio, and V. I. Larkina, "Precipitation of high-energy captured particles in the magnetosphere above the epicenter of an incipient earthquake," *Cosmic Research*, vol. 30, pp. 89–106, 1992.

[118] A. Buzzi, M. Parrot, and J. A. Sauvaud, "Precipitation of particles by intense electromagnetic harmonic waves during magnetic storms," in *Proceedings of the International Demeter Workshop*, Toulouse, France, June 2006.

[119] V. V. Krechetov, "Cerenkov radiation of protons in the magnetosphere as a source of VLF waves preceding an earthquake," *Geomagnetism and Aeronomy*, vol. 35, no. 5, pp. 688–691, 1996.

[120] M. Hayakawa and H. Sato, "Ionospheric perturbations associated with earthquakes, as detected by sub-ionospheric VLF propagation," in *Electromagnetic Phenomena Related to Earthquake Prediction*, M. Hayakawa and Y. Fujinawa, Eds., pp. 391–397, TERRAPUB, Tokyo, Japan, 1994.

[121] V. A. Morgounov, T. Ondoh, and S. Nagai, "Anomalous variation of VLF signals associated with strong earthquakes $M \geq 7.0$," in *Electromagnetic Phenomena Related to Earthquake Prediction*, M. Hayakawa and Y. Fujinawa, Eds., pp. 409–428, TERRAPUB, Tokyo, Japan, 1994.

[122] I. Gufeld, G. Gusev, and O. Pokhotelov, "Is the prediction of earthquake dates possible by the VLF radiowave monitoring method?" in *Electromagnetic Phenomena Related to Earthquake Prediction*, M. Hayakawa and Y. Fujinawa, Eds., pp. 381–389, TERRAPUB, Tokyo, Japan, 1994.

[123] H. Fujiwara, M. Kamogawa, M. Ikeda et al., "Atmospheric anomalies observed during earthquake occurrences," *Geophysical Research Letters*, vol. 31, Article ID L17110, 4 pages, 2004.

Hindawi Publishing Corporation
International Journal of Geophysics
Volume 2012, Article ID 583097, 13 pages
doi:10.1155/2012/583097

Review Article

Precursor-Like Anomalies prior to the 2008 Wenchuan Earthquake: A Critical-but-Constructive Review

Tengfei Ma and Zhongliang Wu

Institute of Geophysics, China Earthquake Administration, Beijing 100081, China

Correspondence should be addressed to Zhongliang Wu, wuzl@cea-igp.ac.cn

Received 7 August 2011; Accepted 31 October 2011

Academic Editor: Rodolfo Console

Results published since the last three years on the observations of the precursor-like anomalies before the May 12, 2008, Wenchuan, M_s8.0 earthquake are collected and analyzed. These retrospective case studies would have provided heuristic clues about the preparation process of this inland great earthquake and the predictability of this destructive event if the standards for the rigorous test of earthquake forecast schemes were strictly observed. At least in some of these studies, however, several issues still need to be further examined to confirm or falsify the connection of the reported observations with the Wenchuan earthquake. Some of the problems are due to the inevitable limitation of observational infrastructure at the recent time, but some of the problems are due to the lack of communication about the test of earthquake forecast schemes. For the interdisciplinary studies on earthquake forecast, reminding of the latter issue seems of special importance for promoting the works and cooperation in this field.

1. Introduction

At least partly due to the tremendous loss of life and property and the intense social impact [1], the Wenchuan earthquake that occurred on May 12, 2008, in Sichuan Province of southwest China, has attracted widespread attention not only in seismological communities but also in other scientific communities. Since the occurrence of the Wenchuan earthquake, there have been some 300 papers published related to the precursor-like anomaly observations prior to this great earthquake, making it necessary for a systematic collection and comprehensive analysis of these materials. The necessity of such collection and analysis is further highlighted by the fact that over 3/4 of these publications are in Chinese with/without English abstract (with some of them being similar to, or just simply a repetition of the English publications) and quite a few of these publications are actually not known to international seismological communities. This is, similar to the situation of other developing countries [2], a characteristic of the scientific publications in China.

In the study of earthquake forecast/prediction, China seems of special features in that earthquake forecast/prediction has been kept for a long time as a nationwide scientific goal, even if there were intense debates on the predictability of earthquakes in the international seismological communities [3]. From merely the number of papers published, the Wenchuan earthquake might be one of the special, or even unique, events with so many studies on its forecast or preshock anomalies. If these anomalies could be confirmed, it would be an important event in the study on earthquake predictability; otherwise if these anomalies could not be confirmed, then it would be a useful sample for reminding of how the studies on earthquake forecast/prediction should be conducted in an efficient way. After the Wenchuan earthquake, there have been several studies trying to collect, compare, and analyze the (published and/or internal) data, including the data from the authors themselves (e.g., [4–11]). There are also some papers on the reflection of the earthquake forecast/prediction approaches based on the lessons of this earthquake [3, 12–15], with a diversity of ideas and data. The present paper is, to much extent, a continuation and extension of such collection and analysis works, but with different emphases in the analysis, highlighting the test of earthquake forecast/prediction schemes, and with a wider range of collection stressing interdisciplinary studies.

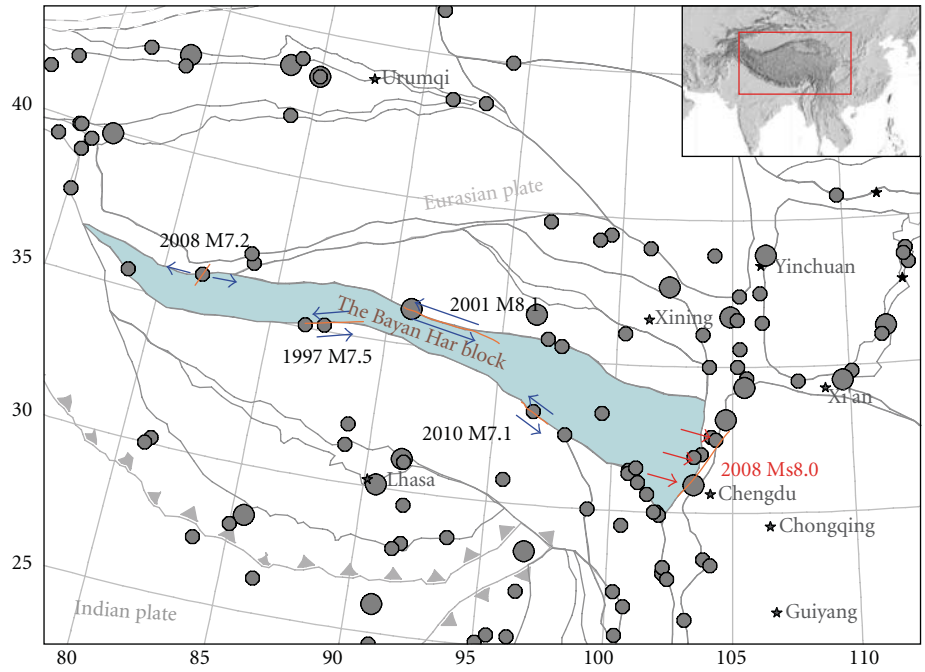

Figure 1: Distribution of major-to-great earthquakes around the Bayan Har block since 1997, with the 2008 Wenchuan earthquake located to the east, as shown by the text and arrows in red. To the top right is the indexing figure showing the position of the map. In the figure, orange lines show the earthquake ruptures, and blue arrows show the focal mechanism types of the earthquakes. Gray dots show the epicenters of historical major to great earthquakes. Gray solid lines indicate the boundaries of the tectonic blocks (according to [19]), with the Bayan Har block highlighted in the figure.

2. Materials Collected and Used for the Analysis

Although it has been only three years since the 2008 Wenchuan earthquake, because publications related to the precursor-like anomalies are within different research fields, the collection of such publications is still difficult to be completed. The collecting process was in two steps. For the materials published in English, searching terms "(ti = Wenchuan or ts = Wenchuan) and (ti = precursor or ts = precursor or ti = before or ts = before or ti = prior or ts = prior)" were used to the SCI-E database via the Web of Science (http://www.isiknowledge.com/). From 2008 to mid-2011, a total of 151 results hit the search. Removing the terms not directly related to the main topics, which are basically on the subjects of earthquake engineering and geological disasters, 61 articles were selected. For the materials published in Chinese, the China National Knowledge Infrastructure (CNKI) database (http://www.cnki.net/) was used with ("topic/title/keywords" = "(wenchuan) and (precursor or before or prior to)", in Chinese) as the search terms. Another two databases, the VIP database (http://www.cqvip.com/) and the Wanfang database (http://www.wanfangdata.com.cn/), were used as complementary sources. Using the screening criteria similar to that of the English publications, 261 articles in Chinese were collected. Abstracts of symposia [16–18] are not included, since most of the results were published after these meetings. Due to the same reason, diplomatic theses are not included in the References. We eliminated the "repeated publications" as much as we could. If there are two papers with exactly the same contents in English and in Chinese, respectively, we just keep the English one in the reference list. If there were two papers, with extremely similar contents and similar author teams, but published in different journals, then we just leave one of them (in the journal with higher impact factors) in the reference list. To keep the paper as concise as it could be, we also screened out the publications which are concentrating on the mechanisms of the phenomenology based on other studies rather than providing the ("fresh") phenomenological report.

Ranking by the number of papers published, these papers appear mainly in Journal of Geodesy and Geophysics (Wuhan, with the English edition Geodesy and Geophysics), Earthquake (Beijing), Acta Seismologica Sinica (the Bulletin of the Seismological Society of China, Beijing, with the English edition Acta Seismologica Sinica, changing to Earthquake Science since 2009), and Chinese Journal of Geophysics (the Bulletin of the Chinese Geophysical Society, Beijing, with the English edition Acta Geophysica Sinica or Chinese Journal of Geophysics), publishing no less than 15 papers in each of them. Journals publishing the related papers numbers up to 53, reflecting the diversity of the related results.

3. Characteristic Anomalies Reported and Characteristic Time Scales

As a background of the geology and seismicity related to the Wenchuan earthquake, Figure 1 shows the distribution and

size of the major-to-great earthquakes around the Bayan Har block since 1997 (using the earthquake catalogue from the China Earthquake Networks Center (CENC)). During this time period, the Bayan Har block is the unique contributor to the major-to-great earthquake activity in continental China. Before this period, for more than 2 decades, there was no major-to-great earthquake occurring around the Bayan Har block. This provides the concepts of the geodynamic origin of the Wenchuan earthquake, and its preparation process.

Precursor-like anomalies, observed at different time scales prior to the Wenchuan earthquake, are in a wide range. Following is a brief summary of the main observations.

3.1. Anomalous Seismicity. Decade-scale quiescence along the Longmenshan fault zone [20, 21]; variation of monthly number of earthquakes since 2000 along the Longmenshan fault zone [22]; six-and-half-year-scale gap of seismicity above M_L4.0, disrupted 1 year before the Wenchuan earthquake [23]; five-year-scale PI "hotspots" along the Longmenshan fault zone, and five-year-scale "accelerating seismic release (ASR)" [21, 24, 25]; five-year-scale preshock increasing activity of intermediate-depth earthquakes [26]; three-year scale quiescence of seismicity above M_L6.0 [10, 27]; three-year-scale large-range seismicity pattern [28]; one-to-three-year-scale variation of "load-unload response ratio (LURR)" presented by seismicity [29, 30]; variation of "modulated earthquakes" 2 years before the Wenchuan earthquake [31]; two-year-scale variation of the homogeneity in seismicity [32]; variation of several statistical parameters of seismicity since the beginning of 2008 [33, 34]; half-year-scale seismic activation identified by PI method [35]. Besides, there are also studies on the potential tidal triggering effect which determines the origin time of the earthquake [36], and relation between Earth rotation and microseismicity [37].

3.2. Anomalies in Deformation Measurement. Decade-scale "locking" along the Longmenshan fault [38–40]; tilt variation from 2005 to 2006 [41]; accelerating fault activity since 2006 [42]; three-to-one-year-scale accelerating deformation [43]; "Oscillation anomalies" of GPS time series since 2007 [44]; one-year scale GPS baseline variation [45]; anomalous changes near the epicenter recorded by tiltmeter, since November 2007 [5]; anomalies of deformation (with resolution 3 months) before the Wenchuan earthquake identified retrospectively by wavelet analysis [46]; anomalies of tilt tidal factor in Shaanxi 3 months prior to the earthquake [47]; half-month-scale anomalous tilt [48]; and anomalies of deformation 3 days and 1 hour before the Wenchuan earthquake [40].

3.3. Anomalies in Strain/Stress Measurements. Five-year-scale perturbation of regional stress field before the Wenchuan earthquake by focal mechanism data [49]; increasing compressional strain since 2004 [50]; two-year-scale increase of regional stress [51]; two-year-scale micro-earthquake swarm, with focal mechanisms approaching to homogeneous [52]; months-to-year-scale disturbance in borehole strain measurement [53] and change of predominant focal-mechanisms of small earthquakes [54]; strain anomalies 3 months before the earthquake, with dominant frequencies depending on the epicentral distance [55]; changes of crustal stress since the end of April, 2008 [11]; week-scale variation of in-situ stress [56]; anomalous variation in in-situ stress measurement 48, 30, 8 hours and 37 minutes before the Wenchuan earthquake [57]; half-an-hour-scale abrupt anomaly recorded by strainmeter near to the epicenter [5, 58].

3.4. Possible Structure Variation. Four-year-scale preshock variation of seismic wave velocity [59]; three-year-scale [10, 60], one-year-scale [61], and two-to-one-month-scale variation of Earth resistivity [60, 61]; two-month-scale step-like resistivity anomalies [62]; one-month-scale increase of gas well pressures in a gas-field in Sichuan [63]; variation of noise correlation function (NCF) five days before the Wenchuan earthquake near the Longmenshan fault zone [64].

3.5. Anomalous Signals Observed in Broadband Seismic Recordings and Gravity Recordings. Decade-scale variation of gravity before the Wenchuan earthquake [65–68]; anomalous signals (tremors?) in broadband seismic recordings and gravity recordings, starting from about May 9∼10, 2008 [69–75].

3.6. Geomagnetic Anomalies. Geomagnetic anomalies revealed by fractional Brownian motion (fBM) analysis 2 to 3 months before the earthquake [76] and electromagnetic anomalies 2∼1 months before the earthquake [77]; and anomalies 3 days before the Wenchuan earthquake, within a large range surrounding the epicenter [78, 79].

3.7. Ionospheric Anomalies. Ionospheric anomalies 13, 6, 5 days [80], 6 days [11, 81–83], 6∼7 days [84–86], 5 days [87–89], 8∼4 days [90–93], 4 days [94], and 2∼3 days [81–83, 88, 94–118] before the Wenchuan earthquake.

3.8. Geothermal and Atmospheric Anomalies. Extreme meteorological condition 21 months and 10 months before the Wenchuan earthquake [119]; temperature variation near the epicenter since November 2007 [5]; half-year-scale decrease of precipitation [120]; temperature variation since January 2008 [121]; large-scale satellite infrared thermal anomaly, appeared since March 2008 [122]; infrared radiation anomalies about 2 months before the Wenchuan earthquake [123–125]; anomalies of outgoing long-wave radiation 40 days before the Wenchuan earthquake [126]; one-month-scale decrease of the SNR of the VLF radio signal detected by satellite [127]; higher temperature in Sichuan in May, 2008, comparing to the last 30 years [128]; abnormal infrasonic waves received 10 days before the Wenchuan earthquake [11]; abnormal increase of temperature since May 5 [129]; abnormal surface latent heat flux 7 days before the earthquake [130]; abnormal variation in thermosphere 3 days before the Wenchuan earthquake [131]; "earthquake cloud" 5 hours before the earthquake [132].

Additionally, preshock macroanomalies [133–137], including animal behaviors [138, 139] and vegetation degeneration [140], are also collected and analyzed. This can act as

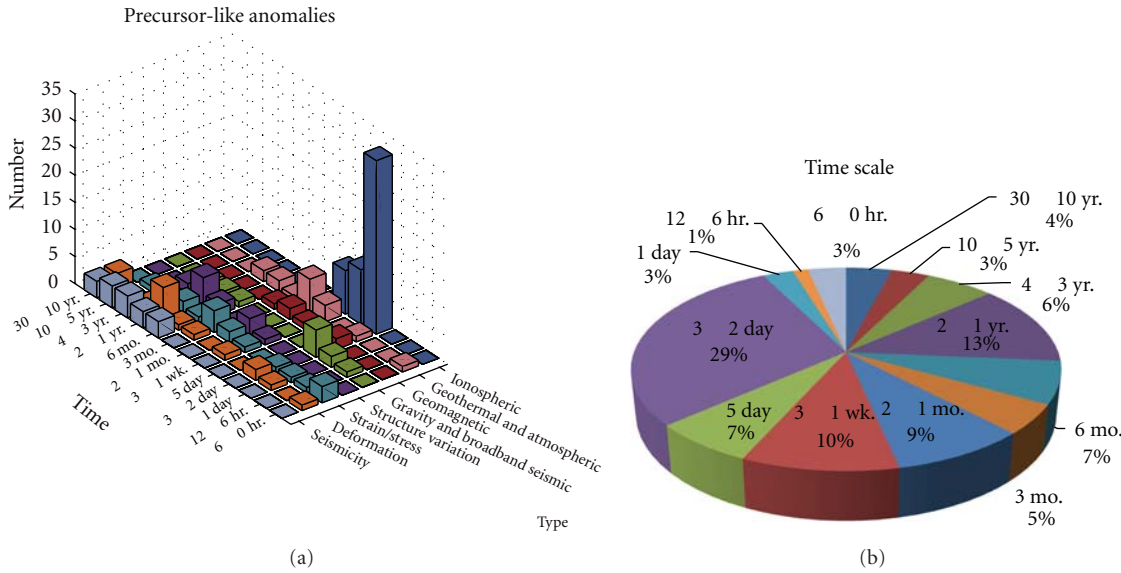

Figure 2: (a) Temporal distribution of the appearance of different types of reported anomalies, as summarized in Section 3. (b) Temporal distribution of the appearance of all the reported anomalies, as summarized in Section 3.

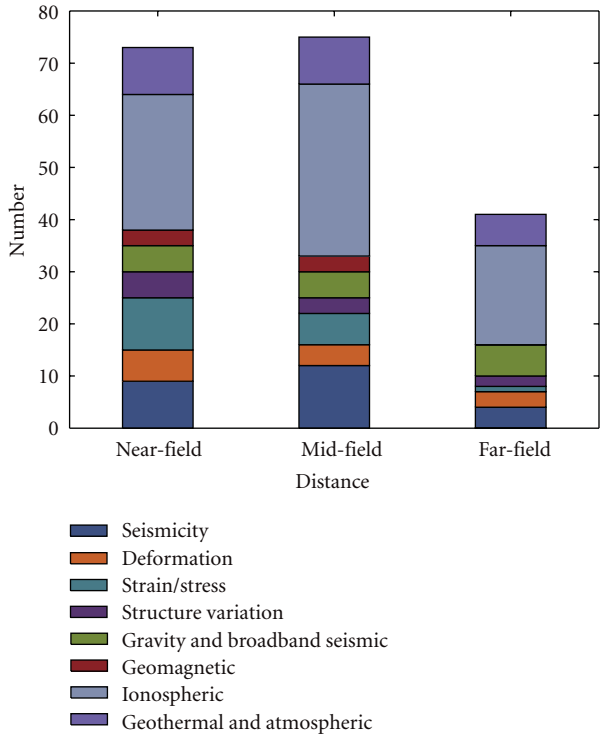

Figure 3: Distance ranges of the reported anomalies, as summarized in Section 3.

a useful reference, but how to confirm or falsify these (almost unrepeatable) observations needs further careful consideration.

At present, it is still hard to draw any definite conclusion on whether the above-mentioned observations, some are independent of others, while some are intercorrelated, may lead to a "unified description" of the earthquake preparation process. Some of the works are not understandable to us at present time regarding their methodology or observational phenomenology (e.g., [141–143]). However, it turns out that some characteristic times seem relatively important. Figure 2 shows, based on the analysis in this section, the "anomaly times" reported. It can be seen from the figure that anomalies detected by seismic, deformation, strain/stress, structure variation, gravity and broadband seismic recordings, geomagnetic, geothermal and atmospheric, and ionosphere observations appeared successively approaching the earthquake. The presently accessible data prevents from a detailed analysis of anomaly-distance dependence. As a conceptual picture, Figure 3 shows the statistics of anomalies with different distance ranges, in which "near-field" means the locations near to the earthquake fault, "mid-field" means the region within the circle centered at the epicenter and radius 1,000 km, and "far-field" means the regions beyond this circle. For those cases with distributed anomalies (an "anomaly field", as detected by satellite TEC), we take the locations within the above three ranges, respectively, in the counting of observation reports. It can be seen that the majority of the reports are within the "near-field" and the "mid-field" regions, with cautions necessary that the sampling of observational sites is by no means homogeneous.

4. Problems in Need of Further Considerations in Future

Except a few studies [10, 24, 25, 35, 79, 144, 145], there are few discussions on the statistical significance of the correlation between the anomalies observed and the earthquake. This is to much extent a problem which needs to be considered seriously in future, because in the test of earthquake forecast/prediction schemes, statistical significance is one of

the key factors in need of consideration. Without a rigorous statistical test, some of the arguments, such as the year-to-month-scale long-range low-temperature before strong earthquakes [146], seems questionable.

The role of a single station analysis is, to some extent, double sided: on one hand, there might be some "special" stations which are especially "sensitive" to some precursory anomalies, even if the anomalies are associated with remote earthquakes; on the other hand, it is hard to draw any definite conclusion only by the records of a single station, while other stations have almost no "reflections." Result of Cheng et al. [8] indicates that, despite the anomalies registered at some individual sites, the routine precursor monitoring networks had no significant anomalies recorded. In the publications, anomalies retrospectively reported at individual stations/sites, ranging by distances from the epicenter, include abnormal strain changes observed at Guza, Sichuan, about one year before the Wenchuan earthquake [147], with epicentral distance ∼1.6°; increasing compressional stress in Wudu, Gansu, 7 months before the Wenchuan earthquake [148], and electronic anomalies in Longnan, Gansu [149]; water level variation in Guanzhong, Shaanxi [150]; deformation anomalies in Liujiaxia, Gansu [151]; water level and ground gas Hg anomalies in Zhouzhi, Shaanxi [152, 153]; ground fluid anomalies and electronic anomalies in Yunnan [154–157], with epicentral distance ∼5.5°; abnormal variation of fluid temperature in Qinghai [158]; abnormal ground fluid variation at sites as far as Huangyuan, Ningxia [159]; anomalous pre-Wenchuan-earthquake deformation/strain/stress recorded in Shanxi [160–164], with epicentral distance ∼10°; electromagnetic radiation anomaly in Gaobeidian and Ningjin, Hebei [165]; anomalous tilt in Tai'an, Shandong [166, 167]; anomalous deformation in Yixian, Hebei [168]; anomalous Earth resistivity from the end of April, 2008, in Qingdao, Shandong [169]; anomalous water level and water temperature variation 6 days before the Wenchuan earthquake, observed at Changli, Hebei [170]; anomalies of water temperature and Radon content in Ningbo, Zhejiang [171], with epicentral distance ∼15.6°. Variation of cosmic rays deals with the stations from Yangbajing, Tibet [172] to Guangzhou, Beijing, Irkutsk, Nagoya, and Moscow [173], with epicentral distance up to ∼51°. Because the Wenchuan earthquake is a great one, its preparation process may have an extremely large spatial scale. Therefore, we try not to be too skeptical about the reliability of these "remote" anomalies. However, when dealing with such a large spatial scale, and dealing with the situation that only a few sites have the anomalies, some statistical test is important.

For some of the observations, the anomalous/alarmed regions are so large that intuitive visual inspection is hard to provide correct judgments. In this case, statistical test is of special importance. An example is the ionospheric anomalies and the satellite-detected thermal anomalies as mentioned in the last section. Several days before the Wenchuan earthquake, abnormal TEC of ionosphere could be observed even in south China [174, 175], with distance about 11°, giving the idea of the size of the "warning region."

Length of data for "baseline comparison" is another concern when reading the related reports. In quite a few studies, the data for checking the "background variations" are only since 2007. This is to much extent an inevitable problem because several observational facilities are just at their beginning stage. However, this limitation prevents from getting concrete conclusions about the anomalies in the case that there is a lack of sufficient knowledge about the *normal* state. Evidently the continuous accumulation of observations is needed. Some of the papers mentioned objectively that there is still lack of the experiences of a great earthquake (e.g., [176]).

Coseismic changes, or changes before and after the earthquake, are presented by a few analysis (e.g., [39, 57, 81, 91, 127, 147, 177]). But generally, lack of analysis on the coseismic variation seems to be one of the problems for some of the investigations. This is also a problem in need of serious consideration, since in the study of the candidate precursors, coseismic variation may provide useful constraints on the mechanism of such precursors.

Based on the above discussions, we suggest that in future works, the following issues should be paid special attention to (1) Statistical evaluation of the correlation between the anomalies reported and the earthquake needs to be considered, semiquantitatively or quantitatively if possible; (2) distance from the observation station and the "target" earthquake has to be taken into serious consideration, especially, if the distance is too large, then theoretical concepts as per the size of earthquake preparation (e.g., [178]) have to be accounted for, and statistical consideration is needed for the large-scale anomalies; (3) information about the "normal" state, or the "baseline" variations, has to be accounted for in identifying the potential anomalies; (4) comparison of preseismic, coseismic, and postseismic changes would be of help to understand the earthquake preparation process as well as the characteristics of the anomalies.

The above-mentioned "problems," however, do not imply that the publications introduced in this paper are not acceptable. As a matter of fact, all these observations are contributions to the study of the predictability of this earthquake. Especially valuable, among the publications, there are papers debating on the causes of the observed variations [179–182]. Some papers provide "negative" results [144, 183–190] which are useful in excluding the misleading information. Some papers objectively report that some of the observational systems did not show significant anomalies [8, 191], or that some of the observation systems are shown to be unable to capture the precursors [192, 193]. There are reports stating that among the whole set of monitoring stations, the stations with anomalies only occupy a small portion (e.g., [194]). Some works also try to exclude the effect of other factors in identifying the anomalies [195, 196]. Some of the reports (e.g., [197–206]) just provided the observation (before, or before and after the earthquake) but were too prudent to reach any direct conclusion related to earthquake precursors. Analysis tools such as ROC test [25], RTL analysis [10], and RTP [207] were used to the forecast test. If applied to geomagnetic data (e.g., [155]), then more objective conclusions about the correlation between the variation

or fluctuation of geomagnetic field and the earthquake could be obtained. The same need exists for the tidal data (e.g., [208]), fluid data [209], electromagnetic radiation data [210], or fault deformation data [211]. Even if for "traditional" seismicity analysis (e.g., [212, 213]), such statistical test would be of help. But generally, however, it is somehow "abnormal" that there have been not so many "alternative" explanations in such a field with so many complexities and controversies. Maybe time is a remedy to this problem.

Last but not least, very few discussions (e.g., [214, 215]) are concerning how to apply the knowledge from these retrospective case studies, such as the observed patterns of seismicity, practically to the decision-making approaches to "operational earthquake forecast" [216]. Complexity of the deformation-related precursors and fluid-related precursors has caused some attentions [217–220]. Considering the observation that earthquakes occur after the restore of some of the anomalies, such as LURR [29], the anomaly-based alarm-oriented forecast problem is shown to be more complicated. Based on gravity measurement, a forward intermediate-term forecast was made [221], but the forecast did not contribute to the reduction of earthquake disasters.

5. Discussion and Conclusions

Systematic collection and comprehensive analysis of the cases of earthquakes regarding the precursor-like anomalies have been an academic tradition in China. In China, *Earthquake Cases* series have been published (in Chinese with English abstract, by the Seismological Press in Beijing) regularly since the 1970s. Contemporary level of informatics allows search and analysis of different data flow including scientific publications themselves. In the case of Wenchuan, what can be seen is that different observations may have some intrinsic consistency to each other, providing heuristic clues to the preparation process of this great earthquake. Remarkably, several characteristic times, such as 2∼4 days and 1∼2 years, may reveal the preparation and approaching process of this inland great earthquake, which is in need of further investigation.

In the study on earthquake forecast/prediction, it is always much easier and much simpler to be critical or skeptical than to conduct concrete observations. Keeping this in mind, the objective of this paper is firstly to summarize what have been done either in China or in other places of the world; secondly to introduce these works, especially to non-Chinese-speaking communities; thirdly to avoid being too demanding or too skeptical in commenting on these works; and at last to propose, in a constructive way, several problems in need of consideration in future—some of them are not complicated but important. We believe that, if these problems were paid special attention to, then to much extent, more useful conclusions would be obtained, and the study on earthquake forecast/prediction would be "accelerated". And this hint is important not only for China but also for other places all over the world.

Being only 3 years after the Wenchuan earthquake, at the present time this work is still far from the stage of systematic evaluation [222–224] and/or empirical semiquantitative analysis [225–228]. More concrete conclusions need more time, although we have had an apparently good start with pretty rich (but complicated) materials.

Acknowledgments

Thanks to Professor R. Console for invitation to this special issue and patience to tolerate the delay in submission. Discussion with Harsh Gupta, V. Kossobokov, Jie Liu, Xiangchu Yin, and Yongxian Zhang stimulated and improved this investigation. Changsheng Jiang, Hanshu Peng, and Jiancang Zhuang helped in the work. Thanks are due to the staffs of the National Library of China, Beijing, for valuable advice and assistance in accessing to the databases. This work is supported by the WFSD project.

References

[1] Y. Chen and D. C. Booth, *The Wenchuan Earthquake of 2008*, Science Press, Springer, Beijing, China, 2011.

[2] A. M. Cetto, *Scientific journal publishing in the developing world?* ICSU-COSTED Occasional Paper No.3, 1998.

[3] Q. F. Chen and K. L. Wang, "The 2008 Wenchuan earthquake and earthquake prediction in China," *Bulletin of the Seismological Society of America*, vol. 100, no. 5, pp. 2840–2857, 2010.

[4] Y.-T. Che, C.-L. Liu, J.-Z. Yu, Z.-J. Guan, and J. Li, "Underground fluid anomaly and macro anomaly of Ms 8.0 Wenchuan earthquake and opinions about earthquake prediction," *Seismology and Geology*, vol. 30, no. 4, pp. 828–838, 2008 (Chinese).

[5] Z. X. Ouyang, H. X. Zhang, Z. Z. Fu, B. Gou, and W. L. Jiang, "Abnormal phenomena recorded by several earthquake precursor observation instruments before the Ms8.0 Wenchuan, Sichuan earthquake," *Acta Geologica Sinica*, vol. 83, no. 4, pp. 834–844, 2009.

[6] R. Yan, "Analysis of earthquake precursor monitoring data," in *Research Report on the Wenchuan M8.0 Earthquake*, Monitoring and Forecasting Department of China Earthquake Administration, Ed., chapter 6, pp. 170–193, Seismological Press, Beijing, China, 2009 (Chinese).

[7] X.-M. Zhang, J.-H. Ding, X.-H. Shen et al., "Electromagnetic perturbations before Wenchuan M8 earthquake and stereo electromagnetic observation system," *Chinese Journal of Radio Science*, vol. 24, no. 1, pp. 1–8, 2009 (Chinese).

[8] W. Z. Cheng, Z. J. Guan, Q. Su, X. Ruan, and Z. W. Zhang, "Precursory anomalies in Sichuan region before 2008 Wenchuan Ms8.0 earthquake and their statistical analysis," *Acta Seismologica Sinica*, vol. 33, no. 3, pp. 304–318, 2011 (Chinese).

[9] Q. Huang, "Seismicity changes prior to the Ms8.0 Wenchuan earthquake in Sichuan, China," *Geophysical Research Letters*, vol. 35, no. 23, Article ID L23308, 2008.

[10] Q. H. Huang, "Retrospective investigation of geophysical data possibly associated with the Ms8.0 Wenchuan earthquake in Sichuan, China," *Journal of Asian Earth Sciences*, vol. 41, no. 4-5, pp. 421–427, 2010.

[11] C. Y. Liu, J. Y. Liu, W. S. Chen, J. Z. Li, Y. Q. Xia, and X. Y. Cui, "An integrated study of anomalies observed before four major earthquakes: 2004 Sumatra M9.3, 2006 Pingtung M7.0, 2007 Chuetsu Oki M6.8, and 2008 Wenchuan M8.0," *Journal of Asian Earth Sciences*, vol. 41, no. 4-5, pp. 401–409, 2010.

[12] L. Wu, "Misconception analysis and suggestions for earthquake monitoring and predication," *Science & Technology Review*, vol. 26, no. 10, pp. 28–29, 2008 (Chinese).
[13] J. Liu, T. Guo, L. Yang, Y. Su, and G. Li, "Retrospection on the conclusions of earthquake tendency forecast before the Wenchuan Ms8.0 earthquake," *Earthquake Research in China*, vol. 23, no. 2, pp. 119–133, 2009.
[14] Z. C. Zhang and W. Zhang, "Some reflections on the 12 May, 2008 Wenchuan earthquake," *Earthquake*, vol. 29, no. 1, pp. 193–202, 2009 (Chinese).
[15] W. Zhao, "Pondering over the scientific thinking of earthquake prediction from the miss report of Wenchuan earthquake—re-discussing Li Siguang's earthquake prediction thought," *Engineering Science*, vol. 11, no. 6, pp. 4–15, 2009 (Chinese).
[16] The Seismological Society of China, Ed., "Proceedings of the 12th Assembly of the Seismological Society of China," *Recent Development in World Seismology*, no. 11, pp. 1–172, 2008 (Chinese).
[17] The Seismological Society of China, Ed., "Earthquake Prediction Development Forum Paper Abstract Special Collection," *Recent Development in World Seismology*, no. 4, pp. 1–103, 2009 (Chinese).
[18] The Seismological Society of China, Ed., "Abstracts from Cross-Strait Seminar on Wenchuan Earthquake," *Recent Development in World Seismology*, no. 6, pp. 1–24, 2010 (Chinese).
[19] P. Zhang, Q. Deng, G. Zhang et al., "Active tectonic blocks and strong earthquakes in the continent of China," *Science in China D*, vol. 46, supplement 2, pp. 13–24, 2003.
[20] L.-X. Gao, J.-L. Sun, and H. Zhang, "Moderate-to-strong earthquake quiescence is the most significant seismic anomaly before the Wenchuan 8.0 earthquake," *Earthquake*, vol. 30, no. 1, pp. 90–97, 2010 (Chinese).
[21] C. S. Jiang and Z. L. Wu, "Seismic moment release before the May 12, 2008, Wenchuan earthquake in Sichuan of southwest China," *Concurrency Computation Practice and Experience*, vol. 22, no. 12, pp. 1784–1795, 2010.
[22] X.-Z. Chen, X.-Y. Guo, and Y.-E. Li, "Distribution characteristics of the month-scale number for earthquakes occurred on the Longmenshan fault," *Earthquake*, vol. 30, no. 2, pp. 20–28, 2010 (Chinese).
[23] Y. Xue, J. Liu, S. Mei, and Z. Song, "Characteristics of seismic activity before the Ms8.0 Wenchuan earthquake," *Earthquake Science*, vol. 22, no. 5, pp. 519–529, 2009.
[24] C. Jiang, Z. Wu, H. Ma, and L. Zhou, "Sichuan-Yunnan versus Andaman-Sumatra: PI approach and retrospective forecast test," *Acta Seismologica Sinica*, vol. 31, no. 3, pp. 307–318, 2009 (Chinese).
[25] C. S. Jiang and Z. L. Wu, "PI forecast for the Sichuan-Yunnan region: retrospective test after the May 12, 2008, Wenchuan earthquake," *Pure and Applied Geophysics*, vol. 167, no. 6-7, pp. 751–761, 2010.
[26] L. Zou and X. Wang, "Study on the characteristics of the medium-depth seismicity before the Kunlun Mountain earthquake and the Wenchuan earthquake," *Seismological and Geomagnetic Observation and Research*, vol. 31, no. 5, pp. 37–44, 2010 (Chinese).
[27] Y. Su and J. Liu, "Quiescence anomalies of $M \geq 6.0$ earthquakes before the 2008 Wenchuan (M8.0) earthquake in Sichuan-Yunnan region," *Journal of Seismological Research*, vol. 33, no. 2, pp. 119–124, 2010 (Chinese).
[28] H.-B. Zhu, "The similar evolution of seismicity patterns of strong-moderate earthquakes before about Ms8 earthquakes of Qinghai-Tibet block," *Chinese Journal of Geophysics*, vol. 53, no. 7, pp. 1611–1621, 2010 (Chinese).
[29] X.-C. Yin, L.-P. Zhang, Y.-X. Zhang et al., "Large scale LURR anomaly before Wenchuan earthquake," *Earthquake*, vol. 29, no. 1, pp. 53–59, 2009 (Chinese).
[30] H. Yu, J. Cheng, and Y. Wan, "Load/unload response ratio and stress accumulation model before large earthquakes," *Acta Seismologica Sinica*, vol. 32, no. 5, pp. 517–528, 2010 (Chinese).
[31] C. Wang, J. Cao, H. Guo, L. Zhang, and N. Xue, "Short-term earthquake prediction in the region of Sichuan-Yunnan using method of modulated earthquake," *Earthquake Research in China*, vol. 26, no. 2, pp. 210–217, 2010 (Chinese).
[32] P. Lu, X. Zhao, Z. Cui, X. Liu, and Y. Duan, "Space-time evolution characteristics of seismic inhomogeneous degree before Wenchuan earthquake," *Journal of Institute of Disaster-Prevention Science and Technology*, vol. 10, no. 3, pp. 126–130, 2008 (Chinese).
[33] Z. Xie, Y. Zhu, X. Lei, and Z. Song, "Variation of multiple seismicity parameters used to investigate critical behavior of the Wenchuan earthquake preparation," *Acta Seismologica Sinica*, vol. 32, no. 6, pp. 659–669, 2010 (Chinese).
[34] G. Luo, M. Yang, H. Ma, and X. Xu, "Intermediate and short-trem anomalies of seismic activity energy field before the Wenchuan M8.0 earthquake," *Earthquake*, vol. 31, no. 3, pp. 135–142, 2011 (Chinese).
[35] H. C. Li and C. C. Chen, "Characteristics of long-term regional seismicity before the 2008 Wen-Chuan, China, earthquake using pattern informatics and genetic algorithms," *Natural Hazards and Earth System Sciences*, vol. 11, no. 3, pp. 1003–1009, 2011.
[36] S. Zhao, S. Xu, P. Wu, and L. Ma, "Earthquake occurrence correlated with the movement of the Sun and the Moon," *Science & Technology Review*, vol. 29, no. 13, pp. 18–23, 2011 (Chinese).
[37] H. Wang, X. Zhao, Y. Li, and X. Chen, "A study on the relationships between Earth rotation and the occurrences of several strong earthquakes," *Earthquake*, vol. 31, no. 2, pp. 33–41, 2011 (Chinese).
[38] F. Du, X.-Z. Wen, P.-Z. Zhang, and Q.-L. Wang, "Interseismic deformation across the Longmenshan fault zone before the 2008 M8.0 Wenchuan earthquake," *Chinese Journal of Geophysics*, vol. 52, no. 11, pp. 2729–2738, 2009 (Chinese).
[39] G. Gu, W. Wang, G. Meng, and Y. Xu, "Crustal movements before and after the Wenchuan earthquake as detected by GPS observations," *Geomatics and Information Science of Wuhan University*, vol. 34, no. 11, pp. 1336–1339, 2009 (Chinese).
[40] G. Gu, G. Meng, and Y. Fang, "Crustal movement in the earthquake area before and after 2008 Wenchuan earthquake as detected by precise single epoch positioning of GPS observations," *Acta Seismologica Sinica*, vol. 33, no. 3, pp. 319–326, 2011 (Chinese).
[41] C. Zhang, H. Shao, C. Shi, and J. Chen, "Research on surface variation characteristics of ground tilt in Longmenshan fault zone before Wenchuan Ms8.0 earthquake," *Journal of Geodesy and Geodynamics*, vol. 31, supplement, pp. 6–9, 2011 (Chinese).
[42] Q. Jiao, X. Yang, L. Xu, and B. Wang, "Preliminary study on motion characteristics of Longmenshan fault before and after Ms8.0 Wenchuan earthquake," *Journal of Geodesy and Geodynamics*, vol. 28, no. 4, pp. 7–11, 2008 (Chinese).
[43] L. Guo, L. Ta, D. Sun, and X. Du, "Vertical deformation characteristic of Longmenshan fault zone before Wenchuan

Ms8.0 earthquake," *South China Journal of Seismology*, vol. 29, no. 3, pp. 1–8, 2009 (Chinese).

[44] Y. Fang, Z. Jiang, and G. Gu, "Oscillation analysis of GPS horizontal time series before the Wenchuan earthquake," *Journal of Seismological Research*, vol. 33, no. 2, pp. 125–130, 2010 (Chinese).

[45] L. Guo, X. Hu, F. Zhang, C. Chen, and D. Sun, "Baseline variation of GPS continuous sites and current activity of Qinghai-Tibet block," *Journal of Geodesy and Geodynamics*, vol. 29, no. 4, pp. 10–14, 2009 (Chinese).

[46] Y. Zhang and Y. Wu, "Anomaly of fixed deformation data and explain before the 2008 Wenchuan earthquake," *Geomatics and Information Science of Wuhan University*, vol. 35, no. 1, pp. 25–29, 2010 (Chinese).

[47] C. Ke, Z. Li, and M. Dou, "Anomalous response of crust tilt tidal factor γ value in Shanxi before Wenchuan Ms8.0 earthquake," *Journal of Geodesy and Geodynamics*, vol. 28, no. 6, pp. 56–60, 2008 (Chinese).

[48] Y. Jing, H. Zhang, Y. Sun, H. Li, L. Fan, and Y. Xiong, "Abnormal changes of crustal deformation before Wenchuan 8.0 earthquake observed by BSQ model digital tilt meter," *Geological Journal of China Universities*, vol. 15, no. 3, pp. 358–364, 2009 (Chinese).

[49] W. Cheng, X. Ruan, H. Qiao, Z. Zhang, and J. Yong, "Research on the dynamic change of regional stress fields before the Ms8.0 Wenchuan earthquake," *Earthquake Research in China*, vol. 23, no. 3, pp. 244–256, 2009.

[50] Z. S. Jiang, Y. Wu, Y. Fang, P. Li, and W. Wang, "The dynamic characteristics of strain fields and crustal movement before the Wenchuan earthquake (Ms=8.0)," *Earthquake*, vol. 23, no. 3, pp. 257–265, 2009.

[51] G. Fan and Q. Jiao, "Analysis of fault activity characteristics in Sichuan-Yunnan area before Wenchuan Ms8.0 earthquake," *Journal of Geodesy and Geodynamics*, vol. 28, no. 6, pp. 27–30, 2008 (Chinese).

[52] T. Chen, "Seismic rate and small seismic swarm changes before the 2008 Wenchuan M8.0 earthquake," *Earthquake Research in Sichuan*, no. 3, pp. 23–29, 2010 (Chinese).

[53] J. Zhang and Q. Liu, "Processing and analysis of four-component borehole strain observations," *Journal of Geodesy and Geodynamics*, vol. 30, no. 6, pp. 6–9, 2010 (Chinese).

[54] G.-L. Diao, X.-W. Xu, Y. Chen et al., "The precursory significance of tectonic stress field transformation before the Wenchuan Mw7.9 earthquake and the Chi-Chi Mw7.6 earthquake," *Chinese Journal of Geophysics*, vol. 54, no. 1, pp. 128–136, 2011 (Chinese).

[55] Y. Zhang, Y. Wu, and P. Lv, "Characteristics of deformation anomaly obtained from tilt and strain observations before the Wenchuan Ms8.0 earthquake," *Acta Seismologica Sinica*, vol. 31, no. 2, pp. 152–159, 2009 (Chinese).

[56] Q.-L. Guo, C.-H. Wang, H.-S. Ma, and C.-G. Wang, "In-situ hydro-fracture stress measurement before and after the Wenchuan Ms8.0 earthquake of China," *Chinese Journal of Geophysics*, vol. 52, no. 5, pp. 1395–1401, 2009 (Chinese).

[57] H. Peng, X. M. Ma, and J. J. Jiang, "Process analysis of in-situ strain during the Ms8.0 Wenchuan earthquake —data from the stress monitoring station at Shandan," *Acta Geologica Sinica*, vol. 83, no. 4, pp. 754–766, 2009.

[58] A. Niu, L. Zhan, W. Yan, and P. Ji, "Borehole strain measurement and application to earthquake prediction in China," *Journal of Geodesy and Geodynamics*, vol. 31, no. 2, pp. 48–52, 2011 (Chinese).

[59] L. Wang, Y. Li, F. Li et al., "Temporal variation of Vp/Vs, Vp and Vs before and after 2008 Wenchuan earthquake," *Acta Seismologica Sinica*, vol. 33, no. 1, pp. 1–14, 2011 (Chinese).

[60] X. B. Du, "Two types of changes in apparent resistivity in earthquake prediction," *Science China Earth Sciences*, vol. 54, no. 1, pp. 145–156, 2011.

[61] W. Xiao and H. Guan, "Anomalous change features of resistivity before the Wenchuan M8.0 earthquake and other large earthquake in China," *Northwestern Seismological Journal*, vol. 31, no. 4, pp. 349–354, 2009 (Chinese).

[62] X.-M. Zhang, M. Li, and H.-P. Guan, "Anomaly analysis of earth resistivity observations before the Wenchuan earthquake," *Earthquake*, vol. 29, no. 1, pp. 108–115, 2009 (Chinese).

[63] M. Yang, D. Chen, Y. Huang, and H. Gong, "Abnormal gas well pressure of Zhongba gas field, Sichuan, before and after the Wenchuan earthquake," *Acta Seismologica Sinica*, vol. 33, no. 4, pp. 505–514, 2011 (Chinese).

[64] H. S. Peng, Z. L. Wu, and C. S. Jiang, "Pre-seismic changes of noise correlation function (NCF) before the Wenchuan earthquake?" *Concurrency Computation Practice and Experience*, vol. 22, no. 12, pp. 1774–1783, 2010.

[65] Y. Zhu, W. Liang, Y. Xu, S. Guo, and F. Liu, "Dynamic variation of gravity field before and after Wenchuan Ms8.0 earthquake," *Acta Seismologica Sinica*, vol. 32, no. 6, pp. 633–640, 2010 (Chinese).

[66] Y. Q. Zhu, F. B. Zhan, J. C. Zhou, W. F. Liang, and Y. M. Xu, "Gravity measurements and their variations before the 2008 Wenchuan earthquake," *Bulletin of the Seismological Society of America B*, vol. 100, no. 5, pp. 2815–2824, 2010.

[67] Y. Zhu, F. Liu, and S. Guo, "Temporal variation of gravity field before and after Wenchuan Ms8.0 earthquake," *Geodesy and Geodynamics*, vol. 2, no. 2, pp. 33–38, 2011.

[68] Y. Zhu, F. Liu, W. Liang, and Y. Xu, "Gravity variation associated with Wenchuan earthquake in western Sichuan," *Geodesy and Geodynamics*, vol. 2, no. 1, pp. 55–60, 2011.

[69] X. Hao, X. Hu, H. Xu et al., "Gravity disturbance before Wenchuan Ms8.0 earthquake," *Journal of Geodesy and Geodynamics*, vol. 28, no. 3, pp. 129–131, 2008 (Chinese).

[70] X. Hao and X. Hu, "Disturbance before the Wenchuan earthquake detected by broadband seismometer," *Progress in Geophysics*, vol. 23, no. 4, pp. 1332–1335, 2008 (Chinese).

[71] X. Hao and X. Hu, "Are "third microseisms" in anomalous tremor before the great Wenchuan earthquake?" *Progress in Geophysics*, vol. 24, no. 4, pp. 1213–1215, 2009 (Chinese).

[72] L. Yang, "Preliminary study on the tremors with special frequency recorded by seismograph before Wenchuan earthquake and its charaters," *Recent Developments in World Seismology*, no. 1, pp. 14–19, 2009 (Chinese).

[73] L. Yang, J. Wang, J. Feng, Y. Hu, J. Chen, and J. Yao, "Preliminary study and application on the tremors with lower frequency recorded by seismograph before the Wenchuan earthquake," *Earthquake Research in China*, vol. 25, no. 4, pp. 356–366, 2009 (Chinese).

[74] L. Yin and L. Yang, "Research on low-frequency wave of the broadband digital data and the information of short-imminent precursor before strong earthquakes," *Northwestern Seismological Journal*, vol. 32, no. 1, pp. 82–87, 2010 (Chinese).

[75] Y. Zhang, Y. Wu, Y. Lv, J. Hu, and P. Lu, "Anomalies observed by ultra broadband seismometer before Wenchuan earthquake," *Journal of Geodesy and Geodynamics*, vol. 31, no. 1, pp. 15–18, 2011 (Chinese).

[76] M. Li, J. Lu, X. Su, and Z. Feng, "A study on fractal Brownian motion of geomagnetic observations before large earthquakes," *Acta Seismologica Sinica*, vol. 31, no. 6, pp. 650–659, 2009 (Chinese).

[77] Y.-Y. Fan, X.-B. Du, J. Zlotnicki et al., "The electromagnetic phenomena before the Ms8.0 Wenchuan earthquake," *Chinese Journal of Geophysics*, vol. 53, no. 12, pp. 2887–2898, 2010 (Chinese).

[78] J. Hu, W. Liu, M. Guo, and H. Zheng, ""Double low-points" anomaly in daily variation of vertical component of geomagnetic field before the Ms8.0 Wenchuan earthquake," *Earthquake Science*, vol. 22, no. 5, pp. 539–543, 2009.

[79] W. Wang, J. Ding, S. Yu, and Y. Zhang, "Short-term and imminent geomagnetic anomalies of the Wenchuan Ms8.0 earthquake and exploration on earthquake forecast," *Earthquake Science*, vol. 22, no. 2, pp. 135–141, 2009.

[80] H. K. Jhuang, Y. Y. Ho, Y. Kakinami et al., "Seismo-ionospheric anomalies of the GPS-TEC appear before the 12 May 2008 magnitude 8.0 Wenchuan earthquake," *International Journal of Remote Sensing*, vol. 31, no. 13, pp. 3579–3587, 2010.

[81] X. Zhang, X. Hu, and C. Zhang, "Ionospheric response with Wenchuan big earthquake by occulted data," *GNSS World of China*, no. 5, pp. 1–5, 2008 (Chinese).

[82] J. Blecki, M. Parrot, and R. Wronowski, "Studies of the electromagnetic field variations in ELF frequency range registered by DEMETER over the Sichuan region prior to the 12 May 2008 earthquake," *International Journal of Remote Sensing*, vol. 31, no. 13, pp. 3615–3629, 2010.

[83] Y. Y. Zhou, Y. Wu, X. J. Qiao, F. Y. Zhu, and J. Yang, "Anomalous variations of ionospheric VTEC before Ms8.0 Wenchuan earthquake," *Chinese Journal of Geophysics*, vol. 53, no. 3, pp. 556–566, 2010, (with Chinese abstract).

[84] X.-M. Zhang, X.-H. Shen, X.-Y. Ouyang et al., "Ionosphere VLF electric field anomalies before Wenchuan M8 earthquake," *Chinese Journal of Radio Science*, vol. 24, no. 6, pp. 1024–1032, 2009 (Chinese).

[85] H. Yu, H. Zhou, and X. Qiao, "Study on wave propagation of ELF emission anomaly before Ms8.0 Wenchuan earthquake," *Acta Seismologica Sinica*, vol. 32, no. 6, pp. 641–648, 2010 (Chinese).

[86] Z. An, Y. Fan, J. Liu et al., "Analysis on ion temperature variation detected by DEMETER before 2008 Wenchuan Ms8.0 earthquake," *Acta Seismologica Sinica*, vol. 32, no. 6, pp. 754–759, 2010 (Chinese).

[87] C. C. Hsiao, J. Y. Liu, K. I. Oyama et al., "Seismo-ionospheric precursor of the 2008 Mw7.9 Wenchuan earthquake observed by FORMOSAT-3/COSMIC," *GPS Solutions*, vol. 14, no. 1, pp. 83–89, 2009.

[88] Z. Nie, F. Zhu, and N. Fu, "Application of Kalman filtering in detecting ionospheric TEC anomaly prior to earthquake," *Journal of Geodesy and Geodynamics*, vol. 31, no. 3, pp. 47–50, 2011 (Chinese).

[89] J. Xiong, Y. Wu, Y. Zhou, and J. Lin, "Ionospheric anomalies detected before 2008 Wenchuan earthquake," *Journal of Geodesy and Geodynamics*, vol. 31, no. 2, pp. 28–31, 2011 (Chinese).

[90] J. Lin, Y. Wu, and F. Zhu, "Ionosphere TEC anomalous disturbance of pre-seism," *Geomatics and Information Science of Wuhan University*, vol. 34, no. 8, pp. 975–978, 2009 (Chinese).

[91] S. Sarkar and A. K. Gwal, "Satellite monitoring of anomalous effects in the ionosphere related to the great Wenchuan earthquake of May 12, 2008," *Natural Hazards*, vol. 55, no. 2, pp. 321–332, 2010.

[92] J. Xiong, Y. Wu, F. Zhu, J. Lin, Y. Zhou, and J. Yang, "Anomalous disturbance of ionospheric NmF2 during Wenchuan earthquake," *Journal of Geodesy and Geodynamics*, vol. 28, no. 6, pp. 22–26, 2008 (Chinese).

[93] F. Zhu, Y. Wu, J. Lin, Y. Zhou, J. Xiong, and J. Yang, "Study on ionospheric TEC anomaly prior to Wenchuan Ms8.0 earthquake," *Journal of Geodesy and Geodynamics*, vol. 28, no. 6, pp. 16–21, 2008 (Chinese).

[94] J. W. Lin, "Two-dimensional ionospheric total electron content map (TEC) seismo-ionospheric anomalies through image processing using principal component analysis," *Advances in Space Research*, vol. 45, no. 11, pp. 1301–1310, 2010.

[95] B. Zhao, W. Wan, M. Wang, L. Liu, and B. Ning, "Recent advances on the ionospheric pre-cursors of earthquakes and ionospheric variations prior to Wenchuan earthquake," *Science & Technology Review*, vol. 26, no. 11, pp. 30–34, 2008 (Chinese).

[96] J. Li, G. Meng, M. Wang, H. Liao, and X. Shen, "Investigation of ionospheric TEC changes related to the 2008 Wenchuan earthquake based on statistic analysis and signal detection," *Earthquake Science*, vol. 22, no. 5, pp. 545–553, 2009.

[97] J. Y. Liu, Y. I. Chen, C. H. Chen et al., "Seismoionospheric GPS total electron content anomalies observed before the 12 May 2008 Mw7.9 Wenchuan earthquake," *Journal of Geophysical Research A*, vol. 114, no. 4, Article ID A04320, 2009.

[98] T. G. Yu, T. Mao, Y. G. Wang, and J. S. Wang, "Study of the ionospheric anomaly before the Wenchuan earthquake," *Chinese Science Bulletin*, vol. 54, no. 6, pp. 1080–1086, 2009.

[99] Z.-C. Zeng, B. Zhang, G.-Y. Fang, D.-F. Wang, and H.-J. Yin, "The analysis of ionospheric variations before Wenchuan earthquake with DEMETER data," *Chinese Journal of Geophysics*, vol. 52, no. 1, pp. 11–19, 2009 (Chinese).

[100] X. Zhang, X. Shen, J. Liu, X. Ouyang, J. Qian, and S. Zhao, "Analysis of ionospheric plasma perturbations before Wenchuan earthquake," *Natural Hazards and Earth System Science*, vol. 9, no. 4, pp. 1259–1266, 2009.

[101] Y. Y. Zhou, Y. Wu, X. J. Qiao, and X. X. Zhang, "Ionospheric anomalies detected by ground-based GPS before the Mw7.9 Wenchuan earthquake of May 12, 2008, China," *Journal of Atmospheric and Solar-Terrestrial Physics*, vol. 71, no. 8-9, pp. 959–966, 2009.

[102] F. Zhu, Y. Wu, J. Lin, Y. Zhou, J. Xiong, and J. Yang, "Study on method of detecting ionospheric TEC anomaly before earthquake," *Journal of Geodesy and Geodynamics*, vol. 29, no. 3, pp. 50–54, 2009 (Chinese).

[103] F. Zhu, Y. Wu, J. Lin, Y. Zhou, J. Xiong, and J. Yang, "Anomalous response of ionospheric VTEC before the Wenchuan earthquake," *Acta Seismologica Sinica*, vol. 31, no. 2, pp. 180–187, 2009 (Chinese).

[104] Z.-H. Ding, J. Wu, S.-J. Sun, J.-S. Chen, and P.-P. Ban, "The variation of ionosphere on some days before the Wenchuan earthquake," *Chinese Journal of Geophysics*, vol. 53, no. 1, pp. 30–38, 2010 (Chinese).

[105] Y. Kakinami, J. Y. Liu, L. C. Tsai, and K. I. Oyama, "Ionospheric electron content anomalies detected by a FORMOSAT-3/COSMIC empirical model before and after the Wenchuan earthquake," *International Journal of Remote Sensing*, vol. 31, no. 13, pp. 3571–3578, 2010.

[106] S. A. Pulinets, V. G. Bondur, M. N. Tsidilina, and M. V. Gaponova, "Verification of the concept of seismoionospheric coupling under quiet heliogeomagnetic conditions, using the Wenchuan (China) earthquake of May 12, 2008, as an example," *Geomagnetism and Aeronomy*, vol. 50, no. 2, pp. 231–242, 2010.

[107] T. Xu, Y. Hu, J. Wu, Z. Wu, Y. Suo, and J. Feng, "Giant disturbance in the ionospheric F2 region prior to the M8.0 Wenchuan earthquake on 12 May 2008," *Annales Geophysicae,*, vol. 28, no. 8, pp. 1533–1538, 2010.

[108] X. M. Zhang, X. H. Shen, J. Liu, X. Y. Ouyang, J. D. Qian, and S. F. Zhao, "Ionospheric perturbations of electron density before the Wenchuan earthquake," *International Journal of Remote Sensing*, vol. 31, no. 13, pp. 3559–3569, 2010.

[109] B. Q. Zhao, M. Wang, T. Yu, G. R. Xu, W. X. Wan, and L. B. Liu, "Ionospheric total electron content variations prior to the 2008 Wenchuan earthquake," *International Journal of Remote Sensing*, vol. 31, no. 13, pp. 3545–3557, 2010.

[110] Y. Zhao, X. Zhang, and J. Liu, "Perturbation analysis of the ionospheric TEC before and after the Wenchuan earthquake," *Progress in Geophysics*, vol. 25, no. 2, pp. 447–453, 2010 (Chinese).

[111] F. Zhu, Y. Wu, J. Lin, and Y. Zhou, "Temporal and spatial characteristics of VTEC anomalies before Wenchuan Ms8.0 earthquake," *Geodesy and Geodynamics*, vol. 1, no. 1, pp. 23–28, 2010.

[112] F. Zhu, Y. Wu, and N. Fu, "Application of Kalman filter in detecting pre-earthquake ionospheric TEC anomaly," *Geodesy and Geodynamics*, vol. 2, no. 2, pp. 43–47, 2011.

[113] M. V. Klimenko, V. V. Klimenko, I. E. Zakharenkova, S. A. Pulinets, B. Zhao, and M. N. Tsidilina, "Formation mechanism of great positive TEC disturbances prior to Wenchuan earthquake on May 12, 2008," *Advances in Space Research*, vol. 48, no. 3, pp. 488–499, 2011.

[114] J. W. Lin, "Use of principal component analysis in the identification of the spatial pattern of an ionospheric total electron content anomalies after China's May 12, 2008, M = 7.9 Wenchuan earthquake," *Advances in Space Research*, vol. 47, no. 11, pp. 1983–1989, 2011.

[115] Y. Wu, N. Fu, J. Lin et al., "Research on TEC anomalies before Ms8.0 Wenchuan earthquake by using Kalman filtering," *Journal of Geodesy and Geodynamics*, vol. 31, no. 2, pp. 23–27, 2011 (Chinese).

[116] T. Xu, Y. L. Hu, J. A. Wu et al., "Anomalous enhancement of electric field derived from ionosonde data before the great Wenchuan earthquake," *Advances in Space Research*, vol. 47, no. 6, pp. 1001–1005, 2011.

[117] T. Xu, J. Wu, Z. Zhao et al., "Monitoring ionospheric variations before earthquakes using the vertical and oblique sounding network over China," *Natural Hazards and Earth System Sciences*, vol. 11, no. 4, pp. 1083–1089, 2011.

[118] J. Yang, Y. Wu, and Y. Zhou, "Probe into seismo-ionospheric anomaly of Wenchuan Ms8.0 earthquake based on computerized ionospheric tomography," *Journal of Geodesy and Geodynamics*, vol. 31, no. 1, pp. 9–14, 2011 (Chinese).

[119] L. Li, J. Yang, J. Huang, and Q. Wu, "Analysis about the specific background of rare drought and intense heat and great floodwater which should not be ignored before Wenchuan earthquake," *Plateau Earthquake Research*, vol. 20, no. 4, pp. 69–75, 2008 (Chinese).

[120] X. Jiang and Y. Li, "The statistical analysis of earthquake and precipitation in Sichuan Province," *Plateau and Mountain Meteorology Research*, vol. 28, no. 2, pp. 33–36, 2008 (Chinese).

[121] J. Li and S. Liu, "On the anomalies of crustal deformation & surface temperature and its correlation: a case study of Wenchuan earthquake," *Geography and Geo-Information Science*, vol. 25, no. 1, pp. 79–83, 2009 (Chinese).

[122] L. J. Wei, J. F. Guo, J. H. Lu, Z. Q. Lu, H. B. Li, and H. Cai, "Satellite thermal infrared earthquake precursor to the Wenchuan Ms8.0 earthquake in Sichuan, China, and its analysis on geo-dynamics," *Acta Geologica Sinica*, vol. 83, no. 4, pp. 767–775, 2009.

[123] L. Wei, J. Guo, H. Cai, H. Li, and Z. J. John, "Satellite thermal infrared anomaly: a short-term and impending earthquake precursor before the Wenchuan Ms8.0 earthquake in Sichuan, China," *Acta Geoscientica Sinica*, vol. 29, no. 5, pp. 583–591, 2008 (Chinese).

[124] X. Guo, Y. Zhang, M. Zhong, W. Shen, and C. Wei, "Variation characteristics of OLR for the Wenchuan earthquake," *Chinese Journal Geophysics*, vol. 53, no. 6, pp. 980–988, 2010.

[125] Y. S. Zhang, X. A. Guo, M. J. Zhong, W. R. Shen, W. Li, and B. He, "Wenchuan earthquake: brightness temperature changes from satellite infrared information," *Chinese Science Bulletin*, vol. 55, no. 18, pp. 1917–1924, 2010.

[126] F. Jing, X.-H. Shen, C.-L. Kang, Q.-Y. Meng, and P. Xiong, "Anomalies of outgoing longwave radiation before some medium to large earthquakes," *Earthquake*, vol. 29, no. 4, pp. 117–122, 2009 (Chinese).

[127] Y. F. He, D. M. Yang, H. R. Chen, J. D. Qian, R. Zhu, and M. Parrot, "SNR changes of VLF radio signals detected onboard the DEMETER satellite and their possible relationship to the Wenchuan earthquake," *Science in China D*, vol. 52, no. 6, pp. 754–763, 2009.

[128] W. Min and X. Xu, "Primary analysis of the variation of surface air temperature before and after Wenchuan earthquake," *Plateau and Mountain Meteorology Research*, vol. 28, no. 2, pp. 42–46, 2008 (Chinese).

[129] W. Ma, "Abnormal phenomenon of NCEP before Wenchuan earthquake," *Science & Technology Review*, vol. 26, no. 10, pp. 37–39, 2008 (Chinese).

[130] M. Li, C. Kang, Z. Li, F. Jing, Y. Xue, and W. Yan, "Abnormal surface latent heat flux prior to the Wenchuan Ms8.0 earthquake," *Earthquake*, vol. 30, no. 3, pp. 64–71, 2010 (Chinese).

[131] H. Zeng, G. Zhu, G. Qin, H. Chen, and Y. Li, "Abnormal variation of thermosphere atmospheric density during the period of big earthquake," *Chinese Journal of Space Science*, vol. 31, no. 3, pp. 318–322, 2011 (Chinese).

[132] L. Wu, S. Liu, Y. Chen, B. Ma, and L. Li, "Satellite thermal infrared and cloud abnormities before Wenchuan earthquake," *Science & Technology Review*, vol. 26, no. 10, pp. 32–36, 2008 (Chinese).

[133] X.-T. Zhang, Y.-X. Zhang, and D.-H. Xu, "Investigation of the macroscopic anomalies before and after the Wenchuan M8.0 earthquake," *Earthquake*, vol. 29, no. 2, pp. 104–117, 2009 (Chinese).

[134] W. Cheng, X. Wu, Z. Guan, H. Zhu, and Z. Lu, "Discussion on the macroscopic anomaly phenomenae reported before the Wenchuan M8.0 earthquake," *Earthquake Research in Sichuan*, no. 1, pp. 1–7, 2010 (Chinese).

[135] D. Xu, "Field investigation of macro-anomalies before the Wenchuan Ms8.0 earthquake, Sichuan, China," *Earthquake*, vol. 30, no. 2, pp. 121–133, 2010 (Chinese).

[136] X. T. Zhang, Y. X. Zhang, and D. H. Xu, "Investigation of the macroscopic anomalies before and after the M8.0 Wenchuan earthquake," *Earthquake Research in China*, vol. 24, no. 1, pp. 48–69, 2010.

[137] W. Yan, C. Zhu, X. Li, and H. Zhang, "Investingation and analysis on macroscopic anomalies of earthquake before and after Wenchuan Ms8.0 earthquake in Longnan area of Gansu Province," *Northwestern Seismological Journal*, vol. 33, no. 1, pp. 67–70, 2011 (Chinese).

[138] Y. Li, Y. Liu, Z. Jiang et al., "Behavioral change related to Wenchuan devastating earthquake in mice," *Bioelectromagnetics*, vol. 30, no. 8, pp. 613–620, 2009.

[139] L. L. Chen, X. A. Hu, J. A. Zheng et al., "Increases in energy intake, insulin resistance and stress in rats before Wenchuan

earthquake far from the epicenter," *Experimental Biology and Medicine*, vol. 235, no. 10, pp. 1216–1223, 2010.

[140] B. Ma, L. Wu, and S. Liu, "NDVI variation features before Wenchuan Ms8.0 earthquake," *Science & Technology Review*, vol. 28, no. 13, pp. 52–57, 2010 (Chinese).

[141] Y. Li, "Possibility to detect Wenchuan M8 earthguake by the earthquake warning system," *Progress in Geophysics*, vol. 23, no. 7, pp. 969–971, 2008 (Chinese).

[142] F. Jiang and Q. Gao, "Application of seismo-geochemical methods for Sichuan Province in Wenchuan 8.0 magnitude earthquake of middle-term prediction succeed at according analysis," *Frontier Science*, vol. 3, no. 2, pp. 13–21, 2009 (Chinese).

[143] F. Y. Qian, B. R. Zhao, W. Qian et al., "Impending HRT wave precursors to the Wenchuan Ms8.0 earthquake and methods of earthquake impending prediction by using HRT wave," *Science in China D*, vol. 52, no. 10, pp. 1572–1584, 2009.

[144] L. S. Zhou, Z. H. Qiu, and L. Tang, "Statistical test of precursory waves before Wenchuan Ms8.0 earthquake," *Journal of Geodesy and Geodynamics*, vol. 29, no. 2, pp. 24–28, 2009 (Chinese).

[145] D. Rong and Y. Li, "The changing characteristics of seismic correlation length before Wenchuan M8.0 earthquake," *Northwestern Seismological Journal*, vol. 32, no. 1, pp. 54–58, 2010 (Chinese).

[146] L. Ming, "An explanation on short term low-temperature climate before strong earthquakes," *Journal of Institute of Disaster-Prevention Science and Technology*, vol. 12, no. 3, pp. 133–137, 2010 (Chinese).

[147] Z. Qiu, B. Zhang, S. Chi, L. Tang, and M. Song, "Abnormal strain changes observed at Guza before the Wenchuan earthquake," *Science China Earth Sciences D*, vol. 54, no. 2, pp. 233–240, 2010.

[148] S. Gao, X. Du, Y. Su et al., "The variation characteristics of precursor data in Wudu Seismic Station and the earthquake activity in the boundary area between Gansu and Sichuan Province in recent years," *Northwestern Seismological Journal*, vol. 31, no. 2, pp. 167–173, 2009 (Chinese).

[149] S. D. Gao, J. Tang, X. B. Du et al., "The change characteristics of electromagnetic field before to after Wenchuan Ms8.0 earthquake," *Chinese Journal of Geophysics*, vol. 53, no. 3, pp. 512–525, 2010 (Chinese).

[150] X. Xing, J. Mao, H. Shao, and S. Zhang, "Converted wavelet applied in analysis of well level data in Guanzhong area," *Plateau Earthquake Research*, vol. 21, no. 4, pp. 1–8, 2009 (Chinese).

[151] F. An, "Analysis on short-imminent anomalies of Liujiaxia deformation before Wenchuan earthquake," *Plateau Earthquake Research*, vol. 21, no. 2, pp. 28–31, 2009 (Chinese).

[152] S. Zhang, W. Fang, Y. Shu, J. Li, and Y. Peng, "Study on the anomaly characteristics of observation data in Zhouzhi deep borehole before Wenchuan earthquake," *Journal of Institute of Disaster-Prevention Science and Technology*, vol. 11, no. 1, pp. 20–27, 2009 (Chinese).

[153] X. Zhao, F. Huang, X. Wang, S. Zhang, D. Chen, and D. Shi, "Anomalous characteristics of gas Hg in Zhouzhi well, Shaanxi Province during Wenchuan Ms8.0 earthquake and its aftershocks," *Inland Earthquake*, vol. 24, no. 3, pp. 236–240, 2010 (Chinese).

[154] J. Zhang, X. Liu, T. Tang, and J. Ma, "Research on dynamic evolution characteristics of geomagnetic field in Chinese mainland before and after Wenchuan Ms8.0 earthquake," *Journal of Seismological Research*, vol. 32, no. 3, pp. 231–234, 2009 (Chinese).

[155] J. Zhang, X. Liu, L. Yao, X. Ma, Y. Yuan, and X. Yin, "Study on anomalous change characters of electromagnetic disturbance before the Wenchuan Ms8.0 earthquake," *Seismological and Geomagnetic Observation and Research*, vol. 31, no. 5, pp. 56–60, 2010 (Chinese).

[156] L. Zhang, "The typical precursor anomaly of ground fluid before Wenchuan earthquake in Yunnan region," *Seismological and Geomagnetic Observation and Research*, vol. 31, no. 6, pp. 40–44, 2010 (Chinese).

[157] L. Zhang, D. He, B. Shen, and Y. Su, "Probing the long-term anomaly of groundwater level of Shuifu in Yunnan area before the Wenchuan Ms8.0 earthquake," *Journal of Seismological Research*, vol. 33, no. 2, pp. 159–163, 2010 (Chinese).

[158] P. Qiu, Y. Wang, and G. Yang, "Analysis on underground water temperature anomaly in Qinghai before Wenchuan Ms8.0 earthquake," *Journal of Institute of Disaster-Prevention Science and Technology*, vol. 12, no. 1, pp. 73–78, 2010 (Chinese).

[159] Y. Zhang, X. Liu, Q. Chang, Q. Kang, and Y. Chen, "Analysis on the anomalies of Wenchuan earthquake and characteristics of postseismic effect," *Plateau Earthquake Research*, vol. 21, no. 3, pp. 22–27, 2009 (Chinese).

[160] P. Zhang, D. Zhang, W. Zhu, L. Fan, R. Chen, and J. Yan, "Anomalous Earth stress of the Ms8 Wenchuan earthquake in Sichuan, China—recording from piezomagnetic frequency measurement to the Earth stress," *Acta Geologica Sinica*, vol. 82, no. 12, pp. 1788–1799, 2008 (Chinese).

[161] Z. Song, Z. Wang, Y. Lv, S. Li, and J. Li, "Study on body strain characteristics of Xiyang Seismological Station, Shanxi, before Wenchuan, Sichuan, 8.0 earthquake and coseismic effect," *Earthquake Research in Shanxi*, vol. 2, pp. 19–20, 2009 (Chinese).

[162] S. Zhang, R. Liu, Y. Ning, L. Tang, and B. Li, "Analysis of characteristics of precursor wave of low frequency in Shanxi before Wenchuan Ms8.0 earthquake," *Journal of Geodesy and Geodynamics*, vol. 29, no. 6, pp. 35–39, 2009 (Chinese).

[163] Z. Liu, X. Yang, S. Xue, B. Li, and M. Song, "Analysis on anomalous variations in observation data of Shanxi Crustal Deformation Network before several earthquake," *Earthquake Research in Shanxi*, no. 2, pp. 31–33, 2010 (Chinese).

[164] J. Yang and C. Zhang, "Discussion on the correlation between metal pendulum ground tiltmeters data at Hancheng, Shannxi Seismological Station and its surrounding seismic activities," *Earthquake Research in Shanxi*, vol. 4, pp. 27–29, 2010 (Chinese).

[165] M. Li, J. Lu, Y. Chang, and X. Liu, "ULF electromagnetic anomaly observed at Gaobeidian and Ningjin seismic stations before Wenchuan 8.0 earthquake," *Recent Developments in World Seismology*, vol. 7, pp. 76–82, 2009 (Chinese).

[166] H. Yin, J. Li, X. Dong, and P. Xu, "On characteristics of crustal movement of Shandong and surrounding areas before and after Wenchuan Ms8.0 earthquake," *Journal of Geodesy and Geodynamics*, vol. 29, no. 3, pp. 23–27, 2009 (Chinese).

[167] S. Lu, Q. Wang, X. Lin et al., "Analysis of anomalies about pendulum tiltmeter at Taian seismostation before Wenchuan earthquake," *Journal of Geodesy and Geodynamics*, vol. 31, supplement, pp. 19–23, 2011 (Chinese).

[168] S. Su, J. Li, Q. Zhang, S. Yang, and Z. Song, "The response of crustal deformation data in Yixian Seismic Station to Wenchuan Ms8.0 earthquake," *North China Earthquake Sciences*, vol. 27, no. 2, pp. 54–58, 2009 (Chinese).

[169] J. Zhang, G. Zhao, J. Wang, T. Tang, and L. Qi, "Preliminary study on the relationship between the Ms8.0 Wenchuan earthquake of 2008 and the anomalies of earth resistivity

observed at Qingdao seismic station," *Seismology and Geology*, vol. 32, no. 3, pp. 409–416, 2010 (Chinese).

[170] H. Zhang, J. Guo, Z. Xue, C. Yu, F. Li, and J. Zhou, "Analysis on geothermal and water level response to Wenchuan earthquake in Changli Well," *North China Earthquake Sciences*, vol. 27, no. 4, pp. 46–49, 2009 (Chinese).

[171] D. Liu, "Discussion on relation between anomalies of water temperature and Radon in Ningbo station and Wenchuan Ms8.0 earthquake," *Journal of Geodesy and Geodynamics*, vol. 28, no. 6, pp. 53–55, 2008 (Chinese).

[172] J. Zhang, J. Ding, X. Shen et al., "Abnormal count rate of Yangbajing neutron-muon telescope before Wenchuan earthquake," *Chinese Journal of Radio Science*, vol. 25, no. 2, pp. 227–233, 2010 (Chinese).

[173] J. Wang, Y. Chen, Z. Ye, and S. Liu, "Property analysis of cosmic rays before and during the great Wenchuan earthquake," *Progress in Geophysics*, vol. 25, no. 1, pp. 137–142, 2010 (Chinese).

[174] B. Deng, M. Yang, J. Huang, and W. Zhao, "Study on VTEC anomaly of ionosphere in south China before and after Wenchuan earthquake," *South China Journal of Seismology*, vol. 29, no. 4, pp. 8–15, 2009 (Chinese).

[175] M. Yang, B. Deng, W. Zhao, and J. Huang, "Study on abnormal characteristics of ionosphere TEC above South-China responding to two strong earthquakes," *Journal of Geodesy and Geodynamics*, vol. 29, no. 6, pp. 13–17, 2009 (Chinese).

[176] W. Bo and G. Yang, "Crustal deformation measured by mobile observation before Wenchuan Ms8.0 earthquake," *Journal of Geodesy and Geodynamics*, vol. 28, no. 6, pp. 11–15, 2008 (Chinese).

[177] G. Zhao, W. Ma, J. Wang, and A. He, "Geothermal earthquake precursor network and its response to Ms8.0 Wenchuan earthquake," *Journal of Seismological Research*, vol. 32, no. 3, pp. 248–252, 2009 (Chinese).

[178] I. P. Dobrovolsky, S. I. Zubkov, and V. I. Miachkin, "Estimation of the size of earthquake preparation zones," *Pure and Applied Geophysics*, vol. 117, no. 5, pp. 1025–1044, 1979.

[179] X. G. Hu and X. G. Hao, "The short-term anomalies detected by broadband seismographs before the May 12 Wenchuan earthquake, Sichuan, China," *Chinese Journal of Geophysics*, vol. 51, no. 6, pp. 1726–1734, 2008 (Chinese).

[180] X. G. Hu and X. G. Hao, "An analysis of the influences of typhoon on anomalous tremors before the great Wenchuan and Kunlunshan earthquakes," *Chinese Journal of Geophysics*, vol. 52, no. 5, pp. 1363–1375, 2009 (Chinese).

[181] R. S. Fu, K. S. Wan, J. J. Chong, and T. X. Xue, "Earthquake auspice or other factor? Discuss with authors of the paper "The short-term anomalies detected by broadband seismographs before the May 12 Wenchuan earthquake, Sichuan, China"," *Chinese Journal of Geophysics*, vol. 52, no. 2, pp. 584–589, 2009 (Chinese).

[182] X.-G. Hu, X.-G. Hao, and X.-X. Xue, "The analysis of the non-typhoon-induced microseisms before the 2008 Wenchuan earthquake," *Chinese Journal of Geophysics*, vol. 53, no. 12, pp. 2875–2886, 2010 (Chinese).

[183] Z. H. Qiu, L. S. Zhou, and S. L. Chi, "Study on precursory strain changes of Wenchuan earthquake with ORA method," *Journal of Geodesy and Geodynamics*, vol. 29, no. 4, pp. 1–4, 2009 (Chinese).

[184] Z. H. Qiu, L. Tang, L. S. Zhou, and B. X. Kan, "Observed strain changes from 4-component borehole strainmeter network before 2008 Wenchuan earthquake," *Journal of Geodesy and Geodynamics*, vol. 29, no. 1, pp. 1–5, 2009 (Chinese).

[185] Q. Su, H. Zhu, and Y. Yang, "Short-line leveling anomaly at Gengda and Wenchuan Ms8.0 earthquake," *Journal of Geodesy and Geodynamics*, vol. 29, supplement, pp. 103–105, 2009 (Chinese).

[186] J. Wei, H. Hao, K. Kang et al., "Gravity disturbance of high frequcncy at Chengdu seismostation before Wenchuan Ms8.0 earthquake," *Journal of Geodesy and Geodynamics*, vol. 29, supplement, pp. 15–19, 2009 (Chinese).

[187] W. Liu, H. Chen, F. Zhao, X. Liu, B. Yuan, and J. Zhang, "Characteristics of spatio-temporal relation of strong earthquakes in China before and after the Sichuan Wenchuan Ms8.0 earthquake," *Earthquake*, vol. 30, no. 3, pp. 140–146, 2010 (Chinese).

[188] H. Zhu, J. P. Deng, and G. Yang, "Discussion on the causes of 2 anomalies before the Wenchuan M8.0 earthquake," *Earthquake Research in Sichuan*, no. 1, pp. 13–17, 2010 (Chinese).

[189] H. Zhu, Q. Su, T. Yang, X. Z. Wen, and S. X. Wang, "Identifying anomalous change of short-line leveling on Gengda site pre- and after Ms8.0 Wenchuan earthquake," *Acta Seismologica Sinica*, vol. 32, no. 6, pp. 649–658, 2010 (Chinese).

[190] W. Cheng, Q. Su, and Y. Sun, "Study on the datum anomalies of crust deformation in Sichuan region before the 2008 M8.0 Wenchuan earthquake," *Earthquake Research in Sichuan*, no. 1, pp. 1–10, 2011 (Chinese).

[191] W. Cheng, Y. Ren, and X. Wu, "Analyzing the anomalies of geo-electrical and geo-magnetic observation data in Sichuan Province before the 2008 Wenchuan M8.0 earthquake," *Earthquake Research in Sichuan*, no. 2, pp. 2–9, 2010 (Chinese).

[192] P. Cheng, J. Mi, H. Wang, Y. Cai, and Y. Huang, "Time-variations of some domestic IGS sites during the Wenchuan earthquake," *GNSS World of China*, vol. 33, no. 5, pp. 11–15, 2008 (Chinese).

[193] J. Liu, "On geothermal earthquake observation network and Wenchuan 8.0 earthquake," *Journal of Institute of Disaster-Prevention Science and Technology*, vol. 12, no. 3, pp. 48–54, 2010 (Chinese).

[194] P. Qiu, Y. Wang, G. Yang, X. Bai, and S. Zhao, "Research on the anomalous changes of water surface temperature before and after Wenchuan Ms8.0 earthquake," *Northwestern Seismological Journal*, vol. 32, no. 4, pp. 367–375, 2010 (Chinese).

[195] J. Dong, R. Yan, J. Zhang, X. Zhang, and J. Liu, "Analysis of earthquake-related information in ionosphere based on DEMETER satellite data-applicated to Wenchuan and Donghai earthquakes," *Earthquake*, vol. 29, supplement, pp. 67–75, 2009 (Chinese).

[196] G. Gu and W. Wang, "Vertical crustal movement before and after the great Wenchuan earthquake obtained from GPS observations in the regional network," *Earthquake*, vol. 31, no. 3, pp. 1–8, 2011 (Chinese).

[197] W. Bo and L. Zhang, "The Ms8.0 Wenchuan earthquake: precursor analysis of fault deformation," *Journal of Seismological Research*, vol. 31, supplement, pp. 419–423, 2008 (Chinese).

[198] S. Zhang, X. Zhang, S. Wang, F. Xue, and L. Liu, "Analysis of crustal vertical deformation before and after Wenchuan Ms8.0 earthquake," *Journal of Geodesy and Geodynamics*, vol. 28, no. 6, pp. 43–46, 2008 (Chinese).

[199] Z.-S. Jiang, Y.-Q. Wu, Y. Fang, P. Li, and W.-X. Wang, "Dynamic characteristics of the strain fields and crustal movements before the Wenchuan Ms8.0 earthquake," *Earthquake*, vol. 29, no. 1, pp. 68–76, 2009 (Chinese).

[200] Z.-S. Jiang, Y. Fang, Y.-Q. Wu, M. Wang, F. Du, and J.-J. Ping, "The dynamic process of regional crustal movement and

deformation before Wenchuan Ms8.0 earthquake," *Chinese Journal of Geophysics*, vol. 52, no. 2, pp. 505–518, 2009 (Chinese).

[201] X. Shan, X. Song, Y. Han, C. Qu, G. Zhang, and G. Zhang, "The characteristics of surface vertical deformation before the Wenchuan Ms8.0 earthquake from InSAR," *Chinese Journal of Geophysics*, vol. 52, no. 11, pp. 2739–2745, 2009 (Chinese).

[202] R. Xie, Q. Li, J. Qin, R. Zhang, S. Xu, and J. Feng, "Study on gravity change around Wenchuan Ms8.0 earthquake recorded in Ji-Lu-Yu junction area," *Journal of Geodesy and Geodynamics*, vol. 29, no. 1, pp. 27–30, 2009 (Chinese).

[203] G. A. Yang and Y. Mi, "Thermal anomalies and earthquakes: evidence from Wenchuan, China," *Earthquake Research in China*, vol. 23, no. 1, pp. 48–55, 2009.

[204] Q. Cui, Y. Shu, Z. Wang, J. Fan, and W. Liu, "Suspected correlation between anomalies of body strain observation data at Xi'an Seismological Station and Wenchuan M8.0 earthquake," *Earthquake Research in Shanxi*, no. 4, pp. 30–33, 2010 (Chinese).

[205] J. Shi, W. Wang, and J. Wen, "The meteorological anomalies before and after the Wenchuan earthquake," *Astronomical Research & Technology*, vol. 7, no. 1, pp. 78–84, 2010 (Chinese).

[206] L. Wu, L. Zhang, G. Li, and H. Guo, "The relative calibration and its application of 4-component borehole strain observation in HaiYuan Station," *Journal of Seismological Research*, vol. 33, no. 4, pp. 318–322, 2010 (Chinese).

[207] W.-B. Liu, "Reverse tracing of the seismicity before strong earthquakes in Mainland China," *Earthquake*, vol. 30, no. 2, pp. 46–53, 2010 (Chinese).

[208] Z. Chen, P. Lu, Z. Li, B. Zhao, and S. Lin, "Analysis of tidal data before Wenchuan Ms8.0 earthquake," *Journal of Geodesy and Geodynamics*, vol. 29, no. 4, pp. 48–50, 2009 (Chinese).

[209] X.-F. Fan, J.-Y. Wang, and M.-Y. Lu, "Preliminary study on some typical medium-term subsurface fluid anomalies before the Wenchuan 8.0 earthquake," *Earthquake*, vol. 29, no. 1, pp. 132–140, 2009 (Chinese).

[210] Y. Ding, H. Chen, and J. Zhang, "The preliminary research on anomalous variation character of electromagnetic radiation before the Wenchuan Ms8.0 earthquake," *Seismological and Geomagnetic Observation and Research*, vol. 30, no. 3, pp. 11–15, 2009 (Chinese).

[211] S. Zhou, Y. Wu, S. Shi, and Z. Chen, "Anomalous change of fault deformation before Wenchuan Ms8.0 earthquake and its comparison with response of other large earthquakes," *Acta Seismologica Sinica*, vol. 31, no. 2, pp. 140–151, 2009 (Chinese).

[212] S.-R. Mei, Y. Xue, and Z.-P. Song, "Anomalous seismic characteristics before Wenchuan M8.0 and Kunlunshan M8.1 earthquakes and their implications," *Earthquake*, vol. 29, no. 1, pp. 1–14, 2009 (Chinese).

[213] L. Chen, H. Fu, and X. Zhao, "Comparative study of M≥5 seismic activities before some large earthquakes," *Earthquake*, vol. 30, no. 4, pp. 22–31, 2010 (Chinese).

[214] W. Cheng and Y. Zhang, "Discussion on the seismicity and seismic tendency of Sichuan Province before the 2008 Wenchuan M8.0 earthquake," *Earthquake Research in Sichuan*, no. 3, pp. 1–7, 2009 (Chinese).

[215] L. Chen and H. Fu, "The contrast study of Wenchuan M8.0 earthquake precursor anomalies," *Inland Earthquake*, vol. 24, no. 4, pp. 289–297, 2010 (Chinese).

[216] T. H. Jordan, Y. T. Chen, P. Gasparini et al., "Operational earthquake forecasting: state of knowledge and guidelines for utilization," *Annals of Geophysics*, vol. 54, no. 4, pp. 315–391, 2011.

[217] A.-F. Niu, L.-K. Zhang, W. Yan, X.-D. Jia, and X.-F. Li, "On the characteristics of ground deformation anomalies in the middle and northern part of the south-north seismic belt prior to the Wenchuan earthquake," *Earthquake*, vol. 29, no. 1, pp. 100–107, 2009 (Chinese).

[218] L. Zhang, M. Yu, and D. Sun, "Analysis on fault deformation anomaly of Longmenshan fault zone before Ms8.0 Wenchuan strong earthquake," *North China Earthquake Sciences*, vol. 27, no. 1, pp. 34–38, 2009 (Chinese).

[219] M.-Y. Lu, Z.-F. Fang, and L.-K. Zhao, "Discussion on the long-time trend change characteristics of subsurface fluid before the Wenchuan Ms8.0 earthquake," *Earthquake*, vol. 30, no. 1, pp. 61–72, 2010 (Chinese).

[220] H. Zhang, Z. Ouyang, Z. Fu, B. Gou, and W. Jiang, "Abnormal phenomena recorded by several earthquake precursor observation instruments before the Ms8.0 Wenchuan, Sichuan earthquake," *Progress in Geophysics*, vol. 26, no. 1, pp. 99–109, 2011 (Chinese).

[221] Y. Zhu, W. Liang, and Y. Xu, "Medium-term prediction of Ms8.0 earthquake in Wenchuan, Sichuan by mobile gravity," *Recent Developments in World Seismology*, no. 7, pp. 36–39, 2008 (Chinese).

[222] M. Wyss, Ed., *Evaluation of Proposed Earthquake Precursors*, American Geophysical Union, Washington, DC, USA, 1991.

[223] M. Wyss and R. Dmowska, Eds., "Earthquake Prediction, State-of-the-Art," *Pure and Applied Geophysics*, vol. 149, no. 1, pp. 1–264, 1997.

[224] R. D. Cicerone, J. E. Ebel, and J. Britton, "A systematic compilation of earthquake precursors," *Tectonophysics*, vol. 476, no. 3-4, pp. 371–396, 2009.

[225] T. Rikitake, *Earthquake Prediction*, Elsevier, New York, NY, USA, 1976.

[226] T. Rikitake, "Classification of earthquake precursors," *Tectonophysics*, vol. 54, no. 3-4, pp. 293–309, 1979.

[227] T. Rikitake, "Earthquake prediction: an empirical approach," *Tectonophysics*, vol. 148, no. 3-4, pp. 195–210, 1988.

[228] K. Mogi, *Earthquake Prediction*, Academic Press, Orlando, Fla, USA, 1985.

Hindawi Publishing Corporation
International Journal of Geophysics
Volume 2012, Article ID 304235, 14 pages
doi:10.1155/2012/304235

Research Article

Probabilistic Seismic Hazard Analysis for Yemen

Rakesh Mohindra,[1] Anand K. S. Nair,[1] Sushil Gupta,[1] Ujjwal Sur,[1] and Vladimir Sokolov[2]

[1] *Risk Modeling & Insurance Group, RMSI Pvt. Ltd., A-7 Sector 16, Noida 201 301, India*
[2] *Geophysical Institute, Karlsruhe Institute of Technology (KIT), Karlsruhe, Germany*

Correspondence should be addressed to Rakesh Mohindra, rakesh.mohindra@rmsi.com

Received 28 June 2011; Revised 14 October 2011; Accepted 2 November 2011

Academic Editor: Yamaoka Koshun

A stochastic-event probabilistic seismic hazard model, which can be used further for estimates of seismic loss and seismic risk analysis, has been developed for the territory of Yemen. An updated composite earthquake catalogue has been compiled using the databases from two basic sources and several research publications. The spatial distribution of earthquakes from the catalogue was used to define and characterize the regional earthquake source zones for Yemen. To capture all possible scenarios in the seismic hazard model, a stochastic event set has been created consisting of 15,986 events generated from 1,583 fault segments in the delineated seismic source zones. Distribution of horizontal peak ground acceleration (PGA) was calculated for all stochastic events considering epistemic uncertainty in ground-motion modeling using three suitable ground motion-prediction relationships, which were applied with equal weight. The probabilistic seismic hazard maps were created showing PGA and MSK seismic intensity at 10% and 50% probability of exceedance in 50 years, considering local soil site conditions. The resulting PGA for 10% probability of exceedance in 50 years (return period 475 years) ranges from 0.2 g to 0.3 g in western Yemen and generally is less than 0.05 g across central and eastern Yemen. The largest contributors to Yemen's seismic hazard are the events from the West Arabian Shield seismic zone.

1. Introduction

The tectonic movement and interaction of the Arabian and the African plates constituting rifts of the Red Sea and Gulf of Aden are the principal cause of earthquakes in Yemen, which are known from historical sources over the last millenniums [1–3]. Earthquakes that affect Yemen are mainly associated with rifts of the Red Sea and the Gulf of Aden [4]. However, small- to moderate-sized earthquakes, which occur inside the Arabian Plate within 200 to 300 km of the axis of the Red Sea [5, 6], may also have some impact on the territory (Figure 1).

In general, seismic history of Yemen indicates the occurrence of large earthquakes with 20- to 30-year recurrence periods [2]. We can mention the Dhamar earthquake of 13 December 1982 ($M = 6$), which was felt over a large area and which killed and injured more than 15,000 people and destroyed about 1,500 settlements, as the deadliest earthquake of Yemen [8]. Two significant earthquakes occurred in 1941 and 1909. The main event ($M = 6.5$) and two aftershocks ($M = 5.8$ and $M = 5.2$) in 1941 killed about 1,200 people and damaged about 1,400 homes. In the 1909 earthquake event, about 300 people were killed and approximately 400 houses were destroyed.

Seismic hazard analysis for the territory of Western Arabia and Yemen was performed by several researchers [9–11]. The conventional Cornell approach [12] has been applied in almost all studies, and the results were not suitable for seismic loss analysis. The goal of this study is the development and testing of a stochastic-event probabilistic seismic hazard model for the territory of Yemen, which considers the influence of local site conditions and which can be used further for estimates of seismic loss and seismic risk analysis.

2. The Approach

The information related to the expected seismic effect and expressed in terms of earthquake ground motion parameters, such as seismic intensity and peak amplitudes of ground

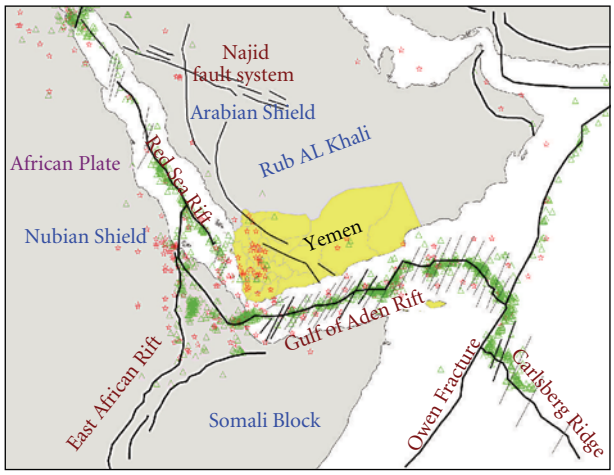

Figure 1: Earthquake catalogue events from two sources (AMB: Ambraseys et al. [7] and ANSS: Advanced National Seismic System Worldwide catalogue) plotted over the generalized seismotectonic feature map.

motion, is necessary for estimation of seismic losses and design of buildings and structures in earthquake-prone regions. Thus, the specification of engineering ground-motion parameters is the goal of seismic hazard analysis.

Probabilistic seismic hazard analysis (PSHA) involves the quantitative estimation of ground shaking hazard at a particular site taking into account characteristics of potentially dangerous earthquakes around the site. The principles of PSHA are well established within the scientific community. In this study, the source zone approach together with stochastic event generation has been used for developing a probabilistic seismic hazard model for Yemen. The main features of the approach are as follows: seismic source zones, which are considered as a potential source of earthquakes in the future, are divided into a series of linear sources (faults) and further into a system of elementary segments. Possible earthquakes may occur along the segments, and earthquake occurrence is assumed to be a stationary random process. Every elementary linear segment is characterized by the following parameters: (a) magnitudes of individual earthquake event and (b) annual rate of earthquake recurrence. Parameters of earthquake ground motion are calculated for every stochastic event (earthquake generated by elementary segment) along the territory of interest. The scheme allows using different parameters of seismicity and earthquake characteristics for different zones, as well as various ground-motion prediction equations.

3. Earthquake Catalogue

A primary component of the PSHA model is the earthquake catalogue for the region. Yemen has a long and relatively well-documented history of important past earthquake events including historical chronicles [2]. As historical data is not based on instrumental observations, the earthquake magnitude, intensity, and epicenter in such database have been estimated based on the description in historical documents. The development in instrumental seismology in Yemen started after the occurrence of the December 13, 1982, Dhamar earthquake [3].

A composite and updated catalogue has been compiled for the present study using two basic sources. The first source is the database collected by Ambraseys et al. [7]. The data has been divided by the authors into two subsets, which cover two periods from 184 BC to 1899 AD and from 1899 to 1987. In the first subset, epicenters of earthquakes were determined from macroseismic data, and, therefore, in most cases they reflect centres of the most heavily affected area. The accuracy of earthquake location in such cases depends on the availability of observations. The second subset combines instrumental data with macroseismic information. The original locations of all events were reexamined and, in most cases, parameters of earthquakes were reassessed using teleseismic and macroseismic information. The second source of earthquake data is the World-ANSS (Advanced National Seismic System) worldwide catalogue hosted by the Northern California Earthquake Data Center. The ANSS catalogue has been created by merging the master earthquake catalogues from contributing ANSS institutions and by removing duplicate solutions for the same event. Besides these two main sources of the data, parameters of important historical earthquakes of Yemen were checked using other literature sources [2, 13–15].

When compiling the composite catalogue in this study, the following has been considered. The catalogue of Ambraseys et al. [7] is a more authentic and reliable source of data than the other sources, because each event in the catalogue has been carefully reexamined. However, location and magnitude of many earthquakes depend entirely on macroseismic data and the event coverage is not uniform in time and area. Many events with no felt effects may have been neglected in the database. From 1963 onward, the ANSS catalogue has been compiled using the data from automatic recordings seismographs. Thus, the composite catalogue (Figure 2) has been created considering (1) all records from Ambraseys et al. [7] from 182 BC to 1962 and (2) all data from the ANSS catalogue from 1963 onward. Aftershocks were removed from the composite catalogue using the declustering method of Gardner and Knopoff [16]. The procedure defines a space D and time T window after each event, which is supposed to be a main shock [16, 17]. All subsequent events within this window are declared dependent events and omitted from the declustered catalogue—unless their magnitude exceeds the main-shock magnitude. Window thresholds D and T usually depend on the main-shock magnitude and they are assumed universal for the entire study region and study period.

Several magnitude scales (local magnitude M_L, body wave magnitude M_b, surface wave magnitude M_S, moment magnitude M_w, etc.) have been used by various researchers to characterize earthquakes in the region [18, 19]. In our study, we have considered moment magnitude M_w, which

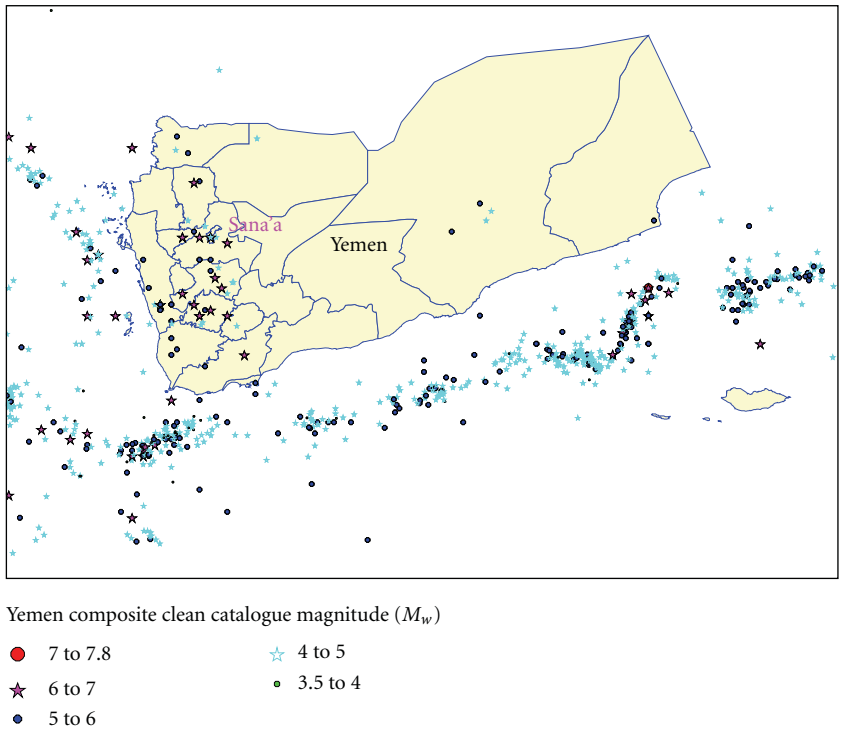

Figure 2: Yemen composite catalogue.

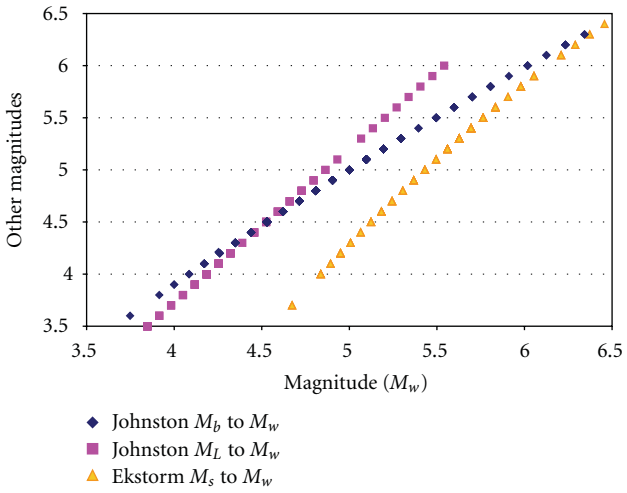

Figure 3: Empirical relationships for conversion between magnitudes scales.

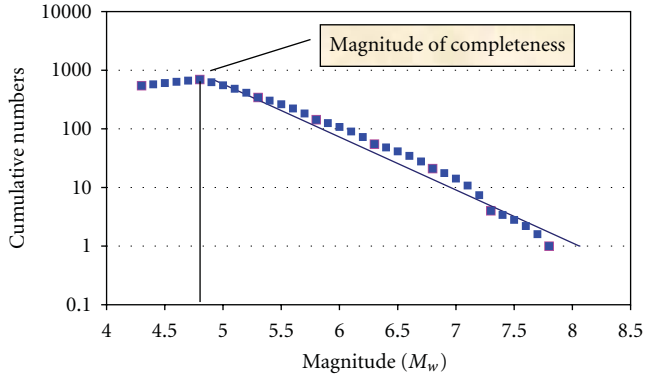

Figure 4: Frequency-magnitude distribution for Yemen and surrounding seismic regions.

is consistent with ground motion computation. Thus, if necessary, magnitudes in the composite catalogue were recalculated. The empirical equations suggested by Johnston et al. [20] which were developed using worldwide datasets, were used for M_b-M_w and M_L-M_w conversion; the empirical equation suggested by Ekström and Dziewonski [21] has been used for M_S-M_w conversion (Figure 3).

The most important requirement for any earthquake catalogue is to judge completeness of the catalogue with respect to magnitude and time of event occurrence. Magnitude of completeness (M_c) is the lowest magnitude, at which 100% of the events are detected in a space and time. Below M_c, some parts of events are missed in the catalogue due to the influence of several factors including the network limitation. A traditional method of frequency-magnitude distribution, which describes the relationship between the frequency of occurrence and magnitude of earthquakes, has been used to estimate M_c, which describes the relationship between the frequency of occurrence and magnitude of earthquakes. The frequency-magnitude curves in Figure 4 show a higher frequency of earthquakes at certain magnitudes and after that it is decreased exponentially for higher magnitude and M_c is picked up as 4.8 ± 0.1, at the point where the curve becomes exponential.

Table 1: Catalogue completeness with respect to time and magnitude range.

Magnitude	Catalogue completeness period (in years)
3.5 to 4.0	20
4.5 to 5.5	50
5.5 to 6.0	80
6.0 to 7.0	110

Although historical data goes as far back as 184 BC, the reporting is not homogeneous for the entire span of the catalogue to derive correct parameters. To compute catalogue completeness with respect to time and magnitude, events have been plotted for various broad regions at 0.2 and 0.5 magnitude interval ranges. It is observed that despite compiling the Yemen seismic regions catalogue from various sources, the earthquake catalogue is not complete uniformly for all magnitude ranges. Catalogue completeness has been computed following the method of Stepp [22]. For magnitude 6.0 and above, the catalogue is complete for the last 110 years, while for magnitudes between 3.5 and 4.0 the catalogue is observed to be complete for only the last 20 years. Table 1 shows the catalogue completeness times for Yemen seismic regions, which have been taken into account while computing recurrence parameters.

4. Seismic Sources

One of the main features of seismic hazard analysis involves identification of seismic sources. Seismic sources are geographical areas that have experienced seismic activity in the past and serve as potential sources of earthquakes in the future. Seismic sources are delineated based on seismotectonic features of the region and it is assumed that the past earthquake activity is a reliable predictor of the future activity.

A cluster of earthquakes occurred in the southwestern part of the Arabian plate near a complex triple junction of active spreading ridges along the Red Sea, Gulf of Aden, and Afar depression (Figure 1). In general, the seismic activity around Yemen is most pronounced along the spreading ridges. However, some small- to moderate-sized events occurred also within the Arabian plate at distances up to 200–300 km from the axis of the Red Sea [5].

A total of 12 seismic sources reflecting peculiarities of seismicity have been delineated in the studied area on the basis of seismotectonic maps, clustering of epicenters, and smoothening of seismicity (Figure 5). Also, the results of the Global Seismic Hazard Assessment Programme [23] and corresponding studies [24] were considered. Due to errors associated with locations of preinstrumental earthquake events and catalogue incompleteness, both the seismotectonic province approach and the epicenter smoothing Frankel approach [25] have been used to demarcate the area of source zones.

The epicenter-smoothing approach [25] has been considered as a lower bound estimator for seismic hazard and helps in decision making in moderate seismicity regions where source zone definition and estimation of maximum possible magnitudes can lead to a wide variety of estimates. In each broad seismic region, using the Gutenberg-Richter magnitude frequency distribution, a-value (total number of earthquakes per year greater than $M_w = 0$) and the slope (b-value) at each 10 km grid cell have been computed. Then, using the Frankel approach, the cumulative annual earthquake occurrence rates have been computed in 0.1 magnitude increments in each 10 km grid with a correlation distance of 50 km [25, 26]. A thematic map of the smoothed a-value at the grid level is presented in Figure 5 together with the defined seismic sources.

In each seismic region, the parameters of the Gutenberg-Richter magnitude frequency distribution

$$\log N_{m>M} = a + bM, \tag{1}$$

where N is the cumulative number of events greater than magnitude M and a-value (a) and b-value (b) are the regression parameters, were estimated.

For each source, the constants a-value and b-value of the recurrence relationship have been obtained from regression analysis on the yearly rate of occurrence of historical events (Figure 6). While estimating yearly rate of occurrences, catalogue completeness by magnitude bins has been considered. The rate of occurrence of future events is calculated by binning events into half magnitude increments. The rate of occurrence of events in a given bin has been equal to the difference between the cumulative rate of occurrence of that bin and the cumulative rate of occurrence of the next bin ($0.25M_w$ larger). The rate of occurrence of Mmax has been calculated in the same manner, taking the next bin as Mmax plus $0.25M_w$.

Demarcated seismic sources have unique tectonic regimes and are different from adjacent sources in terms of stress accumulations and event recurrence characteristics. Based on clustering and homogeneity in historic seismic activity, earthquake source zones that have similar geophysical characteristics within a geographic area have been delineated. Ideally, each area source should have been considered as an independent seismic source to compute recurrence parameters. However, difficulties were encountered due to low seismicity for some sources. Some seismic areas especially within the Yemen Arabian Plate have sparse distribution of historical seismicity. The western region of Yemen has a high potential of seismic hazard as compared to the eastern part. In order to overcome the problem of low seismicity in the source area, events from certain sources have been merged for the purpose of estimating recurrence parameters. For example, parameters for seismic source Red Sea Al Darb have been computed by taking into account the individual source events as it had enough events for regression. However, five sources in the Arabian shield regions comprising sources 1 to 5 have been merged to derive the hazard parameters.

In estimating the seismic rate, we considered truncated exponential magnitude recurrence relationships (Figure 6)

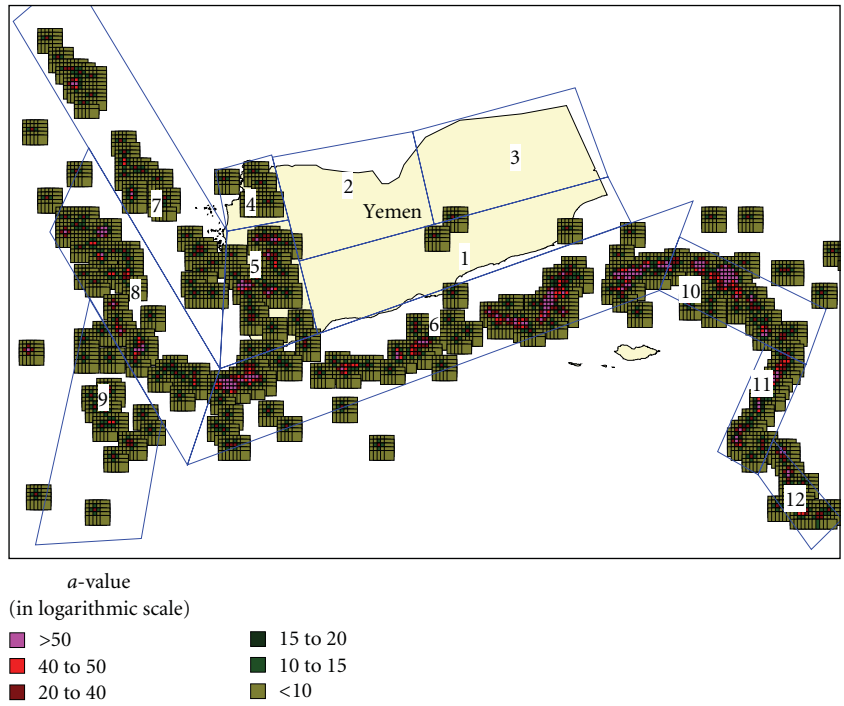

Figure 5: Delineated seismic sources (1–12) plotted upon the thematic map of the Frankel smoothed a-values. Source names are provided in Table 2.

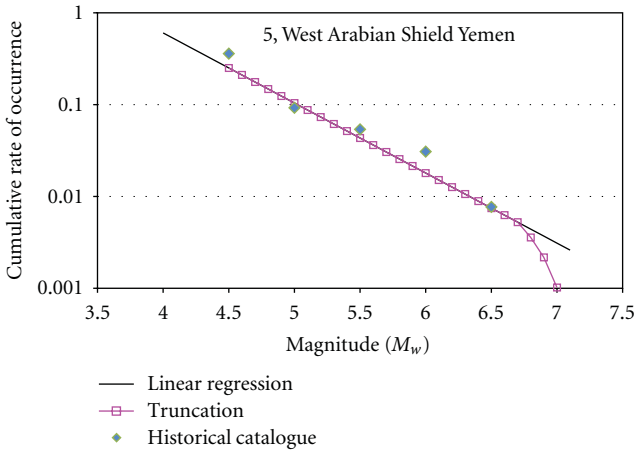

Figure 6: Normal regression and truncation model plot of cumulative number of events per year for the source 5, West Arabian Shield Yemen. Cumulative rates from historical catalogue, showing the Poissonian distribution, are compared with that of regression.

in which recurrence frequencies for upper magnitude are truncated [27]. This approach is important in order to (a) provide compatibility with the physical limitations of magnitudes that are specific to various seismogenic zones and (b) lead to realistic results of recurrence characteristics of local hazard at various locations, in cases when local hazard is analyzed (as it should be) on the basis of probabilistic convolutions between the magnitude recurrence laws and the random attenuation laws.

After recurrence relations were determined for the major sources with merged data the seismicity represented by relation was redistributed to each area source. In the process, it was assumed that the b-value remains the same in all major seismic regions having association with 3–5 area-sources and only appropriate a-value had to be assigned. Characteristics of the seismic zones are listed in Table 2.

5. Stochastic Events

Seismic area source zones have been used to model the earthquake occurrence in areas where observed seismicity exhibits a diffuse pattern and where specific earthquake-generating faults cannot be identified to link with historical seismicity. Thus, it is assumed that earthquakes can occur by rupturing any part of the source area zone. In performing seismic hazard analysis, normally many researchers including computer code such as EQRISK [28] are using point source for generating earthquake events by subdividing the area seismic zone into grids of equal sizes [29]. In reality occurrence of an earthquake event is never a point source, rather the source is always a fault rupture. This can be observed by elongated isoseismal lines and elongated pattern of aftershocks around an event. Instead of considering point sources, we have considered line sources (fault segments) in seismic hazard simulation. In our approach, the area zones have been subdivided into a series of line sources (fault segments) and possible seismic events occur along

Table 2: Characteristics of seismic source zones.

Source ID	Seismic source name	a-value	b-value	Mmax	Elementary fault segments	Stochastic events
1	Central Rub Al-Khali Arabian Shield	1.959	0.763	6.6	256	2,048
2	North Rub Al-Khali Arabian Shield	1.563	0.763	6.6	175	1,400
3	East Rub al Khali Arabian Shield	1.646	0.763	6.6	216	1,728
4	NW Yemen Arabian Shield	1.889	0.763	7.1	45	495
5	Yemen West Arabian Shield	2.832	0.763	7.1	126	1,386
6	Gulf of Aden	5.199	0.988	7.4	249	2,988
7	Red Sea-Al Darb	4.056	0.869	7.4	144	1,728
8	Red Sea	4.152	0.878	7.1	105	1,155
9	East African Rift	3.049	0.742	7.1	147	1,617
10	East Sheba Ridge	5.216	1.084	7.4	54	648
11	Sheba Ridge	4.886	1.084	7.7	32	416
12	Sheba Ridge south	4.738	1.084	7.1	34	374
	Total				**1,583**	**15,983**

the line sources (Figure 7). Ideally, the length of the fault segments depends on magnitude-rupture length relationship and orientation should be along the identified natural faults. Since there is no comprehensive model available for the regions, in this study we assumed the same length for all segments. In reality, there is always a bias on distribution of natural faults within an area source. To avoid uneven seismic distributions, a systematic fault line along the preferred tectonic orientation has been assumed for stochastic events (Figure 7). Although the distribution and orientation of stochastic faults look unnatural, this assumption has two advantages: (a) occurrence of an earthquake event can be considered by rupturing a fault line, not a point source, and (b) seismic annual rate of occurrences can be distributed uniformly.

With an assumption that there is an equal probability for an event of particular magnitude to occur by rupturing any part of the delineated seismic area source zone, a number of stochastic faults have been compiled. Following the Poisson process, seismic activity of the given seismic source zone has been redistributed to the line source taking into consideration the length of the fault segment. These demarcated stochastic faults are treated as individual area line sources. The stochastic earthquake events set along these sources, with associated rate of occurrences, have been generated for earthquake simulation for ground motion footprints.

It is assumed that every segment can produce earthquakes within a considered range of magnitudes (from minimum considered magnitude Mmin to maximum possible magnitude Mmax). To capture possible scenarios, the set of stochastic events, which is associated with each line source, has been created at 0.2 magnitude interval starting from Mmin = 4.5. A total of 15,983 stochastic events with their annual rate of occurrences, associated with 12 seismic sources and 1,583 fault segments, have been generated for hazard simulations. Table 2 shows the characteristics of seismicity assigned to seismic source zones and the corresponding number of segments and stochastic events.

6. Ground Motion Model

The level of ground shaking in seismic hazard analysis is usually expressed in terms of peak ground amplitudes (acceleration PGA, velocity PGV, or displacement PGD), spectral acceleration at discrete frequencies, and seismic intensities (on MMI or MSK intensity scale). The estimations have been obtained using an appropriate ground-motion prediction equation taking into account dependence between the given ground-motion parameter, earthquake magnitude M, source-to-site distance R, and local site conditions.

The unavailability of strong motion models for the Yemen region makes it necessary to select attenuation equations derived from statistically significant data sets from the literature. The collections of ground-motion prediction models, which were developed during the last decades, are described, for example, by Douglas [30, 31] and Abrahamson et al. [32]. However, the applicability of the generalized worldwide models should be carefully studied for the regions lacking the data to avoid additional uncertainty.

Ground-motion models in terms of PGA were developed for the region by several authors [33, 34]. The most recent model for the southern Dead Sea Transform region has been proposed by Al-Qaryouti [35] for the larger value from the two horizontal components as follows:

$$\log_{10}(\mathrm{PGA}) = -3.451 + 0.498M - 0.38\log_{10}\left(R_{\mathrm{rup}}\right) - 0.00253R_{\mathrm{rup}} \pm 0.313, \quad (2)$$

where PGA is expressed in units of g and R_{rup} is the closest distance to rupture. Thenhaus et al. [36] suggested a region-specific adjustment to the Campbell [37] relation to make it suitable for Saudi Arabia as follows:

$$\ln(\mathrm{PGA}) = -3.303 + 0.85M - 1.25[R - 0.313\ln R + 0.087\exp(0.678M)] \pm 0.5, \quad (3)$$

where PGA is expressed in units of g and R is the closest distance to rupture. The model has been used by Al-Haddad

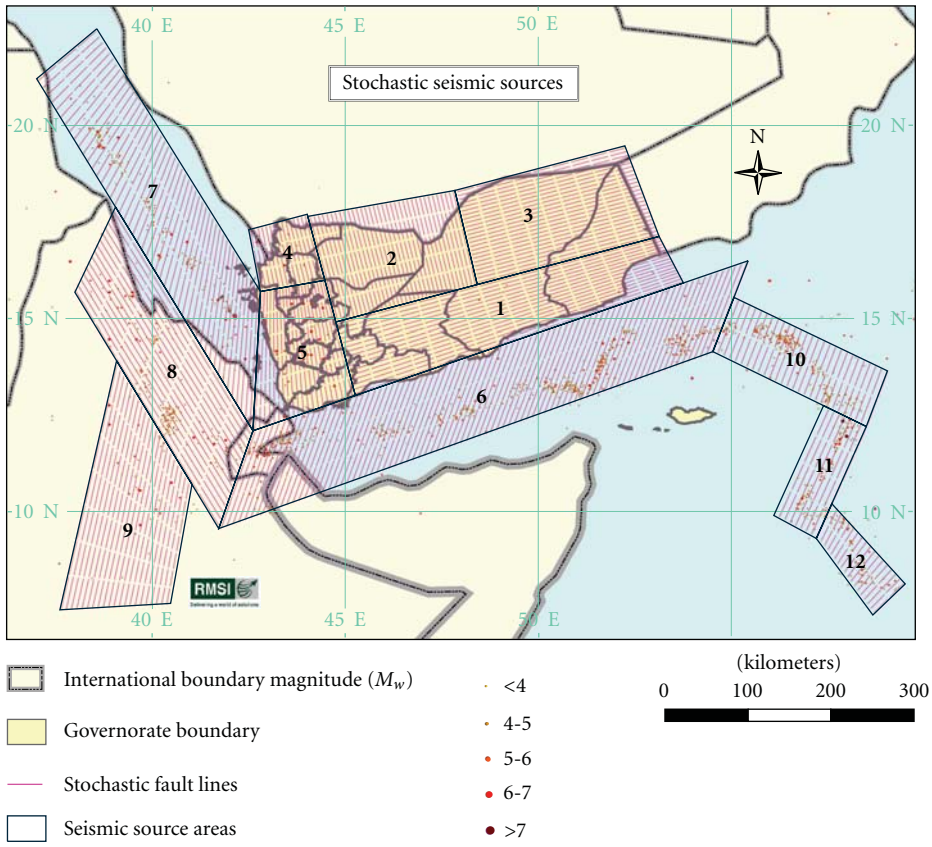

Figure 7: Delineated seismic sources (area seismic sources converted into fault lines for generation of stochastic events). Source details are provided in Table 2.

et al. [24] for evaluation of seismic hazard and design criteria for Saudi Arabia. In developing seismic hazard and design criteria for Saudi Arabia Al-Haddad et al., 1994 had used these attenuation equations for all seismic sources in the vicinity of the Arabian Peninsula including Yemen. Youngs et al. [38] developed ground motion models for subduction interface zones and intraslab regions using worldwide data. Here, we used the following model that relates to subduction intraslab events and rock sites:

$$\ln(\mathrm{PGA}) = 0.2418 + 1.414M - 2.552\left[R_{\mathrm{rup}} + 1.7818\exp(0.554M)\right] + 0.00607H \pm \mathrm{SD}, \quad (4)$$

where PGA (geometrical mean of two horizontal components) is expressed in units of g and R_{rup} is the closest distance to rupture, H is the source depth, and SD is the magnitude-dependent standard deviation, SD = 1.45 − 0.1M.

Seismicity of Yemen is attributed mainly to earthquakes from the transform fault region and the stable continent region. Attenuation 1 is the most recent model for transform region, attenuation 2 is an established equation for stable Arabian continent, and (4) is the global model. In this study we selected these regional attenuation models, which represent ground motion for rock condition (2)–(4), to be applied in seismic hazard analysis for Yemen. In order to capture epistemic uncertainty in ground motion estimations, these three models were used with equal weight. The expected values of ground motion parameters from all stochastic events were estimated from averaged attenuation equations as shown in Figure 8.

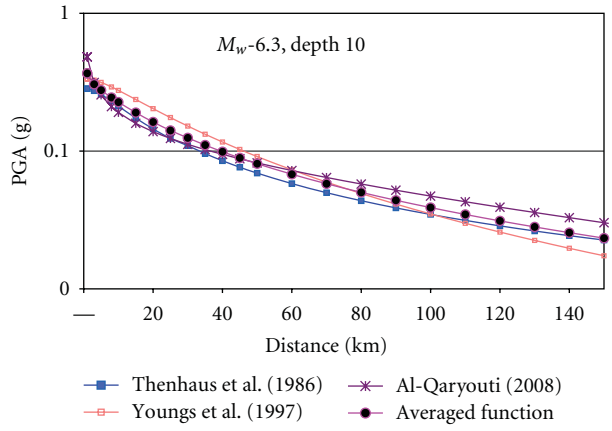

Figure 8: Hazard attenuation curves of PGA from three different studies [35, 36, 38] for an earthquake event of M_w 6.5 and averaged curve used in the study.

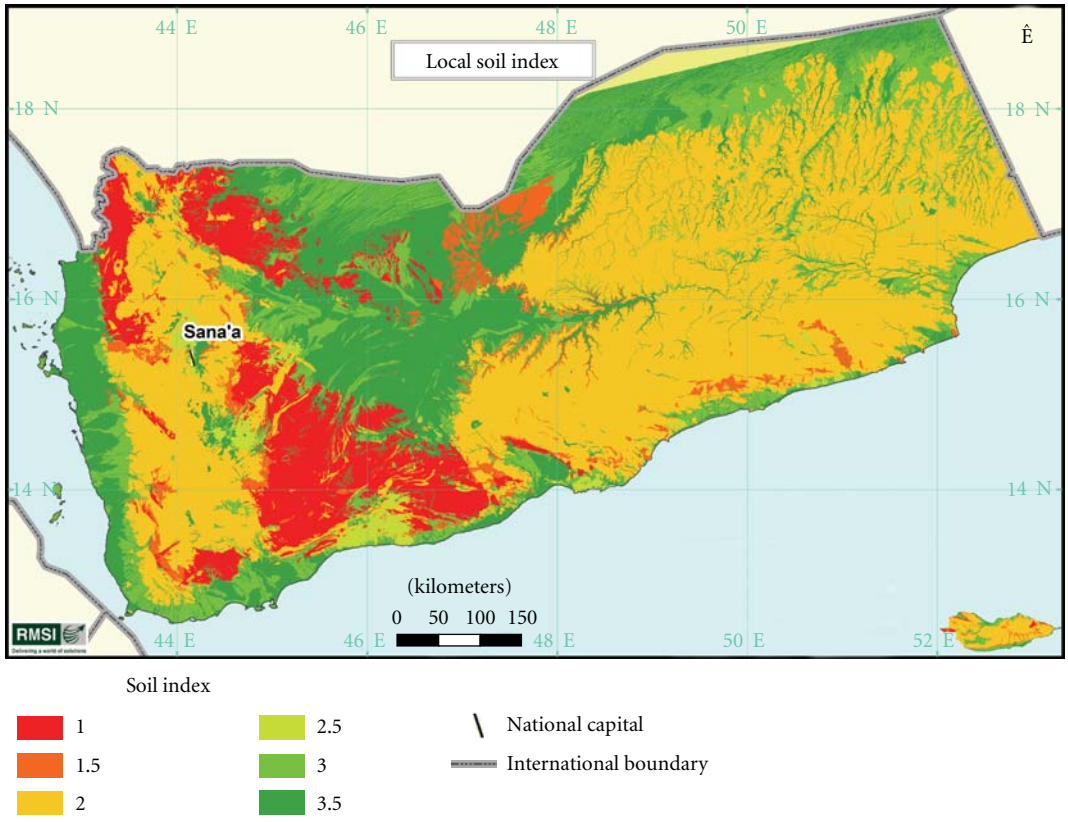

Figure 9: V_{S30} (soil index) map of Yemen generated from classification of geological formations.

Table 3: Soil classification scheme based on shear wave velocities.

Soil index value	NEHRP/CDMG class	Brief description	Shear wave velocities (V_{S30}) m/s
1.0	AB	Very hard to firm rocks mostly metamorphic and igneous rocks	**>760**
1.5	BC	Firm sedimentary rocks (mid-Miocene age) and weathered metamorphic	**760**
2.0	C	Sedimentary formation midlower Pleistocene age	**550–760**
2.5	CD	Weak rock to gravelly soils-deeply weathered and highly fractured bedrock	**270–550**
3.0	D	Holocene alluvial soils	**180–270**
3.5	DE	Young alluvium/water-saturated alluvial deposits	**90–180**

7. Soil Modifications

It is well understood that near-surface geological conditions may strongly affect earthquake ground motion at a particular site amplifying the shaking amplitude and changing frequency of the motion. In certain cases (e.g., building code provisions), a few generalized site classes have been selected to describe the variety of local soil conditions and to characterize their effect on ground motion. A widely used site classification system has been based on the properties of the top 30 m of the soil column, disregarding the characteristics of the deeper geology. Six site categories have been defined on the basis of average shear wave velocity.

The upper geological layer (soil) has been classified for the whole country using type of bedrock, lithology, and age of the surface layers, as well as some other characteristics taken from detailed geological maps of Yemen Geological Survey on 1 : 200 k scales (Figure 9). The classification follows the NEHRP soil classification scheme (Table 3), which considers seven soil classes and their associated shear wave velocities V_{S30} ranging from hard rocks (soil index 1.0) to soft soil young water-saturated alluvial deposits (soil index 3.5). In the absence of a Yemen-specific relationship between soil indexes and amplification effects, the widely used NEHRP site amplification procedure [39] has been used in this study. This procedure, together with the RMSI soil classification scheme, provides the amplification factors to scale the ground motion from one soil condition to another. Nonlinear two-dimensional soil amplification factors modified from Choi and Stewart [40], having nonlinear

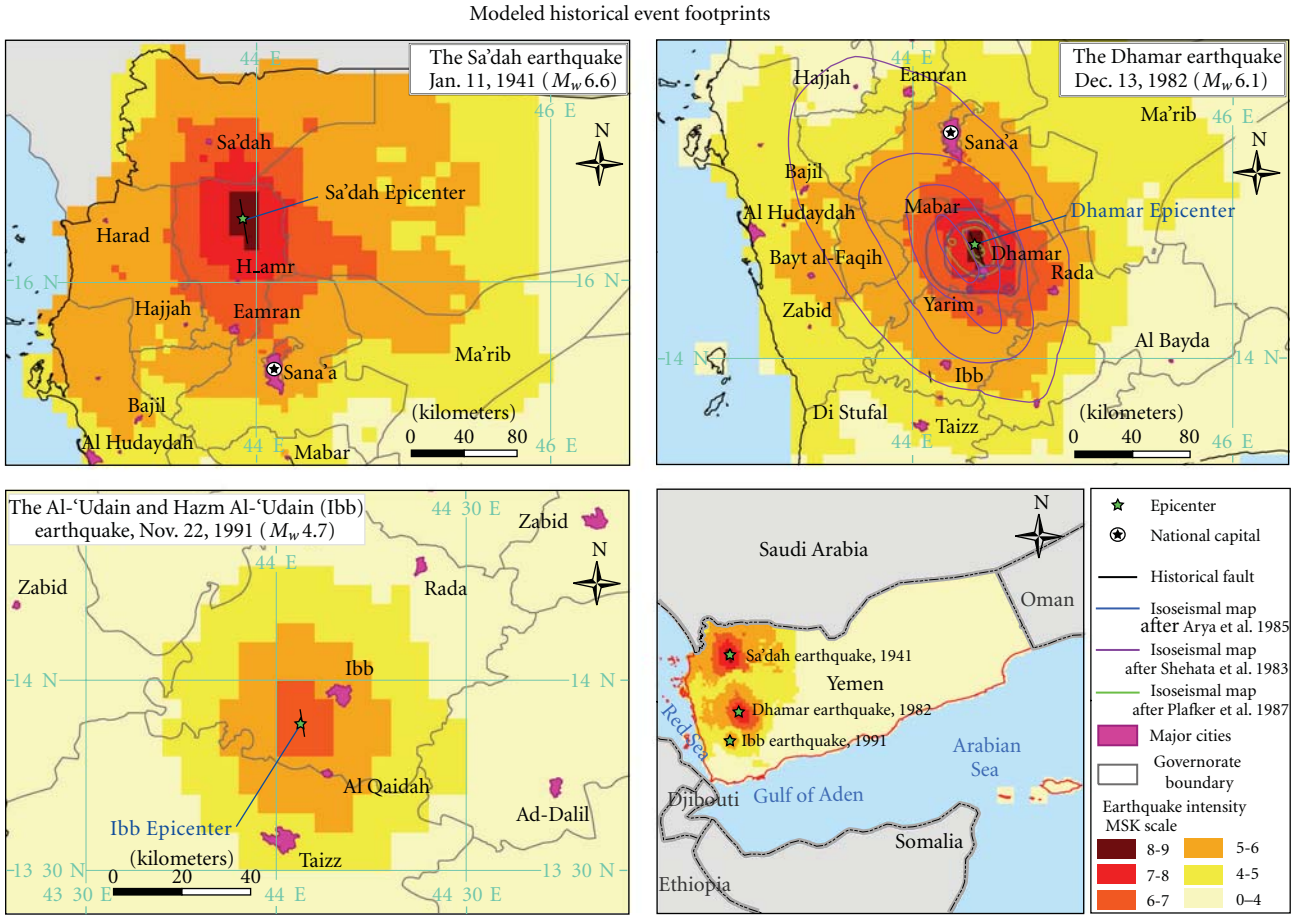

Figure 10: Modeled intensities of historical events, compared by observed intensities surveys by various authors for the Arya et al. [8], Shehata et al. 1983 [42], and Plafker etal. [6] Dhamar event.

multipliers based on the level of ground motion (PGA) and averaged soil index assigned for a given location, have been used in the study as site-dependent amplification factors.

8. Verification of Ground Motion Estimation Scheme

Before probabilistic hazard calculations, we checked the applicability of the developed strong motion prediction scheme for estimation of ground motion parameters along the territory of Yemen. The intensity data obtained during historical earthquakes (11 January 1941; 13 December 1982, and 13 October 1991, see Figure 10) were used for comparison with the model output. Ground-motion footprints in terms of PGA values under rock site condition were calculated using the averaged values resulting from accepted attenuation equations. The source-to-site distance was estimated as the shortest distance between the fault plane and centroid of a grid/population agglomeration area. Using the V_{S30} (soil index) map, the average values within the grid/population agglomeration area were estimated with GIS (Geographical Information System) overlay analysis. Based on the average soil index value and the estimated PGA values (rock site), two-dimensional soil amplification factors were computed and applied to the rock PGA values. The soil-dependent PGAs were converted into MSK intensities using the PGA-MSK relation shown in Table 4.

The Sa'dah Earthquake of January 11, 1941. This earthquake (epicenter 16.4°N and 43.5°E, intensity MSK VIII) is considered amongst the largest earthquakes in the recent history of Yemen [9]. It caused 1,200 deaths, injured 200 people, and damaged 1,700 houses, out of which 300 were destroyed, 400 were damaged beyond repair, and the rest received minor damage [7]. The magnitude of the earthquake was estimated as M_S 6.5 [2].

The Dhamar Earthquake of December 13, 1982. A large area in Dhamar province of Yemen was rocked by a destructive earthquake (M_b = 6.0, epicenter 14.7°N and 44.2°E) on 13 December 1982. This moderate shallow event that occurred in a densely populated region about 70 km south of Sana'a resulted in 2,500 deaths and injured 1,500 people [7, 8]. More than 70,000 dwellings were damaged and 500,000 people were affected. Most casualties occurred in the highly populated villages that were having rubble stone masonry

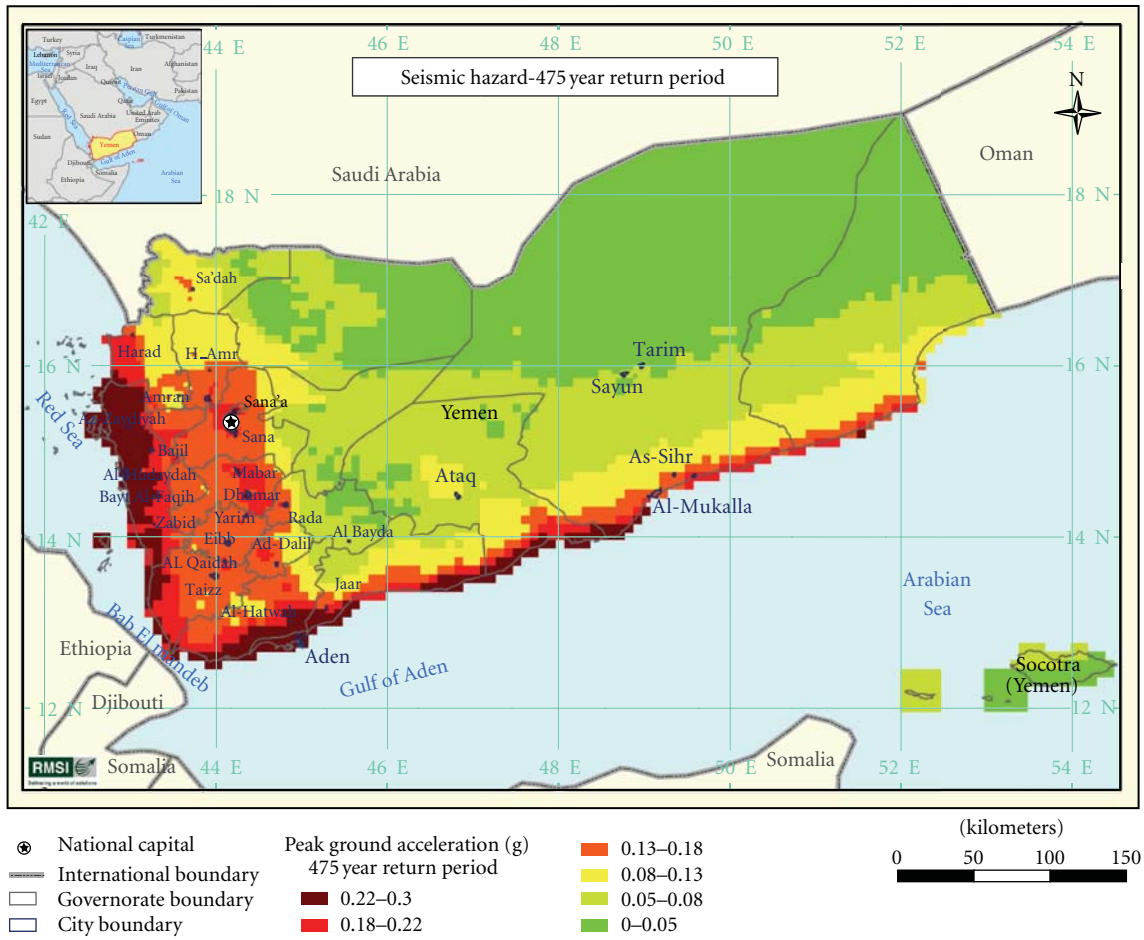

Figure 11: PGA probabilistic seismic hazard maps for 10% probability in 50 years that is, 475-year return period.

Table 4: PGA-MSK intensity conversation table.

PGA (in g)	Intensity in MSK scale
0	0
0.03	4
0.05	5
0.092	6
0.18	7
0.32	8
0.52	9
0.82	10
1.2	11
1.6	12

and unburned brick houses. Such houses suffered heavy damage in the form of large and deep cracks in walls and the collapse of the outer and inner masonry walls that resulted in partial or complete collapse of the whole construction.

The Al-"Udain and Hazm Al-"Udain (Ibb) Earthquake of November 22, 1991. The November 22, 1991 earthquake (M_S 4.5, epicenter 13.9°N, 44.1°E) caused widespread damage to housing and infrastructure in Yemen. The most affected areas were the Al-"Udain and Hazm Al-"Udain districts in the Ibb region. Preliminary surveys indicate that 7,150 buildings were damaged and 1,578 were destroyed [41]. However, the reinforced concrete structures in the epicentral area suffered no structural damage indicating the high vulnerability of traditional buildings, especially those constructed on slopes without proper foundation [7].

Obviously, it is not possible to expect a perfect agreement between the available intensity observations and the results of modeling. However, as can be seen from Figure 10, the general features of the regional earthquake effect (epicentral intensity and intensity attenuation) are reproduced quite adequately by the applied scheme of ground-motion modeling.

9. Results of Probabilistic Seismic Hazard Analysis

The following scheme has been applied for the analysis. Ground motion parameter from the stochastic event was calculated at every particular point of the studied territory (centroid of population agglomeration areas, and 10 km

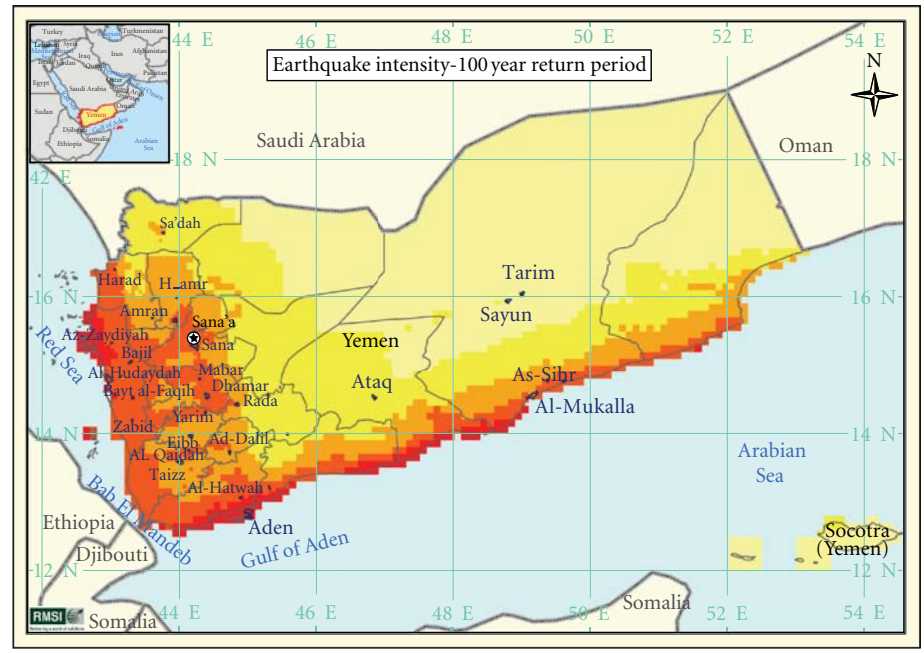

(a)

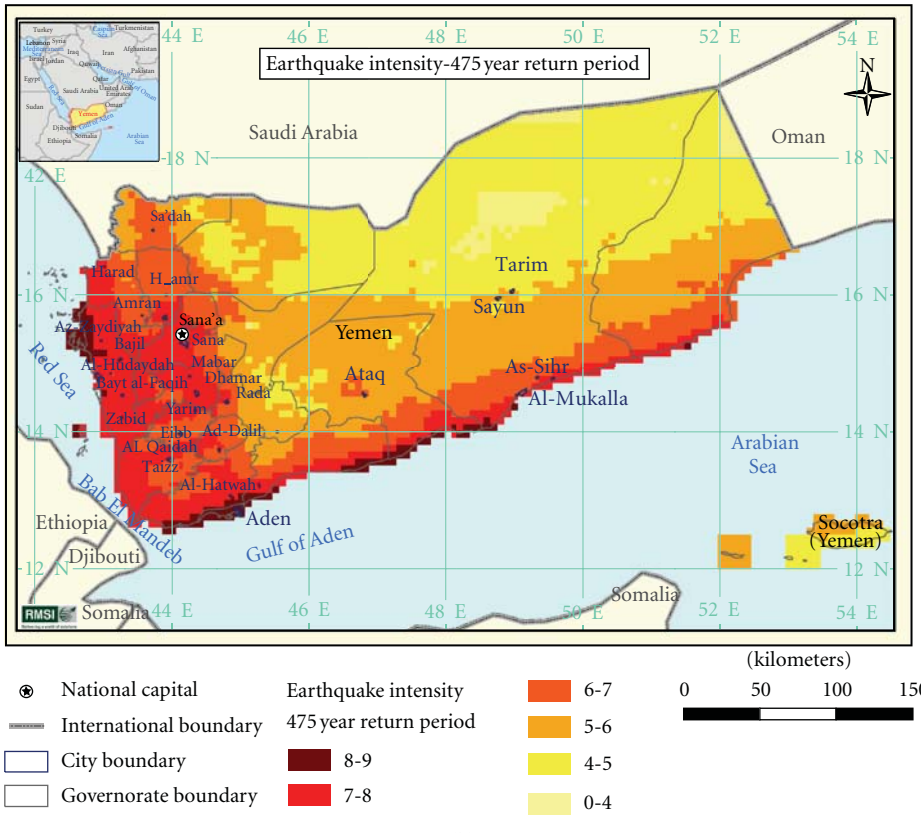

(b)

Figure 12: 100- and 475-year return period probabilistic seismic hazard maps for earthquake intensity in Yemen.

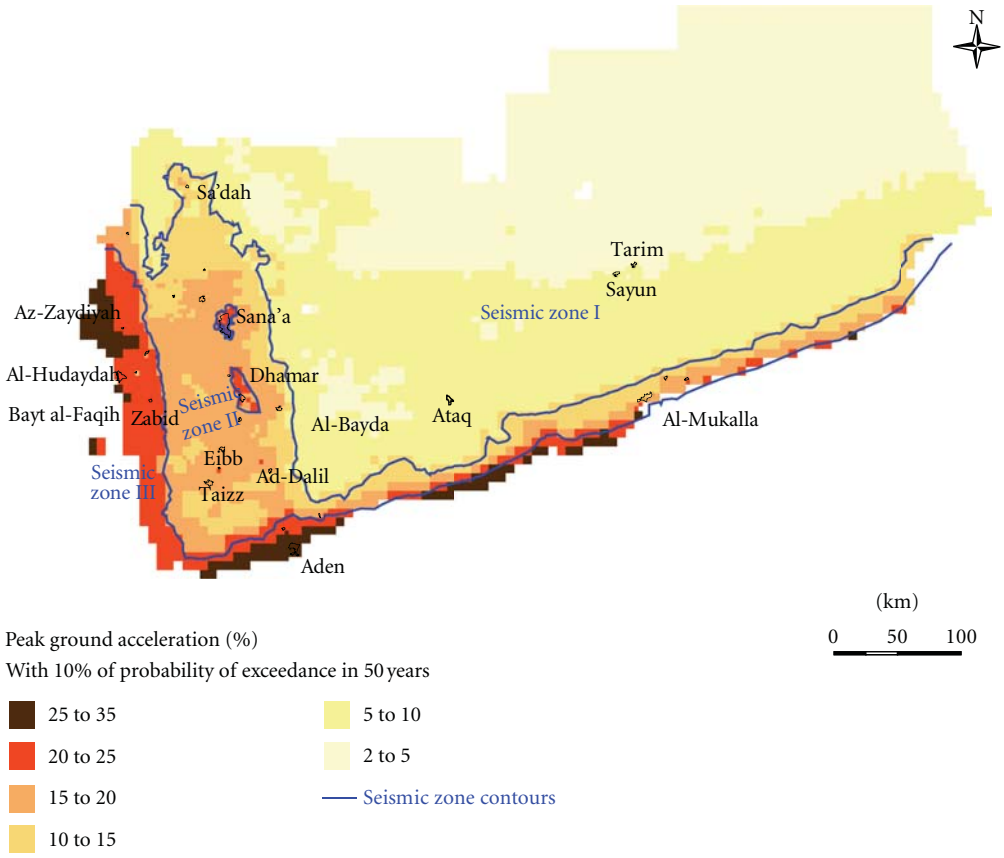

Figure 13: Seismic zoning in Yemen.

grid) using selected ground-motion prediction models and the soil-dependent amplification factor. Every stochastic event is characterized by a return period of occurrence, which depends on the characteristics of seismicity of the given source zone and the magnitude of the event. Thus, the same return period is assigned to the level of ground motion generated by the event. The complete master database of median ground shaking values from all stochastic earthquakes with their rates of occurrence at all locations considering their average site conditions has been prepared. This master database has been used for (a) development of probabilistic seismic hazard maps, that is, return period of particular PGA threshold values at the individual sites, and (b) seismic zoning of the country.

The hazard maps in terms of PGA and MSK intensity with a 39% probability of being exceeded in 50 years (100-year return period) and with a 10% probability of being exceeded in 50 years (475-year return period) are shown in Figures 11 and 12. Note that the site effect has already been incorporated into the hazard assessment. As can be seen, the western and southern parts of Yemen are characterized by the highest level of seismic hazard and the hazard is low across the central and the eastern parts. The largest contributors to Yemen seismic hazard are events from the West Arabian Shield seismic zone.

A seismic zoning scheme for Yemen has been suggested based on hazard values calculated for the 475-year return period. This is the first attempt in developing seismic zoning of the country. The territory of Yemen has been subdivided into 3 seismic zones (Figure 13). By definition, each zone is characterized by a constant hazard, quantified by a different value of the reference peak horizontal ground acceleration as shown in Table 5. Yemen capital area and the Dhamar area are located inside the zone with the highest level of hazard (zone I). Note that the Dhamar area had experienced the destructive earthquake (M_b = 6.0) of 13 December 1982.

Table 5: Parameters of seismic zonation in Yemen.

Seismic zone	Maximum horizontal ground acceleration with 10% exceedance probability in 50 years	Median value of PGA
I	0.20–0.30 g	0.25 g
II	0.10–0.20 g	0.15 g
III	<0.10 g	0.05 g

Although expected seismic hazard values are calculated at over 30,000 rural and urban population agglomeration areas in Yemen, the hazard values in 30 major cities of Yemen in terms of PGA for 100- and 475-year return periods are presented in Table 6 together with information on the city population from the Yemen 2004 Census.

Table 6: Estimated probabilistic seismic hazard for 100- and 475-year return periods for major cities in Yemen.

Major city	Population 2004	100-year return period PGA (in g)	475-year return period PGA (in g)
Sana'a	1,976,081	0.151	0.244
Aden	570,551	0.217	0.292
Taizz	458,933	0.087	0.154
Al-Hudaydah	402,560	0.163	0.247
Eibb	208,844	0.083	0.151
Al-Mukalla	176,942	0.083	0.137
Dhamar	144,273	0.107	0.188
Amran	76,863	0.111	0.194
Sayun	58,037	0.036	0.061
Bajil	55,016	0.153	0.242
Sa'dah	49,422	0.062	0.128
Rada	49,419	0.097	0.180
Tarim	47,674	0.032	0.055
As-Sihr	47,060	0.119	0.191
Yarim	46,498	0.093	0.162
AL Qaidah	39,254	0.108	0.185
Bayt al-Faqih	39,116	0.156	0.237
Hajjah	34,136	0.064	0.116
Al-Bayda	29,059	0.029	0.056
Jaar	28,529	0.122	0.194
Ad-Dalil	27,139	0.090	0.162
Al-Hatwah	25,471	0.146	0.227
Harad	24,280	0.089	0.161
Mabar	24,262	0.114	0.197
Al-Marawiah	22,990	0.084	0.149
Zabid	21,440	0.128	0.211
Gayl Bawazir	20,969	0.091	0.152
Az-Zaydiyah	18,341	0.158	0.246
H_amr	15,036	0.078	0.145
Ataq	13,995	0.051	0.092

10. Conclusions

This study is a part of the "The Yemen National Probabilistic Risk Assessment" project funded by The World Bank Global Facility for Disaster Reduction and Recovery (GFDRR). The broad objectives of the project were to apply the principals of probabilistic risk assessment for assessing risks from earthquake, flood, storm surge, tsunami, and landslide in order to develop an analysis of risk exposure and financial response capacity for Yemen. The main output of the project is (i) analysis of the applications of catastrophic risk modeling for hazard risk management in Yemen and (ii) a natural hazard risk atlas for Yemen. The outcome of research described in this paper is a model for probabilistic seismic hazard assessment, which provides necessary inputs for earthquake loss estimation and risk planning on the country level. It is necessary to note that no building code has been developed so far in the country and the constructed seismic zonation scheme may be used as the basis for the code.

We realize, of course, that there are some limitations and shortcomings in our study. We do not consider epistemic uncertainty in all the inputs to the hazard assessment, which usually is incorporated using the logic tree approach, as well as aleatory uncertainty in PGA-intensity conversion. The choice of the attenuation relations used in this study may have some regional biases. The developments of regional ground motion prediction models, as well as the testing of applicability of the recently proposed generalized worldwide ground-motion models, are a matter of high importance. The applied procedure for soil modification requires additional study. For practical calculations, requiring the estimation of the median hazard and loss values, these simplified approaches have been applied.

Acknowledgments

The authors are grateful to the Risk Modeling and Insurance Group, RMSI Pvt. Ltd., Noida (India) for providing necessary facilities. Financial assistance from the World Bank Grant (Contract no. 7149613) is thankfully acknowledged. The authors wish to express their gratitude to Pushpendra Johri. Upamanyu Mahadevan and other members of the Risk Modeling and Insurance Group, RMSI Pvt. Ltd. for their critical reading of the paper. They acknowledge thoughtful comments and suggestions by two anonymous reviewers, which enhanced the quality of paper significantly.

References

[1] J. P. Poirier and M. A. Taher, "Historical seismicity in the near and Middle East, North Africa and Spain, from Arabic documents (VIIth – XVIIth century)," *Bulletin of the Seismological Society of America*, vol. 70, no. 6, pp. 2185–2201, 1980.

[2] S. A. Alsinawi and A. Al Aydrus, *Seismicity of Yemen*, Obadi Studies and Publishing Center, Sana'a, Republic of Yemen, 1999.

[3] M. M. Al-Saud, "Seismic characteristics and kinematic models of Makkah and central Red Sea regions," *Arabian Journal of Geosciences*, vol. 1, pp. 49–61, 2008.

[4] R. D. Adams and M. Barazangi, "Seismotectonics and seismology of Arab region: a brief summary and future plans," *Bulletin of the Seismological Society of America*, vol. 74, pp. 1011–1030, 1984.

[5] N. N. Ambraseys and C. P. Melville, "Seismicity of Yemen," *Nature*, vol. 303, no. 5915, pp. 321–323, 1983.

[6] G. Plafker, R. Agar, A. Asker, and M. Hanif, "Surface effects and tectonic setting of the 13 December 1982 North Yemen earthquake," *Bulletin of the Seismological Society of America*, vol. 77, pp. 2018–2037, 1987.

[7] N. N. Ambraseys, C. P. Melville, and R.D. Adams, *The Seismicity of Egypt, Arabia and the Red Sea: a historical review*, Cambridge University Press, 1994.

[8] A. S. Arya, L. S. Srivastave, and S. P. Gupta, "Survey of damages during the Dhamar earthquake of 13 December 1982 in the Yemen Arab Republic," *Bulletin of the Seismological Society of America*, vol. 75, no. 2, pp. 597–610, 1985.

[9] A. A. Al Aydrus, "Seismic hazard considerations for Yemen," in *Proceedings of the International Conference on the Geology of the Arab World (GAW4 '97)*, pp. 1106–1129, Cairo University, Cairo, Egypt, 1997.

[10] S. A. Alsinawi and A. Al Aydrus, "Seismic hazard considerations for Yemen," in *Proceedings of the International Conference on Geology of Arab World (GAW4 '99)*, pp. 1106–1129, Cairo University, Cairo, Egypt, 1999.

[11] S. A. Alsinawi, "Seismological considerations of the Eastern Arab region," in *Proceedings of the EuroMediterranean Seminar on Natural, Environmental and Technological Disasters*, Algers, Algeria, 2001.

[12] C. A. Cornell, "Engineering Seismic risk analysis," *Bulletin of the Seismological Society of America*, vol. 58, no. 5, pp. 1583–1606, 1968.

[13] N. A. A. Razaq, N. M. Al Mukhadri, and A. H. A. Ahmed, *Evaluation of Seismic Ground Motion for Sana'a Region, Ministry of Oil and Mineral Resources*, Yemen General Corporation for Mineral Resources and Geological Survey, National Seismological Observatory Center, Dhamar, Yemen, 1997.

[14] E. A. M. Al-Heety, "Historical seismicity of the stable continental regions (SCRs) in the Arabian plate (Preliminary Study)," *MESF Cyber Journal of Earth Science*, vol. 3, pp. 22–41, 2005.

[15] L. M. Sykes and M. Landisman, "The seismicity of East Africa, the Gulf of Aden and the Arabian and Red Seas," *Bulletin of the Seismological Society of America*, vol. 54, pp. 1927–1940, 1964.

[16] J. K. Gardner and L. Knopoff, "Is the sequence of earthquakes in Southern California with aftershocks removed, Poissonian?" *Bulletin of the Seismological Society of America*, vol. 64, pp. 1363–1367, 1974.

[17] G. M. Molchan and O. E. Dmitrieva, "Aftershock identification: methods and new approaches," *Geophysical Journal International*, vol. 109, no. 3, pp. 501–516, 1992.

[18] D. Gardini, M. Di Donato, and E. Boschi, "Calibration of magnitude scales for earthquakes of the Mediterranean," *Journal of Seismology*, vol. 1, no. 2, pp. 161–180, 1997.

[19] R. Ulusay, E. Tuncay, H. Sonmez, and C. Gokceoglu, "An attenuation relationship based on Turkish strong motion data and iso-acceleration map of Turkey," *Engineering Geology*, vol. 74, no. 3-4, pp. 265–291, 2004.

[20] A. C. Johnston, K. J. Coppersmith, L. R. Kanter, and C. A. Cornell, "The earthquakes of stable continental regions: assessment of large earthquake potential," EPRI Report TR–102261, Electric Power Research Institute, Calif, USA, 1994.

[21] G. Ekström and A. M. Dziewonski, "Evidence of bias in estimations of earthquake size," *Nature*, vol. 332, no. 6162, pp. 319–323, 1988.

[22] J. C. Stepp, "Analysis of completeness of the earthquake sample in the Puget Sound area and its effect on statistical estimates of earthquake hazard," in *Proceedings of the1st International Conference on Microzonazion*, vol. 2, pp. 897–910, Seattle, Wash, USA, 1972.

[23] G. Grunthal, C. Bosse, S. Sellami, D. Mayer-Rosa, and D. Giardini, "Compilation of the GSHAP regional seismic hazard for Europe, Africa and the Middle East," *Annali di Geofisica*, vol. 42, no. 6, pp. 1215–1223, 1999.

[24] M. Al-Haddad, G. H. Siddiqi, R. Al-Zaid, A. Arafa, A. Necioglu, and N. Turkelli, "A basis for evaluation of Seismic hazard and design criteria for Saudi Arabia," *Earthquake Spectra*, vol. 10, no. 2, pp. 231–257, 1994.

[25] A. Frankel, "Mapping seismic hazard in the central and eastern United States," *Seismological Research Letters*, vol. 66, no. 4, pp. 8–21, 1995.

[26] A. D. Frankel, M. D. Petersen, C. S. Mueller et al., "Documentation for the 2002 update of the national seismic hazard maps," *U.S. Geological Survey Open-File Report*, vol. 02-420, p. 33, 2002.

[27] C. A. Cornell and E. H. Vanmarcke, "The major influences on Seismic risk," in *Proceedings of the 4th World Conference of Earthquake Engineering*, vol. 1, pp. 69–83, Santiago, Chile, 1969.

[28] R. K. McGuire, "FORTRAN computer program for seismic risk analysis," *U.S. Geological Survey, OpenFile Report*, pp. 67–76, 1976.

[29] J. A. Abdalla and A. S. Al-Homoud, "Seismic hazard assessment of united arab emirates and its surroundings," *Journal of Earthquake Engineering*, vol. 8, no. 6, pp. 817–837, 2004.

[30] J. Douglas, "Earthquake ground motion estimation using strong-motion records: a review of equations for the estimation of peak ground acceleration and response spectral ordinates," *Earth-Science Reviews*, vol. 61, no. 1-2, pp. 43–104, 2003.

[31] J. Douglas, "Errata and additions to Ground motion estimation equations 1966–2003," BRGM/RP-54603-FR, 2006.

[32] N. Abrahamson, G. Atkinson, D. Boore et al., "Comparisons of the NGA ground-motion relations," *Earthquake Spectra*, vol. 24, no. 1, pp. 45–66, 2008.

[33] A. F. Amrat, "Empirical relations characterizing earthquake ground motion attenuation in Jordan," *Bulletin of Jordan Seismological Observatory*, vol. 28, pp. 37–45, 1996.

[34] A. I. Husein Malkawi and K. J. Fahmi, "Locally derived earthquake ground motion attenuation relations for Jordan and conterminous areas," *Quarterly Journal of Engineering Geology*, vol. 29, no. 4, pp. 309–319, 1996.

[35] M. Y. Al-Qaryouti, "Attenuation relations of peak ground acceleration and velocity in the Southern Dead Sea Transform region," *Arab Journal of Geosciences*, vol. 1, pp. 111–117, 2008.

[36] P.C. Thenhaus, S. T. Algermissen, D. M. Perkins, S. Hanson, and W. H. Diment, "Probabilistic estimates of seismic ground motion hazard in Western Saudi Arabia, Kingdom of Saudi Arabia," *USGS Open File Report*, no. OF-06-b, p. 64, 1986.

[37] K. W. Campbell, "Strong motion attenuation relations: a ten-year perspective," *Earthquake Spectra*, vol. 1, no. 4, pp. 759–804, 1985.

[38] R. R. Youngs, S. J. Chiou, W. J. Silva, and J. R. Humphrey, "Strong ground motion attenuation relationships for subduction zone earthquakes," *Seismological Research Letters*, vol. 68, no. 1, pp. 58–73, 1997.

[39] Building Seismic Safety Council (BSSC), "NEHRP recommended provisions for seismic regulations for new buildings and other structures," FEMA 302/303, Part 1 (Provisions) and Part 2 (Commentary), developed for the *Federal Emergency Management Agency*, Washington, DC, USA, pp. 337, 1997.

[40] Y. Choi and J. P. Stewart, "Nonlinear site amplification as function of 30 m shear wave velocity," *Earthquake Spectra*, vol. 21, no. 1, pp. 1–30, 2005.

[41] UNDHA, "YemenEarthquake Nov 1991," UNDRO Situation Reports, pp. 1–5, 1991, http://reliefweb.int/node/34314.

[42] W. M. Shehata, A. Kazi, F.A. Zakir, A. M Allam, and A. A. Satan, "Preliminary Investigations on Dhamar earthquake, North Yemen , of December 13, 1982," *Bulletin of King Abdulaziz University*, pp. 23–52, 1983.

Hindawi Publishing Corporation
International Journal of Geophysics
Volume 2012, Article ID 364318, 12 pages
doi:10.1155/2012/364318

Research Article

The New Avalanche-Like Stochastic Model for Parameterization of Seismicity and Its Application to the South Sakhalin Island Seismicity

M. V. Rodkin[1,2] and I. N. Tikhonov[2]

[1] *Institute of Earthquake Prediction Theory and Mathematical Geophysics, Russian Academy of Sciences (RAS), Moscow 117997, Russia*
[2] *Institute of Marine Geology & Geophysics, Russian Academy of Sciences Far Eastern Branch (FEB RAS), Yuzhno-Sakhalinsk 693022, Russia*

Correspondence should be addressed to I. N. Tikhonov, tikhonov@imgg.ru

Received 9 August 2011; Revised 25 December 2011; Accepted 18 January 2012

Academic Editor: Yamaoka Koshun

Seismic process is usually considered as an example of occurrence of the regime of self-organizing criticality (SOC). A model of seismic regime as an assemblage of randomly developing episodes of avalanche-like relaxation, occurring at a set of metastable subsystems, can be the alternative of such consideration. The model is defined by two parameters characterizing the scaling hierarchical structure of the geophysical medium and the degree of metastability of subsystems of this medium. In the assemblage, these two parameters define a model b-value. An advantage of such approach consists in a clear physical sense of parameters of the model. The application of the model for parameterization of the seismic regime of the south part of Sakhalin Island is considered. The models of space changeability of the scaling parameter and of temporal changeability of the parameter of metastability are constructed. The anomalous increase of the parameter of metastability was found in connection with the Gornozavodsk and Nevelsk earthquakes. At the present time, high values of this parameter occur in the area of the Poyasok Isthmus. This finding is examined in comparison with other indications of an increase in probability of occurrence of a strong earthquake in the South Sakhalin region.

1. Introduction

Seismic process is usually considered as an example of realization of the self-organized criticality—the SOC-model [1–3]. However, as it was argued in [4] the SOC model has a rather limited possibility in interpretation of real seismotectonic processes. Besides, there is no clear interpretation in terms of this model of a difference between regions of high and low seismic activity. Moreover, the analogue between critical phenomena and seismic process is not satisfying enough. The critical phenomena (the second-order phase transitions, for example) proceed without discharge or absorption of energy; and this is their fundamental peculiarity, in many respects determining other features of the critical behavior. But earthquakes are accompanied by release of huge amounts of energy, and this is their fundamental property. Thus it can be concluded, that consideration of a seismic process in terms of the SOC-model is not quite satisfactory. Therefore, alternative approaches are of interest.

For quantitative statistic modeling of seismicity regime, the Generalized Omori law and the Epidemic-Type Aftershock-Sequence (ETAS) model are used at the present time [5–7]. However, these models have a formal statistical character; the determination of parameters of the models and even the findings of statistical relations between the parameter values do not result in an essential progress in understanding of the physics of the seismic process.

The fundamental properties determining the process of seismicity are the scaling hierarchical properties of the structure of the Earth's crust and the irreversibility of the processes ongoing in the Earth's interior. A natural model for understanding of the process of seismicity would be a statistical

model treating seismicity in terms of these fundamental characteristics. The model of seismic process as an assemblage of avalanche-like episodes of relaxation, occurring occasionally at a set of uniform metastable subsystems [8, 9], meets such demands. As it was shown in [8], this model appears to be the most simple, providing the realization of power law distributions typical of dynamical dissipative systems [10]. In case of seismicity, metastability is connected with elastic energy stored in the geophysical media and abruptly released during earthquakes. In application to the earthquake process, we will name this model the statistical earthquake model (SEM). The main parameters of the SEM model are two parameters, characterizing the scaling properties of the geophysical media and the level of irreversibility (metastability) of processes taking place in this media. The SEM model, which was discussed in detail in [9], is presented and used below in the examination of the seismic regime of the south part of Sakhalin Island.

2. Model

We will model seismic regime as an assemblage of episodes of avalanche-like relaxation, occurring occasionally at a set of statistically identical metastable subsystems. Let us describe this statistical earthquake model (SEM) in terms of recurrent scheme (or equivalently in terms of multiplicative process) as it was presented in [8, 9]. A longer description of a continuous case is presented in [11].

Let us imagine that an ongoing stochastic process (here earthquake), that had released energy X_i by time moment t_i, continues its development with probability p or cancels with probability $(1 - p)$. In a case when the process interrupts on this ith step, the quantity of event (the amount of energy released in the event) will be equal to X_i. In a case when the process of relaxation of metastable subsystem continues, we suggest that the energy released in this event will grow up by the next moment of time t_{i+1} to the value

$$X_{i+1} = r \times X_i, \tag{1}$$

where r can be a random parameter with mean value exceeding one. In a continuous case [11], the avalanche-like differential equation instead of recurrent relation (1) is used. This approach models an avalanche-like process of release of metastable systems.

For simplicity of the mathematical manipulations presented below, we will suggest that the constant X_0 value at the first step being equal to $X_0 = 1$ and $r = \text{const}$. In this case, in scheme (1) the probability of interrupting of the process on nth stage and correspondingly obtaining of the value $X_n = r^n$ is equal to $(1 - p) \times p^n$. From this, we observe that the tail of the function of distribution $F(X_n > X)$ is equal to

$$\begin{aligned}(1 - F(X)) &= (1 - p) \times p^n \times (1 + p + p^2 + \cdots p^{\infty}) \\ &= p^n.\end{aligned} \tag{2}$$

We have also $\lg(X) = n \times \lg(r)$, and thus $n = \lg(X)/\lg(r)$ and $\lg(1 - F(X)) = n \times \lg(p) = \lg(X)/\lg(r) \times \lg(p)$. From here, we have

$$(1 - F(X)) = X^{\lg(p)/\lg(r)}; \tag{3}$$

thus we receive a power law dependence for the tail of the distribution function $(1 - F(X))$ from X, as it takes place in the distribution law of the seismic moment and seismic energy values and in many other cases [12]. It can be shown that this result is valid for the case of stochastic r values (for mean r value >1) and in case of random normal distribution of X_0 values that has a minor influence on the final type of distribution (3).

The scheme thus described treats a development of an earthquake as a process of sequential transition to higher hierarchical levels. At constant parameter r value, we have a discrete and log-periodical distribution of the energy values of earthquakes. With a growth of random spread in r values, the step-by-step character of model distributions becomes smoother, and at the limit we receive a monotonic distribution with quasirectilinear relation in coordinates $\{\lg(X), \lg(1 - F(X))\}$ with a slope of recurrence relation equal to

$$b = -\frac{\lg(p)}{\lg(r)}, \tag{4}$$

where b characterizes the power distribution of quantities X and has a meaning similar to the b-value in the Gutenberg-Richter law (for the energy or seismic moment earthquake values). The sign minus is added in (4) to get a positive b-value used in seismology.

Thus, in terms of the SEM model, the b-value is defined by two parameters, one of them (r) characterizes scaling properties of the medium, whereas the second (p) answers a probability of a continuation of avalanche-like relaxation of metastable sub-systems. Thus it characterizes the degree of metastability of the medium. We will name these two parameters further as a scaling parameter r and a metastability parameter p.

It is not difficult to pick up the values of r and p parameters of the SEM model and initial X_0 value so that the received b parameter from (4) will agree with b-value of a typical seismic regime, and $\lg(X)$ will have values typical of earthquake magnitudes. If we take some average number N of avalanche-like processes occurring in a time unit, and the suitable $r(t)$ and $p(t)$ values, the model will give the sequence of magnitudes of main (independent) events $\lg(X_j)$ similar with a sequence of magnitudes of earthquakes (without aftershocks) occurring in a real seismic process.

As an example, we take a case with weak (with amplitude 0.2) and periodic ($T = 1000$ time units) change of parameter p producing the similar periodicity in a model b-values. The mean intensity of seismic flow $N = 500$ events per unit time is suggested, and variations in N number are assumed to follow the Poisson law. In Figure 1, an example of such model process of duration of 5000 time units is presented. For the every one time unit, the model maximal magnitude $M_{\max}$

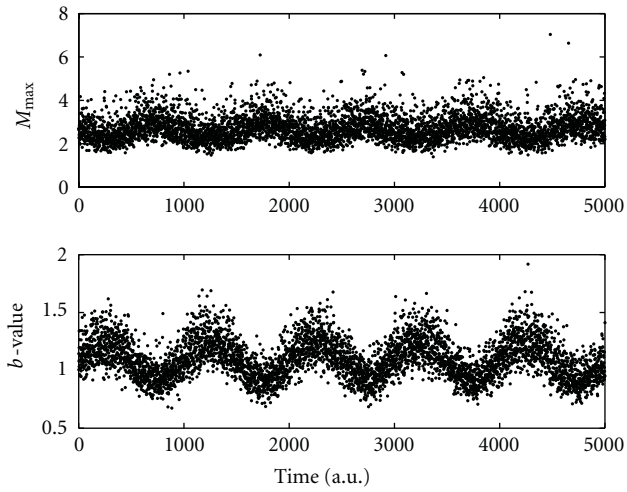

Figure 1: An example of realization of the SEM model of a seismic regime; (a) maximal magnitude values M_{max}; (b) the b-values. On an abscissa axis, the arbitrary time units are given (500 events in average in each).

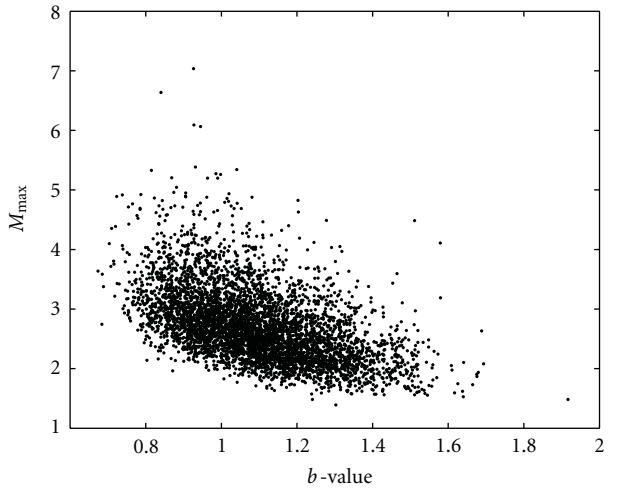

Figure 2: Model relationship between the b-value and maximal magnitude M_{max} value occurred in the next time interval.

value and the b-value are calculated. The b-values are calculated for the every one time unit from the maximum likelihood approach [13] and the model magnitude values $\lg(X_i)$. The received M_{max} and the b-values appear to be similar visually with typical behavior of a real seismic process (besides of an artificially taken periodical character of change in b-values with time).

It is easy to see that even such a very simple model is not trivial. It produces the well-known "prognostic" feature—the decrease in b-values precedes the intervals of time of occurrence of strong earthquakes. To see such dependence (distinct also in Figure 1) more clearly, in Figure 2 the graph of relationship of maximal magnitudes $M_{max} = \lg(X_i)$ values versus b-values in preceding time interval was shown.

An appearance of model correlation given in Figure 2 is clear. Actually, the values of p and r parameters that correspond statistically to occurrence of larger M_{max} values correspond also to lesser b-values. This relation has a stochastic character. It is worth mentioning that the decrease of b-values in the SEM model is not an indicator of developing of process of a "preparation" of a strong event (it is not correct to speak about the preparation of a "strong earthquake" in the case of a sequence of independent events), but it is a parameter correlated with an increase of probability of occurrence of a strong event.

Thus the increase of the values of parameters p and r is an indicator of increase of probability of occurrence of a strong earthquake, and so the evaluation of these parameters and their changeability can be used for monitoring of a probability of a strong earthquake occurrence. In the SEM model, it appears naturally (but not obligatory) to consider the scaling parameter r as depending on the Earth's crust segmentation (so parameter r is spatially dependent and constant or slow changeable through time), whereas the parameter metastability p is suggested to be time dependent.

The SEM model is used below for examination of the seismic regime of the south of Sakhalin Island. However, before discussing the results of such examination, we should briefly characterize the seismicity of the Sakhalin Island and the used database.

3. Patterns of Seismicity of the Sakhalin Island and the Available Earthquake Catalogs

Sakhalin Island (Russia) is located in the Pacific-Eurasia transition zone. In the island, on average 1 earthquake with magnitude $M \geq 6$ and about 10 events with $M \geq 5$ takes place every 10 years. The events with $M \geq 7$ occurred nearly once per century. The strongest known Moneron earthquake M 7.5 took place here in 1971.

The seismicity of Sakhalin can be divided into shallow (h = 0–30 km) and deep (mainly in depth interval of 280–350 km) seismicity. Deep earthquakes are connected with the Kurile Islands subduction zone. In Sakhalin Island, deep-focus earthquakes do not represent a substantial seismic danger, and shallow seismicity appears to be not dependent on deep seismicity. Below, only shallow earthquakes with the depth $h < 30$ km are considered.

Within Sakhalin Island and the adjacent shelf, four major deep fault systems were identified that generate almost all crustal earthquakes with $M \geq 5.5$: the Rebun-Moneron, the Western Sakhalin, the Central Sakhalin, and the Eastern-Sakhalin fault systems (Figure 3).

The Rebun-Moneron fault system, situated near the Moneron and Rebun Islands, was revealed to be active when the century's strongest shallow-focus Sakhalin earthquake (M_S 7.5, September 5, 1971) took place here.

The Western Sakhalin fault system extends below the floor of the Tatar Straight along the western shore of the island and then merges with the Central Sakhalin faults. In this zone strong earthquakes in 1907 (Alexandrovsk-Sakhalinsk, M_S 6.5), 1924 (Lesogorsk-Uglegorsk, M_S 6.9), and in 2000 (Uglegorsk, M_S 7.2) took place. No strong earthquakes ($M > 5.0$) were registered in the southern part of this fault zone until

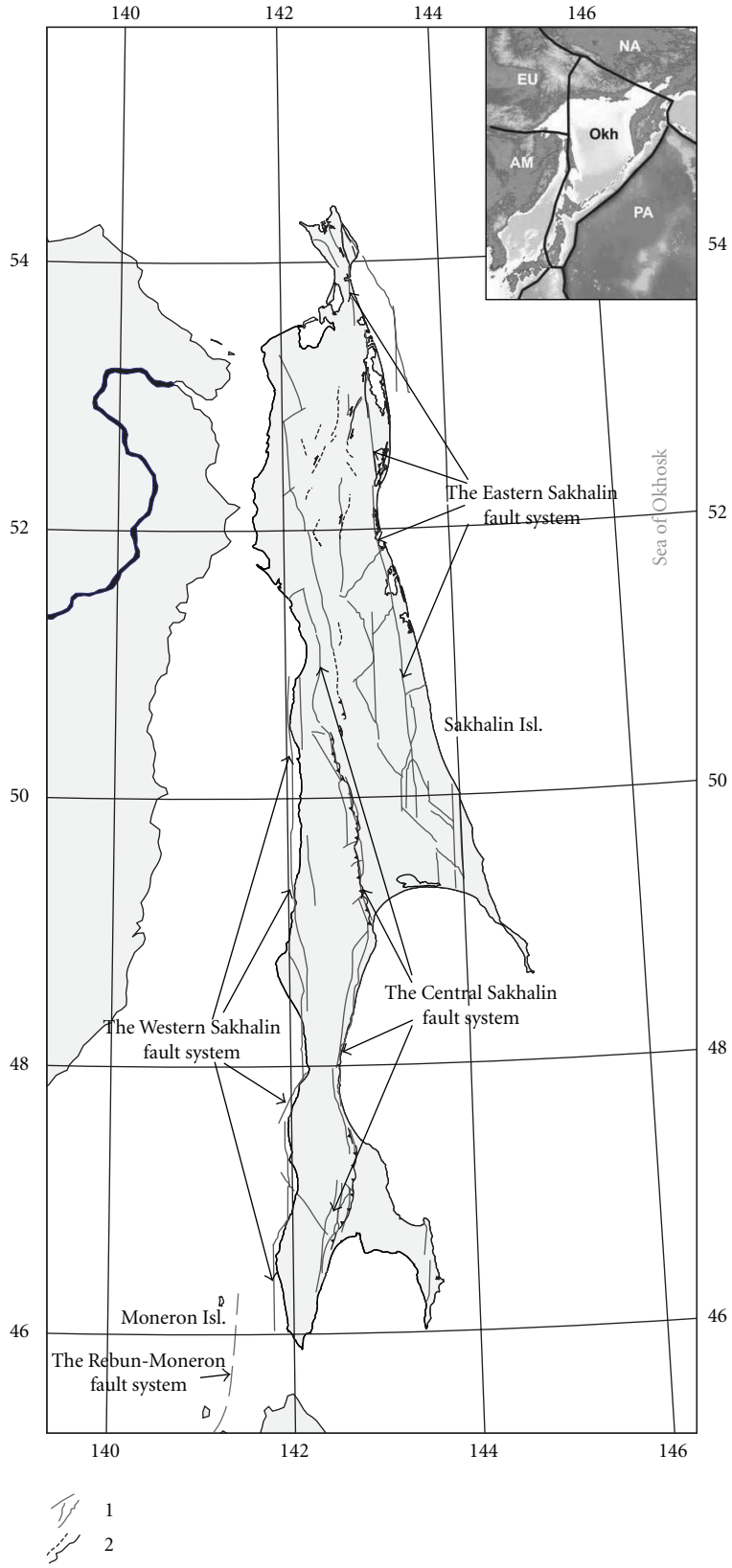

Figure 3: Active faults of the Sakhalin region. Insert—regional scheme of plate boundaries in the model NUVEL-1A and its modifications [14]. NA—North American, EU—Eurasian, PA—Pacific, OKH—Okhotsk plates.

the 17 August 2006, M_W 5.6 Gornozavodsk earthquake and the 2 August 2007, M_W 6.2 Nevelsk earthquake have occurred here [15, 16].

The Central Sakhalin fault system, and more specifically, its southern segment, is traceable from south to north along the western coast of Aniva Bay (Krilion Peninsula), farther on westward from Yuzhno-Sakhalinsk, and along the eastern shore of the island to Poronaisk, and then merges with the Western Sakhalin faults. Two strongest earthquakes that occured in this fault zone since 1905 (February 2, 1951 Aniva earthquake (M_S 5.5) and the September 1, 2001 Takoe earthquake (M_S 5.6)) took place within the southern segment of the fault.

The Eastern Sakhalin fault system extends along the north-eastern shore of the island. Prior to the May 28, 1995 Neftegorsk earthquake (M_S 7.2), there was no evidence of a significant earthquake occurrence here. Investigation of active faults of the North Sakhalin began after the Neftegorsk earthquake [17–19]. Paleoseismological reconstructions showed that recurrence time of the strong (M 7.0–7.5) earthquake here appears to be from some hundreds to thousand years.

The most complete data about the Sakhalin Island earthquakes during the historical and instrumental periods of observations are collected in the regional catalogue [20] (see Figure 4). The catalogue is unified, and all earthquakes are characterized in M_{LH} magnitude scale. 3566 events with magnitudes $M_{LH} \geq 3.0$ occurring in 1905–2005 are given in the catalog. The representativeness of the catalog changes considerably with time. The catalog is believed to be representative (the Gutenberg-Richter frequency-magnitude relation is fulfilled) for the events with $M_{LH} \geq 5.5$ since 1930, and for the events with $M_{LH} \geq 3.5$ since 1970. This catalog named below as catalog 1 is used for the examination of spatial change of the scaling parameter r of the SEM model.

Let us consider the main features of the spatial distribution of epicenters with $M_{LH} \geq 3.5$ (Figure 4). As it is seen in the figure, three areas with higher seismicity are observed in the Sakhalin Island and the adjoining shelf: (1) western part of the Southern Sakhalin with adjacent shelf southward 47.0°N; (2) western and Central parts of the Central Sakhalin with adjacent shelf between 48.5° and 51.5°N; (3) eastern part of the Northern Sakhalin with adjacent north-eastern shelf northward 51.5°N. All the earthquakes with $M_{LH} \geq 5.5$ occurred within these three areas; in these regions the most part of the shocks with $M_{LH} \geq 4.5$ have also occurred.

It can be noticed that localization of the strong earthquakes appears to agree with a suggested location of the boundary of Okhotsk Sea plate in this region. It is suggested [21] that this boundary in the south goes along the western shore of the island up to the latitude 51°N, then it turns to the east and crosses the island along the valley of Tym River and extends further northward along the eastern shore of the island. There are, however, a number of gaps in localization of strong seismicity along this tentative plate boundary zone. Below, the most southern gap in strong seismicity taking place along the western shore of the Sakhalin Island between 47.0°N and 49°N neighboring to the location of the M_W 6.2 Nevelsk and M_S 7.5 Moneron earthquakes (Figure 5) will be examined. This site was argued earlier [22] as a seismic gap—a potential area of the origin of a next strong earthquake [23].

More detailed information about the seismicity of the South Sakhalin area is available since 2003 because of the installation of the seismic networks "Datamark" and "DAT." The catalog obtained from these networks is presented in unified M_L magnitude scale. In the latest version of this catalog published last year [24], which was used, it is argued that the network provides the registration of $M \geq 2.5$ earthquakes throughout the South Sakhalin and adjacent shelf area and $M \geq 2.0$ earthquakes in the central part of the South Sakhalin area. The Gutenberg-Richter frequency-magnitude relation of the catalog data is found to be valid for the earthquakes with $M \geq 2.0$. This catalog named below as catalog 2 is used below for the examination of the spatial change of the parameter of metastability p of the SEM model. The Gutenberg-Richter relations for both catalogs 1 and 2 are presented in Figure 6. This Figure shows the suitable representativeness of earthquakes with magnitude $M \geq 3.5$ and $M \geq 2.0$ for catalog 1 and catalog 2 correspondingly.

4. Parameterization of Seismicity of the South of Sakhalin in the Framework of the SEM Model

We have used the catalogue 1 [20] and its continuation to examine the spatial model of change of the scaling parameter r. Firstly, the b-values were estimated in the surroundings of every event of the used catalogue. Estimation of the b-value was performed for the groups including 50 events closest to the given earthquake. For the b-values estimation the maximum likelihood method was used [13]:

$$b = \frac{\lg(e)}{M_{\text{av}} - M_c}, \tag{5}$$

where $e = 2.7183\cdots$, M_{av} is the average magnitude for the given subset of data and M_c is the lower magnitude limit. Estimates from (5) are known to be suitably stable for number of events exceeding 50. Then by formula (4) the value of parameter r_i for spatial surrounding of the ith earthquake was estimated. At this step, the value of probability p was taken to be fixed $p = 0.5$. For the further use, the scaling parameter r_i values were spatially averaged in cells 1/3° of latitude ×1/3° of longitude to obtain $R(\varphi, \lambda)$ values. This way we have got $R(\varphi, \lambda)$ values as spatially averaged scaling parameter r values.

Having in mind the change in representativeness of the catalog 1 through time the different variants of time interval and magnitude limitation were used for r_i and $R(\varphi, \lambda)$ calculation. One of the received $R(\varphi, \lambda)$ models obtained for the case of $M_{LH} > 3.5$ earthquakes occurring since 1970 (there are 1224 such events in the catalog 1) is shown in Figure 7. In all examined cases of different time intervals and limitation of magnitude range, the main features of the $R(\varphi, \lambda)$ map are similar. We have considerable increase in $R(\varphi, \lambda)$ values in the area adjacent to the location of occurrence of the strongest Moneron and Nevelsk earthquakes, and a slight tendency of a decrease in scaling parameter value from south to north

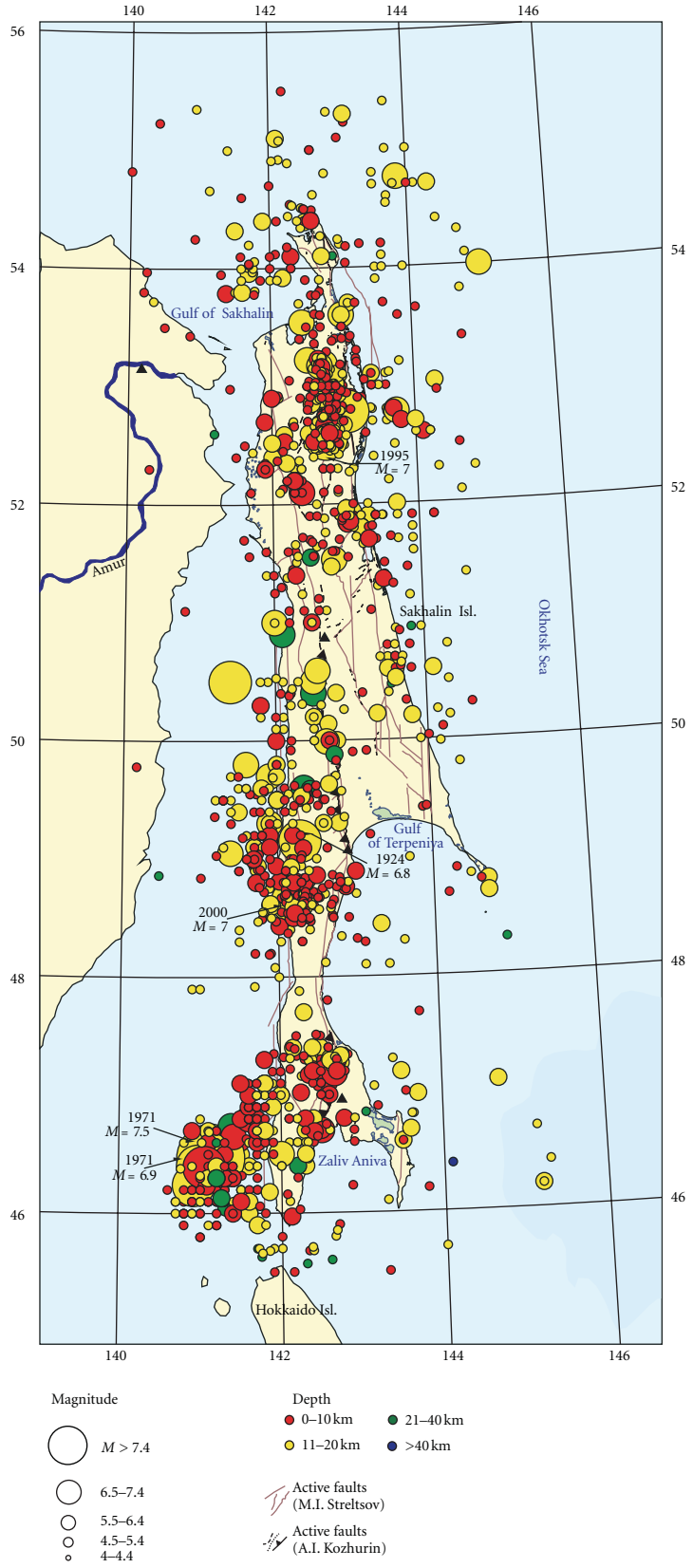

FIGURE 4: Map of crustal $M_S \geq 3.5$ earthquake of the Sakhalin region, 1906–2010. Date and magnitude is given for the strongest earthquakes.

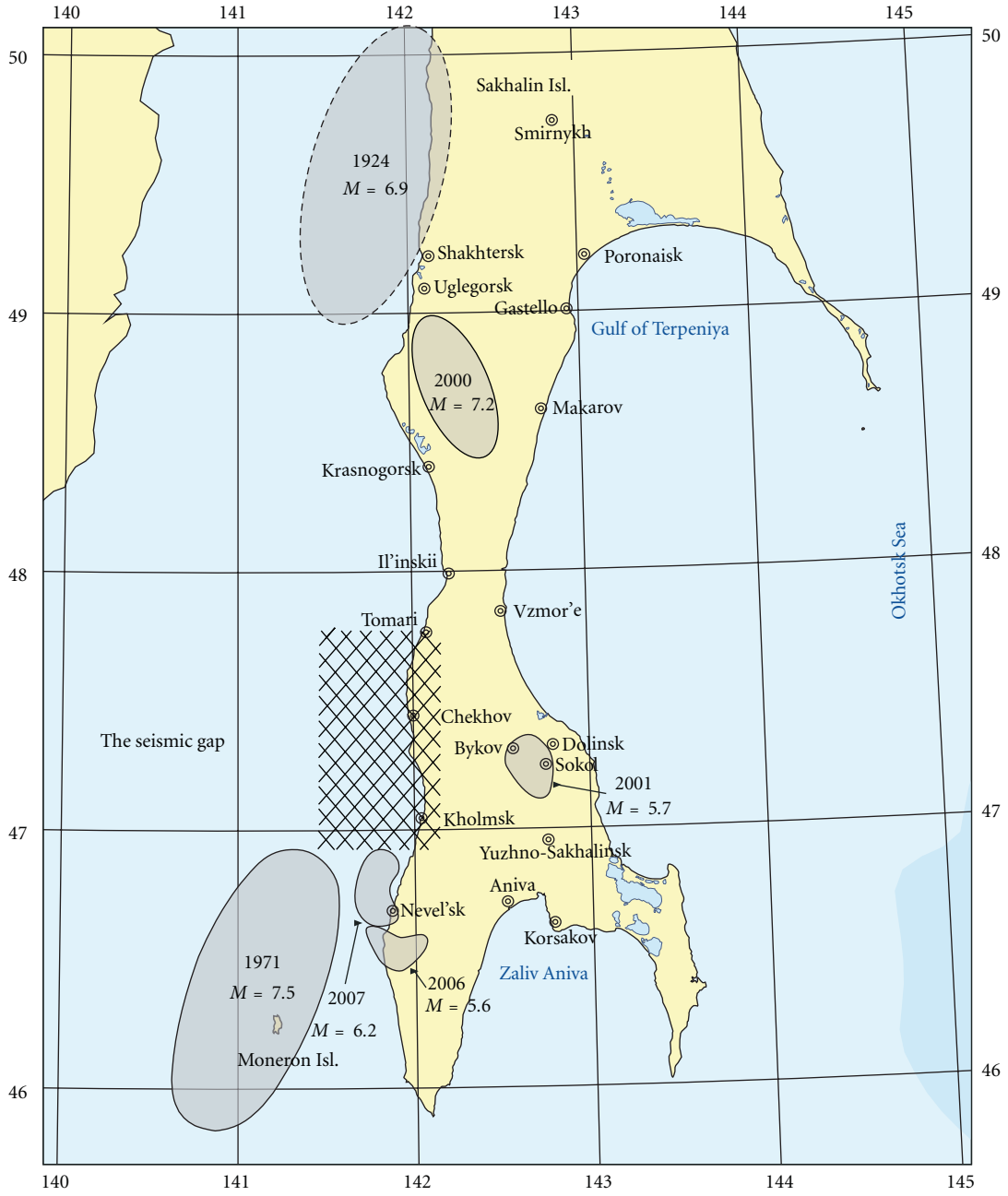

Figure 5: Sources of large earthquakes at the western coast of Sakhalin Island (grey ovals) and the approximate location of the seismic gap (hatched rectangle).

in the South Sakhalin region. Note also that the range of change of $R(\varphi, \lambda)$ values is slightly larger than it was expected. This can occur due to changeability of other factors factually included at this step in change of $R(\varphi, \lambda)$ value (remember, that parameter p was suggested to be constant, $p = 0.5$).

For earthquake prediction, however, the time changes of probability p are of the main interest. In estimation of temporary changeability of parameter of metastability p, the errors in determination of $R(\varphi, \lambda)$ values do not play an essential role, because the values $R(\varphi, \lambda)$ are suggested to be constant in time and so the errors of their determination have a minor importance in examination of change in parameter metastability p values with time.

The estimation of time changeability of parameter of metastability p was carried out using the detailed catalogue 2 obtained from the networks "Datamark" and "DAT" and the obtained before model of spatial changeability of scaling parameter, that is, from $R(\varphi, \lambda)$ values. As above, in the case of the $R(\varphi, \lambda)$ values determination different variants of time and magnitude intervals were examined. In the version presented below, we have examined earthquakes with $M \geq 2.5$, 1789 events altogether. Firstly, we calculated local

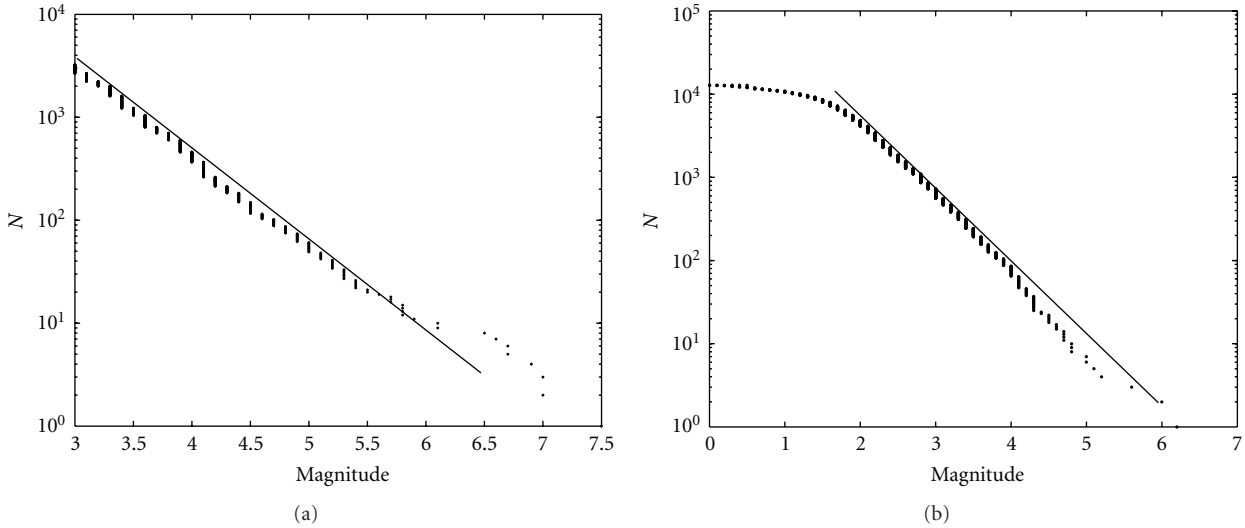

Figure 6: Gutenberg-Richter relations for both catalogs 1(a) and 2 (b); points—earthquakes of magnitude M in descending order, line shows the limits of validity of Gutenberg-Richter relation.

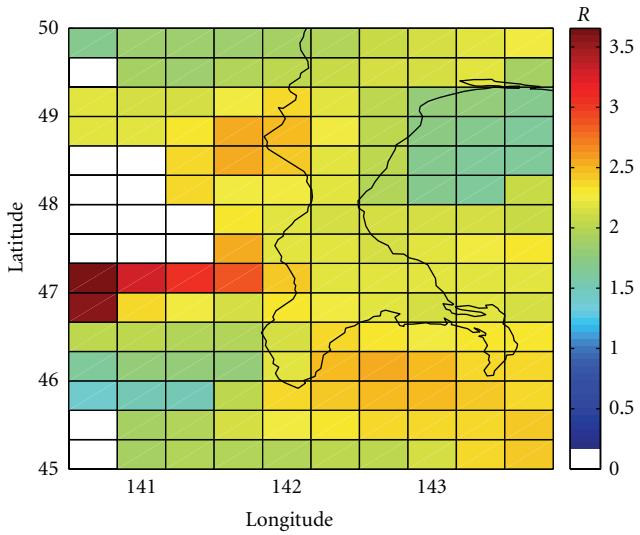

Figure 7: Scheme of changes of the values $R(\varphi, \lambda)$, spatial component of the SEM model.

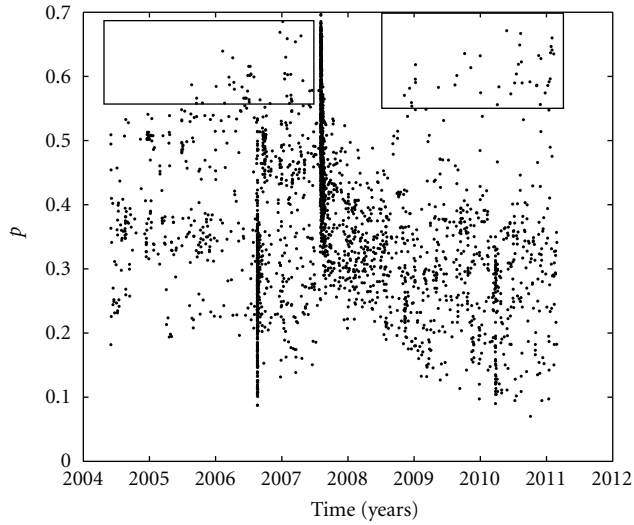

Figure 8: Temporary component of the SEM model—sequence of values of parameter of metastability p in spatial-temporary surrounding of earthquakes of the catalogue 2. The groups of the events with higher p values ($p > 0.55$), occurred before and after the Nevelsk earthquake, are marked out by the rectangles.

b-values for the spatial-temporal surrounding of every of these earthquakes. As above, 50 events spatially closest to every given ith earthquake were chosen to estimate the corresponding b-value from relation (5); however, the selection was done not from all the assemblage of the epicenters, but only from a temporal subsequence of events from $(i-500)$ to $(i+500)$; the length of the sequence decreases for the events adjacent to the ends of the temporary area. The quantity of parameter p_i was estimated then from (4) with due account of the value of the scaling parameter $R(\varphi, \lambda)$ corresponding to given coordinates and the obtained time-local b-value.

In Figure 8, the values $p(t)_i$ for every ith event of catalogue 2, obtained by the described method are shown. In Figure two temporary areas of high concentration of the earthquakes, corresponding to the Gornozavodsk (17 August 2006, 46.51°N and 141.92°E, M_W 5.6) and Nevelsk (2 August, 2007, 46.83°N and 141.76°E, M_W 6.2) earthquakes, are well seen. Some tendency of an increase in parameter p values before the Nevelsk earthquake, and a clear tendency of decrease after the Nevelsk earthquake occurrence can be seen. This tendency is fairly valid. In terms of the SEM model, this feature points out the growth of probability of occurrence of a strong earthquake that has realized in the Nevelsk earthquake occurrence. On this background the groups of events with anomalously high (>0.55) parameter p values are highlighted. The first such group takes place before the Nevelsk

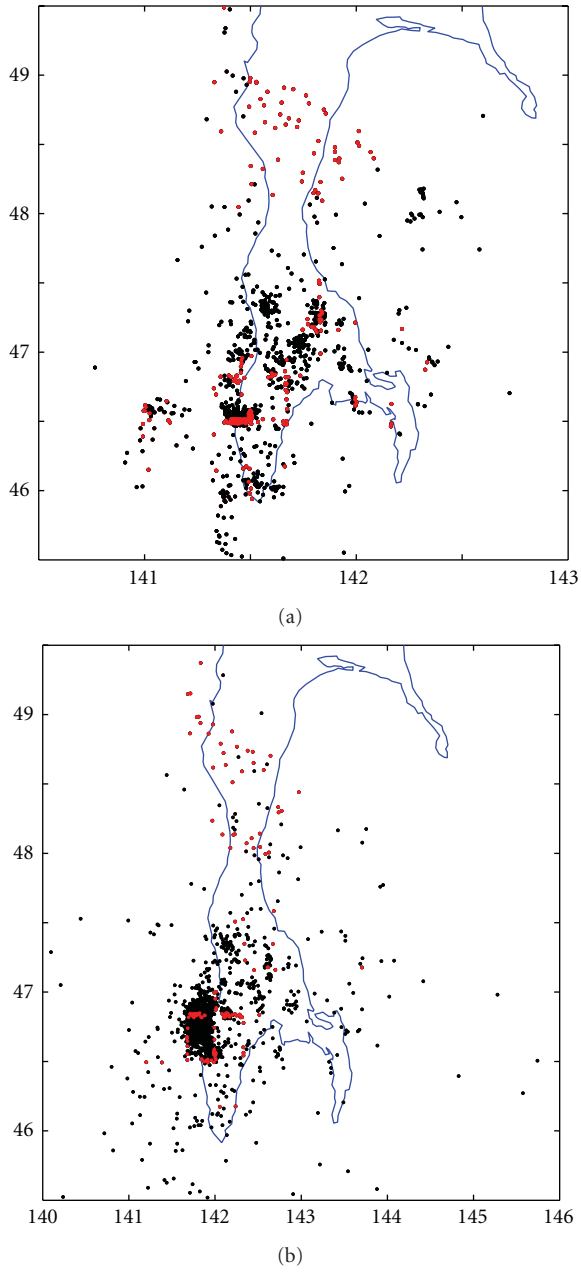

Figure 9: Location of earthquakes with typical ($p < 0.55$, black points) and with increased values of parameter of metastability ($p > 0.55$, red points). (a) events occurred before the Nevelsk earthquake; (b) events occurred after the Nevelsk earthquake.

earthquake, and the second group begins in one year after the Nevelsk earthquake occurrence and prolongs till now. These two groups are highlighted in Figure 8 by the rectangles. In Figures 9(a) and 9(b), spatial location of epicenters of the examined events of the catalogue 2 occurring before and after the Nevelsk earthquake are given. In both cases, the events with metastability parameter p values exceeding 0.55 are given as red points. We cannot explain some regularity in location of events with parameter p values exceeding 0.55, probably it can be connected with some quantization of latitude and longitude values in the catalog.

The groups of the epicenters with $p > 0.55$, occurring before the Nevelsk earthquake took place in a number of locations connected with epicenters of strong earthquakes and earthquake swarms occurring in this time interval. Besides, during the same time interval events with higher values of parameter of metastability p were found to be typical of the more distant area located in the Poyasok Isthmus region with latitude values in interval 48-49°N.

The higher level of parameter of metastability revealed in the area of the Poyasok Isthmus can be connected probably with the Southern Sakhalin fault [25, 26], which represents a large transversal nonconformity across the Sakhalin Island. The greater activity of this structure before the Nevelsk earthquake could be explained probably by an analogy with the effect of activity of transverse structures in the straits of the Kuril Islands in connection with the strong earthquakes occurring at the adjacent segments of the subduction zone. Such analogy is substantiated by close correlation of the areas of strong earthquakes occurrence in the Sakhalin Island with the tentative location of the Okhotsk Sea plate boundary.

After the Nevelsk earthquake of August 2, 2007, the earthquakes with higher parameter p value timely disappeared (Figure 8). However, such earthquakes arose again one year later. The events with $p > 0.55$ took place in a few areas connected with the Nevelsk earthquake occurrence and in the Poyasok Isthmus area. Besides, a few events with high parameter metastability value are dispersed irregularly around the studied area; those can be caused by stochastic errors.

According to the catalog 1 [20], the Poyasok Isthmus area corresponds to the seismic gap between two segments of high seismic activity taking place in the last century, so it can be suggested that a considerable seismic activity could occur in this gap also. Having this possibility in mind we have examined the seismicity in the Poyasok Isthmus area in more detail. The growth of seismic danger is associated rather frequently with a nonlinear growth of a number of events and released seismic energy with time. To check this effect, the graphs of a number of events and released seismic energy in the zone (rectangle area 47.8°–49°N and 141.5°–144°E) were calculated from the catalog 2 data. In Figure 10(a), the cumulative graph of a number of events occurring here since 2005 is given, and all earthquakes with magnitude exceeding 2 were taken into account to increase a statistics. In Figure 10(b), the graph of cumulated seismic energy released here since 2009 is shown (if we could show data for an earlier period of time, the changes in flow of seismic energy after 2009 would become badly visible).

In Figure 10(a), several intervals of nonlinear growth of a number of events are seen. These time intervals appear to be associated with the strongest earthquakes which occurred during this time interval in the south of Sakhalin Island. The moments of these earthquakes occurrence are marked by vertical lines and figures: 1—Nevelsk, 2—Gornozavodsk, and 3—the event of February 24, 2007 with M_S 4.6 and coordinates 48.95°N, 142.06°E. The first two events are the strongest earthquakes occurring in the studied time interval in the south of Sakhalin. The third event is the strongest earthquake, which occurred in the Poyasok Isthmus region

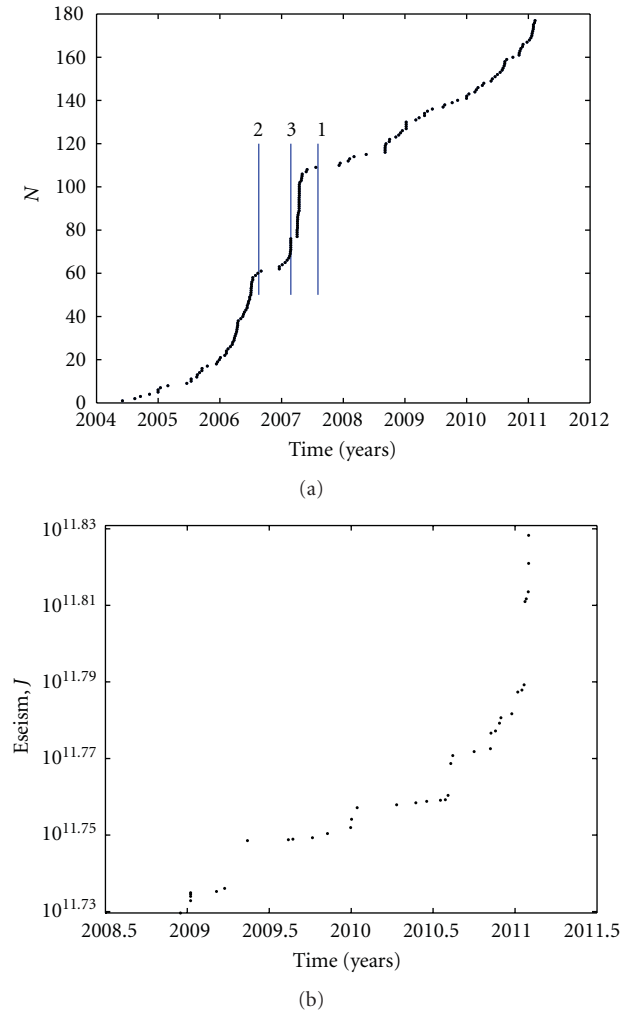

Figure 10: Cumulative graphs of a number of the events (a) and of released seismic energy (b) inside the area 48°-49°N and 141.5°–143°E. Vertical lines and figures show the moments of the Nevelsk (1), Gornozavodsk (2) earthquakes, and the strongest earthquake of February 24, 2007, $M = 4.6$ (3) occurred in the pointed area.

in this time interval. A prominent nonlinear growth of a number of earthquakes preceded the first two events and coincides with the moment of the third event occurring in the Poyasok Isthmus area. The last case is an example of a typical fore- and aftershock behavior. The first two cases of nonlinear increases in seismic activity with the subsequent seismic silence agree with the seismic behavior found in the distant vicinity of the strong earthquakes in [27]. In this work, an increase in seismic activity replaced by the seismic silence was found in a distant vicinity of generalized strong earthquake with approaching the strong earthquake occurrence moment.

A nonlinear growth of a number of earthquakes takes place in the Poyasok Isthmus area also since 2010. Besides, the nonlinear growth of released seismic energy takes place here since the middle of 2010 (Figure 10(b)).

It should be noted also that the intervals of time of nonlinear growth of a number of events and of released seismic energy (occurring in 2007-2008 and since the middle of 2010) correspond to the intervals of time of occurrence of events with higher (>0.55) values of parameter of metastability p in the Poyasok Isthmus area. Thus one can conclude that the seismic regime behavior taking place now in the Poyasok Isthmus area repeats the one that took place here before the strong Nevelsk earthquake and testifies for the increase of probability of a strong earthquake occurrence.

5. Discussion

Seismic regime is usually considered in terms of the SOC-model. This model suggests the spontaneous evolution of dynamic system to a critical state. However, the physical mechanism of such evolution in the case of seismicity has not been suggested. It is also not clear how to explain the difference of seismically active and aseismic areas in terms of the SOC-model. The analogy between seismic regime and the second-order phase transitions also seems disputable. The principal feature of the second-order phase transitions is that the transformation goes without absorption (emission) of energy. In contrast to it, a huge explosion-like release of energy takes place during strong earthquakes.

The alternative model of the seismic regime as a set of episodes of avalanche-like relaxation of metastable sub-systems (SEM model) is suggested. In the case of seismicity the origin of metastable sub-systems is connected with storage of elastic energy. The discharge of accumulated elastic energy can be initiated by the excess of stress level [2] and/or by local temporal decrease of strength of geomaterial occurring in connection with processes of (fluid) metamorphic transformations [28–30].

In the simple variant of the SEM model (without memory of the medium), the geophysical medium is described by two parameters [9]. The first parameter characterizes a spatial hierarchy (scaling) of the medium; this parameter r is easily identified with the coefficient of hierarchy according to Sadovsky [31]. The second parameter characterizes a degree of metastability of the medium; it is parameter p, a probability of continuation of the process of on-going avalanche-like relaxation of the stored energy. In assemblage, these two parameters define spatial-time change of the b-value.

The presence of two latent parameters specifying one empirically determining characteristic b-value gives place for choice. It seems natural to describe the spatial changeability by scaling parameter r and a temporal changeability by parameter of metastability p. The spatial model of change of scaling parameter for Sakhalin $R(\varphi, \lambda)$ was obtained using the catalogue for 1905–2005; at this step parameter p was suggested to be constant $p = 0.5$. The model of time changeability of parameter of metastability $p(\varphi, \lambda, t)$ was obtained with the use of values $R(\varphi, \lambda)$ on the basis of the detailed ($M \geq 2$) catalogue of seismicity of the south of Sakhalin for the time interval 06/07/2003–02/27/2011, when strong Gornozavodsk and Nevelsk earthquakes (M_W 5.6 and M_W 6.2) had occurred.

As a result of the estimate of the parameter of metastability $p(\varphi, \lambda, t)$, a few spatial-time groups of earthquakes with

higher p parameter values were revealed. In terms of the SEM model such increase corresponds to the growth of probability of the strong earthquake occurrence. One of the groups, observed before the Nevelsk earthquake, corresponds to the causative fault of this earthquake. After the Nevelsk earthquake, occurrence of the higher values of parameter p was not observed for a year. Then such earthquakes appeared again in the area of the Poyasok Isthmus, as it was before the Nevelsk earthquake. Since March 2010 in this area, the shocks with still higher (>0.6) values of the parameter p have appeared. It can be suggested that such behavior testifies for an increase of the probability of a strong earthquake origin in the south of Sakhalin.

The results of parameterization of the seismic regime in the framework of the SEM model complement the results received previously from the examination of the seismic gaps. According to these results, the gap along the western coast of the South Sakhalin was only partly (in its southern part up to the latitude 47°N) closed as a result of the Nevelsk earthquake (Figure 5). At present, it is not clear whether the finding of increase in seismic activity in the Poyasok Isthmus area shows a higher probability of the origin of a stronger earthquake in this area or a stronger earthquake can occur in the larger area corresponding to the seismic gap along the western coast of the Sakhalin Island. If the period of accelerated growth of seismic activity changes by the period of seismic silence (as it was just before the Nevelsk and Gornozavodsk earthquakes), it can be an indicator of a stronger and more remote earthquake.

Note that the revealed features in the behavior of parameters of the SEM model could be explained in terms of change of b-value. In this case, the discussed anomaly in parameter p increase in the vicinity of strong Nevelsk earthquake corresponds to the well-known tendency of decrease in b-value in vicinity of strong earthquakes. But the used approach of the SEM model has some advantage for the interpretation because of the more clearly physical sense of the parameters of the SEM model.

6. Conclusion

Seismic regime is usually considered as an example of the regime of self-organizing criticality (SOC-conception). The alternative SEM model treats the seismic regime as an assemblage of random episodes of avalanche-like relaxation, taking place at a set of uniform metastable sub-systems. The SEM model in its simple form without memory of the system is defined by two parameters, characterizing scaling in spatial structure of the Earth's crust and the degree of metastability of the geophysical medium. This model is used for the description of seismic regime of the south of Sakhalin Island. The models of spatial changeability of the scaling parameter and temporal changeability of the parameter of metastability are constructed. The anomalous growth of the parameter of metastability preceded the occurrence of the Gornozavodsk and Nevelsk earthquakes. At the present time, the anomalously high (and growing over time) values of this parameter are observed in the area of the Poyasok Isthmus (in the vicinity of latitude 48°N). Clear nonlinear growth of the flow of a number of seismic events and of seismic energy is noticeable in this area before the Gornozavodsk and Nevelsk earthquakes and after 2009.

Acknowledgments

This paper was supported by the Russian Foundation for Basic Research, Grant no. 11-05-00663, and the European Grant FP7 no. 262005 SEMEP.

References

[1] P. Bak, C. Tang, and K. Wiesenfeld, "Self-organized criticality," *Physical Review A*, vol. 38, no. 1, pp. 364–374, 1988.

[2] G. A. Sobolev and A. V. Ponomarev, *Physics of Earthquakes and Precursors*, Nauka, Moscow, Russia, 2003.

[3] D. L. Turcotte, "Seismicity and self-organized criticality," *Physics of the Earth and Planetary Interiors*, vol. 111, no. 3-4, pp. 275–293, 1999.

[4] Y. Ben-Zion, "Collective behavior of earthquakes and faults: continuum-discrete transitions, progressive evolutionary changes, and different dynamic regimes," *Reviews of Geophysics*, vol. 46, no. 4, Article ID RG4006, 2008.

[5] Y. Ogata, "Statistical models for earthquake occurrence and residual analysis for point processes," *Journal of the American Statistical Association*, vol. 83, pp. 9–27, 1988.

[6] Y. Ogata, "Space-time point-process models for earthquake occurrences," *Annals of the Institute of Statistical Mathematics*, vol. 50, no. 2, pp. 379–402, 1998.

[7] P. A. Reasenberg and L. M. Jones, "Earthquake hazard after a mainshock in California," *Science*, vol. 243, no. 4895, pp. 1173–1176, 1989.

[8] V. Pisarenko and M. Rodkin, "Heavy-tailed distributions in disaster analysis," *Advances in Natural and Technological Hazards Research*, vol. 30, 2010.

[9] M. V. Rodkin, "Alternative to SOC concept—model of seismic regime as a set of episodes of random avalanche-like releases occurring on a set of metastable subsystems," *Izvestiya, Physics of the Solid Earth*, vol. 47, no. 11, pp. 966–973, 2011.

[10] B. B. Mandelbrot, *The Fractal Geometry of Nature*, W.H. Freeman and Company, 1982.

[11] M. V. Rodkin, V. F. Pisarenko, and T. A. Rukavishnikova, "Parameterization of regime of rare strong catastrophes-events," *Geoecology*, no. 2, pp. 164–172, 2007 (Russian).

[12] Sornette D., *Critical Phenomena in Natural Sciences, Chaos, Fractals, Self-organization and Disorder: Concepts and Tools*, Springer Series in Synergetics, Heidelberg, Germany, 2nd edition, 2004.

[13] T. Utsu, "A method for determining the value of b in a formula $\log n = a - bm$ showing the magnitude-frequency relation for earthquakes," *Geophysical bulletin of Hokkaido University*, vol. 13, pp. 99–103, 1965.

[14] D. Wei and T. Seno, "Determination of the Amuruan plate motion," in *Mantle Dynamics and Plate Interactions in East Asia*, vol. 27 of *Geodynamics Series*, p. 419, AGU, Washington, DC, USA, 1998.

[15] B. V. Levin, Ch. U. Kim, and I. N. Tikhonov, "The Gornozavodsk earthquake of August 17(18), 2006, in the south of Sakhalin Island," *Russian Journal of Pacific Geology*, vol. 1, no. 2, pp. 194–199, 2007.

[16] I. N. Tikhonov and Ch. U. Kim, "Confirmed prediction of the 2 August 2007 MW 6.2 Nevelsk earthquake (Sakhalin Island, Russia)," *Tectonophysics*, vol. 485, no. 1–4, pp. 85–93, 2010.

[17] A. I. Kozhurin and M. I. Streltsov, "Seismotectonic consequences of the May 28, 1995 Northern Sakhalin Earthquake," *Russia's Federal System of Seismological Networks and Earthquake Prediction. Information and Analytical Bulletin. The Neftegorsk Earthquake of May 27(28), 1995*, pp. 95–100, 1995.

[18] T. Shimamoto, M. Watanabe, Suzuki et al., "Surface faults and damage associated with the 1995 Neftegorsk earthquake," *The Journal of the Geological Society of Japan*, vol. 102, no. 10, pp. 894–907, 1996.

[19] M. I. Streltsov, *The May 27(28),1995 Neftegorsk Earthquake on Sakhalin Island*, Yanus-K, Moscow, Russia, 2005.

[20] L. N. Poplavskaya, A. I. Ivaschenko, L. S. Oskorbin et al., *Regional catalog of Sakhalin Earthquakes 1905–2005*, Institute of Marine Geology and Geophysics Far Eastern Branch RAS, Yuzhno-Sakhalinsk, Russia, 2006.

[21] S. M. Saprygin, V. E. Kononov, and V. N. Senachin, "Horizontal motions and plate boundaries in Sakhalin and Hokkaido," *Doklady Earth Sciences*, vol. 398, no. 7, pp. 1043–1046, 2004.

[22] I. N. Tikhonov, *Methods of Earthquake Catalog Analysis for Purposes of Intermediate- and Short-Term Prediction of Large Seismic Events*, Institute of Marine Geology and Geophysics Far Eastern Branch RAS, Vladivostok, Russia, 2006.

[23] K. Mogi, *Earthquake Prediction*, Academic Press (Harcourt Brace Jovanovich, Publishers), New York, NY, USA, 1985.

[24] B. V. Levin, Ed., *Catalog of Earthquakes of the South Sakhalin Area since 2000 until 2010 years*, Vladivostok, Russia, 2011.

[25] S. M. Saprygin, "Detailed seismic zoning of Sakhalin," *Russian Journal of Pacific Geology*, vol. 2, no. 2, pp. 158–164, 2008 (Russian).

[26] N. A. Bogdanov, Ed., *Tectonic Map of the Sea of Okhotsk Region in 1:2500000 Scale*, ILOVM RAS, Moscow, Russia, 2000.

[27] M. V. Rodkin, "Seismicity in the generalized vicinity of large earthquakes," *Journal of Volcanology and Seismology*, vol. 2, no. 6, pp. 435–445, 2008.

[28] V. A. Kalinin, M. V. Rodkin, and I. S. Tomashevskaya, *Geodynamic Effects of Physicochemical Transformations in a Solid Medium*, Nauka, Moscow, Russia, 1989.

[29] M. V. Rodkin, A. D. Gvishiani, and L. M. Labuntsova, "Models of generation of power laws of distribution in the processes of seismicity and in formation of oil fields and ore deposits," *Russian Journal of Earth Sciences*, vol. 10, no. 5, 2008.

[30] D. Sornette, "Earthquakes: from chemical alteration to mechanical rupture," *Physics Report*, vol. 313, no. 5, pp. 237–291, 1999.

[31] M. A. Sadovskii, Ed., *Discrete Properties of Geophysical Media*, Nauka, Moscow, Russia, 1989.

Hindawi Publishing Corporation
International Journal of Geophysics
Volume 2012, Article ID 543482, 8 pages
doi:10.1155/2012/543482

Research Article

Evaluating the RELM Test Results

Michael K. Sachs,[1] Ya-Ting Lee,[2] Donald L. Turcotte,[3] James R. Holliday,[1] and John B. Rundle[1,3,4]

[1] *Department of Physics, University of California, Davis, Davis CA 95616, USA*
[2] *Graduate Institute of Geophysics, National Central University, Jhougli 320, Taiwan*
[3] *Department of Geology, University of California, Davis, Davis CA 95616, USA*
[4] *Theory Section, Santa Fe Institute, Santa Fe, NM 87501, USA*

Correspondence should be addressed to Michael K. Sachs, mksachs@ucdavis.edu

Received 15 July 2011; Revised 2 December 2011; Accepted 19 December 2011

Academic Editor: RodoÌfo Console

We consider implications of the Regional Earthquake Likelihood Models (RELM) test results with regard to earthquake forecasting. Prospective forecasts were solicited for $M \geq 4.95$ earthquakes in California during the period 2006–2010. During this period 31 earthquakes occurred in the test region with $M \geq 4.95$. We consider five forecasts that were submitted for the test. We compare the forecasts utilizing forecast verification methodology developed in the atmospheric sciences, specifically for tornadoes. We utilize a "skill score" based on the forecast scores λ_{fi} of occurrence of the test earthquakes. A perfect forecast would have $\lambda_{fi} = 1$, and a random (no skill) forecast would have $\lambda_{fi} = 2.86 \times 10^{-3}$. The best forecasts (largest value of λ_{fi}) for the 31 earthquakes had values of $\lambda_{fi} = 1.24 \times 10^{-1}$ to $\lambda_{fi} = 5.49 \times 10^{-3}$. The best mean forecast for all earthquakes was $\overline{\lambda}_f = 2.84 \times 10^{-2}$. The best forecasts are about an order of magnitude better than random forecasts. We discuss the earthquakes, the forecasts, and alternative methods of evaluation of the performance of RELM forecasts. We also discuss the relative merits of alarm-based versus probability-based forecasts.

1. Introduction

Earthquakes do not occur randomly in space. Large earthquakes occur preferentially in regions where small earthquakes occur. Earthquakes are complex phenomena, but they do obey several scaling laws. One example is Gutenberg-Richter frequency-magnitude scaling. The cumulative number of earthquakes N with magnitudes greater than M in a region over a specified period of time is well approximated by the relation

$$\log N = a - bM, \tag{1}$$

where b is a near universal constant in the range $0.8 < b < 1.1$ and a is a measure of the level of seismicity. Small earthquakes can be used to determine a and (1) can be used to determine the probability of occurrence of large earthquakes. Kossobokov et al. [1] utilized the number of $M \geq 4$ earthquakes in $1^\circ \times 1^\circ$ areas to map the global seismic hazard.

A question that has been studied by many groups is whether there are temporal variations in seismicity that can be used to forecast the occurrence of future earthquakes. Earthquakes on major faults (say the San Andreas in California) occur quasiperiodically. A reasonable hypothesis would be that the rate of regional seismicity would accelerate during the period between the major earthquakes. There is no evidence that this occurs systematically. Background seismicity in California appears to be stationary. With the exception of years with large aftershock sequences, Rundle et al. [2] (Figure 1) showed that seismic activity in Southern California in the magnitude range $1.5 < m < 4$ for the period 1983 to 2000 was well represented on a yearly basis by (1) taking $a = 5.4$ and $b = 1.0$.

Intermediate-term earthquake forecasting algorithms based on pattern recognition of variations in regional seismicity were developed by Keilis-Borok and colleagues [3]. These forecasts were alarm based, when a threshold of anomalous behavior was reached a warning of a time of

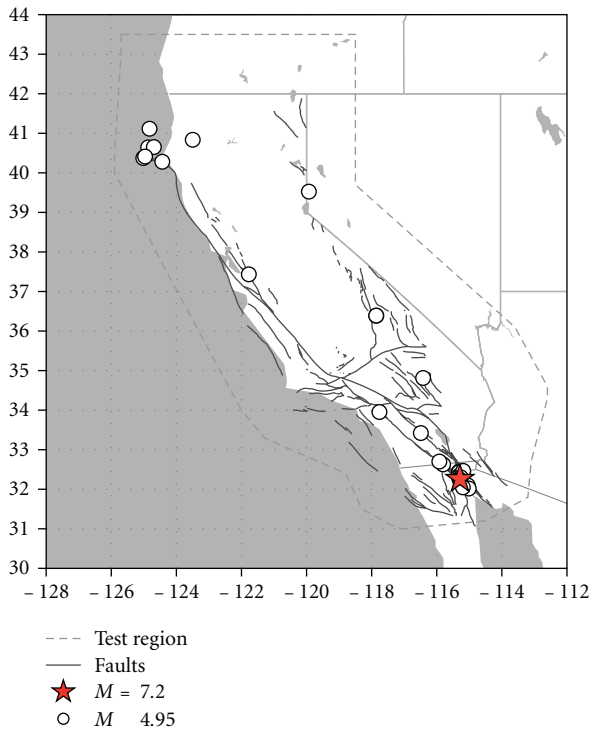

Figure 1: Map of the test region, the coast of California, major faults, and the 31 earthquakes with $M \geq 4.95$ that occurred in the test region. The earthquakes are given in Table 1.

increasing probability (TIP) of an earthquake was issued. A relatively high success rate was found including the 1988 Armenian earthquake and the 1989 Loma Prieta earthquake [4], but there were also notable false alarms and failures to predict.

The focus of this paper is to study the implications of the RELM test of earthquake forecasts in California. This was a prospective test of forecasts for $m > 5$ earthquakes during the period 2006–2010. Forecast submission was required prior to the starting date. In our study of the RELM test results we will utilize the methodology developed in the atmospheric sciences [5], specifically for tornadoes. Tornado forecasts are alarm based. Two levels of alarms are issued: (1) a tornado watch is issued for a specified area and time if atmospheric conditions appear conducive to tornados, (2) a tornado warning is issued if one or more tornados have been observed. The evaluation of tornado forecasts is based on the number of failures to predict and on the number of false alarms. A quantitative measure of success is the skill score, the skill score is unity for a perfect forecast and zero for a random (no skill) forecast. RELM forecasts were probabilistic rather than alarm based, that is a continuous range forecast probabilities were required. In an alarm-based forecast an area of high risk is specified. We will discuss the implications of the two alternative approaches.

The forecasts submitted to the RELM test were primarily based on precursory seismic activity. There are a variety of approaches to the quantification of this activity. In Section 2 of this paper we will discuss the relative intensity (RI) and pattern informatics (PI) approaches. The RI approach extrapolates the occurrence of small earthquakes during a specified precursory time window. High activity (activation) indicates high risk. The PI approach is related but includes both activation and quiescence. In Section 3 the problems with retrospective forecasts are discussed. In Section 4 the RELM test is discussed and the test earthquakes are described in Section 5. The submitted forecasts are discussed in Section 6 and are evaluated in Section 7.

An objective of this paper is to understand the relationship of the forecasts to the distribution of seismicity during the test period. We discuss what we believe is a well-defined precursory activation.

2. PI and RI

A pattern informatics (PI) approach to earthquake forecasting was proposed by Rundle et al. [2, 6] and Tiampo et al. [7]. In forecasting $M \geq 5$ earthquakes a region is divided into a grid of $0.1^\circ \times 0.1^\circ$ regions. The rates of seismicity in the regions are studied to quantify anomalous behavior. Precursory changes that include either increases or decreases in seismicity are identified during a prescribed time interval. If changes exceed a prescribed threshold hot-spots are defined. The forecast is that future $M \geq 5$ earthquakes will occur in the hot spot regions in a 10-year time window. Thus, the PI method is alarm based. Utilizing the PI method Rundle et al. [8] made a forecast of California hot spots valid for the period 2000–2010. Holliday et al. [9] reported that 16 of the 18 earthquakes that occurred during the period 2000–2005 occurred in hot spot regions. The PI forecast is time dependent because it is based on temporal changes in background seismicity.

A closely related forecasting technique is the relative intensity (RI) approach. The RI forecast is based on the direct extrapolation of the rate of occurrence of small earthquakes using (1). The RI forecast can be time dependent if the time span of the background seismicity is relatively short. The success of the PI method described above led to a discussion as to whether the PI method is significantly better than the RI method. Comparisons of these approaches have come to different conclusions regarding their validity [10, 11]. These comparisons emphasize the difficulties in evaluating the performance of seismicity forecasts.

3. Prospective versus Retrospective Forecasts

A prospective forecast is a true forecast of future earthquakes. No knowledge of these earthquakes exists. A retrospective forecast is a forecast of earthquakes that have occurred in the past (say 2000–2010) based on data available before the start of the period. The existence of the forecast earthquake is known. In principal a retrospective forecast can be carried out fairly; however, in many cases these forecasts are biased by the existence of the forecast earthquakes.

The PI forecast by Rundle et al. [8] was prospective. However, the successful forecast of 16 out of 18 earthquakes

in California led to a retrospective challenge of the results [11].

It became clear that it would be desirable to sponsor a contest in which research groups would provide prospective forecasts of earthquakes under well-defined conditions. This was the origin of the RELM test, which will be described in the next section. Some of the rules were based on the prospective forecast made by Rundle et al. [8]. The test region was California. Forecasts were made for $M > 5$ earthquakes on a grid of $0.1^\circ \times 0.1^\circ$ forecast cells. The forecast period was 1 January 2006 to 31 December 2010. The results will also be summarized in this paper.

4. RELM Test

In order to test methods for forecasting future earthquakes the Southern California Earthquake Center (SCEC) formed the working group for Regional Earthquake Likelihood Models (RELM) in 2000 [12]. For the first time a competitive test of prospective earthquake forecasts was to be carried out. Research groups were encouraged to submit forecasts of future earthquakes in California. At the end of the test period, the forecasts would be compared with the actual earthquakes that occurred.

The ground rules for the RELM test were as follows.

(1) The test region to be studied was the state of California; however the selected region extended somewhat beyond the boundaries of the state as shown in Figure 1.

(2) The objective was to forecast the largest earthquakes for which a reasonable number could be expected to occur in a reasonable time period. A five-year time period for the test was selected extending from 1 January 2006 to 31 December 2010. Earthquakes with $M \geq 5$ were to be forecast. This magnitude cutoff was chosen because at least 20 $M \geq 5$ earthquakes could be expected in this period. For $M \geq 6$, only about 2 would be expected so the 5-year period would be much too short. The applicable magnitudes were taken from the Advanced National Seismic System (ANSS) online catalog (http://www.ncedc.org/anss/anss-detail.html).

(3) Participants were required to submit the number of earthquakes expected to occur in specified spatial cells and magnitude bins during the test period. In order to do this, the test region was subdivided into $N_c = 7682$ spatial cells with dimensions $0.1^\circ \times 0.1^\circ$ (approximately 10 km × 10 km). These spatial cells were further divided into 41 magnitude bins: $4.95 \leq M < 5.05$, $5.05 \leq M < 5.15$, $5.15 \leq M < 5.25$,..., $8.85 \leq M < 8.95$, and $8.95 \leq M < \infty$. The participants were required to specify the forecast number of earthquakes N_{fmi} in magnitude bin m ($m - 0.05 < M < m + 0.05$) that would occur during the test period in cell i.

It is important to note that the RELM forecasts were continuous (probabilistic) rather than alarm based. The numbers of earthquakes expected to occur in each spatial cell and each magnitude bin was required. Continuous and alarm-based forecasts each have advantages and disadvantages. Continuous forecasts are useful for setting insurance premiums but the numbers of predicted earthquakes are so small that they have little meaning to the general public. Alarm-based forecasts specify where earthquakes are most likely to occur.

Nineteen forecasts were submitted by eight groups. Before discussing these forecasts in some detail we will discuss the earthquakes that occurred in the test region during the test period with $M \geq 4.95$.

5. The Earthquakes

During the test period 1 January 2006 to 31 December 2010, there were $N_e = 31$ earthquakes in the test region with $M \geq 4.95$. The times of occurrence, locations, and magnitudes of these earthquakes are given in Table 1. The locations of the test earthquakes are also shown in Figure 1.

The 31 earthquakes occurred in $N_{ce} = 22$ cells. The association of earthquakes with cells is given in Table 2. Five of the 22 cells had multiple earthquakes. The occurrence of five test earthquakes in cell A is not surprising since this is in the Cerro Prieto geothermal area that is recognized as having a high level of seismicity. Earthquakes occurred in 22 of the 7682 $0.1^\circ \times 0.1^\circ$ test cells in the test area.

The major earthquake that occurred during the test period was the $M = 7.2$ El Mayor-Cucapah earthquake on 4 April 2010 (event 22 in Table 1). This earthquake was on the plate boundary between the North American and Pacific plates. The epicenter was about 50 km south of the Mexico-United States border, but occurred within the test region as shown in Figure 1. Events 23, 24, 25, 26, 27, 28, 29, and 31 are well-defined aftershocks of the El Mayor-Cucapah earthquake. Events 1, 7, 8, 9, 10, 14, 16, and 19 constitute a precursory swarm of eight test earthquakes in this region in the magnitude range 4.97 to 5.80, including four in the 10-day period between 9 February and 19 February 2008 (events 7–10). These events were located some 5 km to 20 km north of the subsequent epicenter of the El Mayor-Cucapah earthquake and lie outside the primary aftershock region of that event. This swarm of earthquakes certainly cannot be considered foreshocks due to their relatively small magnitudes and early occurrence but may represent a seismic activation. We will discuss this activation in terms of AMR later in this paper.

Another swarm of earthquakes occurred in the northwest corner of the test region adjacent to Cape Mendocino. This sequence (events 23, 4, 5, 20, and 21) had magnitudes in the range 5.0 to 6.5. This is a region of high seismicity, and this concentration of events is expected. Event 21 may or may not be an aftershock of event 20. The pair of earthquakes 17 and 18 are interesting. It is very likely that the $M = 5.0$ earthquake on 1 October 2009 was a foreshock of the $M = 5.19$ earthquake on 3 October 2009.

6. Submitted Forecasts

The submitted forecasts have been discussed in some detail [13]. The nineteen forecasts submitted by eight groups are available on the RELM website (http://relm.cseptesting.org/). In order to have a common basis for comparison, we will only consider forecasts that cover the entire test region.

Table 1: Times of occurrence, locations, and magnitudes of the 31 earthquakes in the test region with $M \geq 4.95$ from 1 January 2006 until 31 December 2010. The $M = 7.2$ El Mayor-Cucapah earthquake is in bold.

No.	Origin time (UTC)	Lat.	Long.	M
1	2006/05/24 04:20:26.01	32.3067	−115.2278	5.37
2	2006/07/19 11:41:43.46	40.2807	−124.4332	5.00
3	2007/02/26 12:19:54.48	40.6428	−124.8662	5.40
4	2007/05/09 07:50:03.83	40.3745	−125.0162	5.20
5	2007/06/25 02:32:24.62	41.1155	−124.8245	5.00
6	2007/10/31 03:04:54.81	37.4337	−121.7743	5.45
7	2008/02/09 07:12:04.55	32.3595	−115.2773	5.10
8	2008/02/11 18:29:30.53	32.3272	−115.2568	5.10
9	2008/02/12 04:32:39.24	32.4475	−115.3175	4.97
10	2008/02/19 22:41:29.66	32.4325	−115.3130	5.01
11	2008/04/26 06:40:10.60	39.5253	−119.9289	5.00
12	2008/04/30 03:03:06.90	40.8358	−123.4968	5.40
13	2008/07/29 18:42:15.71	33.9530	−117.7613	5.39
14	2008/11/20 19:23:00.19	32.3288	−115.3318	4.98
15	2008/12/06 04:18:42.85	34.8133	−116.4188	5.06
16	2009/09/19 22:55:17.84	32.3707	−115.2612	5.08
17	2009/10/01 10:01:24.67	36.3878	−117.8587	5.00
18	2009/10/03 01:16:00.31	36.3910	−117.8608	5.19
19	2009/12/30 18:48:57.33	32.4640	−115.1892	5.80
20	2010/01/10 00:27:39.32	40.6520	−124.6925	6.50
21	2010/02/04 20:20:21.97	40.4123	−124.9613	5.88
22	**2010/04/04 22:40:42.15**	**32.2587**	**−115.2872**	**7.20**
23	2010/04/04 22:50:17.08	32.0972	−115.0467	5.51
24	2010/04/04 23:15:14.24	32.3000	−115.2595	5.43
25	2010/04/04 23:25:06.95	32.2462	−115.2978	5.38
26	2010/04/05 00:07:09.07	32.0180	−115.0172	5.32
27	2010/04/05 03:15:24.46	32.6282	−115.8062	4.97
28	2010/04/08 16:44:25.92	32.2198	−115.2760	5.29
29	2010/06/15 04:26:58.48	32.7002	−115.9213	5.72
30	2010/07/07 23:53:33.53	33.4205	−116.4887	5.43
31	2010/09/14 10:52:18.00	32.0485	−115.1982	4.96

Seven forecasts were submitted that gave the predicted number, N_{fmi}, for $M \geq 4.95$ earthquakes in 0.1 magnitude bins during the five-year test period for all $N_c = 7682$ $0.1^\circ \times 0.1^\circ$ cells.

The submitted forecasts are based on a variety of approaches. The Bird and Liu forecast [14] was based on a kinematic model of neotectonics. The Ebel et al. forecast [15] was based on the average rate of $M \geq 5$ earthquakes in $3^\circ \times 3^\circ$ cells for the period 1932 to 2004. The Helmstetter et al. forecast [16] was based on the extrapolation of past seismicity. The Holliday et al. forecast [17] was based on the extrapolation of past seismicity using a modification of the pattern informatics (PI) technique. The Wiemer and Schorlemmer forecast [18] was based on the asperity-based likelihood model (ALM).

We will now discuss the Holliday et al. forecast in somewhat greater detail. The basis of this RELM forecast followed the format introduced in the PI forecast methodology [7, 8]. The magnitude range $M \geq 5$ and the cell dimensions $0.1^\circ \times 0.1^\circ$ were the same. However, the PI method was alarm based. Earthquakes were forecast to either occur or not occur in specified regions (hotspots) in a specified time period. In the PI-based RELM forecast, all hotspot cells are given equal probabilities of an earthquake. For the values in Table 2, $\lambda_{fi} = 3.32 \times 10^{-2}$. Instead of being alarm based, the RELM test was based on probabilities of occurrence of an earthquake in each cell in the test region. This required a continuous assessment of risk rather than a binary, alarm-based assessment. To do this, the Holliday et al. [17] forecast introduced a uniform probability of occurrence for hotspot regions and added smaller probabilities for nonhotspot regions based on the relative intensity (RI) of seismicity in the region. A map of the Holliday et al. [17] forecast is given in Figure 2.

As stated in our description of the RELM test, each participant submitted a forecast for the number of earthquakes N_{fmi} in magnitude bin m that would occur in cell i. Thus $41 \times 7682 = 314962$ values of N_{fmi} were submitted in each

Table 2: Cell scores λ_{fi} of an earthquake with $M \geq 4.95$ for the 22 cells in which earthquakes occurred during the test period. The association of cell IDs (A–V) with the earthquake IDs (1–31) from Table 1 is given. Five submitted forecasts are given: (1) Bird and Liu (B and L), (2) Ebel et al. (Ebel), (3) Helmstetter et al. (Helm.), (4) Holliday et al. (Holl.), and (5) Wiemer and Schorlemmer (W and S). The highest (best) scores are in bold.

Cell ID	EQ ID	B and L	Ebel	Helm.	Holl.	W and S
(A)	1,7,8,16,24	$1.99e-2$	$2.20e-2$	$1.17e-1$	$3.32e-2$	**$1.24e-1$**
(B)	2	$1.41e-2$	$3.40e-2$	**$7.20e-2$**	$3.32e-2$	$4.99e-2$
(C)	3	$7.40e-3$	$6.59e-3$	$7.41e-3$	**$3.32e-2$**	$7.91e-3$
(D)	4	$3.54e-2$	$3.29e-2$	**$6.97e-2$**	$3.32e-2$	$3.59e-2$
(E)	5	**$7.23e-3$**	$1.10e-3$	$2.29e-3$	$9.72e-5$	$1.58e-7$
(F)	6	$9.37e-3$	$2.85e-2$	$3.07e-2$	$3.32e-2$	**$4.55e-2$**
(G)	9,10	$9.11e-3$	$5.49e-3$	$2.55e-2$	**$3.32e-2$**	$2.38e-2$
(H)	11	$3.42e-4$	**$5.49e-3$**	$9.15e-4$	$1.62e-4$	$2.06e-4$
(I)	12	$2.14e-3$	$1.10e-3$	$3.65e-3$	$2.05e-4$	**$9.89e-3$**
(J)	13	$1.68e-3$	$8.78e-3$	$1.11e-2$	**$3.32e-2$**	$1.13e-2$
(K)	14	$3.12e-2$	$2.20e-2$	$3.30e-2$	$3.32e-2$	**$5.90e-2$**
(L)	15	$2.07e-3$	$5.49e-3$	**$6.93e-3$**	$3.32e-3$	$2.64e-3$
(M)	17,18	$1.74e-3$	$2.20e-3$	$5.78e-3$	**$3.32e-2$**	$5.38e-4$
(N)	19	**$5.83e-2$**	$6.59e-3$	$1.49e-2$	$3.32e-2$	$7.44e-3$
(O)	20	$1.25e-2$	$1.43e-2$	$9.45e-3$	**$3.32e-2$**	$1.62e-2$
(P)	21	$6.48e-3$	$3.29e-2$	$2.71e-2$	**$3.32e-2$**	$7.46e-3$
(Q)	22,25,28	$2.88e-2$	$2.20e-2$	$2.84e-2$	$3.32e-2$	**$5.23e-2$**
(R)	23,26	**$3.06e-2$**	$1.54e-2$	$1.43e-2$	$1.73e-4$	$1.58e-2$
(S)	27	$2.13e-2$	$5.49e-3$	$1.26e-2$	**$3.32e-2$**	$1.19e-2$
(T)	29	$1.83e-2$	$1.32e-2$	$2.43e-2$	$3.32e-2$	**$4.99e-2$**
(U)	30	$1.26e-2$	$3.07e-2$	**$1.03e-1$**	$3.32e-3$	$5.16e-2$
(V)	31	$6.76e-3$	$1.54e-2$	$5.55e-3$	**$3.32e-2$**	$2.64e-3$

forecast. In order to better understand the implications of the forecasts we sum the probabilities in the magnitude bins for each spatial cell to give the number of forecast earthquakes N_{fi} in cell i with magnitude $M \geq 4.95$:

$$N_{fi} = \sum_{m=5}^{9} N_{fmi}. \tag{2}$$

The reason we carry out this sum is so that we can directly apply the "skill score" methodology developed in the atmospheric sciences. In terms of forecasting tornadoes, the question is whether a tornado occurs, not its strength. Since the RELM test was for earthquakes with $M \geq 4.95$ our scoring is whether such an earthquake occurs or does not occur in a spacial cell.

The sum of the N_{fi} over all cells is the total number of earthquakes N_f with $M \geq 4.95$ forecast to occur during the test period:

$$N_f = \sum_{i=1}^{N_c} N_{fi}, \tag{3}$$

where N_c is the total number of cells. Our objective is to separate the forecast of the total number of earthquakes from the forecast of their locations. In order to do this we introduce a cell score λ_{fi} defined by

$$\lambda_{fi} = \frac{N_{ce} N_{fi}}{N_f}, \tag{4}$$

where N_{ce} is the number of cells in which an earthquake occurred during the test period. Note that from (3) and (4) we have

$$\sum_{i=1}^{N_c} \lambda_{fi} = N_{ce}. \tag{5}$$

Thus, the sum of λ_{fi} over all cells is the same for each submitted forecast. The cell score λ_{fi} is a direct measure of the probability of occurrence of a test earthquake in cell i. A perfect forecast (a perfect skill score) would have $\lambda_{fi} \geq 1$ for the cells in which earthquakes occur and $\lambda_{fi} = 0$ for all other cells. In principal λ_{fi} can be as big as N_{ce}. However, because we are only concerned with whether an earthquake occurs in a cell, not how many occur—a point we discuss in the next paragraph—all values of $\lambda_{fi} > 1$ are just treated as 1 for that particular cell. In practice this does not occur due to the small values of N_{fmi} provided by the RELM forecasts.

Since the forecasts are for specific $0.1^\circ \times 0.1^\circ$ cells, it is necessary to consider how to handle the forecasts when more than one earthquake occurs in a cell. As stated above, in our analysis a cell in which more than one earthquake occurred is treated the same as a cell in which only one earthquake occurred. This follows the practice used in tornado forecasting. How many tornadoes occur in a region during the forecast period is not considered, only whether one or more occur. For the test earthquakes given in Table 1, events 1, 7, 8, 16, and 24 occurred in the same cell, similarly

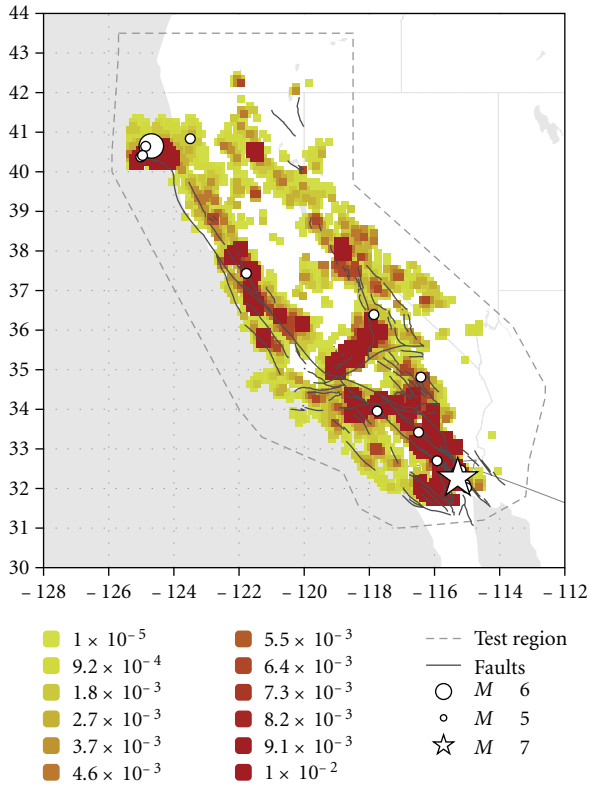

Figure 2: Map of the normalized probabilities λ_{fi} given for the testregion by Holliday et al. [17] using their PI-based forecast. The "hotspots" are shown in red. The test earthquakes are also shown.

Table 3: Comparisons of the forecasts: Column 1. the number of maximum cell scores $N_{\lambda\max}$. Column 2: the mean cell scores forecast $\bar{\lambda}_f$. Column 3: the number of earthquakes N_f predicted by each forecast. The best scores in each category are in bold.

	$N_{\lambda\max}$	$\bar{\lambda}_f$	N_f
Bird and Liu	3	$1.53e-2$	56
Ebel et al.	1	$1.51e-2$	115
Helmstetter et al.	4	**$2.84e-2$**	35
Holliday et al.	**8**	$2.45e-2$	**30**
Wiemer and Schor.	6	$2.66e-2$	24

for events 9 and 10, events 17 and 18, events 22, 25, and 28, and events 23 and 26. This multiplicity is shown in Table 2. Thus, we will consider forecasts made for 22 cells.

Taking the actual number of cells in which earthquakes occurred to be $N_{ce} = 22$ and the total number of earthquakes forecast in each submission N_f using (3), we obtained the forecast scores λ_{fi} using (4).

The seven submitted forecasts included two submissions with separate forecasts with and without aftershocks. Different numbers of events were forecast but the relative scores of locations were the same. Thus, we consider five submissions. The forecast scores λ_{fi} for each of the five submissions are given in Table 2 for the $N_{ce} = 22$ cells in which an earthquake occurred. A perfect forecast in which only the 22 cells were forecast to have earthquakes would have $\lambda_{fi} = 1$ in each of the 22 cells. A random forecast in which all $N_c = 7682$ cells were given the same $N_{fi} = a$ would yield

$$\lambda_{fi}^{\text{random}} = \frac{N_{ce}a}{N_f} = \frac{N_{ce}}{N_c} = \frac{22}{7682} = 2.86 \times 10^{-3}. \quad (6)$$

The submitted forecast scores in Table 2 have a wide range of values from $\lambda_{fi} = 1.58 \times 10^{-7}$ to $\lambda_{fi} = 1.24 \times 10^{-1}$.

7. Evaluation of Results

During the formulation of the RELM project a comprehensive testing strategy was also developed [19]. A suite of likelihood tests were proposed, which would be implemented through a testing center [20]. The approach utilized an L-test, an N-test, and an R-test. These tests were applied to the raw submitted data. This approach was applied to the first 2.5 years of RELM results by Schorlemmer et al. [13]. Zechar et al. [21] recognized a problem with the original proposed likelihood tests and proposed a modification.

This is certainly one approach to the evaluation of results, the primary purpose of this paper is to present a complementary approach. Our approach has the advantage that the evaluation of the numbers of earthquakes forecast can be separated from the forecast of their locations.

Lee et al. [22] proposed the modified approach to the evaluation of RELM test results that is used in this paper. In their short paper they compared the forecasts that had been submitted for all of California. In this paper we consider a subset of those forecasts and relate the results to the concept of alarm-based forecasts.

The results given in Table 2 can be used to compare the forecast scores for each of the cells in which earthquakes occurred. The highest scores between the models are shown in bold. Clearly there are many ways in which to evaluate the results of the forecasts. There is a tradeoff between good forecasts with large λ_{fi} and poor forecasts with small λ_{fi}. We first consider the forecasts that had the highest forecast scores. The Holliday et al. [17] forecast had the largest λ_{fi} for 8 of the 22 cells in which (target) earthquakes occurred. The Wiemer and Schorlemmer [18] forecast had 6 of the largest λ_{fi}. The Helmstetter et al. [16] forecast had 4 of the largest λ_{fi}. Finally, the Bird and Liu [14] forecast had 3 of the largest λ_{fi}. These values are also given in Table 3. The range of the highest cell scores was from $\lambda_{fi} = 1.24 \times 10^{-1}$ for event 1 to $\lambda_{fi} = 5.49 \times 10^{-3}$ for event 11.

It is also of interest to compare the mean cell forecast scores for the 22 cells in which earthquakes occurred. These values $\bar{\lambda}_f$ are given in Table 3. The Helmstetter et al. [16] forecast had the highest $\bar{\lambda}_f = 2.84 \times 10^{-2}$, the Wiemer and Schorlemmer [18] forecast had $\bar{\lambda}_f = 2.66 \times 10^{-2}$, and the Holliday et al. [17] forecast had $\bar{\lambda}_f = 2.45 \times 10^{-2}$. The Helmstetter et al. [16] forecast did the best in an average sense but did relatively poorly in providing the best cell forecasts. It should be noted that the best average forecast $\bar{\lambda}_f = 2.84 \times 10^{-2}$ is one order of magnitude better than the random (no skill) forecast $\lambda_{fi}^{\text{random}} = 2.86 \times 10^{-3}$.

As noted above, the Holliday et al. [17] forecast is primarily an alarm-based (hotspot) forecast. The PI method was used to determine the cells in which earthquakes were most likely to occur (hotspots). In the cell forecasts given in Table 2, these cells had forecast scores $\lambda_{fi} = 3.32 \times 10^{-2}$ and consisted of 8.3% of the total area of the test region (637 of the 7682 cells). Of the 22 cells in which earthquakes occurred, 17 occurred in hotspot cells. In 8 of the 17 cells, the forecast cell scores given by the Holliday et al. [17] forecast were the highest.

8. Discussion

The RELM test provides a well-defined set of prospective earthquake forecasts and a well-defined set of test earthquakes. In this paper we present a method for evaluating the RELM forecasts. We believe our approach has significant advantages but look forward to comparing our results with those obtained by other authors.

RELM forecasts provide the numbers N_{fmi} of earthquakes expected to occur in magnitude bins m and spatial cells i. The basis of our approach is

(1) to use (2) to determine the forecast number N_{fi} of earthquakes with $M \geq 4.95$ expected to occur in spatial cell i,

(2) to use (3) to determine the total forecast number N_f of earthquakes,

(3) to use (4) to determine the cell score λ_{fi}.

We first compared the actual number of earthquakes that occurred during the test period, 31 with the forecast values. The closest forecast values were those of Holliday et al. [17] with $N_f = 30$ as shown in Table 3.

We next compared the forecast scores λ_{fi} of an earthquake with $M \geq 4.95$ occurring in cell i. We noted that the values of λ_{fi} were the same for the two submissions in which both main shocks and aftershocks plus main shocks were submitted. These forecasts gave different values for the numbers N_{fmi}, N_{fi}, and N_f of earthquakes but the forecast distributions in space were identical.

In a perfect forecast the forecast score would have been $\lambda_{fi} = 1$ for each of the 22 cells in which one or more earthquakes occurred and $\lambda_{fi} = 0$ in the other 7660 cells. The mean forecast scores for the 22 cells in which earthquakes occurred for the five forecasts ranged from a high value $\overline{\lambda}_f = 2.84 \times 10^{-2}$ to a low value of $\overline{\lambda}_f = 1.53 \times 10^{-2}$. The range of values was relatively small, about a factor of two. The random (no skill) forecast assuming equal probabilities for the 7682 cells in the test region gives a forecast score $\lambda_{fi}^{\text{random}} = 2.86 \times 10^{-3}$ for all cells. The best forecast score $\lambda_{fi} = 2.84 \times 10^{-2}$ was about a factor of 10 better than the random forecast but a factor of 100 worse than a perfect forecast.

As we have previously discussed earthquake forecasts can be either probabilistic or alarm based. The submission rules for RELM were probabilistic. The only forecast that had an alarm-based distribution of forecasts was that of Holliday et al. [17]. A question of interest for future tests of earthquake forecasts is whether they should be alarm or probability based. A systematic study of alarm-based forecasts could be of considerable interest.

Another interesting question is whether the forecasts have a temporal component. Is there a time-dependent component in the data used that changes forecast probabilities significantly? As discussed previously, eight of the test earthquakes were aftershocks of the El Mayor-Cucapah earthquake and eight of the test earthquakes were associated with a precursory swarm. Thus, 17 of the 31 of the test earthquakes were associated with this earthquake. It appears reasonable to conclude that precursory activation prior to the El Mayor-Cucapah earthquake may have played a significant role in the success of forecasts.

Another swarm of 6 earthquakes during the test period adjacent to Cape Mendocino did not lead to a subsequent larger event during the test period. Swarms of activity in this region occur regularly. In terms of precursory activation this activity would lead to a false alarm. The contrast between the two regions (Cape Mendocino and El Mayor-Cucapah) is an indication of the difficulties in forecasting earthquakes utilizing precursory activation.

Glossary

M: Earthquake magnitude
m: Bin magnitude $m - 0.05 \leq M \leq m + 0.05$
N_e: Number of actual earthquakes
N_f: Number of forecast earthquakes
N_c: Number of cells
N_{ce}: Number of cells with earthquakes
N_{fi}: Number of forecast earthquakes in cell i
N_{fmi}: Number of forecast earthquakes in magnitude bin m and cell i
λ_{fi}: Forecast score, related to the probability that an earthquake with $M \geq 4.95$ will occur in cell i
$\overline{\lambda}_f$: Mean forecast score for the 22 cells in which earthquakes occurred
$\lambda_{fi}^{\text{random}}$: A random (no skill) forecast $\lambda_{fi}^{\text{random}} = 2.86 \times 10^{-3}$
$N_{\lambda\,\max}$: The number of maximum cell scores.

Acknowledgments

Y. T. Lee is grateful for research support from both the National Science Council (ROC) and the Institute of Geophysics (NCU, ROC). J. B. Rundle and J. R. Holliday have been supported by Nasa Grant NNXO8AF69G.

References

[1] V. G. Kossobokov, V. I. Keilis-Borok, D. L. Turcotte, and B. D. Malamud, "Implications of a statistical physics approach for earthquake hazard assessment and forecasting," *Pure and Applied Geophysics*, vol. 157, no. 11-12, pp. 2323–2349, 2000.

[2] J. B. Rundle, W. Klein, K. Tiampo, and S. Gross, "Linear pattern dynamics in nonlinear threshold systems," *Physical Review E*, vol. 61, no. 3, pp. 2418–2431, 2000.

[3] V. I. Keilis-Borok, "The lithosphere of the earth as a nonlinear system with implications for earthquake prediction," *Reviews of Geophysics*, vol. 28, pp. 19–34, 1990.

[4] V. Keilis-Borok and A. A. Soloviev, *Nonlinear Dynamicsof the Lithosphere and Earthquake Prediction*, Springer, New York, NY, USA, 2003.

[5] I. T. Jolliffe and D. B. Stephenson, *Forecast Verification*, John Wiley & Sons, Chichester, UK, 2003.

[6] J. B. Rundle, D. L. Turcotte, R. Shcherbakov, W. Klein, and C. Sammis, "Statistical physics approach to understanding the multiscale dynamics of earthquake fault systems," *Reviews of Geophysics*, vol. 41, no. 4, p. 1019, 2003.

[7] K. F. Tiampo, J. B. Rundle, S. McGinnis, S. J. Gross, and W. Klein, "Eigenpatterns in southern California seismicity," *Journal of Geophysical Research*, vol. 107, no. B12, p. 2354, 2002.

[8] J. B. Rundle, K. F. Tiampo, W. Klein, and J. S. S. Martins, "Self-organization in leaky threshold systems: the influence of near-mean field dynamics and its implications for earthquakes, neurobiology, and forecasting," *Proceedings of the National Academy of Sciences of the United States of America*, vol. 99, 1, pp. 2514–2521, 2002.

[9] J. R. Holliday, J. B. Rundle, K. F. Tiampo, and D. L. Turcotte, "Using earthquake intensities to forecast earthquake occurrence times," *Nonlinear Processes in Geophysics*, vol. 13, no. 5, pp. 585–593, 2006.

[10] J. R. Holliday, K. Z. Nanjo, K. F. Tiampo, J. B. Rundle, and D. L. Turcotte, "Earthquake forecasting and its verification," *Nonlinear Processes in Geophysics*, vol. 12, no. 6, pp. 965–977, 2005.

[11] J. D. Zechar and T. H. Jordan, "Testing alarm-based earthquake predictions," *Geophysical Journal International*, vol. 172, no. 2, pp. 715–724, 2008.

[12] E. H. Field, "Overview of the working group for the development of regional earthquake likelihood models (RELM)," *Seismological Research Letters*, vol. 78, no. 1, pp. 7–16, 2007.

[13] D. Schorlemmer, J. D. Zechar, M. J. Werner, E. H. Field, D. D. Jackson, and T. H. Jordan, "First results of the regional earthquake likelihood models experiment," *Pure and Applied Geophysics*, vol. 167, no. 8-9, pp. 859–876, 2010.

[14] P. Bird and Z. Liu, "Seismic hazard inferred from tectonics: California," *Seismological Research Letters*, vol. 78, no. 1, pp. 37–48, 2007.

[15] J. E. Ebel, D. W. Chambers, A. L. Kafla, and J. A. Baglivo, "Non-poissonian earthquake clustering and the hidden Markov model as bases for earthquake forecasting in California," *Seismological Research Letters*, vol. 78, no. 1, pp. 57–65, 2007.

[16] A. Helmstetter, Y. Y. Kagan, and D. D. Jackson, "High-resolution time-independent grid-based forecast for $m \geq 5$ earthquakes in California," *Seismological Research Letters*, vol. 78, no. 1, pp. 78–86, 2007.

[17] J. R. Holliday, C. C. Chen, K. F. Tiampo, J. B. Rundle, D. L. Turcotte, and A. Donnellan, "A RELM earthquake forecast based on pattern informatics," *Seismological Research Letters*, vol. 78, no. 1, pp. 87–93, 2007.

[18] S. Wiemer and D. Schorlemmer, "ALM: an asperity-based likelihood model for California," *Seismological Research Letters*, vol. 78, no. 1, pp. 134–140, 2007.

[19] D. Schorlemmer, M. C. Gerstenberger, S. Wiemer, D. D. Jackson, and D. A. Rhoades, "Earthquake likelihood model testing," *Seismological Research Letters*, vol. 78, no. 1, pp. 17–29, 2007.

[20] D. Schorlemmer and M. C. Gerstenberger, "RELM testing center," *Seismological Research Letters*, vol. 78, no. 1, pp. 30–36, 2007.

[21] J. D. Zechar, M. C. Gerstenberger, and D. A. Rhoades, "Likelihood-based tests for evaluating space-rate-magnitude earthquake forecasts," *Bulletin of the Seismological Society of America*, vol. 100, no. 3, pp. 1184–1195, 2010.

[22] Y.-T. Lee, D. L. Turcotte, J. R. Holliday et al., "Results of the Regional Earthquake Likelihood Models (RELM) test of earthquake forecasts in California," *Proceedings of the National Academy of Sciences of the United States of America*, vol. 108, no. 40, pp. 16533–16538, 2011.

Hindawi Publishing Corporation
International Journal of Geophysics
Volume 2012, Article ID 307517, 6 pages
doi:10.1155/2012/307517

Research Article

Medium-Term Earthquake Forecast Using Gravity Monitoring Data: Evidence from the Yutian and Wenchuan Earthquakes in China

Yiqing Zhu[1,2] and F. Benjamin Zhan[3,4]

[1] *Institute of Geodesy and Geophysics, Chinese Academy of Sciences, Wuhan 430077, China*
[2] *Second Crust Monitoring and Application Center, China Earthquake Administration, Xi'an 710054, China*
[3] *School of Resource and Environmental Science, Wuhan University, Wuhan 430079, China*
[4] *Texas Center for Geographic Information Science, Department of Geography, Texas State University, San Marcos, TX 78666, USA*

Correspondence should be addressed to F. Benjamin Zhan, zhan@txstate.edu

Received 15 July 2011; Accepted 28 December 2011

Academic Editor: Jiancang Zhuang

Gravity changes derived from regional gravity monitoring data in China from 1998 to 2005 exhibited noticeable variations before the occurrence of two large earthquakes in 2008 in China—the 2008 Yutian (Xinjiang) $M_s = 7.3$ earthquake and the 2008 Wenchuan (Sichuan) $M_s = 8.0$ earthquake. Based on these gravity variations, a group of researchers at the Second Crust Monitoring and Application Center of China Earthquake Administration made a suggestion in December of 2006 that the possibility for the Yutian (Xinjiang) and Wenchuan (Sichuan) areas to experience a large earthquake in either 2007 or 2008 was high. We review the gravity monitoring data and methods upon which the researchers reached these medium-term earthquake forecasts. Experience related to the medium-term forecasts of the Yutian and Wenchuan earthquakes suggests that gravity changes derived from regional gravity monitoring data could potentially be a useful medium-term precursor of large earthquakes, but significant additional research is needed to validate and evaluate this hypothesis.

1. Introduction

In December 2006, a group of researchers at the Second Crust Monitoring and Application Center of China Earthquake Administration suggested that the possibility for the areas surrounding Yutian (Xinjiang) and Wenchuan (Sichian) to experience a large earthquake in either 2007 or 2008 was high [1]. The forecasted location, magnitude, and timeframe of the two earthquakes are summarized in Table 1. These researchers used gravity changes derived from regional gravity monitoring data in China from 1998 to 2005 as the primary precursory information to make these suggestions. In this paper, we first review ground gravity surveys conducted in China in 1998, 2000, 2002, and 2005 and then report how the researchers used gravity monitoring data to make medium-term (less than three years) forecasts of the Yutian and Wenchuan earthquakes. In addition, we make a few observations about possible connections between gravity changes and the occurrence of a large earthquake and provide some discussions about future research directions in earthquake research using gravity monitoring data.

2. Nationwide Gravity Survey Campaigns in China

China began establishing an ambitious countrywide crustal movement observation network in 1998—Crustal Movement Observation Network of China (CMONOC) (Figure 1). Among other types of observation stations, the network consisted of 25 absolute gravity observation stations and 360 relative gravity observation stations at the end of 2005. The absolute gravity observation stations serve as a control network through which a stable and uniform gravity field throughout the country can be computed. Gravity field dynamics throughout the country then can be determined

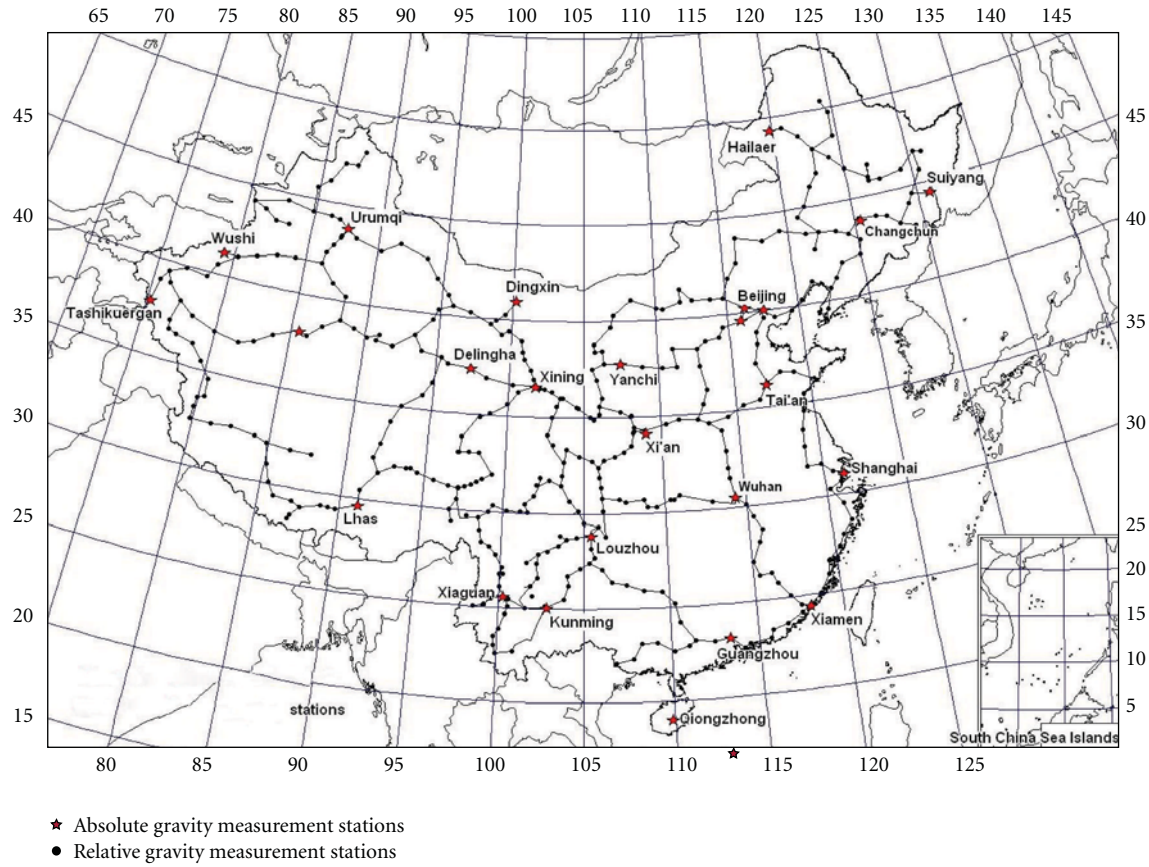

Figure 1: Crustal Movement Observation Network of China (CMONOC).

Table 1: Summary of the three elements of the two forecasted and actual earthquakes.

Earthquake parameters	Forecasted	Actual
The Yutian earthquake [1, 4]		
Epicenter	36.0°N, 80.0°E	35.6°N, 81.6°E
Magnitude	Ms6.0-Ms7.0	Ms7.3
Timeframe	2007-2008	March 21, 2008
The Wenchuan earthquake [1, 5]		
Epicenter	31.6°N, 103.7°E	31.0°N, 103.4°E
Magnitude	Ms6.0–Ms7.0	Ms8.0
Timeframe	2007–2008	May 12, 2008

through repeated mobile gravity surveys at the 360 relative gravity stations. China Earthquake Administration, the Chinese Academy of Sciences, and China State Bureau of Surveying and Mapping coordinated four rounds of nationwide ground gravity surveys in 1998, 2000, 2002, and 2005. Because details of the gravity surveys and data processing are provided in two recent papers [2, 3], we only briefly describe the surveys as well as procedures for data processing in the rest of this section and in the next section.

Surveyors with significant field observation experience from three different organizations—the Institute of Geodesy and Geophysics of the Chinese Academy of Sciences, the Institute of Seismology of China Earthquake Administration, and the State Bureau of Surveying and Mapping in China—conducted the absolute gravity surveys using FG-5 gravimeters. The accuracy of the observed absolute gravity survey at each station was higher than 5×10^{-8} m/s^2 [2, 6, 7].

After field survey, absolute gravity data at the absolute gravity observation stations were adjusted for earth-tide, speed of light, local air pressure, polar motion, and vertical gradient. The adjusted data then were used for subsequent analysis and integration with the relative gravity survey data. Both the absolute and relative gravity surveys were all conducted during the months from July through November in 1998, 2000, 2002, and 2005. This arrangement of conducting the gravity surveys in the same months of different years was designed to reduce possible seasonal hydrological effects on gravity observed at the same location in different years.

The mobile relative gravity surveys were completed through joint efforts by two organizations of China Earthquake Administration—the Institute of Seismology and the Second Crust Monitoring and Application Center. Surveyors used the LaCoste and Romberg gravimeters (model G (LCR-G)) in the relative gravity surveys. The accuracy of LCR-G gravimeters was higher than 10×10^{-8} m/s^2, and the drifts of null reading values of the LCR-G gravimeters were within $\pm 5 \times 10^{-8}$ ms^{-2}/hour. Field surveyors followed the Chinese national field work procedures and guidelines when conducting the mobile relative gravity surveys to ensure that the relative gravity survey data were in the best possible quality [2, 6, 7].

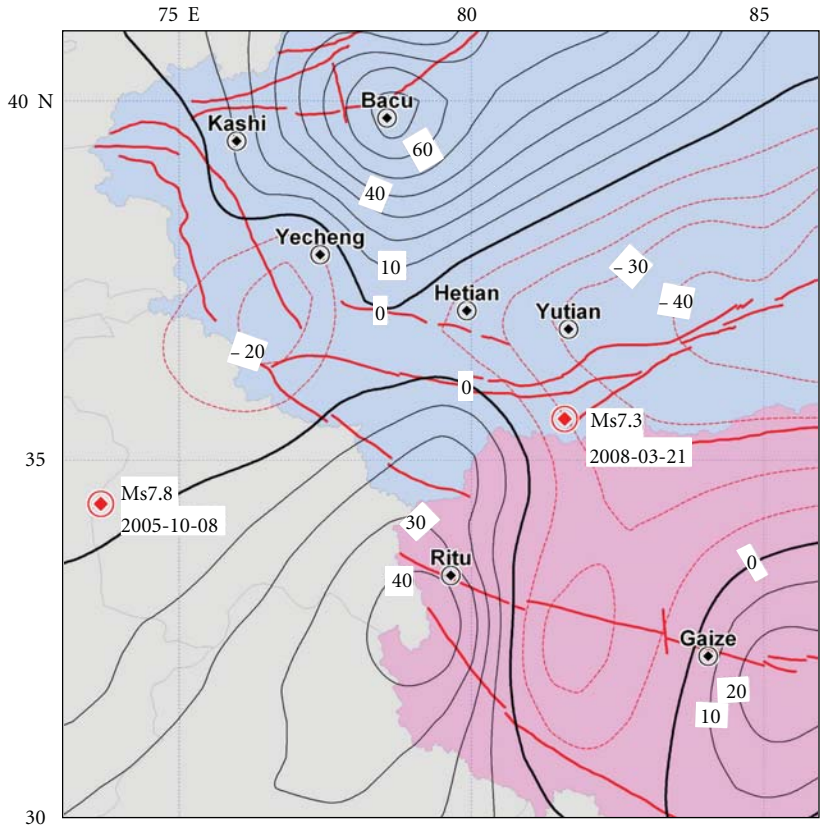

Figure 2: A contour map showing gravity changes (in 10^{-8} m/s^2) from 1998 to 2005 before the Yutian Earthquake. The contours on the map were produced using a resolution of 0.25 geographic degrees.

3. Processing of Field Gravity Survey Data

The key in processing the field gravity data described previously is to integrate the high precision absolute gravity survey data with the mobile relative gravity survey data and then compute the absolute gravity at each of the relative gravity observation stations. A 3-step procedure was used to determine the final gravity data at each relative gravity observation station. First, relative gravity survey data were adjusted for solid earth-tide, air pressure, first-order item, and height of gravimeters. Second, a preliminary analysis of the gravity survey data across all four rounds of surveys was conducted to eliminate data with possible gross errors. Third, the Adjustment Program for Mobile Gravimetric Data Measured by LaCoste and Romberg Gravimeters (LGADJ) software package recommended by China Earthquake Administration was used to obtain the (absolute) gravity data at the location of each observation station for each of the four time periods. The LGADJ software package is a standard computational tool that can be used to integrate absolute and relative gravity survey data to obtain the final absolute gravity data at each of the relative gravity observation stations [8, 9]. The average accuracy of the final adjusted gravity data at each relative observation station was better than 15×10^{-8} m/s^2 across all four years.

Least-squares collocation was used to calculate gravity data at the intersections of a grid with a resolution of 0.25 geographic degrees in the region in question based on the computed gravity data at the observation stations mentioned above. The least-squares collocation method treats observed gravity data at the observation stations and gravity data to be estimated at other locations on the grid as random variables. The method provides the best possible estimation of ground gravity data at locations where observation data did not exist. After obtaining the gravity data on the grid, the MapGIS software was used to produce the contour maps of gravity changes between different time periods.

4. Gravity Changes before the Yutian Earthquake

As can be seen from Figure 2, there were significant gravity changes in the region shown in Figure 2 from 1998 to 2005. Based on empirical experience, when the difference between the largest positive gravity change and the highest negative gravity change in the region in question exceeds 80×10^{-8} m/s^2, the gravity changes in the region are considered significant. The gravity change gradient extended from the southwest part of the region shown in Figure 2 to the northeast part of the region. Positive gravity changes occurred in the southwest part of the region, and negative gravity changes took place in the northeast part of the region. The difference between the positive and negative gravity changes was as great as 80×10^{-8} m/s^2. Based on the contour map shown in Figure 2, a belt with a steep gravity change gradient can be identified. This belt extended from Yutian to Hetian.

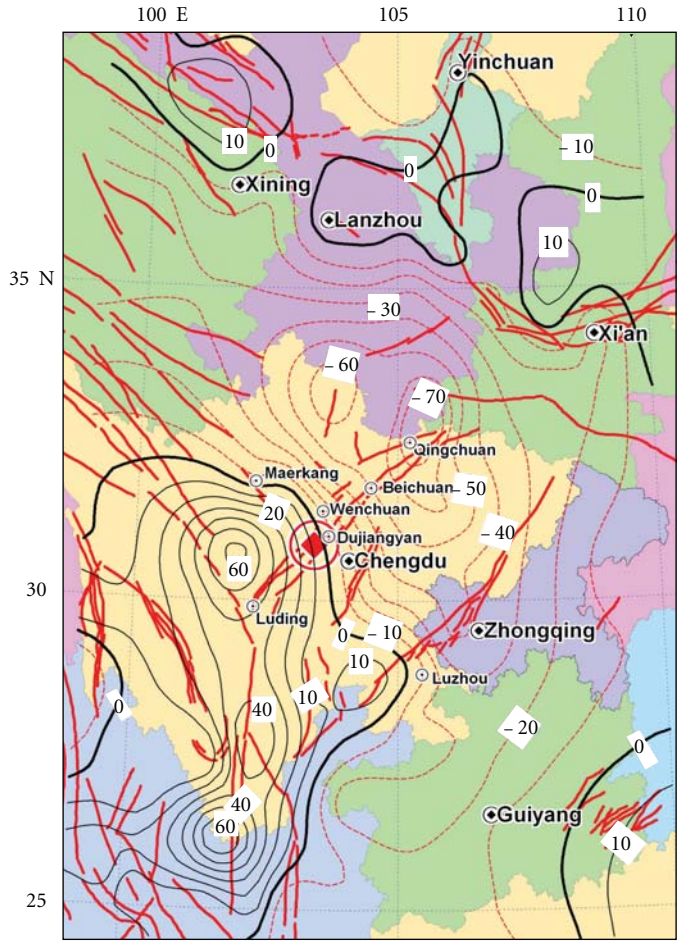

Figure 3: A contour map illustrating gravity changes from 1998 to 2005 before the Wenchuan earthquake. The contours on the map were produced using a resolution of 0.25 geographic degrees.

5. Gravity Changes before the Wenchuan Earthquake

Characteristics of gravity changes from 1998 to 2005 before the Wenchuan earthquake are shown in Figure 3. Within the region, the rhombus-shaped Chuan-Dian (Sichuan-Yunnan) Plate showed positive gravity changes from 1998 to 2005 as great as 60×10^{-8} m/s^2, whereas areas surrounding the Chuan-Dian Plate exhibited negative gravity changes during the same period with a negative peak gravity change value as large as 60×10^{-8} m/s^2. These positive and negative gravity changes and their differences were particularly evident in northern Sichuan where the difference of gravity changes was as great as 60×10^{-8} m/s^2. This difference was particularly evident in a belt with a steep gravity change gradient. This belt extended from Luzhou, through Wenchuan, to Maerkang (Figure 3).

6. Medium-Term Forecasts of the Yutian and Wenchuan Earthquakes

As stated at the beginning of this paper, the forecast location, magnitude, and timeframe of the Yutian and Wenchuan earthquakes are summarized in Table 1. For the Yutian earthquake [1], the *location* of the earthquake was determined based on analysis results of past earthquakes and an observation that an earthquake typically occurs at the intersection of the zero gravity change contour line in the area with high gravity change gradients and the fault that is mostly likely to accumulate sufficient energy for a major earthquake, the Kangxiwar-Altyn Tagh Fault in this case. The *magnitude* of the Yutian earthquake was estimated to be between $M_s = 6.0$ and $M_s = 7.0$ based on the highest value (60×10^{-8} m/s^2) of the differences of gravity changes in the region from 1998 to 2005 (Figure 2). Again, this estimation was based on empirical data about the relationships between the magnitudes of earthquakes occurred before the Yutian earthquake and values of the differences of gravity changes before these past earthquakes. The determination of the *timeframe* of the forecasted Yutian earthquake was also based on past experience and empirical data. Earthquakes typically occur within one to two years after a period of significant gravity changes in the region in question. Because the region experienced significant gravity changes from 1998 to 2005, it was forecasted that the earthquake would occur sometime in 2007 or 2008.

Table 2: Nine large ($M_s \geq 6.8$) earthquakes occurred within or near China from 2001 to 2008 and gravity changes before these nine earthquakes as detected by the Crustal Monitoring Network of China (CMONOC) [3].

ID	Earthquake (province or equivalent)	Magnitude (M_s)	Location of actual epicenter	Date of earthquake	Observed peak-to-valley difference of gravity changes (in 10^{-8} m/s^2) (time period) and region of change
1	Kunlun (Xinjiang)	8.1	36.2°N, 90.9°E	14-Nov-2001	130 (1998–2000); bordering areas between Qinghai and Xinjiang
2	Offshore east of Taiwan	7.5	24.4°N, 122.1°E	31-Mar-2002	80 (1998–2000); coastal area in Fujian facing Taiwan
3	Wangqing (Jilin)	7.2	43.5°N, 103.6°E	29-Jun-2002	60 (1998–2000); the Wangqing-Changchun-Suiyang area in Jilin
4	Jashi (Xinjiang)	6.8	39.5°N, 77.2°E	24-Feb-2003	60 (1998–2000); the Kashi-Wushi-Kuerle area in southwest Xinjiang
5	The bordering areas between China and Russia near Northern Xinjiang	7.9	49.9°N, 87.9°E	28-Sep-2003	60 (2000–2002); northern Xinjiang
6	Gaizhe (Tibet)	6.9	32.5°N, 85.2°E	9-Jan-2008	80 (2002–2005); the Gaize and Nima area in Tibet
7	Yutian (Xinjiang)	7.3	35.6°N, 81.6°E	21-Mar-2008	90 (2002–2005); the Yutian and Hetian area in Xinjiang
8	Wenchuan (Sichuan)	8.0	31.0°N, 103.4°E	12-May-2008	130 (1998–2005); northern Sichuan along Luzhou-Wenchuan-Maerkang
9	Zhongba (Tibet)	6.8	31.0°N, 83.6°E	25-Aug-2008	90 (2002–2005); the Zhongba and Nima area in Tibet

A similar procedure was used to forecast the Wenchuan earthquake [1, 5]. The forecasted location of the Wenchuan earthquake was determined to be at the intersection of the Longmenshan Fault and the zero gravity change line shown in Figure 3. The magnitude was forecasted to be between $M_s = 6.0$ and $M_s = 7.0$ based on the highest value of the differences of gravity changes in the region. The timeframe—sometime in 2007 or 2008—was estimated based on the observation that the earthquake would occur in about one to two years from 2005 after a period of significant gravity changes from 1998 to 2005. Again, this timeframe of the earthquake forecast was based on empirical data and experience of the researchers. Additional research is needed to remove the subjective nature in the determination of the timeframe of a forecasted earthquake.

7. Conclusions and Discussions

Despite many years of research, short- to medium-term earthquake forecast has remained a difficult task [10–12]. Although the potential of using gravity data for earthquake research was recognized nearly 50 years ago [13–20], there existed few cases demonstrating the usefulness of gravity monitoring data for useful earthquake forecast. Based on discussions presented above, we argue that information derived from large-scale regional gravity monitoring data has the potential to be used as a precursor for forecasting large earthquakes in a medium-term of no more than five years, particularly when that information is combined with expert knowledge about historic seismic activities, seismicity rate, as well as geological and tectonic conditions in the region in question.

The benefits of medium-term earthquake forecast are obvious. At a minimum, the forecast will help delineate high risk areas within a short timeframe of usually two to three years, enable decision makers to deploy limited resources to targeted areas, and hopefully help save lives and protect properties. An immediate need in advancing this line of research is to support and continue empirical research for medium-term earthquake forecasts using gravity monitoring data at a regional scale. We advocate that countries in high-risk earthquake zones establish regional scale gravity monitoring networks in areas covering these earthquake zones. A procedure similar to the one used in China can be employed to periodically collect ground gravity survey data [4–7]. These procedures can be modified, improved, and replicated to suite situations in other parts of the world.

Gravity data reported in this paper suffer a number of limitations. First, there are several uncertainties in the data that affect the usefulness and reliability of the gravity changes derived from the gravity monitoring data. These uncertainties include gravity variations due to hydrological effects and vertical crustal displacements, as well as inevitable errors in ground gravity surveys across a large region. Second, the density of the monitoring network as measured by the number of gravity observation stations was low. This low density undoubtedly would affect the results of the gravity monitoring data. Third, the time interval of the ground gravity survey was two or three years in the four rounds of gravity surveys discussed in this paper. Gravity monitoring data of the same nature with higher frequency would improve the usefulness of the data. Future efforts of data collection and data processing should strive to reduce the uncertainties and limitations mentioned above.

There are a number of significant research questions that warrant additional research. The first question is whether there were significant gravity changes before other large earthquakes in China and its neighboring regions during the same time period. A recent article by Zhan and his colleagues demonstrated that significant gravity changes were observed before all nine large earthquakes that ruptured within or near mainland China from 2001 to 2008 [3]. Table 2 provides

a summary of the significant gravity changes before these nine earthquakes. However, it remains to be evaluated whether these gravity changes are indeed associated with the large earthquakes and if similar observations can be made in other parts of the world.

The second research question is how to remove the subjective nature in the determination of the magnitude, location, and timeframe of a forecasted large earthquake. The forecast examples presented in this paper heavily relied on subjective expert knowledge and empirical experience of the researchers. What is missing is a set of objective computational procedures that are generally applicable to other parts of the world for determining the magnitude, location, and timeframe of a pending large earthquake [21].

Third, once the method is fully developed, the statistical significance of gravity changes and their relationships with the occurrence of large earthquakes will have to be evaluated using historical data. In addition, a quest of enormous value is to investigate the *physical* processes that lead to gravity changes before large earthquakes and determine how those physical processes may be used in earthquake forecast. Progresses about research addressing the questions stated above will be reported in future publications.

Acknowledgments

Most of this paper was written in the summers of 2009 and 2010 while F. B. Zhan. was visiting Wuhan University in China. He appreciates the support from the Chang Jiang Scholars Award Program and Wuhan University. Y. Zhu's work was in part supported by a grant from the National Science Foundation of China (no. 40874035) and by a special earthquake research project grant (no. 200908029) from China Earthquake Administration.

References

[1] Y. Zhu, W. Liang, Y. Xu, and L. Liu, "Spatial-temporal characteristics of gravity field dynamics in mainland China and forecast of earthquake trends," in *Annual Research Report about Earthquake Trends in China in 2007*, pp. 111–119, Second Crust Monitoring and Application Center, China Earthquake Administration, Xi'An, China, 2010.

[2] Y. Zhu, F. B. Zhan, J. Zhou, W. Liang, and Y. Xu, "Gravity measurements and their variations before the 2008 Wenchuan earthquake," *Bulletin of the Seismological Society of America*, vol. 100, no. 5, pp. 2815–2824, 2010.

[3] F. B. Zhan, Y. Zhu, J. Ning, J. Zhou, W. Liang, and Y. Xu, "Gravity changes before large earthquakes in China: 1998–2005," *Geo-Spatial Information Science*, vol. 14, no. 1, pp. 1–9, 2011.

[4] Y. Zhu, Y. Xu, and W. Liang, "Medium-term prediction of Yutian, Xinjiang M_s = 7.3 earthquake in 2008," *Journal of Geodesy and Geodynamics*, vol. 28, no. 5, pp. 13–15, 2008 (Chinese).

[5] Y. Zhu, W. Liang, and Y. Xu, "Medium-term prediction of M_s = 8.0 earthquake in Wenchuan, Sichuan by mobile gravity," *Recent Developments in World Seismology*, vol. 7, pp. 36–39, 2008 (Chinese).

[6] H. Xu, "Function of gravimetry in CMONOC," *Journal of Geodesy and Geodynamics*, vol. 23, pp. 1–3, 2003 (Chinese).

[7] W. M. Zhang, Y. Wang, and X.-H. Zhou, "Expectation and application study of absolute gravity observation technology in China," *Progress in Geophysics*, vol. 23, no. 1, pp. 69–72, 2008 (Chinese).

[8] D. Liu, H. Li, and S. Liu, "A management and analysis system of gravity survey data-LGADJ," in *Proceedings of the Research Symposium of Application of Seismological Prediction Methods*, pp. 339–350, Seismological Press, Beijing, China, 1991.

[9] X. Wu, Y. Chen, H. Li et al., "National network of gravity measurement and assessment of its accuracy," *Earthquake Research of China*, vol. 11, no. 1, pp. 92–98, 1995 (Chinese).

[10] R. J. Geller, "Earthquake prediction: a critical review," *Geophysical Journal International*, vol. 131, no. 3, pp. 425–450, 1997.

[11] R. J. Geller, D. D. Jackson, Y. Y. Kagan, and F. Mulargia, "Geoscience—earthquakes cannot be predicted," *Science*, vol. 275, no. 5306, pp. 1616–1617, 1997.

[12] M. Wyss and D. C. Booth, "The IASPEI procedure for the evaluation of earthquake precursors," *Geophysical Journal International*, vol. 131, no. 3, pp. 423–424, 1997.

[13] H. W. Oliver, M. F. Kane, and L. C. Pakiser, "Gravity anomalies in Central Sierra Nevada, California," *Journal of Geophysical Research*, vol. 66, pp. 4265–4271, 1961.

[14] D. F. Barnes, "Gravity changes during Alaska earthquake," *Journal of Geophysical Research*, vol. 71, pp. 451–456, 1966.

[15] R. Page, "Aftershocks and microaftershocks of Great Alaska earthquake of 1964," *Bulletin of the Seismological Society of America*, vol. 58, pp. 1131–1168, 1968.

[16] Y.-T. Chen, H.-D. Gu, and Z.-X. Lu, "Variations of gravity before and after the Haicheng earthquake, 1975, and the Tangshan earthquake, 1976," *Physics of the Earth and Planetary Interiors*, vol. 18, no. 4, pp. 330–338, 1979.

[17] M. H. Wei, W. Zhao, and L. Ma, "Gravity Changes before and After the Tangshan earthquake of July 28, 1976, and Possible Interpretation," *Journal of Geophysical Research-Solid Earth and Planets*, vol. 90, pp. 5421–5428, 1985.

[18] G. Gu, J. T. Kuo, K. Liu, J. Zheng, H. Lu, and D. Liu, "Seismogenesis and occurrence of earthquakes as observed by temporally continuous gravity variations in China," *Chinese Science Bulletin*, vol. 43, no. 1, pp. 8–21, 1998.

[19] J. T. Kuo, J. H. Zheng, S. H. Song, and K. R. Liu, "Determination of earthquake epicentroids by inversion of gravity variation data in the BTTZ region, China," *Tectonophysics*, vol. 312, no. 2–4, pp. 267–281, 1999.

[20] K. R. Liu, J. X. Zheng, J. T. Kuo et al., "Mobile gravity survey and the combined dilatation model (CDM) in the BTTZ region," in *Advances in Pure and Applied Geophysics*, pp. 167–178, Meteorological Publishing House, Beijing, China, 2002.

[21] F. B. Zhan, Y. Zhu, M. F. Goodchild, and J. Zhou, "An approach for identifying high risk areas of medium-term large earthquakes using gravity monitoring data," Tech. Rep., Department of Geography, Texas Center for Geographic Information Science, Texas State University-San Marcos, 2010.

Hindawi Publishing Corporation
International Journal of Geophysics
Volume 2012, Article ID 610712, 10 pages
doi:10.1155/2012/610712

Research Article

Spatiotemporal Relationship between Geodetic and Seismic Quantities: A Possible Clue to Preparatory Processes of $M \geq 6.0$ Inland Earthquakes in Japan

Masashi Kawamura,[1] Takeshi Kudo,[2] and Koshun Yamaoka[3]

[1] *Department of Earth Sciences and Graduate Institute of Geophysics, National Central University, Jhongda Road no. 300, Taoyuan, Jhongli 32001, Taiwan*
[2] *General Education Division, College of Engineering, Chubu University, Matsumoto-cho 1200, Aichi, Kasugai 487-8501, Japan*
[3] *Research Center for Seismology, Volcanology and Disaster Mitigation, Graduate School of Environmental Studies, Nagoya University, Chikusa-ku, Nagoya 464-8601, Japan*

Correspondence should be addressed to Masashi Kawamura, mkawamu@ncu.edu.tw

Received 23 June 2011; Revised 6 September 2011; Accepted 11 September 2011

Academic Editor: Rodolfo Console

Constructing a statistical model to characterize the physical conditions associated with large earthquake occurrence is crucial for disaster mitigation. With the aim to formulate such a model, we previously developed a statistical evaluation system which assesses the correlation of the spatiotemporal relationship between different kinds of physical quantities with the occurrence times of large inland earthquakes. In this study, we focused on assessing the relationship between geodetic and seismic quantities and attempted to find the pair of related quantities that most likely indicates preparatory processes of large earthquakes in Japan. We assessed the quantities prior to $M \geq 6.0$ inland earthquakes for the period of 2001–2007 in terms of probability gains and error diagram. Our system revealed that the pair of absolute value of dilatation rate and seismic energy showed the highest statistical performance. Further validation of this result is required by updating the database of physical quantities.

1. Introduction

It is an urgent issue for disaster mitigation to develop a statistical model well reflecting crustal activities, which are expected to include the preparatory processes of large inland earthquakes. Resolution of this issue requires a comprehensive understanding and monitoring of crustal activities through more than one kind of physical observation. Therefore, keeping this in mind, in this study, we focused on examining the spatiotemporal relationships between different physical quantities, at least one of which is time-variable. By determining informative combinations of physical quantities, that is, those having some correlation, we aim to develop a monitoring index/indices in crustal activities which feature the preparatory processes of large inland earthquakes for Japan. Imoto [1, 2] insisted that their seismicity model shows higher performance by taking into consideration the correlation between different kinds of geophysical parameters. This implies that there are some correlations between different kinds of observations that may represent different aspects of crustal phenomena or show causality between apparently different crustal phenomena.

As the first step toward formulating a model to capture statistical and physical conditions for the occurrence of large inland earthquakes, we created a database of physical observations with spatially and temporally gridded formats (Figure 1). Furthermore, we constructed a statistical evaluation system to assess the relationship between the occurrence times of target events and interquantity relationship in the physical observation data, at least one of which is time variable [4]. This system comprises some calculation modules corresponding to respective steps in Section 2 and their subordinate functions (not shown in Section 2) to output several parameters which are required for next steps

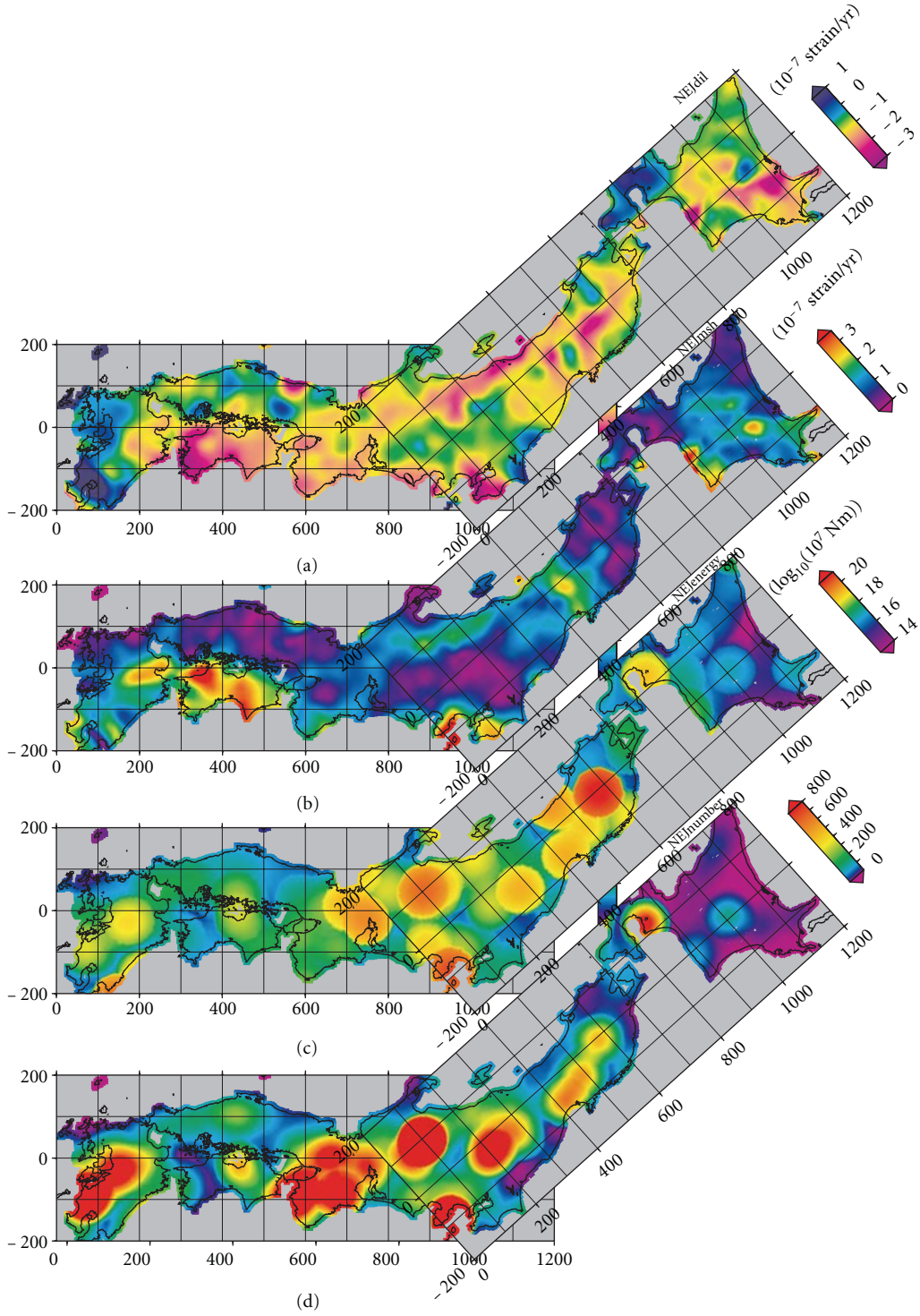

Figure 1: Gridded maps for (a) dilatation rate, (b) maximum shear strain rate, (c) seismic energy [3] within 30 km search radius, and (d) the number of earthquakes within 30 km search radius, respectively, over the Japanese islands.

or to display the final result of statistical evaluation at step 4 (Table 1, Figure 2).

Here, we actually operated the system to examine the relationship between two physical quantities and the occurrence times of M $\geq$ 6.0 mainshocks in Japan. We adopted the spatiotemporal relationship between geodetic quantities (dilatation rate and maximum shear strain rate) and seismic quantities (seismic energy and number of earthquakes) for representative physical observation. We look for the relationship for the earthquake from 2001 through 2007

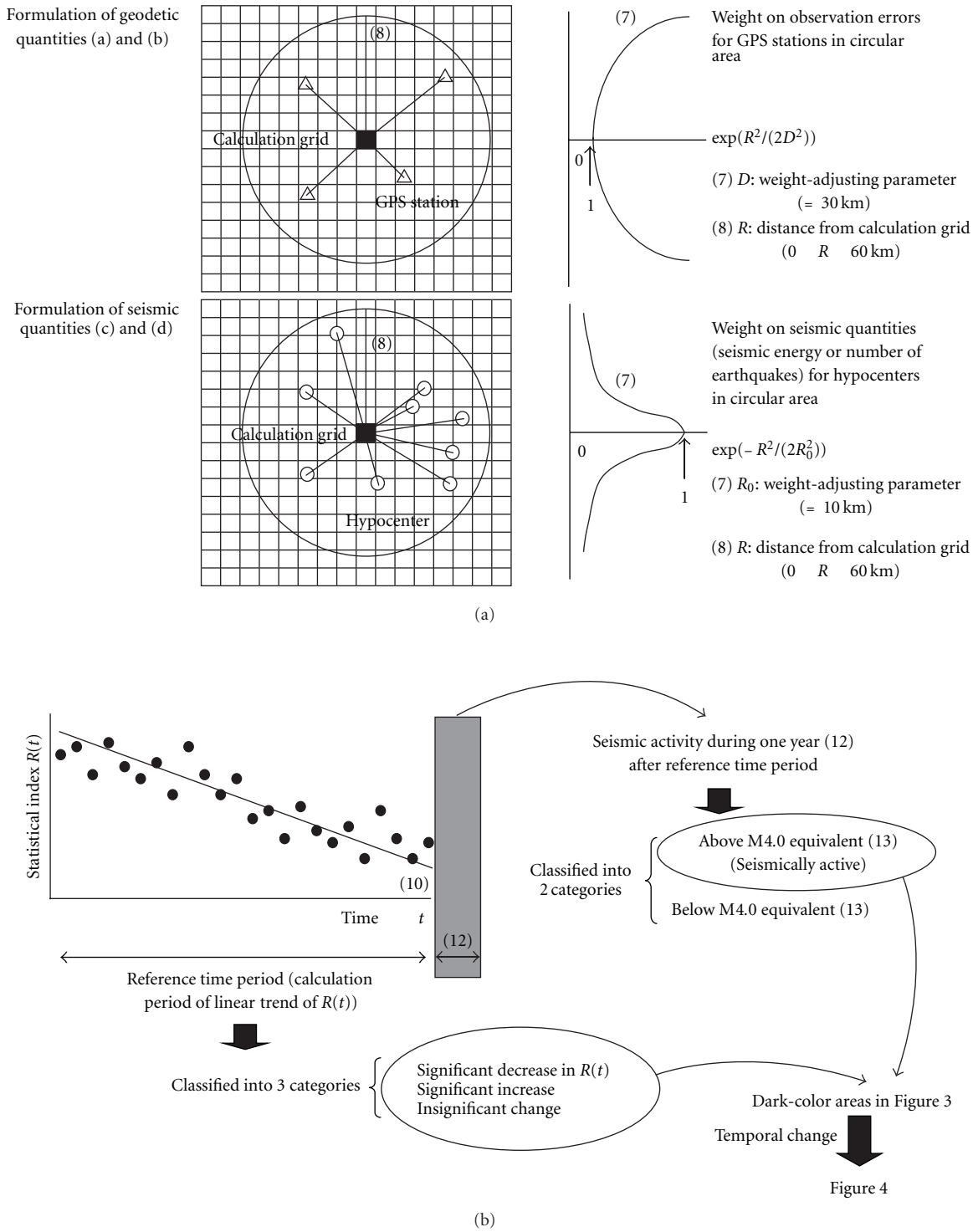

Figure 2: (a) Schematic explanation on the method of obtaining geodetic quantities (dilatation rate and maximum shear strain rate) and seismic quantities (seismic energy and number of earthquakes) for each grid, which were calculated by relating them to the displacement rates for GPS stations (open triangle) and the magnitudes for hypocenters (open circle) in circular area, respectively. We weighted the observation errors for GPS stations and seismic quantities for hypocenters depending on the distances between the calculation grid (black square) and the other grids in circular area, respectively. The vertical axis of each right figure in which weight curve is delineated shows the distances relative to the calculation grid. (b) Schematic explanation on the approach of obtaining Figures 3 and 4. See also text for detail.

Table 1: Tabulated information on input parameters required at each step of statistical evaluation system. The related schematic explanation should be referred to Figure 2.

No.	Parameter
(1)	Range of region for analysis (inland Japan)
(2)	Interval between spatial grids (0.05°)
(3)	Interval between time grids (three month)
(4)	Time period referred to for calculating physical quantities such as dilatation rate for each time grid (two years)
(5)	Range of depth ($0 \leq$ depth ≤ 30 km)
(6)	Range of magnitude ($M \geq 1.0$)
(7)	Smoothing (weight-adjusting) parameters for obtaining spatially gridded physical quantities (refer to Figure 2(a))
(8)	Search radius for applying smoothing parameters to area centered at a calculation grid (Figure 2(a))
(9)	Search radius for calculating statistical index for a calculation grid (60 km)
(10)	Approval method for classifying the temporal change in statistical index $R(t)$ into three categories (Figure 2(b))
(11)	Confidence level for statistical approval (95%)
(12)	Calculation period of total seismic energy released following calculation period of temporal change in statistical index $R(t)$ (Figure 2(b))
(13)	Lower limit of total seismic energy released during period (12) which is regarded as seismically active (Figure 2(b))
(14)	Definition of large inland earthquakes (lower limit of magnitudes) ($M \geq 6.0$)

for inland Japan. In evaluating this relationship, the system computes the statistical performance of a proposed monitoring index which would reflect an aspect of the preparatory process of large earthquake occurrence. We searched for the most informative combination between geodetic and seismic quantities based on evaluating the statistical performance of the proposed monitoring index for $M \geq 6.0$ inland mainshocks. Evaluation of the statistical performance revealed that the time variation of the monitoring index created based on the relationship between the absolute value of dilatation rate and seismic energy was most closely associated with the occurrence times of $M \geq 6.0$ inland mainshocks. Our result revealed the relationship between the absolute value of dilatation rate and seismic energy would best reflect the crustal activities involving preparatory processes of the occurrence of $M \geq 6.0$ inland mainshocks. An important future issue is to further validate the highest performance of the proposed monitoring index by updating the database to increase the number of samples, or large inland earthquakes.

2. Statistical Evaluation of the Relationship between Geodetic and Seismic Quantities

The statistical evaluation system developed by Kawamura et al. [4] statistically assesses the relationship between the spatiotemporal connection in any two kinds of physical quantities and the occurrence times of target physical events of interest We actually operated the system as follows to find a monitoring index, which is created based on a pair of items (a) to (d) in Figure 1, or a pair of geodetic and seismic quantities, such that the index can feature crustal activities which are expected to reflect the preparatory processes of large inland earthquakes.

2.1. Step 1: Making a Database with Spatially and Temporally Gridded Formats. We created a database comprising items (a) to (d) in Figure 1. It shows spatially and temporally gridded maps of four physical quantities: (a) dilatation rate, (b) maximum shear strain rate, (c) seismic energy [3] within 30 km search radius, and (d) the number of earthquakes within 30 km search radius, respectively, over inland Japan. Items (a) and (b) were computed from GEONET (GPS Earth Observation NETwork) data (Figure 2(a)). Items (c) and (d) were calculated from unified hypocenter data operated by Japan Meteorological Agency (Figure 2(a)).

We here explain the method of making physical quantities (a) to (d) (Figure 2(a)). To obtain dilatation rate (a) and maximum shear strain rate (b) with grid formats, we first removed abnormal values from the GEONET coordinate data, where the coordinate data with a standard deviation >3 over half a month before and after each time was regarded as abnormal value. We next calculated the displacement rate at each observation point. We assumed that the displacement rate on an arbitrary coordinate grid can be represented by using a linear function of the displacement rate at its nearby observation point. Then, the displacement rate at observation point is related to the position of grid point as follows:

$$\begin{aligned} U_x &= A_{11} + A_{12}\left(x - x_g\right) + A_{13}\left(y - y_g\right) + E_x, \\ U_y &= A_{21} + A_{22}\left(x - x_g\right) + A_{23}\left(y - y_g\right) + Ey, \end{aligned} \tag{1}$$

where U_x and U_y are east-west and north-south components of displacement rate at each observation point; $x - x_g$ and $y - y_g$ are east-west and north-south components of the position $(x,\ y)$ of observation point relative to the position $(x_g,\ y_g)$ of grid point. E_x and E_y are the error term of respective components. Then, dilatation rate Δ and maximum shear strain rate $\sum$ can be obtained as follows:

$$\left(\Delta, \sum\right) = \left(A_{12} + A_{23},\ \left(\left(A_{12} - A_{23}\right)^2 + \left(A_{13} + A_{22}\right)^2\right)^{1/2}\right). \tag{2}$$

Furthermore, the error term E_x, E_y was weighted depending on the distance between observation and grid points as follows:

$$E_i = \sigma_i \exp\left(\frac{R^2}{2D^2}\right) \quad (i = x, y), \tag{3}$$

where σ_i is each component of the estimation error of the displacement rate at observation point. R is the distance between observation and grid points. D is weight-adjusting parameter. In the following sections, we show the system operation result obtained by setting $D = 30$ km and $0 \le R \le 60$ km.

To obtain seismic energy (c) and the number of earthquakes (d) for each grid point, the earthquakes within a radius of 60 km of grid point with depths shallower than 30 km and magnitudes ≥ 1.0 were collected (Figure 3(b)). Then, the total seismic energy and the total number of earthquakes were calculated, where the seismic energy and the number of each earthquake were weighted depending on the distance between observation and grid points as follows:

$$P = P_i \exp\left(-\frac{R^2}{2R_0^2}\right) \quad (i = 1, n), \tag{4}$$

where P_i is physical quantity related to the ith earthquake, to which 1 is assigned in the case physical quantity is defined as the number of earthquakes, n is the total collected number of earthquakes for grid point, and R is the distance between observation and grid points. R_0 is weight-adjusting parameter. In this way, by taking the distance-depending weight into consideration, the essential event collection radius becomes 30 km. In the following sections, we show the system operation result obtained by setting $R_0 = 10$ km and $0 \le R \le 60$ km.

2.2. Step 2: Comparison between Geodetic and Seismic Quantities. After the selection of one of the four possible pairs (here, the absolute value of dilatation rate and seismic energy (per two years), maximum shear strain rate and seismic energy, absolute value of dilatation rate and the number of earthquakes (per two years), and maximum shear strain rate and the number of earthquakes), its relationship was examined using scatter diagrams for circular regions, each having 60-km radius centered in 0.05°-by-0.05° spatial grids, over inland Japan; each pair was compared for two-year time windows centered in a three-month-interval time grid.

2.3. Step 3: Quantification of the Relationship Between Geodetic and Seismic Quantities. Quantification of the relationship between geodetic and seismic quantities requires us to define an index well characterizing the relationship. We here define the index as a statistical index $R(t)$, where t represents time. One of the simplest indices is correlation coefficient. Scatter diagrams for respective time windows, however, implied that the relationship between geodetic and seismic quantities showed relatively complicated patterns, which forced us to define another index as follows.

Table 2: Model contingency table for explaining the relationship between potential conditions for/against the occurrence of physical events such as large inland earthquakes and their actual occurrence. The relation can be classified into the following four elements: *a*: the number of "yes" warnings accompanied by the occurrence of events, *b*: the number of "yes" warnings not accompanied by the occurrence of events, *c*: the number of "no" warnings accompanied by the occurrence of events, *d*: the number of "no" warnings not accompanied by the occurrence of events.

Potential condition for event occurrence	Event occurrence	
	Yes	No
Positive	*a*	*b*
Negative	*c*	*d*

(1) For a particular circular region centered in a spatial grid and for a two-year time window centered in a time grid, the mean of the absolute value of dilatation rate or the maximum shear strain rate was calculated from the grids ranking in the top 20% in terms of seismic energy or number of earthquakes. We defined this parameter as statistical index $R(t)$, where t represents the midpoint of each two-year time window.

(2) Process (1) was carried out for each time window which is moved by three months. The linear trend of $R(t)$ was then calculated for each time period from 1 January 2001 through 1 October 2007 with reference to the fixed time grid of 1 April 1998. The linear trend of $R(t)$ thus obtained was classified into three categories on the basis of trend significance with a 95% confidence level: significant decrease, significant increase, and insignificant change.

(3) Processes (1) and (2) are carried out for every spatial grid with an interval of 0.05°.

2.4. Step 4: Statistical Evaluation of the Relationship between Geodetic-Seismic Quantity Connection and Large Event Occurrence Times. The relationship between the occurrence times of large inland mainshocks and different types of statistical index $R(t)$ was evaluated by calculating the probability gains of alarm rate (AR) and success rate (SR) for M $\ge$ 6.0 inland mainshocks and drawing an error diagram based on a contingency table. To calculate AR and SR for each pair of physical quantities, we need to tabulate the relationship between the proposed potential condition, which is proposed for the possible occurrence of physical events of interest, and the actual occurrence of the event (Table 2). The items in the row and column of contingency table correspond to the potential condition for event occurrence and the actual occurrence, respectively. Defining the time period for positive potential condition in which the events will be predicted to occur as the period of A and the period of negative potential condition as the period of B, each element

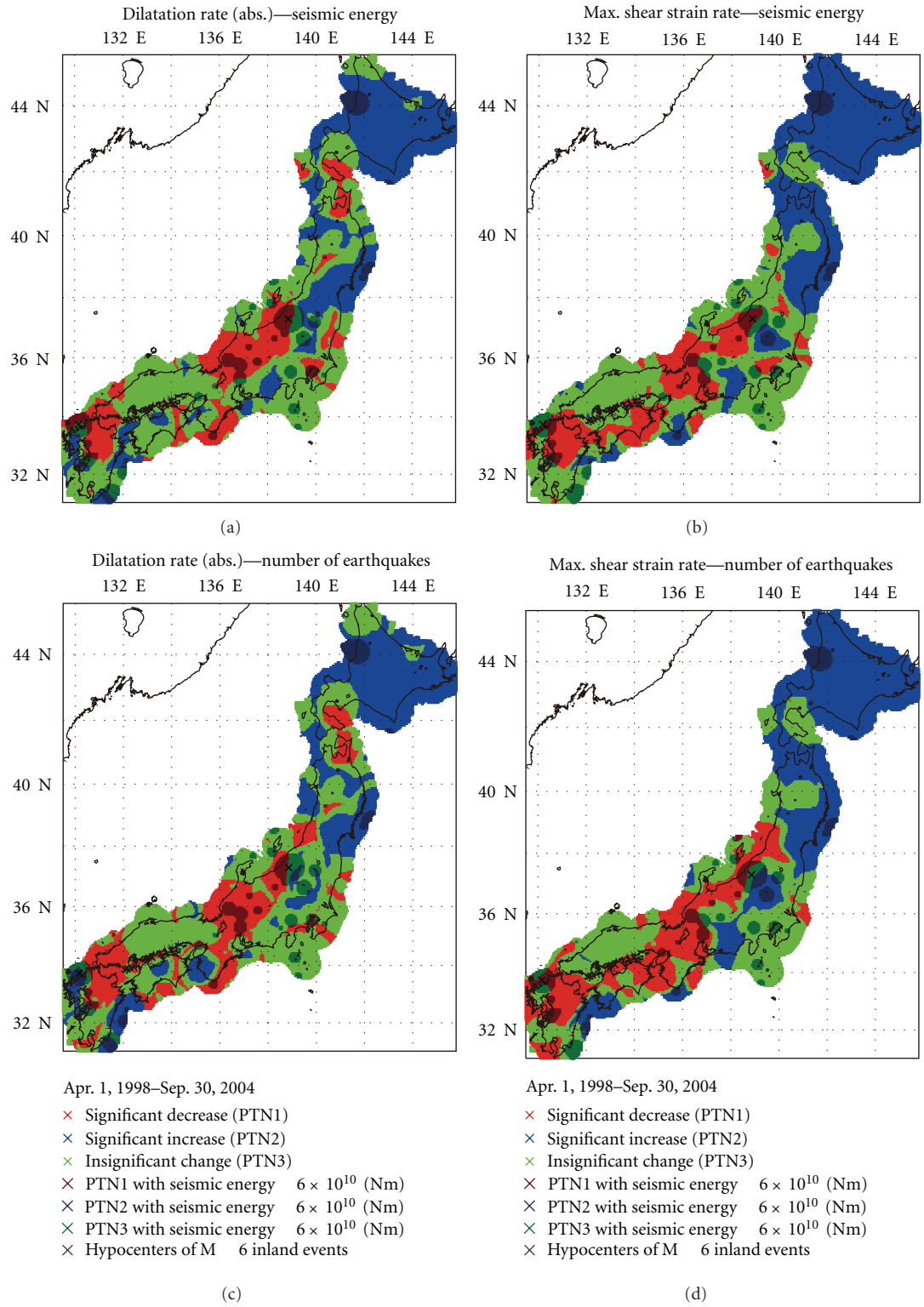

FIGURE 3: Spatial distributions of linear trends of statistical index $R(t)$ (pure red: significant decrease, pure blue: significant increase, pure green: insignificant change), which is obtained by comparison between (a) the absolute value of dilatation rate and seismic energy per two years, (b) maximum shear strain rate and seismic energy per two years, (c) absolute value of dilatation rate and number of earthquakes per two years, (d) maximum shear strain rate and number of earthquakes per two years. Time period for calculating linear trends of $R(t)$ is from 1 April 1998 through 30 September 2004, which is shown in panel (c) and (d). Superimposed in dark colors are the same distributions of areas in which seismic energy more than or equal to M4.0 earthquake (6×10^{10} Nm) was radiated during one year after the time period shown in panel (c) and (d). Linear trends of $R(t)$, which were obtained by least squares fitting, were classified using T approval with a confidence level of 95%. The numbers of dark-red, dark-blue, and dark-green grids, which are normalized by those of their corresponding pure-color ones, are here defined as no. PTN1, no. PTN2, and no. PTN3, respectively, for convenience in Figures 4 and 5.

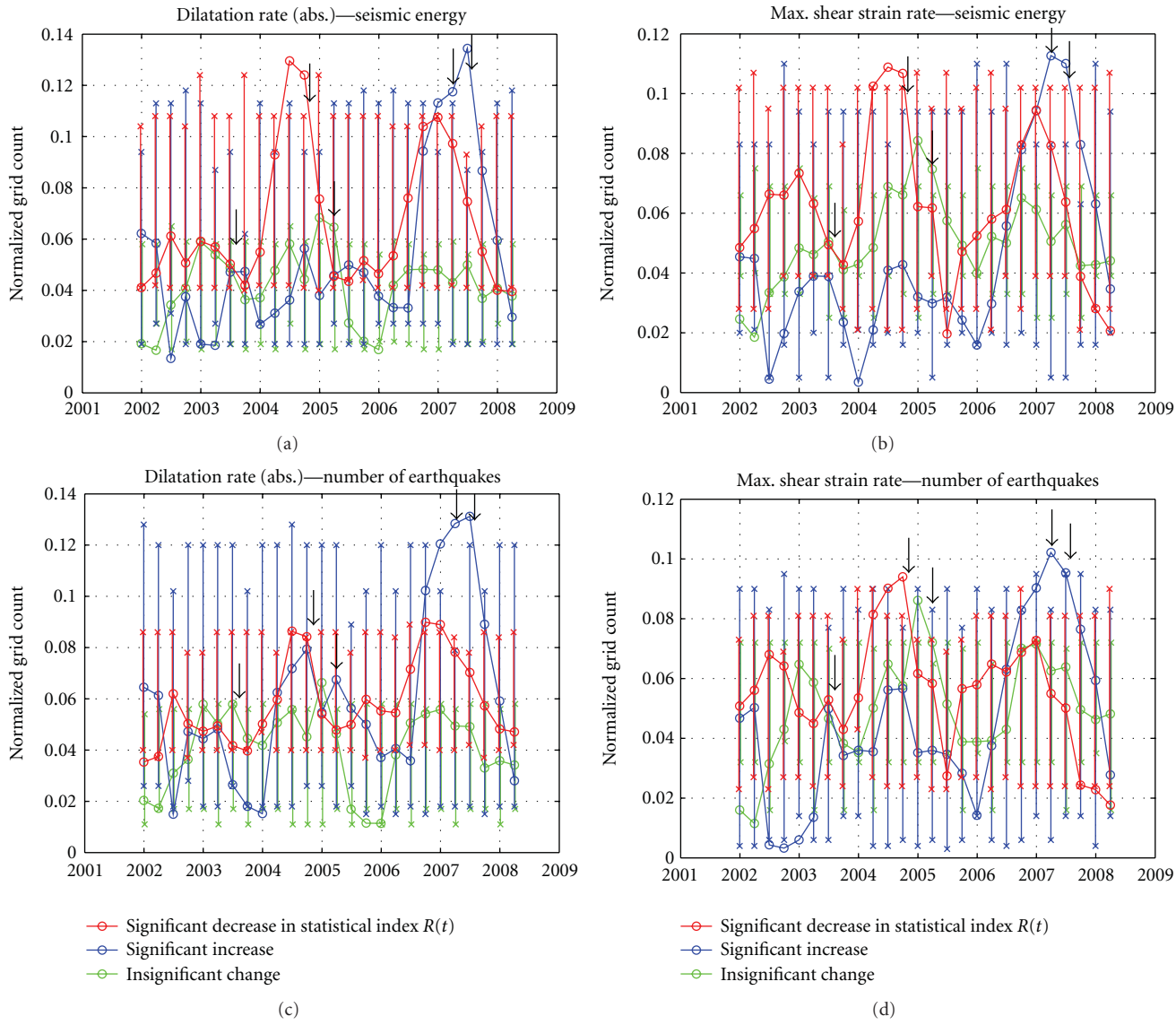

FIGURE 4: Temporal variation in no. PTN1, no. PTN2, and no. PTN3 (ref. Figure 3). Black arrows correspond to the occurrence date of M ≥ 6.0 inland mainshocks. Also shown are the error bars which were obtained by 100 times of shuffling of no. PTN1, no. PTN2, and no. PTN3 in time, respectively. The horizontal axis denotes the time corresponding to the end of the time period referred to for calculation of linear trend of $R(t)$. The beginning of each time period is fixed to April 1, 1998. Panels (a) to (d) correspond to different four pairs of geodetic and seismic quantities, which are the same as those in Figure 3.

of (a, b, c, d) in Table 2 can be explained as follows:

(a) the number of cases in which physical events of interest occur during the period of A,

(b) the number of cases in which physical events did not occur during the period of A,

(c) the number of cases in which physical events of interest occur during the period of B,

(d) the number of cases in which physical events did not occur during the period of B.

By this definition, $a+b$ and $a+c$ can be interpreted as follows.

($a+b$): Total number of the periods of A.

($a+c$): Total number of periods in which physical events of interest occurred.

If an event occurs during the time period of A, one count is added to element a. Using elements of (a, b, c, d), alarm rate (AR), and success rate (SR) can be calculated as follows [5, 6]:

$$\mathrm{AR} = \frac{a}{a+b}, \qquad \mathrm{SR} = \frac{a}{a+c}. \tag{5}$$

The role of this step is to find a useful monitoring index/indices which feature the preparatory crustal activity

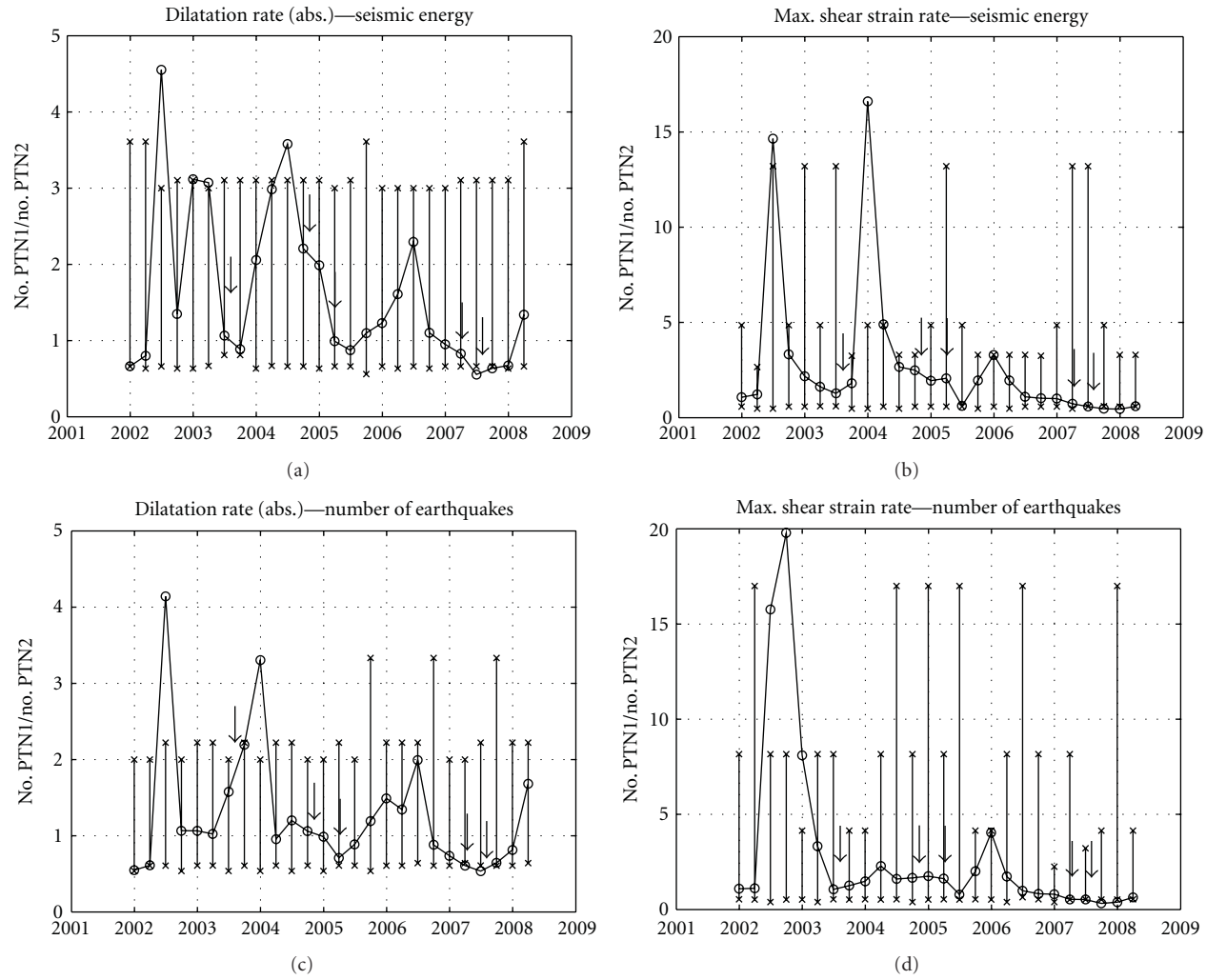

Figure 5: Temporal variation in the ratio of no. PTN1 to no. PTN2 (ref. Figure 3). Black arrows and the horizontal axis denote the same parameters as in Figure 4. Also shown are the error bars which were obtained by calculating the ratio between no. PTN1 and no. PTN2 shuffled in Figure 4. Panels (a) to (d) correspond to different four pairs of geodetic and seismic quantities, which are the same as those in Figures 3 and 4.

of a large inland earthquake through a statistical evaluation process. Such a monitoring index is defined based on the information on grid counts showing a specific (ex. negative significant) trend of $R(t)$ for a time window which are accompanied by high seismic activities. It should be noted that the performance of the monitoring index must be verified and validated in prospective way by updating the database.

We here focused on time variations of spatial grid counts which are accompanied by one-year release of total seismic energy larger than or equal to M4.0 earthquake (6.0×10^{10} Nm); the seismically active grid counts are specifically defined as no. PTN1 for those of significant decrease in $R(t)$, no. PTN2 for those of significant increase in $R(t)$, and no. PTN3 for those of insignificant change in $R(t)$. In addition, the three kinds of grid counts were normalized by their respective total grid counts (pure-color plus dark-color grids in Figure 3) for each time period of calculation. Step 4 tabulates thus calculated spatiotemporal distributions of no. PTNs1–3 and outputs the following figures: Figure 4(a) spatial distributions of no. PTNs1–3 for each time period (Figure 3), Figure 4(b) temporal changes in no. PTN1, no. PTN2, and no. PTN3 (Figure 4), and Figure 4(c) temporal changes in no. PTN1/no. PTN2 (Figure 5); this figure represents superiority or inferiority in the normalized area of PTN1 and PTN2. Assuming the temporal changes in no. PTN1/no. PTN2 reflect the preparatory processes of large inland earthquakes, we attempted to formulate a positive potential condition for the occurrence of large inland earthquakes in terms of a way of temporal changes in no. PTN1/no. PTN2 as shown in the first row of Table 3.

Statistical evaluation process at Step 4 requires the probability gains [7, 8] of alarm rate (AR) and success rate (SR). To calculate the probability gains of AR and SR, we prepared reference AR and SR for each pair of geodetic and seismic quantities in the following way.

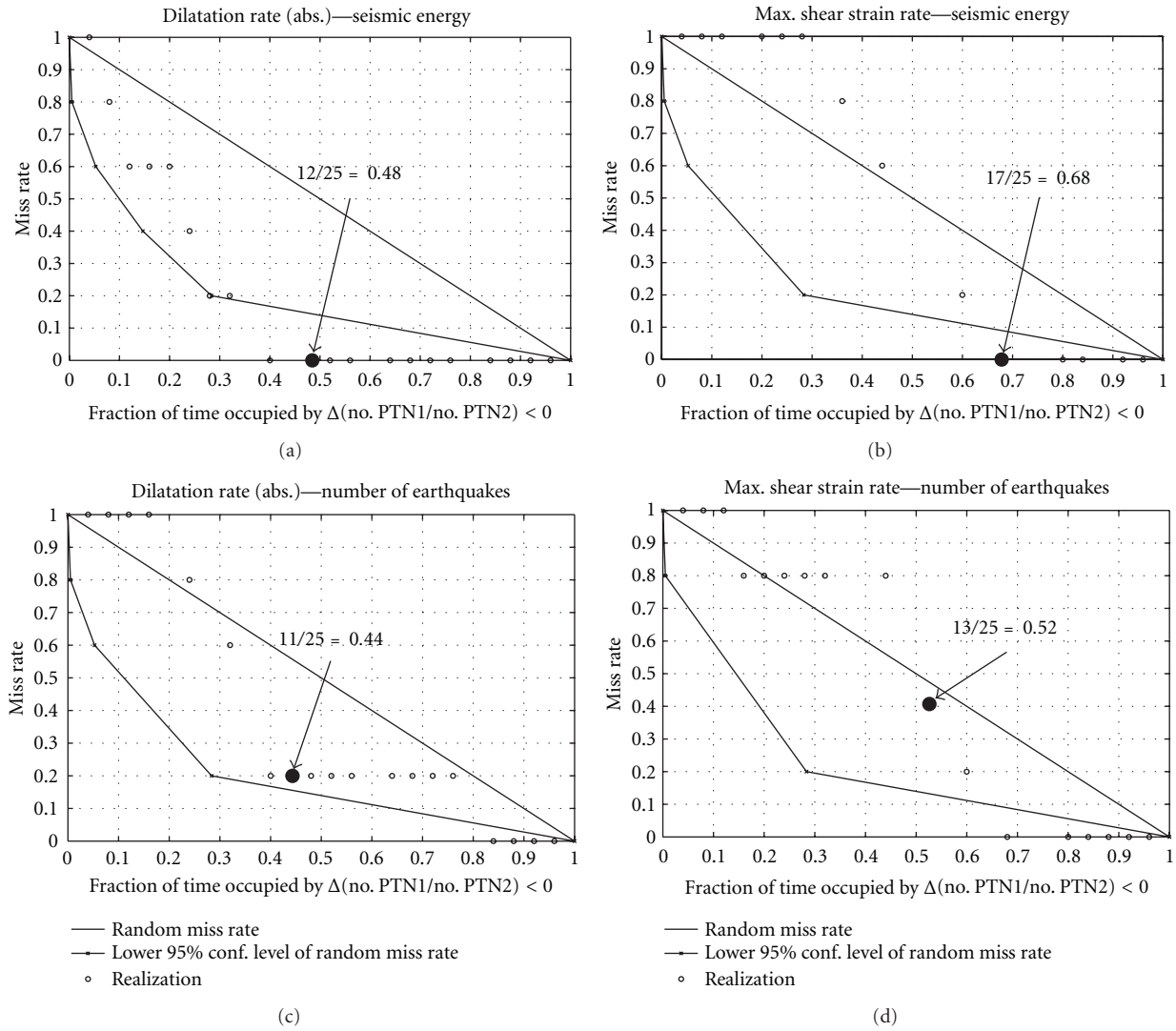

Figure 6: Error diagram (Molchan diagram) for evaluating the significance of the performance of a proposed potential condition for the occurrence of large inland earthquakes.

(1) We applied the bootstrap method to shuffle the spatial distributions of no. PTNs1–3 grids and their corresponding seismically inactive grids for a particular time window.

(2) Process (1) was carried out by moving the time window with its beginning time grid fixed. By repeating this, we obtained the temporal variation of the shuffled spatial distributions.

(3) We applied the bootstrap method to shuffle the temporal variation obtained in process (2).

(4) Processes (1) to (3) were repeated 100 times.

(5) The 100 ARs and SRs obtained were averaged.

Thus, calculated references AR and SR were considered as being due to a random phenomenon.

3. Most Informative Pair of Geodetic and Seismic Quantities

Among the four pairs of geodetic and seismic quantities examined, the pair comprising the absolute value of dilatation rate and seismic energy was found to be the most closely related in terms of probability gains of both alarm rate (AR) and success rate (SR) for $M \geq 6.0$ inland mainshocks (3.56 and 3.58, resp.) (Table 3). This pair showed the best performance even from the viewpoint of the error diagram (Figure 6). This is because the actual plot was located closest to position of the origin in Figure 6, which corresponds to the best performance of a proposed potential condition for event occurrence. The condition is represented in the first row of Table 3 or as the horizontal axis of Figure 6. This result was the same regardless of the approval methods and confidence levels. Figures 4(a) and 5(a) and the leftmost figures of respective elements in Table 3, which correspond to

Table 3: Contingency table showing the relationship between proposed potential conditions associated with the occurrence of M ≥ 6.0 inland mainshocks for four pairs of geodetic and seismic quantities and their actual occurrence times. The four figures for each element correspond to the following four pairs of geodetic and seismic quantities from left: the absolute value of dilatation rate and seismic energy, maximum shear strain rate and seismic energy, absolute value of dilatation rate and the number of earthquakes, and maximum shear strain rate and the number of earthquakes. A proposed potential condition occurring prior to the occurrence of inland mainshocks, Δ(no. PTN1/no. PTN2)<0, implies that the trend of no. PTN1/no. PTN2 is negative (Figure 5).

	Occurrence of inland earthquakes (M ≥ 6)	Nonoccurrence	Alarm rate (AR)
Δ(no. PTN 1/no. PTN2) < 0	5/5/4/3	7/12/7/10	0.417/0.294/0.364/0.231
Δ(no. PTN 1/no. PTN2) > 0	0/0/1/2	13/8/13/10	
Success rate (SR)	1.00/1.00/0.80/0.60		

Probability gains of AR and SR: 3.56/2.49/3.00/1.97 and 3.58/3.49/2.73/2.13.

the pair comprising the absolute value of dilatation rate and seismic energy, indicate that M ≥ 6.0 inland mainshocks are most likely to occur during the time period of the decrease in no. PTN1 relative to no. PTN2 or the increase in no. PTN2 relative to no. PTN1.

On the assumption that this tendency holds for even a small region influenced by a change in Coulomb failure stress (ΔCFS), a possible physical occurrence mechanism of a M ≥ 6.0 mainshock would be related to its preparatory process over a fault system. A mainshock would be triggered at the stage after microseismicity becomes active in the fault system, where stresses are considered to be accumulated on its asperities. Such a region may be accompanied by smaller strain rates. Because only a few samples of M ≥ 6.0 inland mainshocks were available to us, we need to continue to collect observations and further evaluate and validate the condition for event occurrence and the closest relation between geodetic and seismic quantities in the same manner as the one described in this study. We emphasize that this manner must not be changed in validating the condition for event occurrence. Furthermore, it is important to operate the statistical evaluation system to search for other informative pairs of physical quantities to gain a physical understanding of crustal activities as preparatory processes of large inland earthquakes.

4. Summary

Based on the notion that there are some correlations between different kinds of observations that may represent different aspects of crustal phenomena, we began with creating a database of various physical quantities and further constructed a basic system for statistically evaluating and validating a monitoring index which would reflect crustal activities associated with the occurrence of physical events such as large inland earthquakes. We have indicated that the most informative pair of geodetic and seismic quantities comprises the absolute value of dilatation rate and seismic energy in terms of probability gains of alarm rate (AR) and success rate (SR) and error diagram for M ≥ 6.0 inland mainshocks. The probability gains were calculated on the basis of contingency tables which show the relationship between the temporal changes in linear trends of statistical index $R(t)$ in seismically active areas and the occurrence times of M ≥ 6.0 inland mainshocks. Further evaluation and validation of the best pairs and the search for other informative combinations of physical quantities are necessary to gain a physical understanding of crustal activities, particularly, the preparatory processes of large inland earthquakes.

Acknowledgments

The authors deeply acknowledge valuable comments provided by two anonymous reviewers, which highly contributed to the improvement of the manuscript. They are also grateful to Geospatial Information Authority of Japan, and Japan Meteorological Agency for letting them utilize GEONET (GPS Earth Observation NETwork) data and unified hypocenter catalog, respectively.

References

[1] M. Imoto, "Earthquake probability based on multidisciplinary observations with correlations," *Earth, Planets and Space*, vol. 58, no. 11, pp. 1447–1454, 2006.

[2] M. Imoto, "Information gain of a model based on multidisciplinary observations with correlations," *Journal of Geophysical Research B*, vol. 112, no. 5, Article ID B05306, 2007.

[3] B. Gutenberg and C. F. Richter, "Magnitude and energy of earthquakes," *Annali di Geofisica*, vol. 9, pp. 1–15, 1956.

[4] M. Kawamura, T. Kudo, K. Yamaoka, and M. Furumoto, "Understanding of crustal activity with statistical approaches: I. Construction of spatiotemporal database with a unified data format,," *Journal of the Seismological Society of Japan (Second Series)*, vol. 63, pp. 21–33, 2010 (Japanese).

[5] I. T. Jolliffe and D. B. Stephenson, *Forecast Verification*, John Wiley & Sons, New York, NY, USA, 2003.

[6] S. Uyeda and A. Kumamoto, "Evaluation of the Kushida method of short-term earthquake prediction," *Proceedings of the Japan Academy Series B*, vol. 80, no. 3, pp. 140–147, 2004.

[7] K. Aki, "A probabilistic synthesis of precursory phenomena," in *Earthquake Prediction: An International Review*, D. W. Simpson and P. G. Richards, Eds., Maurice Ewing Seires 4, pp. 566–574, AGU, Washington, DC, USA, 1981.

[8] A. Helmstetter, Y. Y. Kagan, and D. D. Jackson, "High-resolution time-independent grid-based forecast for M ≥ 5 earthquakes in California," *Seismological Research Letters*, vol. 78, no. 1, pp. 78–86, 2007.